



Pt, Pd, Ni, Co, Mo). These components can be added to optimize the finished catalyst's acidity, metals activity, porosity, and physical integrity.

One key application of shape selectivity is ExxonMobil's selective catalysts dewaxing technology. Dewaxing rearranges the structure of primarily straight chain molecules to ensure they have the correct flow properties at the desired temperatures. The MSDW-2 catalyst technology is a medium pore zeolite which applies shape selectivity, proper control of acidity, and a metal driven hydrogenation-dehydrogenation function to selectively convert or 'dewax' the straight chain molecules to a slightly branched molecules as it enters the zeolite pore. More bulky or branched molecules, which already have beneficial lubricant properties, are excluded from entering the zeolite pore. Thus, this catalyst technology only works on the molecules that need to be converted.

**Metal Oxide Catalysts.** Another important class of catalytic materials that are widely used in the refining industry are metal oxides. These materials, which are typically mixtures of CoMo or NiMo oxides on silica-alumina supports, are primarily used in key refinery processes called hydroprocessing. This technology uses the catalytic addition of hydrogen to selectively remove sulfur and nitrogen from various refinery streams to produce low sulfur gasoline and diesel. More hydrogen intensive hydroprocessing applications can also reduce other components such as olefins and aromatics.

The prime contributor to sulfur in the gasoline pool is from the cat-cracking unit. While it is possible to hydrotreat the sulfur to very low levels, cat naphtha also contains a considerable amount of valuable olefins, which are high in octane. Thus, the challenge is to selectively remove sulfur while minimizing the saturation of olefins. This is particularly an issue for higher sulfur cat naphthas. ExxonMobil's *SCANfining* technology [5] utilizes a proprietary CoMo catalyst, jointly developed with Akzo Nobel, to selectively reduce the cat naphtha sulfur while minimizing the saturation of high octane olefins (Figure 3).

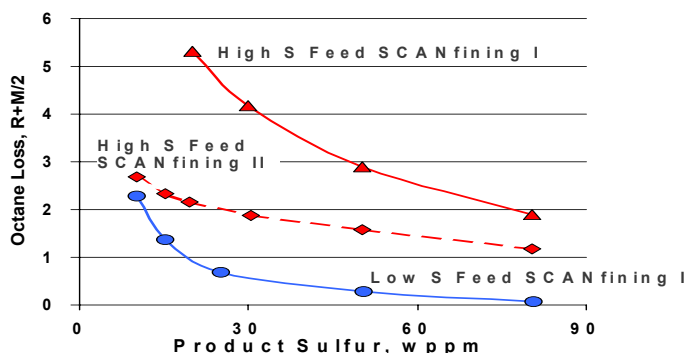


**Figure 3.** ExxonMobil's *SCANfining* technology selectively removes sulfur while minimizing octane loss.

The CoMo system is characterized by high metals dispersion with special attention given to the support-metal interactions. *SCANfining II*, is even more selective particularly for higher sulfur cat naphthas. *SCANfining* has been rapidly commercialized and will be used in 30 units worldwide to manufacture low sulfur gasoline.

A new generation of ultra-high activity catalysts for nitrogen and sulfur removal was recently discovered by ExxonMobil and jointly developed with Akzo Nobel. This catalyst system called *NEBULA™* is unique in that it is a bulk mixed metal oxide, which maximizes the number of active sites per volume of catalyst [6]. *NEBULA™* has shown very high hydrodesulfurization and

hydrodenitrogenation activities compared to conventional catalysts (Figure 4). This performance advantage enables the refiner to produce ultra low sulfur diesel in existing units. *NEBULA™* has been commercialized in a number of distillate hydrotreating and hydrocracking applications.

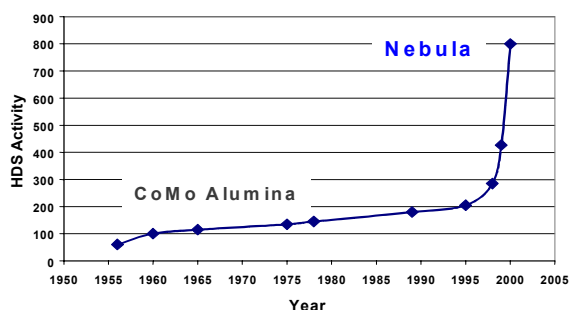


**Figure 4.** *NEBULA™* catalyst technology represents a step change in Hydroprocessing catalysts.

### Future Advances in Catalysis

Catalysis will continue to play a crucial role in the petroleum and petrochemical industries. Fuel and lube compositions are expected to evolve in response to environmental legislation and advanced engine design. In addition, petroleum feedstocks will become heavier and sourer with time. This will require future catalysts, which are higher in activity and selectivity, more poison tolerant and stable for longer periods.

ExxonMobil is committed to accelerate the pace of innovation and delivery through the use of HTE. ExxonMobil and Symyx Technologies, a leader in the development and application of high-speed materials research methods, have formed a technology alliance focused on the application of HTE technology across ExxonMobil's downstream and chemical portfolio. Implementation of HTE methods will enhance ExxonMobil's core competency in catalyst research and development. This alliance includes high throughput catalyst synthesis, characterization, and evaluation tools coupled with an informatics platform to more rapidly discover and implement future catalyst systems.

### References

- (1) Kaufmann, T. G.; Kaldor, A.; Stuntz, G. F.; Kerby, M. C.; Ansell, L. L. *Catalysis Today*, **2000**, *62*, 77.
- (2) Chen, N. Y.; Garwood, W. E.; Dwyer, F. G. *Shape Selective Catalysis in Industrial Applications*, 2<sup>nd</sup> ed., Marcel Dekker, New York, 1996.
- (3) Beck, J. S.; Vartuli, J. C.; Roth, W. J.; Leonowicz, M. E.; Kresge, C. T.; Schmitt, K. D.; Chu, C. T.-W. Olson, D. H.; Sheppard, E. W.; McCullen, J. B.; Higgins, J. B.; Schlenker, J. L. *J. Am. Chem. Soc.* **1992**, *114*, 10834.
- (4) Feng, X.; Frywell, G.E., Wang, L.Q., Kim, A.Y., Liu, J., Kemner, K.M., *Science*, **1997**, *276*, 923
- (5) Riley, K. L.; Kaufman, J. L.; Zaczepinski, S.; Desai, P. H.; Mayo, S. W. *Akzo Nobel Catalyst Symposium, Vol. G-3*, 1998, 1.
- (6) Meijburg G., Brevoort E., Plantenga F., Mayo S., Inoue Y., Fujita K., Lewis W., Sapre A., *NEBULA™ for Hydrocracker Pretreat Operations*, ERTC 2003, London.

## SELECTIVE HYDRODESULFURIZATION OF FCC GASOLINE OVER CoMo/Al<sub>2</sub>O<sub>3</sub> SULFIDE CATALYSTS

Makoto Toba, Yasuo Miki, Yukio Kanda, Takashi Matsui,  
Masaru Harada and Yuji Yoshimura

National Institute of Advanced Industrial Science and Technology,  
Tsukuba Central-5, 1-1-1 Higashi,  
Tsukuba, Ibaraki 305-8565, Japan

### Introduction

FCC gasoline is one of the major components of motor gasoline. It contains high level of sulfur derived from heavy gas oil and atmospheric residue used as FCC raw materials. FCC gasoline also contains valuable olefins which contribute to the octane number of the motor gasoline. Therefore, the selective hydrodesulfurization which minimizes octane loss is highly desired to meet the severe limitation of sulfur content (1~3). In this study, the selective hydrodesulfurization (HDS) of FCC gasoline over new sulfide catalysts was investigated.

### Experimental

Two kinds of FCC gasoline (full-range and 60 °C +) were used here. The properties of them are summarized in Table 1.

**Table 1. Properties of FCC gasoline**

	FCCG (full-range)	FCCG (60°C +)
Density (g/cm <sup>3</sup> @15°C)	0.733	0.771
Sulfur (wtppm)	158.9	234.1
H/C (mol/mol)	1.93	1.83
Average molecular weight	102	112
GC-RON* <sup>1</sup>	90.5	88.9
Hydrocarbon type (vol%)* <sup>1</sup>		
Paraffins (P)	5.5	4.8
Isoparaffins (I)	37.6	32.4
Olefins (O)	26.3	19.7
Naphthenes (N)	9.2	12.4
Aromatics (A)	21.4	30.8

\*1 Research octane number and hydrocarbon type were measured by GC.

Sulfide CoMo and NiMo catalysts were prepared by incipient wetness impregnation of  $\gamma$ -alumina with a mixed solution obtained from molybdenum oxide, cobalt (nickel) carbonate and a special ligand. All catalysts were presulfided in the stream of 5% H<sub>2</sub>S/H<sub>2</sub> gas before reaction.

The selective hydrodesulfurization (HDS) of FCC gasoline was carried out in a high-pressure fixed-bed continuous-flow reactor. The reaction conditions were hydrogen pressure of 1~2 MPa, reaction temperature of 220~260 °C, liquid hourly space velocity (LHSV) of 4 h<sup>-1</sup>, and a volume ratio of hydrogen (NTP) to feed of 100.

The hydrocarbon composition and research octane number (RON) in feedstock and products were analyzed by using PIONA-GC (Agilent 6890N (JIS K2536)-Yokogawa Analytical Systems Co. GPI system). The contents of total sulfur were measured by elemental analysis (Mitsubishi Chemicals Co., TS-100V). Sulfur compounds were analyzed by a GC-SCD (Agilent6890-Sievers355).

### Results and Discussion

Figure 1 shows the time course of HDS percentage, olefin and aromatics hydrogenation percentage during HDS of FCC gasoline (60 °C+) for 56h. HDS activity showed almost constant, while olefin hydrogenation activity decreases drastically in the first 10h and

decreases gradually in the latter 46h. Aromatics hydrogenation activity showed zero except initial stage of reaction.

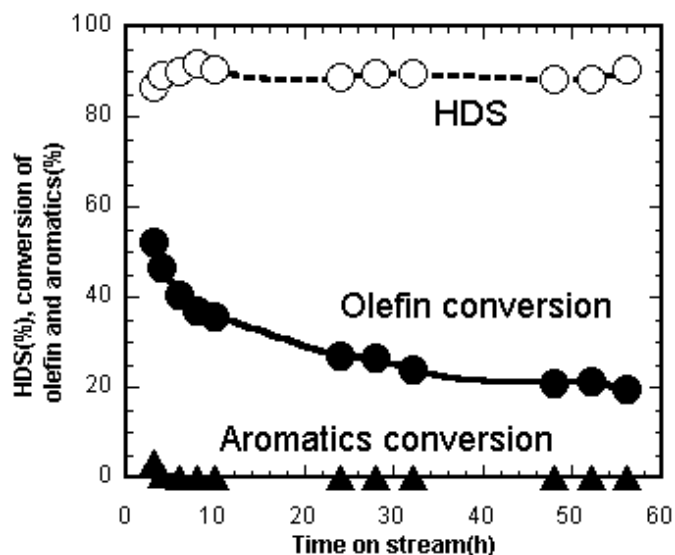


**Figure 1.** Time course of FCC gasoline (60 °C+)

hydrodesulfurization: Reaction conditions: temperature 240 °C; pressure 1MPa, LHSV, 4h<sup>-1</sup>, H<sub>2</sub>/feed ratio 100NL/L; Catalyst: CoMo/Al<sub>2</sub>O<sub>3</sub> (CoO 3.1 wt%, MoO<sub>3</sub> 11.8 wt%)

Effect of catalyst species on properties of product oil in the hydrotreatment of heavy FCC gasoline is shown in Table 2. Both catalysts showed very high HDS activities. NiMo/Al<sub>2</sub>O<sub>3</sub> catalyst gave a much higher olefin hydrogenation activity than CoMo/Al<sub>2</sub>O<sub>3</sub> catalyst. This result means that CoMo/Al<sub>2</sub>O<sub>3</sub> is more suitable for selective hydrogenation of FCC gasoline than NiMo/Al<sub>2</sub>O<sub>3</sub>.

**Table 2. Effect of catalyst species on properties of product oil in the hydrotreatment of heavy FCC gasoline\*<sup>1</sup>**

	FCCG (60 °C+)	NiMo/Al <sub>2</sub> O <sub>3</sub> * <sup>2</sup>	CoMo/Al <sub>2</sub> O <sub>3</sub> * <sup>2</sup>
Temperature (°C)	—	240	240
Time (h)	—	52	52
Density (g/cm <sup>3</sup> @15°C)	0.771	0.766	0.768
Sulfur (wtppm)	234.1	5.6	7.1
HDS (%)	—	97.6	97.0
Olefin conv. (%)	—	80.3	37.2
H/C (mol/mol)	1.83	1.87	1.85
Average molecular weight	112	112	112
GC-RON* <sup>3</sup>	88.9	85.6	87.1
Hydrocarbon type (vol%)			
Paraffins (P)	4.8	9.6	7.3
Isoparaffins (I)	32.4	41.8	36.9
Olefins (O)	19.7	3.8	12.3
Naphthenes (N)	12.4	14.8	13.4
Aromatics (A)	30.8	30.1	30.1

\*1 Reaction conditions: temperature 240 °C; pressure 2MPa, LHSV, 4h<sup>-1</sup>, H<sub>2</sub>/feed ratio 100NL/L

\*2 NiO (CoO) 6.1wt%-MoO<sub>3</sub> 23.6wt%, sulfidation, 340 °C for 3h

\*3 Research octane number measured by GC

Figure 2 shows effect of sulfidation temperature of catalyst on HDS and olefin hydrogenation activities. The reaction carried out at

220, 240 and 260 °C. It is noted that olefin hydrogenation activity of the catalyst sulfided at 319°C is much lower than those of other catalysts, while HDS activity showed almost same level. These results suggest that sulfidation temperature have much larger influence on olefin hydrogenation active sites than the HDS active sites. These phenomena appeared more remarkably at higher temperature. According to the proposed olefin hydrogenation active site, olefin hydrogenation occurs at Mo coordinatively unsaturated sites (CUS) (4). Perhaps, CUS Mo sites of this catalyst may selectively disappear.

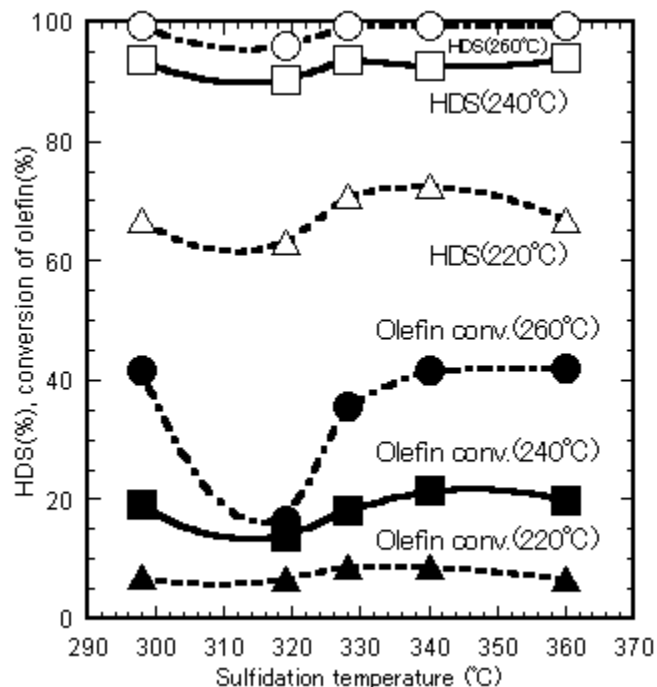


**Figure 2.** Effect of sulfidation temperature of catalyst on HDS and olefin hydrogenation : Reaction conditions: pressure 1MPa, LHSV, 4h<sup>-1</sup>, H<sub>2</sub>/feed ratio 100NL/L : Catalyst: CoMo/Al<sub>2</sub>O<sub>3</sub> (CoO 3.1 wt%, MoO<sub>3</sub> 11.8 wt%)

Figure 3 shows HDS and olefin hydrogenation activity in the hydrotreatment of full-range FCC gasoline. Olefin hydrogenation activity of developed catalyst is relatively low and octane (GC-RON) loss is 0.6 to 1.3 in the range of 220°C to 260°C. However, olefin hydrogenation activity of commercial catalyst drastically increased at 260°C, while HDS activities of both catalysts showed almost same. From the analysis of various C5 and C6 olefin reactivity, terminal olefin hydrogenation activity for the developed catalyst (43.6~49.8%) showed slightly lower than the commercial one (48.2~59.6%). However, internal olefin hydrogenation activity at 260 °C for the developed catalyst (-18.2~5.0%) showed much lower than the commercial one (-17.6~23.6%). These results suggest that internal olefin is less active at olefin hydrogenation active site of developed catalyst. At lower temperature, conversion of internal olefin showed minus value because of formation of internal olefins from terminal olefins by C=C double bond isomerization. These phenomena are effective olefin hydrogenation depression.

Sulfur compounds in full-range FCC gasoline product oils were analyzed by GC-SCD. Benzothiophene and methylbenzothiophene were completely desulfurized. Most of sulfur compounds remaining in the product are thiophene and alkylthiophenes. Slight amounts of sulfur compounds such as 2-pentanethiol which were produced by re-

combination reaction between olefins and hydrogen sulfide were observed.

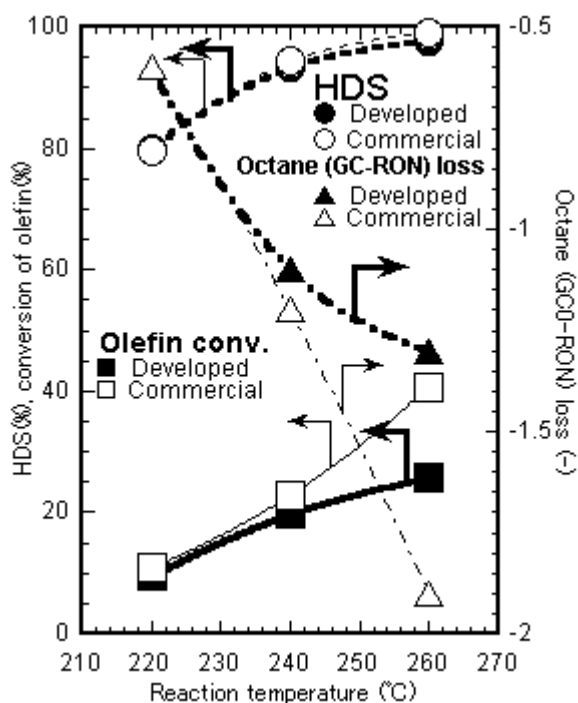


**Figure 3.** HDS and olefin hydrogenation activity in the hydrotreatment of full-range FCC gasoline: Reaction conditions: pressure 1MPa, LHSV, 4h<sup>-1</sup>, H<sub>2</sub>/feed ratio 100NL/L: Catalyst: CoMo/Al<sub>2</sub>O<sub>3</sub> (developed, CoO 3.1 wt%, MoO<sub>3</sub> 11.8 wt%; commercial, CoO 4.5 wt%, MoO<sub>3</sub> 16.9 wt%)

### Conclusions

The developed CoMo/Al<sub>2</sub>O<sub>3</sub> catalyst showed high HDS activity and depressed olefin hydrogenation. The HDS selectivity of the catalyst depended on their sulfidation conditions. Olefin hydrogenation activity of the catalyst sulfided at 319°C less increased with increasing operating temperature than those of other catalysts. At higher temperature, internal olefin hydrogenation activity of the developed catalyst was much lower than that of commercial one.

### References

- (1) S. Hatanaka, M. Yamada, O. Sadakane, *Ind. Eng. Chem. Res.*, **36**, 1519 (1997).
- (2) S. Hatanaka, M. Yamada, O. Sadakane, *Ind. Eng. Chem. Res.*, **37**, 1519 (1998).
- (3) Rosvoll, J. S., Grande, K., Moljord, K., Skjøfsvik, P. A., Thorvaldsen, B., Johansen, S., Kuhnle, S., Sørup, P. Å., Sapre, A. V., Roundtree, E. M., *Hydrocarbon Processing*, **Feb. 2004**, 55 (2004).
- (4) Tanaka, K., Okuhara, T., *Proc. 3<sup>rd</sup> Int. Conf. on Chem. and Uses of Molybdenum*, Barry H. F., Mitchell, P. C. H. Ed. Climax Molybdenum Company, 1979; p.170.

# SELECTIVE SULFUR REMOVAL FROM LIQUID HYDROCARBONS OVER REGENERABLE CeO<sub>2</sub>-TiO<sub>2</sub> ADSORBENTS FOR FUEL CELL APPLICATIONS

Shingo Watanabe, Xiaoliang Ma and Chunshan Song\*

Clean Fuels and Catalysis Program, The Energy Institute and Department of Energy and Geo-Environmental Engineering The Pennsylvania State University  
209 Academic Project Building, University Park, PA 16802  
\*E-mail: csong@psu.edu

## Introduction

In order to improve the air quality, the governments in various countries have announced new regulations to reduce the sulfur contents in transportation fuels. The U.S. Environmental Protection Agency (EPA), for example, has announced a new regulation that mandates refineries to reduce the sulfur content in gasoline to below 30 ppmw from the current average of 300 ppmw and in diesel to below 15 ppmw from the current level of 500 ppmw by year 2006. The interest in the desulfurization of transportation fuels is further motivated by the development of fuel cells to power automobiles, because the fuel-cell-powered vehicles are more efficient energetically and do not emit noxious gases such as SO<sub>x</sub>, NO<sub>x</sub> etc. However, for PEMFC applications the sulfur content in the transportation fuels needs to be further reduced to < 1 ppmw.

Catalytic hydrodesulfurization (HDS) is the conventional method that is being employed by the refineries to produce clean transportation fuels. Although HDS process can remove sulfur compounds from gasoline close to 30 ppmw, it is highly inconvenient and more expensive process to produce fuel cell grade gasoline as the process is conducted at high pressure, high temperature with high hydrogen consumption. Several alternative methods such as adsorption, alkylation, oxidation, extraction etc. have been developed in recent years. Among them the adsorptive desulfurization can be accomplished at low temperature and pressure. Since gasoline contains significant amount of olefins and aromatics, the adsorbent should be able to remove selectively organic sulfur compounds in the presence of the olefins and aromatics.

A new concept is being developed in our laboratory at Penn State University known as "Selective adsorption for removal of sulfur (PSU-SARS)" for the adsorption desulfurization of gasoline, diesel and jet fuels. Several new adsorbents based on zeolites, mixed oxides, supported metal and metal compounds, and activated carbons are being developed and some of them exhibit excellent adsorption capacity for the desulfurization of gasoline and jet fuels.<sup>8</sup>

Owing to its high oxygen storage capacity, redox properties and good metal-support interactions, CeO<sub>2</sub> has been known as an excellent support for base metals and noble metals in a variety of catalytic processes, including auto exhaust three-way catalyst. The CeO<sub>2</sub>-based adsorbents have also been developed in recent years for the removal of H<sub>2</sub>S and SO<sub>x</sub> from flue gas, natural gas and coal-derived gas. CeO<sub>2</sub> has been evaluated as a high temperature regenerable desulfurization sorbent, which yields elemental sulfur upon regeneration<sup>9-11</sup>. Our recent work on the desulfurization of jet fuel indicated that Ce loaded zeolites and CeO<sub>2</sub>-based bimetallic oxides adsorbents exhibit fairly good adsorption properties.

Taking into account of the interesting properties of the CeO<sub>2</sub>, the present study aimed at developing CeO<sub>2</sub>-based regenerable adsorbents for the removal of thiophenic sulfur compounds present in the gasoline, jet and diesel fuels. High surface area CeO<sub>2</sub>-TiO<sub>2</sub> bimetallic oxides with various molar ratios synthesized by coprecipitation have been used as adsorbents for the desulfurization of a model gasoline containing 430 ppmw of sulfur in the form of

thiophene, tetrahydrothiophene, benzothiophene and 2-methylbenzothiophene in a fix-bed flow reactor at ambient temperature and pressure. CeO<sub>2</sub>-TiO<sub>2</sub> mole ratio was swung to investigate organic sulfur compounds adsorption behavior using model fuel and commercial fuel. Regenerability of the adsorbents by air was also tested.

## Experimental

The adsorbents were prepared using cerium ammonium nitrates and titanium oxysulfate sulfuric acid hydrate (Aldrich Chem. Co.) by urea gelation/co-precipitation method.<sup>6</sup> Precipitation was employed at 90~95°C for 8 hours. Precipitants were dried 110°C over night, and calcined at 450°C for 6 hrs in air employing a temperature ramp of 2°C/min. Analysis of the adsorbents was performed by X-ray diffraction (XRD), and surface area was calculated using the BET equation. Pore size distributions were calculated by the Barrett-Joyner-Halender (BJH) method using the desorption branch of the isotherm.

A model gasoline, which contained thiophene, tetrahydrothiophene, benzothiophene and 2-methylbenzo-thiophene (total sulfur concentration: 430 ppmw), toluene and 1-octene in heptane was used in the present study. The composition of the model gasoline is listed in Table 1.

For flow system desulfurization, the powder adsorbent was packed in a stainless steel column with an internal diameter of 4.6 mm and length of 37.5 mm. The adsorbent bed volume was about 0.623 ml. Pretreatment was conducted under the dry airflow at 375°C for 2 hours before adsorption. The model gasoline was fed into the column using a HPLC pump. The feed flow rate was 0.05 ml/min. The adsorption was conducted under ambient temperature and pressure. Antek 9000 Total Sulfur Analyzer (detection limit < 0.5 ppmw) was used to determine the total sulfur concentration of the treated model gasoline. The breakthrough volume and capacity were calculated on the basis of the breakthrough curves considering the sulfur content at the breakthrough point was below 1 ppmw.

Regeneration was conducted under an air flow. Air was flowed through the spent adsorbent bed at room temperature for 5 min. Then, the temperature of the adsorbent bed was increased up to 375°C within 10 min, and kept at 375°C for 45 min. Total time for the regeneration was 60 min. Air was continuously flowing, until temperature was cooled down to room temperature. After the regeneration the adsorptive desulfurization test was conducted again.

Table 1 Model gasoline composition

	FW	d (g/cm <sup>3</sup> )	b.p. (°C)	mole%	S conc. (ppmw)
C <sub>7</sub>	100.2	0.684	98	99.769	-
T	84.1	1.051	-	0.0344	110
THT	88.2	1.000	-	0.0297	95
BT	134.2	1.149	-	0.0359	115
2MBT	148.2	-	-	0.0312	100
Toluene	92.1	0.865	110.6	0.0333	-
1-octene	122.2	0.7515	122	0.0333	-
C <sub>9</sub> (IS)	128.3	0.718	151	0.0333	-
Total				100.00	430

## Results and Discussion

The present study was focused on examining the effect of Ti-Ce atomic ratio on the adsorptive performance of the Ti-Ce bi-metal oxide adsorbents ( $\text{TiO}_2\text{-CeO}_2$ ) and the regenerability of the Ti-Ce bimetal oxide adsorbents. The breakthrough curves of the model gasoline over the bi-metal oxides with different Ti-Ce atomic ratio are shown in Figure 1. The breakthrough amount of the treated model gasoline (gram of the cumulative treated model gasoline per gram of the adsorbent, g/g) increases in the order of  $\text{CeO}_2 < \text{TiO}_2 < \text{Ti}_{0.05}\text{Ce}_{0.95}\text{O}_2 < \text{Ti}_{0.1}\text{Ce}_{0.9}\text{O}_2 < \text{Ti}_{0.9}\text{Ce}_{0.1}\text{O}_2 < \text{Ti}_{0.5}\text{Ce}_{0.5}\text{O}_2$ . It is clear that the bi-metal oxides showed better adsorptive performance than the monometal oxides,  $\text{CeO}_2$  and  $\text{TiO}_2$ , indicating that there is significant synergism of the two metal oxides. It might be because the bi-metal oxides result in a morphological change, which was observed in XRD analysis, and/or a change in the electronic structure on the surface. The smaller crystal size for the bi-metal oxides, which were calculated on the basis of XRD data, than those of the monometal oxides,  $\text{TiO}_2$  and  $\text{CeO}_2$ , was observed. Figure 2 shows that the breakthrough capacity (milligram of sulfur per gram of adsorbent, mg/g) of the bi-metal oxides at the outlet sulfur level of 1 and 30 ppmw as a function of the Ti-Ce atomic ratio. Adding small amount of  $\text{TiO}_2$  into  $\text{CeO}_2$  improved the capacity of the adsorbent significantly. The bi-metal oxide with a Ti-Ce atomic ratio of 1:1 showed the highest adsorptive capacity, being 3.8 mg/g.

Adsorptive selectivity of the bi-metal oxides was also examined. The results showed that the bi-metal oxides have good selectivity for the organic sulfur compounds. Further work in characteristics of the bi-metal oxides is necessary for fundamental understanding the adsorptive mechanism.

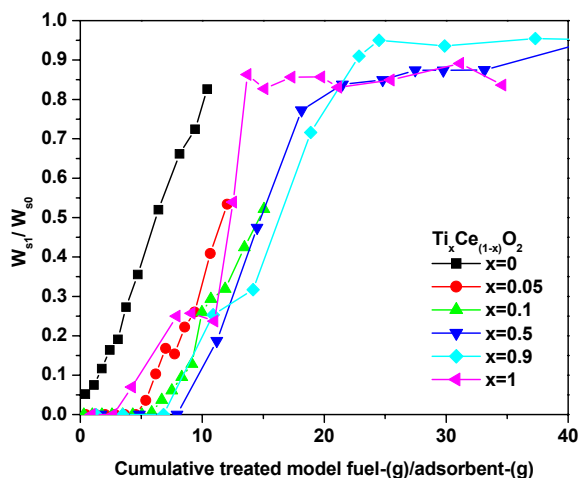


Figure 1 The breakthrough curves of model gasoline over  $\text{TiO}_2\text{-CeO}_2$  adsorbents

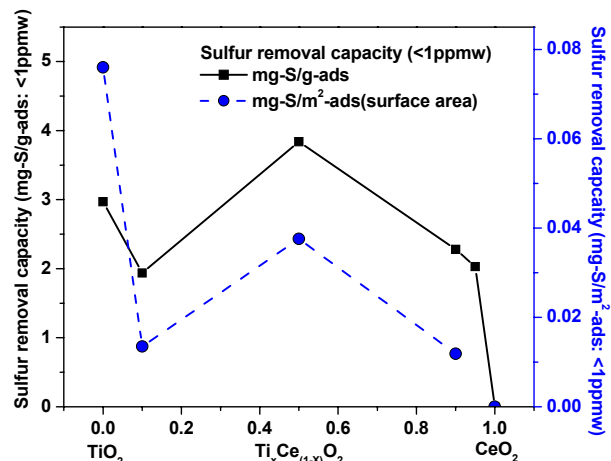


Figure 2 The adsorptive capacities of  $\text{CeO}_2\text{-TiO}_2$  adsorbents as a function of Ti-Ce atomic ratio in  $\text{CeO}_2\text{-TiO}_2$  adsorbents

The spent  $\text{Ti}_{0.1}\text{Ce}_{0.9}\text{O}_2$  adsorbent was regenerated at  $375^\circ\text{C}$  under an air flow. The adsorptive performance of the regenerated  $\text{Ti}_{0.1}\text{Ce}_{0.9}\text{O}_2$  adsorbent was shown in Figure 3 in comparison with that of the fresh one. As seen in this figure, the breakthrough curve for the regenerated adsorbent was almost consistent with that for the fresh one, implying that almost all of the adsorptive capacity of the fresh adsorbent was recovered by the oxidative regeneration with air. More studies are necessary to determine the best regeneration conditions.

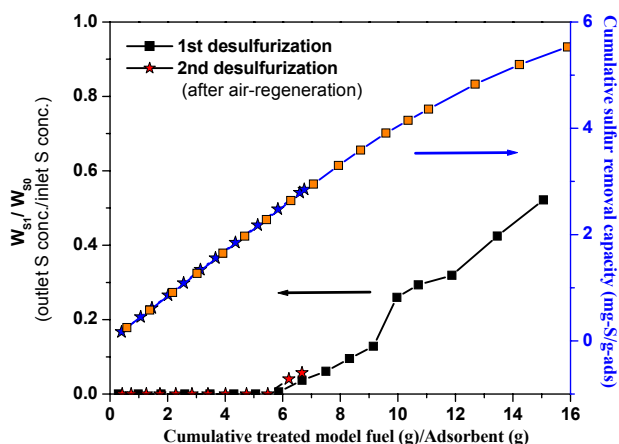


Figure 3 Adsorptive performances of the fresh and regenerated  $\text{Ti}_{0.1}\text{Ce}_{0.9}\text{O}_2$  adsorbents

## Summary

$\text{TiO}_2\text{-CeO}_2$  bimetallic oxides showed higher desulfurization capacity in comparison with the monometallic oxides,  $\text{TiO}_2$  and  $\text{CeO}_2$ . A synergetic effect of the two metal oxides was observed in the adsorptive desulfurization of the model fuel. A potential

advantage of the TiO<sub>2</sub>-CeO<sub>2</sub> binary oxides is that they can be regenerated by the oxidation at 375°C in air.

### Acknowledgments

This work was supported in part by the US Department of Defense and in part by the US Department of Energy.

### References

- (1) Song, C. S. and X.L. Ma, *Applied Catalysis B Environmental*, **2003**, *41(1-2)* 207-238
- (2) Ma, X.L., L. Sun, Z. Yin and C. S. Song, *Preprint Paper – American Chemical Society*, Division Fuel Chemistry **2001**, *46(2)*, 648-649.
- (3) Ma, X.L., M. Sprague, L. Sun and C. S. Song, *Preprint Paper – American Chemical Society*, Division Fuel Chemistry **2002**, *47(2)*, 452-453.
- (4) S. Velu, S. Watanabe, X.L. Ma, L. Sun and C. S. Song, *Preprint Paper – American Chemical Society*, Division Petroleum Chemistry **2003**, *48(2)*, 56-57.
- (5) S. Velu, X.L. Ma and C. S. Song, *Preprint Paper – American Chemical Society*, Division Fuel Chemistry **2002**, *47(2)*, 447-448.
- (6) M. Kobayashi and M. Flytzani-Stephanopoulos, *Industrial and Engineering Chemistry research*, **2002**, *41*, 3115-3123
- (7) S. Watanabe, S. Velu, X. Ma and C.S. Song **2003**, *Preprint Paper – American Chemical Society*, Division Fuel Chemistry *48(2)*: 695-696.
- (8) Song, C. S. **2003**, *Catalysis Today*, **86(1-4)**: 211-263.
- (9) Flytzani-Stephanopoulos, M., T. L. Zhu and Y. Li **2000**, *Catalysis Today*, **62(2-3)**: 145-158.
- (10) Liu, W., C. Wadia and M. Flytzani Stephanopoulos **1996**, *Catalysis Today*, **28(4)**: 391-403.
- (11) Zeng, Y., S. Zhang, F. R. Groves and D. P. Harrison **1999**, *Chemical Engineering Science*, **54(15-16)**: 3007-3017.

# Vapor-Phase Oxidesulfurization (ODS) of Organosulfur Compounds: Carbonyl Sulfide, Methyl Mercaptans and Thiophene

Sukwon Choi and Israel.E. Wachs

Operando Molecular Spectroscopy & Catalysis Laboratory  
Department of Chemical Engineering  
Lehigh University, Bethlehem PA, 18015, USA

## Introduction

Sulfur in transportation fuels remains a leading source of SO<sub>x</sub> emissions from vehicle engines and is a major source of air pollution. Significant reduction in the emissions of sulfur compounds has been targeted as one of the highest priorities by the Environmental Protection Agency (EPA)<sup>1</sup>. The conventional technologies to remove S from organosulfur compounds are via catalytic hydrodesulfurization (HDS) or via direct combustion, which operate under severe conditions (elevated temperatures and/or high pressures). During HDS, H<sub>2</sub> is converted to H<sub>2</sub>S and subsequently reacted with O<sub>2</sub> in the Claus process to H<sub>2</sub>O and elemental sulfur, which is disposed in landfills. Direct combustion leads to the formation of unwanted global warming CO<sub>2</sub>, and an undesirable acid rain precursor SO<sub>2</sub>.

We have investigated an alternative vapor-phase oxidesulfurization (ODS) of the various organosulfur compounds. Under these initiatives, novel catalytic reaction processes of selectively oxidizing various organosulfur compounds typically found in petroleum streams (CH<sub>3</sub>SH, CH<sub>3</sub>SCH<sub>3</sub>, CH<sub>3</sub>SSCH<sub>3</sub>, COS, CS<sub>2</sub>, thiophene, 2,5-dimethylthiophene) into valuable chemical intermediates (H<sub>2</sub>CO, CO, H<sub>2</sub>, maleic anhydride and concentrated SO<sub>2</sub> that can be used for producing H<sub>2</sub>SO<sub>4</sub>) has been extensively studied. This research has primarily focused on establishing the fundamental kinetics and mechanisms of these selective oxidation reactions over well-defined supported metal oxide catalysts.

## Experimental

**Catalyst Preparation.** The catalysts used in this study were prepared by the incipient wetness impregnation method. This technique is described in detail elsewhere<sup>2,3</sup>. The support materials used in this study are TiO<sub>2</sub> (55 m<sup>2</sup>/g), ZrO<sub>2</sub> (39 m<sup>2</sup>/g), Nb<sub>2</sub>O<sub>5</sub> (55 m<sup>2</sup>/g), CeO<sub>2</sub> (36 m<sup>2</sup>/g), Al<sub>2</sub>O<sub>3</sub> (γ, 180 m<sup>2</sup>/g), and SiO<sub>2</sub> (300 m<sup>2</sup>/g).

**Characterization Methods.** *In Situ* Raman spectroscopy was performed with a system comprised of an Ar<sup>+</sup> laser (Spectra Physics, model 2020-50) set at 514.5 nm, and a Spex Triplemate spectrometer (model 1877) connected to a Princeton Applied Research (model 143) OMA III optical multichannel photodiode array detector. The reactivities of the catalysts were obtained from an isothermal fixed-bed reactor system operating at atmospheric pressure. The feed gas contained 1000 ppm of the reactant (COS, CS<sub>2</sub>, CH<sub>3</sub>SH, thiophene), 18% O<sub>2</sub> in He balance, and was introduced into the reactor at a flow rate of 150 ml/min. Sample runs were performed between 200-450 °C. Analysis of the reaction products was accomplished using a FTIR, (model #101250 Midac) or an on-line gas chromatograph (HP 5890A) equipped with a thermal conductivity detector (TCD) and a sulfur chemiluminescence detector (SCD 355, Sievers). Temperature Programmed Surface Reaction Mass Spectrometry (TPSR-MS) was carried out with an AMI-100 system equipped with an online mass spectrometer (Dycor DyMaxion). The adsorption was performed between 35-100 °C using 200 mg of catalyst and was ramped to 500 °C at a heating rate of 10 °C/min in 5% O<sub>2</sub>/He or He at 30 mL/min. *In situ* FT-IR (Fourier Transform Infrared) studies were conducted with

the IRIS<sup>4</sup> setup at TU-Delft, using a Magna-IR spectrometer 550 (Nicolet) under conditions replicating those used for the TPSR experiments.

## Results and Discussion

Steady-state reactivity data showed that COS and CS<sub>2</sub> are selectively oxidized to CO and SO<sub>2</sub> over the sulfur tolerant supported vanadia catalysts between 290-330 °C and 230-270 °C, respectively. CO selectivities as high as 98% and 90% were achieved for COS and CS<sub>2</sub> oxidation, respectively. The major byproduct from CS<sub>2</sub> oxidation is COS, which can be further selectively converted to CO via the ODS of COS. For the selective oxidation of CH<sub>3</sub>SH to H<sub>2</sub>CO and SO<sub>2</sub> over a series of redox supported metal oxide catalysts (supported vanadia, molybdate, tungstates and niobates) also did not exhibit deactivation and were sulfur tolerant. The most selective catalysts for the ODS of COS between 350-400 °C were vanadia supported on ZrO<sub>2</sub>, TiO<sub>2</sub> and SiO<sub>2</sub> (in the 84-89% range at high conversions). Furthermore, supported vanadia catalysts on various metal oxide supports (CeO<sub>2</sub>, ZrO<sub>2</sub>, Al<sub>2</sub>O<sub>3</sub>, SiO<sub>2</sub>, Nb<sub>2</sub>O<sub>5</sub>) were found to exhibit high catalytic activity/selectivity for the ODS of thiophene to maleic anhydride.

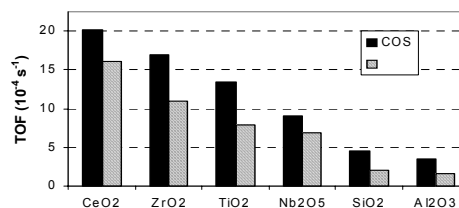


**Figure 1.** Variation of the TOF with the oxide support for COS and CS<sub>2</sub> oxidation at 330°C and 260°C, respectively, over supported vanadia catalysts with monolayer coverage.

Raman spectroscopy revealed that the supported metal oxide phases were 100% dispersed on the oxide substrate. Thus, the exclusive presence of surface metal oxide species allowed the determination of the number of active sites in the catalyst samples since dispersion was 100%. As shown in **Figure 1** for monolayer surface vanadia coverage, where the oxide support cations are essentially not exposed to the reactant gases and are covered by the vanadia overlayer, the turnover frequencies (TOF: Activity per surface metal atom based on the yield of CO) for COS and CS<sub>2</sub> oxidation varied about one order of magnitude with the specific oxide support (CeO<sub>2</sub> > ZrO<sub>2</sub> > TiO<sub>2</sub> > Nb<sub>2</sub>O<sub>5</sub> > Al<sub>2</sub>O<sub>3</sub> ~ SiO<sub>2</sub>). A similar phenomenon was observed for TOFs (based on the yield of H<sub>2</sub>CO) during CH<sub>3</sub>SH oxidation over supported vanadia catalysts at 350 °C. The TOFs varied within one order of magnitude (TiO<sub>2</sub> > ZrO<sub>2</sub> ~ Nb<sub>2</sub>O<sub>5</sub> > Al<sub>2</sub>O<sub>3</sub> ~ SiO<sub>2</sub>). These trends are inversely correlated with the electronegativity of the support cation in the bridging V-O-Support bond and suggests the bridging V-O-Support bond being the active site for these reactions since Raman revealed that the terminal V=O bonds were essentially the same in these supported vanadia catalysts<sup>5</sup>. Furthermore, all three reactions exhibited a zero-order dependence on the oxygen partial pressure (0.5-20%) and a first-order dependence on the COS/CS<sub>2</sub>/CH<sub>3</sub>SH partial pressures (<1%, due to safety concerns), which suggest that the surface vanadia species is essentially fully oxidized under the investigated reaction conditions.

The desorption spectra of CO and SO<sub>2</sub> are shown in **Figure 2** from the 5% V<sub>2</sub>O<sub>5</sub>/TiO<sub>2</sub> catalyst following COS adsorption at 100 °C. The simultaneous desorption of CO and SO<sub>2</sub> suggests that the

oxidation of COS proceeds via the rate-determining step involving cleavage of the C-S bond.

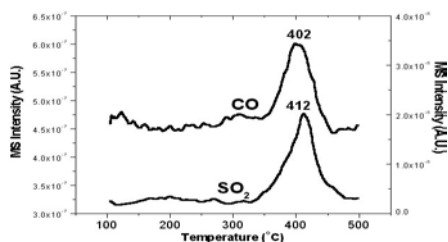
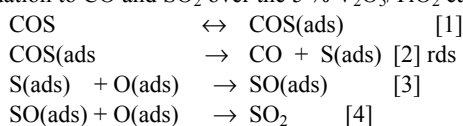
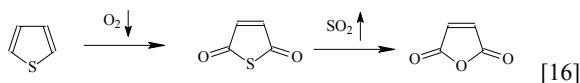
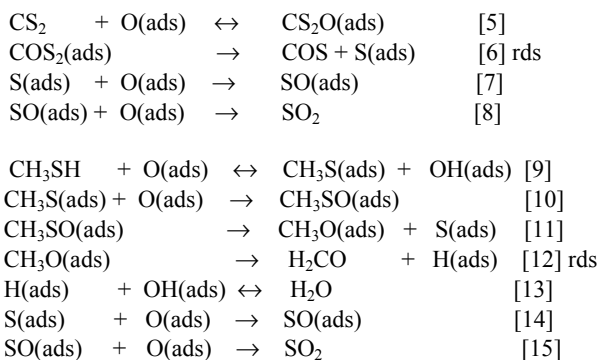


**Figure 2.** TPSR-MS profiles after COS adsorbed at 100 °C on the 5% V<sub>2</sub>O<sub>5</sub>/TiO<sub>2</sub> catalyst, under 5% O<sub>2</sub>/He flow.

The slight delay in the production of SO<sub>2</sub> is consistent with this conclusion since the remaining S(ads) requires the addition of two oxygen atoms. The above suggests the following mechanism for COS oxidation to CO and SO<sub>2</sub> over the 5% V<sub>2</sub>O<sub>5</sub>/TiO<sub>2</sub> catalyst.



Similarly, the TPSR profiles revealed the reaction mechanisms for the oxidesulfurization of CS<sub>2</sub>, CH<sub>3</sub>SH and thiophene over the 5% V<sub>2</sub>O<sub>5</sub>/TiO<sub>2</sub> catalyst, as the following given in reaction steps [1]-[16].



FT-IR studies were conducted to confirm these reaction mechanisms. And the ODS of thiophene is given as an example. *In situ* FT-IR spectroscopy and steady-state reactivity studies have revealed that for the selective oxidation reactions of thiophene to maleic anhydride over various supported vanadia catalysts proceed via thiomaleic anhydride. *In situ* FT-IR results shown in **Figure 3** indicate that thiomaleic anhydride begins to form even at low temperatures near 100 °C over supported vanadia on titania catalysts. The darkened region indicates the typical IR band regions associated with surface adsorbed anhydride species (C=O vibrations, 1770~1860 cm<sup>-1</sup>) that appear at relatively low temperatures, while the shifting of these peaks in this region to higher wave numbers with increases in temperature show the transitioning of thiomaleic anhydride to maleic anhydride. These results are consistent with the Temperature Programmed Surface Reaction Mass Spectroscopy (TPSR-MS) results shown in **Figure 4**. In addition, TPSR experiments revealed that the ODS of thiophene over supported vanadia on titania catalyst followed a Langmuir-Hinshelwood reaction path where gas-phase O<sub>2</sub> is involved in the formation of the

reaction products. This was in contrast to the ODS reactions of the more simple organosulfur compounds (COS, CS<sub>2</sub>, CH<sub>3</sub>SH), which exhibited Mars van Krevelen type behavior. Currently we are investigating the ODS of the sterically hindered 2,5-dimethyl thiophene (2,5-DMT) to maleic anhydride. Preliminary results indicate that during the ODS of 2,5-DMT, the two sterically hindering methyl groups are removed in the initial steps of the reaction to form thiophene and subsequently the ODS reaction proceeds via the thiophene ODS reaction pathway.

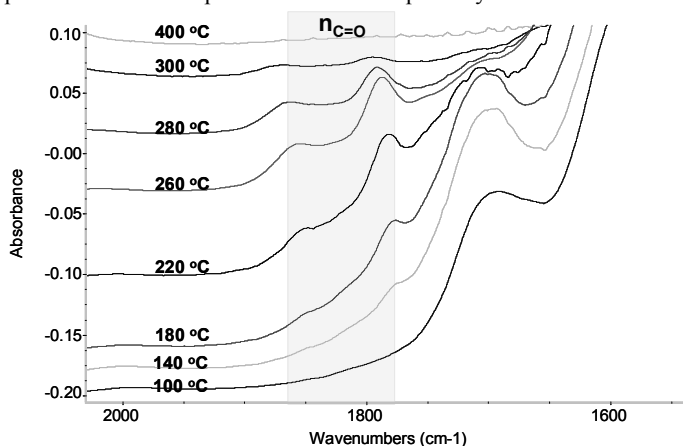


**Figure 3.** *In situ* FT-IR spectra of thiophene ODS at various temperatures over the 5% V<sub>2</sub>O<sub>5</sub>/TiO<sub>2</sub> catalyst.

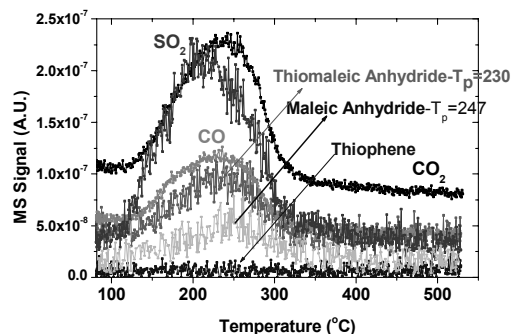


**Figure 4.** TPSR-MS profiles after thiophene adsorbed at 75 °C on the 5% V<sub>2</sub>O<sub>5</sub>/TiO<sub>2</sub> catalyst, under 5% O<sub>2</sub>/He flow.

#### Acknowledgement

The authors gratefully acknowledge the National Science Foundation, Grant NSF-CTS-9901643, for financial support of this research, and professors Guido Mul and Jacob A. Moulijn of Delft University of Technology, for their assistance and support.

#### References

1. EPA-Gasoline, RIA (EPA420-R-99-023), December 1999.
2. EPA-Diesel, RIA (EPA 420-R000-026), December 2000.
3. Deo, G., Wachs, I. E. *J. Catal.* 146 (1994) 323-334.
4. Wachs, I. E., Deo, G., Juskelis, M. V., Weckhuysen, B. M. in: Froment, G. F., Waugh (Eds.), K. C., *Dynamics of Surfaces and Reaction Kinetics in Heterogeneous Catalysis*, Elsevier, Amsterdam, 1997, pp. 305-314.
5. Elst, L.P.A.F., Eijbouts, S., van Langeveld, A. D. Moulijn, J.A., *J. Catal.* 196 (2000) 95-103.
6. Harcastle, F. D. and Wachs, I. E., *J. Phys. Chem.* 95 (1991) 5031-5041.

# PROCESS FOR THE REMOVAL OF THIOLS FROM A HYDROCARBON STREAM BY A HETEROGENEOUS REACTION WITH A METAL OXIDE

James P. Nehlsen, Jay B. Benziger, and Ioannis G. Kevrekidis

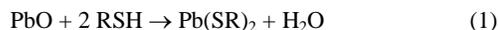
Department of Chemical Engineering  
Princeton University, Princeton, NJ 08544

## Introduction

The removal of sulfur from gasoline fractions is necessary to prevent the poisoning of Pt reforming catalysts as well as reducing the emission of SO<sub>2</sub> with the combustion products from engines. The process we describe here is a simple, low temperature method for the removal of thiols from a hydrocarbon stream. Thiols are common in hydrotreated gasoline, resulting from the reaction of olefins with H<sub>2</sub>S present in the HDS reactor.

In this process, thiols are converted directly to insoluble metal thiolates by a heterogeneous reaction with certain metal oxides or hydroxides. The thiolates are then mechanically filtered from the hydrocarbon stream. The metal and the original thiol can then be recovered in a liquid-liquid extraction step. This process could complement conventional HDS by reducing the sulfur load on an HDS reactor while recovering the thiols for other uses, or to trim refined products that do not meet low-sulfur specifications.

The process is based on thiolate chemistry in which thiols react with metal ions to form metal thiolates. Most work in this area focuses on the reaction of thiols with aqueous solutions of heavy metal salts or with surface reactions on metals and metal oxides. The reaction system applied here is distinct from these works because the reaction removes ions from the surface of the oxide, allowing a dense oxide particle to be completely consumed. An example reaction with PbO is



The recovery of the metal is achieved by extraction with a dilute acid. The choice of acid depends on the metal salt desired. An example reaction is



This simple process<sup>1</sup> uses inexpensive materials and very little energy compared to conventional desulfurization techniques. The process proposed here, shown as Figure 1, is selective for thiols. No reaction is observed between PbO and disulfide, sulfide, or thiophenic species.

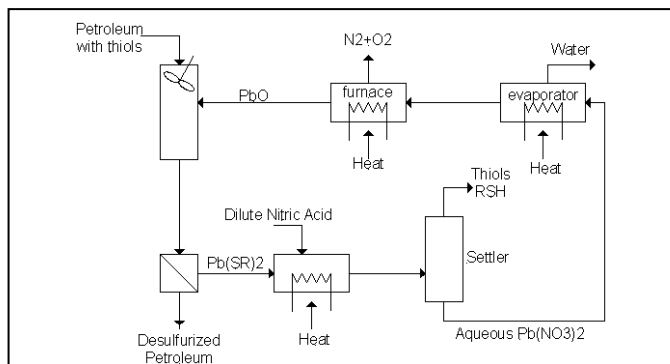


**Figure 1.** Diagram of the thiol removal process using lead oxides, showing the key operations including reaction, filtration, and extraction.

## Experimental

The heterogeneous reaction and the reactive extraction portions of this process were studied. The reaction was carried out in batch

mode with various powdered metal oxides including BaO, Bi<sub>2</sub>O<sub>3</sub>, CaO, CdO, CoO, Cr<sub>2</sub>O<sub>3</sub>, CuO, HgO, MgO, MoO<sub>3</sub>, metallic Pb wire, PbO, Pb<sub>3</sub>O<sub>4</sub>, PbO<sub>2</sub>, Pb(OH)<sub>2</sub>, Pb(NO<sub>3</sub>)<sub>2</sub>, PbS, SbO, SnO, and Sr(OH)<sub>2</sub>.

The primary oxide studied was PbO. Powdered PbO (massicot form, Aldrich) of mass between 0.02 and 0.2 g was added to a glass vial. An *n*-alkanethiol, either 1-hexanethiol, 1-octanethiol, or 1-dodecanethiol (Aldrich), was added to the vial. An inert hydrocarbon, usually cyclohexane or toluene, was sometimes added to prevent the reaction product from becoming a paste. The solid product could be suspended in the hydrocarbon by stirring to facilitate filtration. Some samples were stirred using a magnetic stir bar, and some were heated to about 70°C on a hotplate and cooled before filtering.

The reaction product, a wet powder, was gravity filtered (Whatman #50 hardened circles), then rinsed several times with water, acetone, cyclohexane, and then pentane, and dried at room temperature.

Other metal oxides and hydroxides were tested by adding 1-octanethiol to a small amount (approx. 0.15-0.5 g) of the oxide or hydroxide in a glass vial. The formation of thiolates was evidenced by a dramatic increase in apparent solid volume and in some cases, a color change. Reacted mixtures were filtered and dried as above, then weighed to determine conversion. Active oxides were also mixed in the same manner with butyl disulfide (97%, Aldrich), butyl sulfide (96%, Aldrich), tetrahydrothiophene (99%, Aldrich), and thiophene (99+%, Aldrich) to test for reactivity with other sulfur compounds.

The Pb was extracted from the thiolates by liquid-liquid extraction with dilute (0.2-0.3 M) nitric acid. The solid thiolates were added to cyclohexane and the mixture was heated to the melting point of the thiolate, approximately 70°C. This mixture was added to the nitric acid and agitated by rapid stirring. The hydrocarbon layer was then analyzed for thiol content by gas chromatography (Hewlett Packard HP-1 column, FID). The aqueous layer was evaporated and the Pb was recovered as Pb(NO<sub>3</sub>)<sub>2</sub> crystals.

## Results and Discussion

**Reactions.** All of the tested oxides and hydroxides of Pb, metallic Pb wire with a surface oxide coating, HgO, Ba(OH)<sub>2</sub>, and BaO formed stable, insoluble thiolates of the alkanethiols. These oxides did not react with any of the other organo-sulfur compounds tested.

PbO, Pb<sub>3</sub>O<sub>4</sub>, Pb(OH)<sub>2</sub>, and PbO<sub>2</sub> reacted quickly yielding an insoluble, yellow thiolate. No other reaction products were detected. Reactions were typically complete in about 1 hour without agitation or heat. The thiolate does not appear to foul the surface of the oxide, allowing the reaction to go to completion without agitation. Yields of Pb(SC<sub>8</sub>H<sub>17</sub>)<sub>2</sub> were typically 80-90%, including transfer losses. Heating the product above the melting temperature of the thiolate revealed no remaining solid oxide, indicating that some amounts of sub-thiolate, such as Pb(SC<sub>8</sub>H<sub>17</sub>)(OH), may have been formed, reducing the yield. Pb<sup>4+</sup> compounds only reacted with two thiols per Pb, probably resulting in the formation of PbO(SC<sub>8</sub>H<sub>17</sub>)<sub>2</sub> or Pb(OH)<sub>2</sub>(SC<sub>8</sub>H<sub>17</sub>)<sub>2</sub>.

The lead thiolates were solid at room temperature, but became soluble in hydrocarbon solvents at temperatures above about 50°C. In the presence of cyclohexane, a miscible solution of lead dioctylthiolate, Pb(SC<sub>8</sub>H<sub>17</sub>)<sub>2</sub>, was formed at 54-55°C. The melting temperature of dry dialkylthiolates increased with molecular weight and was 70-80°C for the dioctylthiolate. The observed melting point was lower than reported elsewhere,<sup>2</sup> probably due to impurities or incomplete removal of the hydrocarbon solvent. The thiolates were insoluble in cyclohexane, toluene, acetone, and water at room temperature. The thiolate melts were miscible with cyclohexane and toluene, but immiscible with water.

Figure 2 presents a series of photographs demonstrating the reaction of *n*-octanethiol with PbO<sub>2</sub>. PbO<sub>2</sub> was used in the photographs for color contrast purposes, since the massicot form of PbO and the thiolate product are both yellow. The reaction is marked by a rapid growth in apparent solids volume as the liquid thiol is converted into solid thiolate. The color change from the black PbO<sub>2</sub> to the yellow thiolate is also evident.

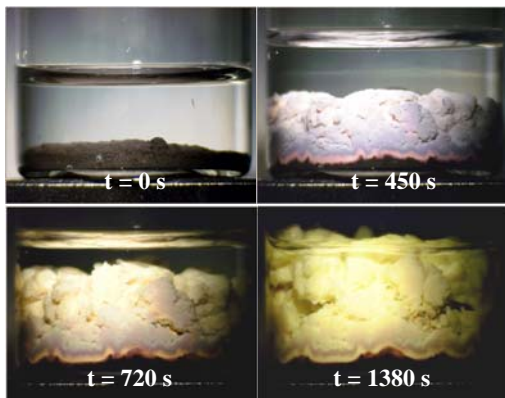


**Figure 2.** Photographs of the reaction of PbO<sub>2</sub> with *n*-octanethiol. Photographs are chronological, starting from top left, occurring at elapsed times shown. The initial mixture was 0.75 g PbO<sub>2</sub>, 4 mL cyclohexane, and 3 mL *n*-octanethiol (added after first picture).

Metallic Pb wire was also active in forming thiolates. The thiol reacted with the natural coating of oxides present on a Pb surface to form an insoluble yellow thiolate. The extent of reaction on a Pb wire was very low when carried out in an inert nitrogen atmosphere. The reaction occurred at the surface of the wire, forming plates of thiolate that were pushed outwards as new thiolate was formed.

An example of this reaction is shown in Figure 3 in which a piece of Pb wire is placed into *n*-octanethiol. The reaction is much slower than the reaction with powdered PbO due to the time required diffusing oxygen to the Pb surface and the lower surface area of the wire compared to the powdered oxides.

Hg(II)O reacted exothermically to generate a white, insoluble thiolate. The yield of Hg(SC<sub>8</sub>H<sub>17</sub>)<sub>2</sub> was 99%. BaO and Ba(OH)<sub>2</sub> also reacted with alkanethiols to generate an insoluble, white thiolate. The reaction was fast and occurred without agitation, but the yield of 54% was lower than for PbO or HgO. The lower yield is again most likely due to the formation of sub-thiolate, Ba(SC<sub>8</sub>H<sub>17</sub>)(OH). This reaction is interesting, however, because of the lower environmental and health risks associated with Ba as opposed to Hg and Pb. No other oxides reacted quickly to yield insoluble thiolates.



**Figure 3.** Photographs of the reaction of Pb wire with *n*-octanethiol. Left: Pb wire in cyclohexane before reaction. Right: After reaction with *n*-octanethiol for 14 days. Initial mixture was 2 mL cyclohexane and 4 mL *n*-octanethiol (added after picture on left).

The thermodynamic limit for the removal of thiols by this reaction can be determined from the heat of reaction. The equilibrium constant *K* is given by

$$-\Delta G_{\text{rxn}} = RT \ln(K) \quad (2)$$

where, from equation 1,

$$K = (a_{\text{Pb(SR)}_2} a_{\text{H}_2\text{O}}) / (a_{\text{RSH}}^2 a_{\text{PbO}}) \quad (3)$$

The solids PbO and Pb(SR)<sub>2</sub> both have unit activity. Assuming an ideal solution, the activity of the water and thiol are equal to their mole fraction in the hydrocarbon solvent. The value of  $\Delta G_{\text{rxn}}$  estimated previously<sup>3</sup> is -121 kJ/mol. The equilibrium constant for this reaction, assuming unit water activity (present as a second liquid phase), is approximately  $1.9 \times 10^{21}$ , permitting the removal of thiol sulfur to 23 ppt. The thermodynamic limit of this reaction permits desulfurization to extremely low levels, although kinetic and mass transfer limitations may prevent this limit from being practically achieved.

**Metal Recovery.** Reactive liquid-liquid extraction with a dilute acid can be performed by heating the thiolates to melting, either with or without the addition of a hydrocarbon solvent. Agitating the thiolates with an acid solution (0.1-0.3 M typically) allows the reaction to reach completion in about 2 hours. Improved contacting between the liquid phases and using more concentrated acids can reduce the time required. The result is an aqueous phase containing the metal salt and a hydrocarbon phase containing the original thiols and any added solvent. A reusable oxide can be obtained by roasting most metal salts in air.

Using this technique, thiolates made from reaction with PbO were extracted with 0.21M HNO<sub>3</sub>. The yellow diluted melt of Pb(SC<sub>8</sub>H<sub>17</sub>)<sub>2</sub> changed to colorless as the reaction proceeded. The recovery of Pb as Pb(NO<sub>3</sub>)<sub>2</sub> was 102%, or essentially all of the lead within experimental error. A second trial with thiolates made from PbO<sub>2</sub> and 0.31M HNO<sub>3</sub> yielded a 95% Pb recovery. Thiol recoveries in the hydrocarbon phase, as measured by GC, for these two runs were 78% and 90%, respectively.

## Conclusions

The heterogeneous reaction of thiols with oxides and hydroxides of Pb, Hg(II), and Ba can be used to remove and recover thiols from a petroleum stream. Experimental results suggest that a simple process consisting of reaction, filtration, and extraction is all that is required to separate and recover the thiols. The metal oxide can be recovered by additional evaporation and roasting steps. Most of the required unit operations have low energy requirements and low reagent material costs.

This process can reduce the sulfur content of fuels for environmental benefits. It could also reduce the load on a conventional HDS unit when sour feedstocks are used by removing the thiols before the feed is introduced to the HDS unit, saving costs in hydrogen and catalyst life. The process also recovers thiols which are a valuable feedstock to the food and fragrance industries<sup>4</sup> as well as the pharmaceutical industry.

**Acknowledgement.** The authors thank Dr. Steffen Berg for his assistance in this work. This work was partially supported by the AFOSR (Dynamics & Control, Dr. B. King).

## References

- (1) Nehlsen, J. P.; Benziger, J. B. and Kevrekidis, I. G. *Energy Fuels* **2004**, ASAP Article.
- (2) Tiers, G. V. D. and Brostrom, M. L. *J. Appl. Crystallogr.* **2000**, 33 (3, Pt. 2), 915-920.
- (3) Nehlsen, J. P.; Benziger, J. B. and Kevrekidis, I. G. *Ind. Eng. Chem. Res.* **2003**, 42 (26), 6919-6923.
- (4) Naim, M.; Zuker, I.; Zehavi, U. and Rouseff, R. L. *J. Agric. Food Chem.* **1993**, 41 (9), 1359-1361.

# PROMOTING EFFECT OF WATER ON COAL HYDROGENATION

Yoshiharu Yoneyama, Aya Kanao, Tatsuya Yamamoto,  
Yi Zhang, Noritatsu Tsubaki

Faculty of Engineering, Toyama University,  
Toyama, Japan 930-8555

## Introduction

Low-cost hydrogen sources are required for converting coals to liquid or gaseous fuels, and chemicals. Water is a promising candidate among hydrogen sources. Many researchers used water as hydrogen source through water-gas shift reaction or as an effective pretreatment method for hydrogenation and pyrolysis of coals.<sup>1</sup> Water at supercritical state or steam has been used as extraction or pretreatment vehicles of coals as well.<sup>2-5</sup> On the other hand in the catalytic hydrogenation of coals, it is well known that water or steam deactivates hydrotreating catalyst.<sup>6,7</sup> Even if it seems that water exhibited negative effect on coal hydrogenation with or without catalysts, addition of water increased the CO<sub>2</sub> formation and the contents of phenolic compounds in the obtained oils.<sup>3-5</sup> These results strongly suggest that water interacts with coals under hydrogenation conditions.

In this study to clarify the role of water in the coal hydrogenation, Wandoan and Argonne premium coal were non-catalytically hydrogenated at 673 K with water addition. For comparison, experiments under nitrogen, and with addition n-undecane (n-C<sub>11</sub>) were also carried out. Aliphatic C-O linkages are important linkages between aromatic moieties of coal structures. In addition, dibenzyl ether was used as a coal-model compound containing ether linkage, and was pyrolyzed with and without water addition in the presence of pyrite in order to determine the cleavage of ether linkages of coal structures under the conditions we used.

## Experimental

Basic data of coals are listed in Table 1. The coals were dried at 333 K under vacuum for over 48 h to constant weight before use. Undecane (n-C<sub>11</sub>) was used without further purification. Super high purity of hydrogen (over 99.999 %) and nitrogen (over 99.999 %) were used to minimize oxidization during the reaction.

Hydrogenation was carried out using coal of 1.5 g with or without adding water of 0.8 g, or adding n-C<sub>11</sub> of 0.8 g in a 25 ml horizontal microautoclave reactor at 673 K for 60 min under an initial hydrogen pressure of 6.9 MPa. For comparison, similar experiment under nitrogen was also conducted. The gaseous product was collected for analysis by gas chromatograph with thermal conductivity detector. The recovered products were placed into a thimble filter and separated to tetrahydrofuran (THF) soluble product by Soxhlet

Table 1. Elemental Analysis of Coals (% ,daf)

Coal	C	H	N	O + S <sup>a</sup>	Pyrite <sup>b</sup>
Beulah-Zap	72.9	4.8	1.1	21.2	0.2
Wandoan	73.4	6.2	1.1	19.4	-
Wyodak	75.0	5.4	1.1	18.5	0.1
Illinois #6	77.7	5.0	1.4	16.0	5.0
Blind Canyon	80.7	5.8	1.6	12.0	0.4
Lewiston-Stockton	82.6	5.3	2.6	9.6	0.3
Pittsburgh #8	83.2	5.3	1.6	9.8	2.5
Upper Freeport	85.5	4.7	1.6	8.3	3.5

<sup>a</sup> By difference <sup>b</sup>wt%, dry base

extraction with THF, followed by rotary-evaporation and dried in a vacuum oven at 333 K. The conversion was defined as the sum of the yields of gases and THF soluble products.

Hydrogenation of dibenzyl ether (DE) was carried out using DE of 0.159g and synthetic pyrite of 0.005g with and without adding water of 0.9g in a 25 ml horizontal microautoclave reactor at 350 °C for 30 min. The products were recovered by washing with acetone. When a residue was present in the reactor, the reactor was washed by ethyl acetate one more to recover the residue completely. After washing the reactor with ethyl acetate, there existed no residual materials in the reactor. After sampling the acetone solution for gc analysis, both the acetone and the ethyl acetate solutions were combined. The combined solution was filtered with a membrane filter, and then the solution was evaporated to weigh the residue.

## Results and Discussion

**Coal Hydrogenation** Figure 1 shows the relationship between the carbon content of original coals and the coal conversions using hydrogen or nitrogen, where water or n-C<sub>11</sub> was added. In the combination of nitrogen and water, with the increasing the carbon content of original coals, the conversions of coals were enhanced, except for Upprt Freeport coal. Addition of n-C<sub>11</sub> did not increase the coal conversion, however addition of water enhanced. On the other

hand, in the combination of hydrogen and water there existed no clear relationship between the carbon content of original coals and the coal conversions. Addition of water had promoting effect on coal conversions under hydrogen also. It was found that the conversions of both Illinois #6 and Pittsburgh #8 coals were irregularly large. The conversion of Illinois #6 coal increased about 20 % with added water, even though added water in nitrogen did not promote the coal conversion significantly. There existed synergistic effect between hydrogen and water on conversion of Illinois #6 and Pittsburgh #8 coals. Since Illinois #6 and Pittsburgh #8 coals contain more pyrite

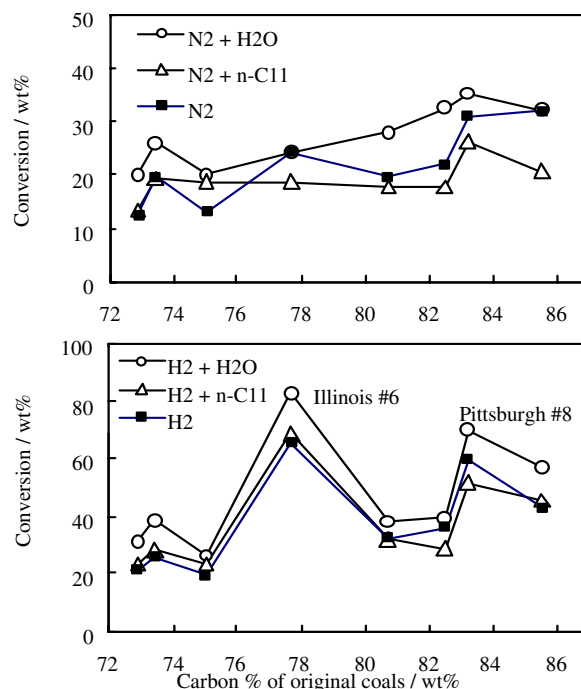


Figure 1. Relationship between carbon % of original coals and the conversion under nitrogen or hydrogen with added water or undecane (n-C<sub>11</sub>). Temperature, 673 K; time, 60 min.

than other coals as compared in Table 1, it is considered that pyrite plays an important role in the promoting effect of water on coal conversions using hydrogen. It is well known that pyrite in coals acts as catalyst in coal hydrogenation.<sup>7</sup>

Figure 2 exhibits the relationship between the pyrite contents of original coals and the conversions of coals in hydrogen. The conversions of coals containing larger amounts of pyrite were larger except for Upper Freeport coal, while the conversion of coals containing less amount of pyrite were lower. Because Illinois #6 and Pittsburgh #8 coals contain large amount of pyrite, synergistic effect between hydrogen and water is considered to be large. It is referred that pyrite plays an important role in the synergistic effect between water and hydrogen on coal conversion.

**Hydrogenation of DE** In order to determine the effectiveness of water on the cleavage of ether linkage in coal, DE was hydrogenated with and without water addition in the presence of pyrite. Table 2 summarizes the conversions and the yields of the products of hydrogenation of DE. Since some products did not elute from the column, both conversions calculated by the sum of the products, and by the unreacted DE are shown. Without pyrite addition, both conversions were close. Water addition was found to inhibit the cleavage of the aliphatic ether linkage. The conversion decreased from 52.8 to 13.8 % with water addition. The yields of benzaldehyde and benzyl alcohol were larger for water addition. On the other hand, without pyrite addition both conversions were close, but with pyrite they were different each other. The residual products, which did not elute from the gc column, formed without water addition in the presence of pyrite. Thus the conversion from the products was lower than that from unreacted DE. The reactions formed the residual products is thought as the retrogressive reactions in the coal hydrogenation. These results suggest that water addition prevents retrogressive reaction occurred in coal hydrogenation using pyrite as a catalyst.

In the hydrogenation with water addition, hydrolysis, pyrolysis and hydrogenation occur. In order to estimate the contribution of hydrolysis and pyrolysis in this hydrogenation, DE was pyrolyzed in N<sub>2</sub>. The conversion and product yields are summarized in Table 3. Under N<sub>2</sub> the residual products were formed in all reactions, however water addition decreased the yield of the residual product. Without pyrite addition, water addition increased the conversion of DE, and promoted hydrolysis reaction. Though pyrite is a hydrogenation catalyst, the conversion of DE increased with pyrite in both reactions with and without water addition. Water addition increased both conversions calculated by the products and by the unreacted DE. Because the yield of benzyl alcohol was increased with water addition, the combination of pyrite and water addition promoted the hydrolysis of DE significantly. It was found that water itself has an inhibitive effect on the formation of the residual product.

These results indicate that the synergistic effect between pyrite and water on coal hydrogenation should be derived from the suppression of the retrogressive reaction occurring in the coal hydrogenations and promoting the cleavage of C-O linkages in coal structures.

## References

- (1) Ross D. S., *Coal Science*, **3**, 301.
- (2) Graff R. A. and Brandes S. D., *Energy Fuels*, 1987, **1**, 84
- (3) Deshpande, G. V.; Holder, G. D.; Bishop, A. A.; Gopal, J.; Wender, I. *Fuel* **1984**, *63*, 956.
- (4) Kershaw, J. R. *Fuel Process. Technol.* **1986**, *13*, 111.
- (5) Artok, L.; Schobert, H. H.; Nomura, M.; Erbatur, O.; Kidena, K. *Energy Fuels* **1998**, *12*, 1200.

- (6) Kamiya, Y.; Nobusawa, T.; Futamura S. *Fuel Process. Technol.* **1988**, *18*, 1.
- (7) Ruether, J. A.; Mima, J. A.; Kornosky, R. M.; Ha, B. C. *Energy Fuels* **1987**, *1*, 198.
- (8) Trewhella, M. Jr.; Grint, A. *Fuel* **1987**, *66*, 1315

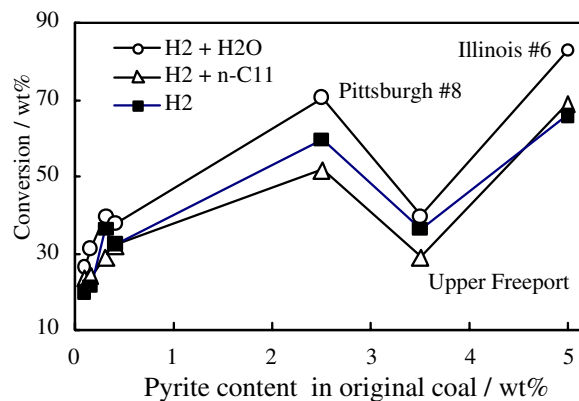


**Figure 2.** Relationship between pyrite content in original coal and the conversion.

**Table 2** Effect of Water Addition on DE hydrogenation

Catalyst	none	none	FeS <sub>2</sub>	FeS <sub>2</sub>
water addition	no	yes	no	yes
Conversion <sup>1</sup>	51.9	13.8	96.2	68.2
Conversion <sup>2</sup>	52.8	13.8	46.0	68.9
Product (mol%)				
benzene	4.9	0	8.0	5.4
toluene	80.0	12.2	61.3	65.7
benzaldehyde	7.2	8.9	10.4	21.3
benzyl alcohol	4.9	6.5	5.8	34.1
bibenzyl	4.2	0	3.3	5.7
residue <sup>3</sup>	0	0	29.5	0

<sup>1</sup> calculated by the unreacted DE; <sup>2</sup> calculated by the products  
<sup>3</sup> polymeric products, wt%; 673K, 6.9MPa H<sub>2</sub>, 30 min

**Table 3** Effect of Water Addition on DE Pyrolysis

Catalyst	none	none	FeS <sub>2</sub>	FeS <sub>2</sub>
water addition	no	yes	no	yes
Conversion <sup>1</sup>	42.3	48.2	75.7	81.5
Conversion <sup>2</sup>	6.3	5	25.9	41.1
Product (mol%)				
benzene	0	0	0	0
toluene	3.8	1.7	15.1	9.3
benzaldehyde	6.7	4.2	25.9	10.7
benzyl alcohol	2.1	4.1	7.7	59.5
bibenzyl	0.0	0	1.5	1.3
residue <sup>3</sup>	64.9	60.5	62.9	48.4

<sup>1</sup> calculated by the unreacted DE; <sup>2</sup> calculated by the products;  
<sup>3</sup> polymeric products, wt%; 673K, 6.9MPa N<sub>2</sub>, 30 min

# HYDROTREATING OF DIESEL FUEL OVER EX SITU PRESULFIDED NiW AND NiMoW CATALYSTS

Guoliang Li, Changlong Yin, Huiji Zhao, Chenguang Liu and Yangchu Li

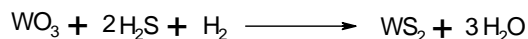
Key Laboratory of Catalysis, CNPC,  
State Key Laboratory of Heavy Oil Processing  
University of Petroleum, Dongying, Shandong 257061, China

## Introduction

The sulfided catalysts for the hydrotreating of petroleum feedstocks have the ability to catalyse hydrogenation and hydrogenolysis reactions in the presence of strong inhibitors such as H<sub>2</sub>S and NH<sub>3</sub>. The conventional method for presulfurizing hydrogenation catalysts is an in-situ (inside reactor) method of presulfurization, using hydrogen sulfide or a straight fraction oil containing carbon disulfide and dimethyl disulfide to convert the hydrogenation-active metal into sulfurization state. The in-situ method of presulfurization has the disadvantages of higher production costs, prolonged time for presulfurization and flammable and poisonous sulfides being used, thus causing environmental pollution. A process which allows the transformation of an oxide into a stable sulfided intermediate has been developed (1-3) and several related technologies has been patented. These processes consist in wetting ex situ the catalysts with elemental sulfur and/or a hydrocarbon solution of a high molecular weight alkylpolysulfide. The ex situ presulfided catalysts only need to introduce hydrogen or hydrogen and oils simultaneously to start up the presulfurization, and subsequently raise the temperature, thus complete the sulfurization activation process. Therefore, ex-situ (outside reactor) method of presulfurization has advantages of simple operation, high efficiency and non-pollution. In this work, two commercial hydrogenation catalysts NiW/Al<sub>2</sub>O<sub>3</sub> and NiMoW/Al<sub>2</sub>O<sub>3</sub> were presulfided with ex-situ and in-situ method of presulfurization, respectively, and the activities of the catalysts were investigated by the hydrotreating of diesel fuel.

## Experimental

**Catalyst preparation.** The catalysts used in this work are two industrial hydrogenation catalysts: NiW/Al<sub>2</sub>O<sub>3</sub> and NiMoW/Al<sub>2</sub>O<sub>3</sub>, the characteristics of which are listed in Table 1. The component of vulcanization agent is: elemental sulfur (60wt%), dimethylsulfoxide (20wt%), tetraethylthiuram disulfide (TETD, 20wt%). The solvent of the vulcanization agent is a mixture of solvent oil and bean oil with weight ratio of 2. The amount of sulfide deposited onto the catalysts was calculated on the basis of the transformation of the oxidic metals phases into sulfided metals, which can be showed as follows:



**Catalyst activity.** Catalytic activity measurements were carried out in a continuous high pressure reactor unit of 24 mm I.D., 100cm in length. 100 ml of the catalyst extrudates were loaded in the reactor. In situ presulfiding is carried out before the reaction at 100°C, and 150 °C for 5 hour, 250 °C for 5 hours, 340 °C for 5 hours with a liquid stream containing 1w% CS<sub>2</sub> in straight-run kerosene. The H<sub>2</sub>/feed ratio is 350:1 for NiW/Al<sub>2</sub>O<sub>3</sub> and 500:1 for

NiMoW/Al<sub>2</sub>O<sub>3</sub> and the LHSV for both catalysts is 2.0h<sup>-1</sup>. The total pressure for NiW/Al<sub>2</sub>O<sub>3</sub> is 6.4MPa and 4.0MPa for NiMoW/Al<sub>2</sub>O<sub>3</sub> catalyst. The FCC diesel feed is then admitted at the same conditions as that for presulfiding. The reaction product was cooled and separated into gaseous and liquid products in a high-pressure separator. For ex situ presulfided catalyst presulfiding is performed by heating the catalyst under hydrogen from room temperature up to 220 °C (heating rate 40 °C/h), at 220 °C for 1 hour, and at 340 °C for 2 hours (heating rate 38 °C/h). The diesel fuel is then fed at test conditions.

Table 1. Characteristics of the Catalysts

Catalysts	NiW/Al <sub>2</sub> O <sub>3</sub>	NiMoW/Al <sub>2</sub> O <sub>3</sub>
Pore volume, cm <sup>3</sup> /ml	0.25	0.34
BET area, m <sup>2</sup> /g	152.0	154.1
Component, wt%		
WO <sub>3</sub>	26.0	19.2
MoO <sub>3</sub>		9.5
NiO	2.6	2.5

## Results and Discussion

Temperature rising during the presulfurization process is a troublesome problem. The heater temperature and sulfurization temperature in catalyst's bed during the process were determined and the curves for the ex situ presulfided NiW/Al<sub>2</sub>O<sub>3</sub> and NiMoW/Al<sub>2</sub>O<sub>3</sub> catalysts were illustrated in Figure 1 and Figure 2, respectively. The temperature curves for the in situ presulfided NiMoW/Al<sub>2</sub>O<sub>3</sub> catalyst were shown in Figure 3. The experimental results show that no obvious temperature rising appears during the treatment of the ex situ presulfided NiW/Al<sub>2</sub>O<sub>3</sub> and NiMoW/Al<sub>2</sub>O<sub>3</sub> catalysts, while the temperature in catalyst's bed is fluctuant acutely during the in situ presulfurization process. Moreover, the time for the treatment of the ex situ presulfided catalyst is shortened to about 11 hours, much less than that for the in situ presulfurization, the latter is about 24 hours.

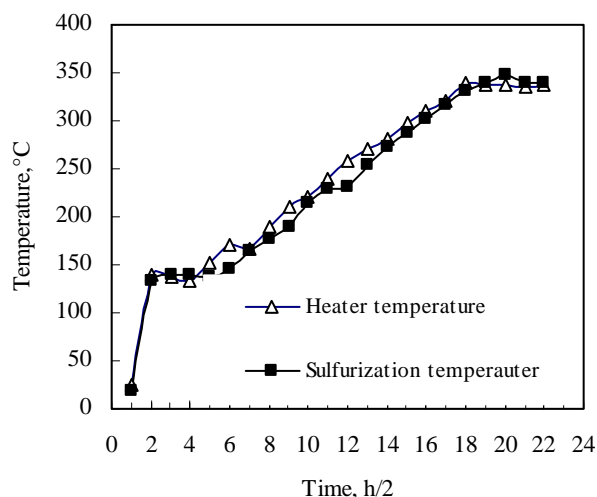
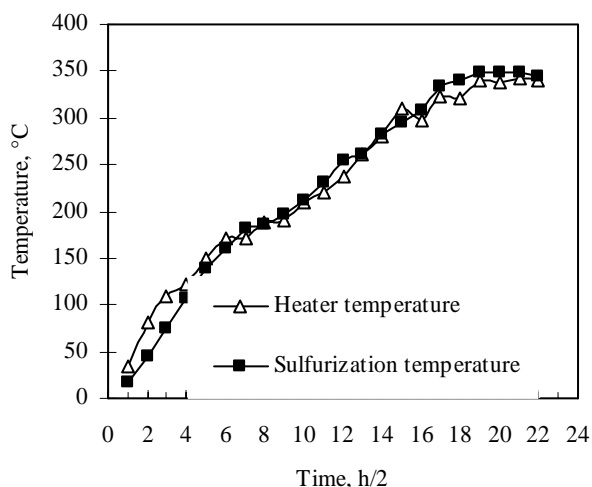
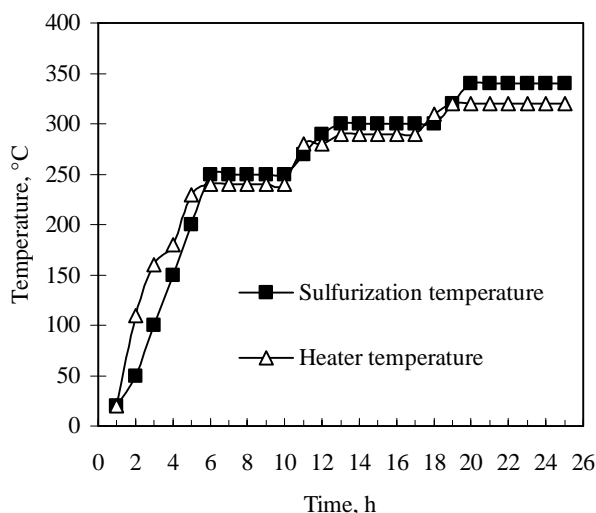


Figure 1. The temperature curve for the ex situ presulfided NiW/Al<sub>2</sub>O<sub>3</sub> catalyst.



**Figure 2.** The temperature curve for the ex situ presulfided NiMoW/Al<sub>2</sub>O<sub>3</sub> catalyst.



**Figure 3.** The temperature curve for the in situ presulfided NiMoW/Al<sub>2</sub>O<sub>3</sub> catalyst.

The activities of the catalysts with different sulfurization method (i.e. in situ and ex situ) were studied according to the characteristics of the hydrotreated products obtained from the hydrotreating of FCC diesel over in situ presulfided and ex situ presulfided catalysts at the same reaction conditions. The characteristics of the hydrotreated products over NiW/Al<sub>2</sub>O<sub>3</sub> catalyst and NiMoW/Al<sub>2</sub>O<sub>3</sub> catalyst were listed in Table 2 and Table 3, respectively. It can be found from the results that the ex situ presulfided catalyst shows the same or even better HDN and HDS activities as/ than in situ presulfided catalyst, and the distillation range of the hydrotreated products over ex situ presulfided catalyst is similar to that over in situ presulfided catalyst. The enhancement of the cetane number of the hydrotreated products indicates that the ex situ sulfurization technology in this work is effective and the activity of the ex situ presulfided catalyst is consistent with or even higher than that of conventional in situ presulfided catalyst.

**Table 2. The Characteristics of the Hydrotreated Products over NiW/Al<sub>2</sub>O<sub>3</sub> Catalyst**

	Feed	In-situ	Ex-situ
Sulfur, µg/g	10600.0	3048.0	2399.0
Nitrogen, µg/g	540.0	233.0	186.0
Cetane Number	47.6	50.8	50.4
HDS, %	-	71.3	77.4
HDN, %	-	56.8	65.6
Distillation range, °C			
IBP	205	89	104
10%	244	244	237
30%	281	277	278
50%	307	303	301
70%	329	325	323
90%	360	355	355
95%	>360	>360	>360

**Table 3. The Characteristics of the Hydrotreated Products over NiMoW/Al<sub>2</sub>O<sub>3</sub> Catalyst**

	Feed	In-situ	Ex-situ
Sulfur, µg/g	10600.0	2192.0	2019.0
Nitrogen, µg/g	540.0	286.0	286.0
Cetane Number	47.6	50.5	50.5
HDS, %	-	79.3	80.9
HDN, %	-	47.0	47.0
Distillation range, °C			
IBP	205	50	50
10%	244	245	247
30%	281	259	260
50%	307	299	298
70%	329	324	327
90%	360	338	355
95%	>360	359	360

### Conclusions

The experimental results reveal that the vulcanization agent with given component in this work can effectively sulfurize NiW/Al<sub>2</sub>O<sub>3</sub> and NiMoW/Al<sub>2</sub>O<sub>3</sub>, and it is shown that no obvious temperature rising appears during the treatment of the ex situ presulfided NiW/Al<sub>2</sub>O<sub>3</sub> and NiMoW/Al<sub>2</sub>O<sub>3</sub> catalysts, while the temperature in catalyst's bed is fluctuant acutely during the in situ presulfurization. The time for the treatment of the ex situ presulfided catalyst is half that for the in situ presulfurization, which means energy consuming can be reduced greatly during the sulfurization process. The results of the evaluation for the catalyst's activity disclose that the HDN and HDS activities of the ex situ presulfided catalyst are the same as or even better than in situ presulfided catalyst. The enhancement of the cetane number of the hydrotreated products indicates that the ex situ sulfurization technology in this work is effective and the activity of the ex situ presulfided catalyst is consistent with or even higher than that of conventional in situ presulfided catalyst.

**Acknowledgement.** Financial support from PetroChina Corporation Limited is greatly appreciated.

### References

- (1) Labruyere F.; Dufresne P.; Lacroix M.; Breyse M. *Catal. Today*, **1998**, *43*, 111.
- (2) Murff S. R.; Carlisle E.A.; dufresne P.; Rabehasaina H. Prepr. Pap. - *Am. Chem. Soc., Div. Petrol. Chem.*, **1993**, *38*(1), 81.
- (3) Neuman D. J.; Klavey H.; Sempey G. K. *NPRA Paper*, **1998**, AM-98-59, San Francisco, California.

## FUTURE CHALLENGES OF HYDROTREATING CATALYST TECHNOLOGY

Henrik Topsøe, Ramus G. Egeberg, and Kim G. Knudsen

Haldor Topsøe A/S, Nymøllevej 55, DK-2800 Lyngby, Denmark

### Summary

In this presentation we will discuss the advent of tighter fuel specifications and in particular how the very low sulfur content allowed in transportation fuels has set a new agenda for the refining industry. Each refiner must decide how to most cost-effectively implement the needed technology upgrading, whilst also being able to shift the product slate composition as demand for different fuels grows. The decision on e.g. whether to revamp an existing HDT unit or build a grassroots unit requires a detailed analysis of the whole refinery and a deep understanding of the detailed kinetics of the hydroprocessing reactions.

In recent years, several scientific advances have provided new fundamental insight into HDS catalysis. Recent scanning tunneling microscopy (STM) experiments and density functional theory (DFT) calculations have shed light on the atomic-scale structure of Co-Mo-S catalysts, the origin of the high-activity Type II sites, and the detailed molecular reactions that take place. We will also discuss the discovery of a metallic edge state on the active catalyst nanoparticles that has spurred the development of a new series of high-activity catalysts based on the so-called BRIM<sup>TM</sup> technology.

### Challenges in Catalyst Technology

The demand for low sulfur transportation fuels requires that refiners evaluate the many different options for reaching the target. Selection of catalyst types is one of the important decisions. As sulfur conversion increases, we are left with the most refractory species – alkylated dibenzothiophenes. Under idealized conditions, the conversion of these molecules that are sterically hindered mainly proceeds via a prehydrogenative route instead of direct desulfurization (1-5). Since NiMo catalysts are generally more active for the indirect hydrogenative route and CoMo catalysts more active for the direct route, one should think that NiMo is the preferred option for ultra deep desulfurization. However, at low hydrogen pressures and high space velocities CoMo catalyst are often seen to outperform NiMo catalysts (4). It has been observed that nitrogen compounds may inhibit the hydrogenative pathway (6-9), and by conducting detailed studies into the influence of such effects under real feed conditions (9) it was found that specific basic nitrogen compounds have a profound effect on HDS and HDN activity. This is presumably a result of competitive adsorption. These nitrogen compounds inhibit both direct and indirect desulfurization but the effect is largest for the latter. Thus, selection of catalyst depends on both feedstock and operation conditions. In addition, issues such as hydrogen availability and other product properties may play a role (10).

Besides the issues related to the legislative drive for removing sulfur the refiners are also faced with a growing demand for diesel fuels. Such a demand may partly be met by producing less low value products such as heating oil. This can be done by converting heavy fractions by hydrocracking or ‘mild hydrocracking’ processes or one may adopt upgrading processes e.g. for light cycle oil. The latter alternative requires new technology that not only removes refractory sulfur species in the presence of high amounts of nitrogen but also perform a certain degree of ring opening to reach a reasonable product cetane number.

The development of new catalysts no longer proceeds by trial-and-error but goes hand in hand with the insight gained from

fundamental desulfurization studies. Some recent developments are highlighted below.

### Support Interaction and Origin of Type I/II Sites

The role of support interactions in desulfurization catalysts has been an important topic for a number of years. Most studies have dealt with alumina-supported NiMo or CoMo sulfides that are predominantly used in the industry. By using alumina as a support, the dispersion of MoS<sub>2</sub> edges is quite high due to the formation of small stable nanoclusters. A high edge dispersion is important since it increases the amount of Co (Ni) that can be accommodated at the edges forming the active Co(Ni)-Mo-S structure (1). However, the support interaction also has important implications for the intrinsic activity of the active sites. Several years ago we observed (11) that increasing the sulfiding temperature from 673 K to 873 K resulted in modified Co-Mo-S structures (Type II Co-Mo-S) with substantially higher activity per active site than those formed at the lower temperature (Type I). The existence of these two different structures is related to the interaction between Mo and surface alumina OH groups during preparation leading to monolayer type structures that are difficult to sulfide. Other studies (12,13) also show some evidence for Mo-O-Al linkage in Type I structures and thus corroborate the idea that a weak support interaction is needed to create Type II sites. The linkages can be broken by high temperature sulfiding but this decreases the MoS<sub>2</sub> edge dispersion and it is therefore preferable to find alternate procedures. This may occur by introduction of additives or chelating agents or by using weakly interacting supports (14-18).

The formation of multi-stack MoS<sub>2</sub> structures has been observed in catalysts containing Type II sites. However, multi-stacking may only be a by-product of weaker support interactions and it is also possible to produce single slab Type II Co-Mo-S samples (1). Furthermore, as discussed below, only the top layer of multi-stacks will expose the special brim sites that seem to play a critical role in hydrogenative desulfurization.

Recently, the origin of intrinsic activity differences between Type I and Type II structures has been the subject of a DFT study (19). Here the direct connection between the presence of linkage to the alumina and HDS activity was addressed by calculating the difference in Mo-S bond strength when oxygen linkages are introduced. It was shown that Mo-O linkages are most probably located on the S edge and the presence of such oxygen linkages was seen to increase the energy required to form sulfur vacancies significantly. Since the sulfur vacancies are necessary for sulfur extraction reactions, this provides us with a consistent picture of the influence of support interaction on the Type I and Type II reactivity.

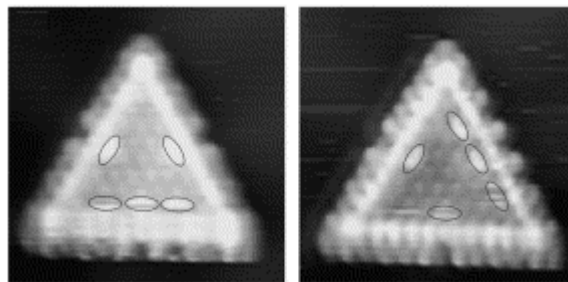


**Figure 1.** Consecutive STM images of thiolate species adsorbed on the brim sites of a MoS<sub>2</sub> nanocrystal. The time lapse between the images recorded at room temperature is *ca.* 1 min showing a high mobility of the adsorbed molecules along the brim. Adapted from (20).

## BRIM™ Technology

The existence of both direct and prehydrogenative desulfurization routes has been known for many years, yet very little information on the precise molecular reaction steps has been available. STM studies have provided interesting clues as to how these reactions proceed. MoS<sub>2</sub> nanoparticles with a triangular geometry possess special brim sites with metallic character. By combining these studies with DFT calculations, it was found (20) that thiophene can be hydrogenated and ring opened on the brim sites, whereafter the butenethiolates diffuse to sulfur vacancies on the cluster edge, where the second sulfur-carbon bond is broken. Consecutive STM images (Figure 1) show how the hydrogenated species are highly mobile supporting the outlined two-step reaction pathway.

In parallel with these findings, Haldor Topsøe has developed a new preparation procedure that provides high activity hydroprocessing catalysts. This new BRIM™ technology not only optimizes the brim site hydrogenation functionality but also increases the direct desulfurization pathway. The first two commercial catalysts based on this technology are Topsøe's TK-558 BRIM™ (CoMo) and TK-559 BRIM™ (NiMo) for FCC pretreatment service. They show superior activity (Figure 2) and have very recently been successfully adopted by many refiners.

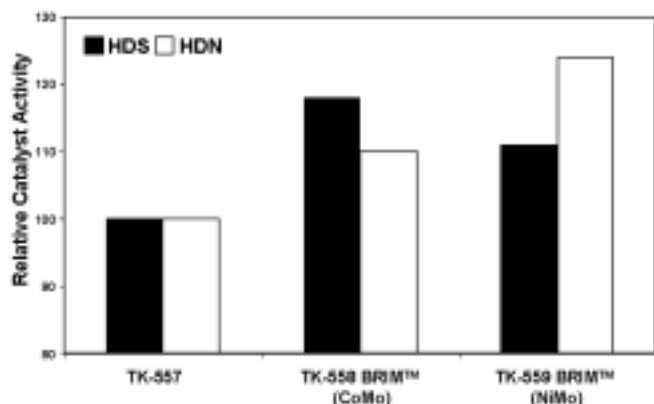


**Figure 2.** Relative activities of Haldor Topsøe's new BRIM™ technology catalysts for FCC pretreatment service. These catalysts rely on the highly active brim sites present on catalyst nanoparticles.

## Conclusions

The challenges that the refining industry is facing now and in the years to come call for major developments within hydroprocessing catalyst technology. To assess how a specific refinery successfully adjusts to the new legislation and market demands, a detailed knowledge of reaction kinetics and catalyst reactivity and selectivity is required. The progress in fundamental HDS studies on support interaction, catalyst morphology and reaction pathways is expected to continue to provide new opportunities for the development of improved commercial catalysts.

## References

- (1) Topsøe, H.; Clausen, B.S.; Massoth, F.E. *Hydrotreating Catalysis – Science and Technology*, Vol 11, Ed. Anderson, J.R and Boudart, M.; Springer Verlag Berlin, 1996.
- (2) Landau, M. V.; *Catal. Today* **1997**, 36, 393.
- (3) Whitehurst, D. D.; Isoda, T.; Mochida, I. *Adv. Catal.* **1998**, 42, 345.
- (4) Knudsen, K. G.; Cooper, B. C.; Topsøe, H. *Appl. Catal. A* **1999**, 189, 205.
- (5) Song, C. *Catal. Today* **2003**, 86, 211.
- (6) Nagai, M.; Kabe, T. *J. Catal.* **1983**, 81, 440.

- (7) Nagai, M.; Sato, T.; Aiba, A. *J. Catal.* **1986**, 97, 52.
- (8) van Looij, F.; van der Laan, P.; Stork, W. H. J.; DiCamillo, D. J.; Swain, J. *Appl. Catal. A* **1998**, 170, 1.
- (9) Zeuthen, P.; Knudsen, K. G.; Whistehurst, D. D. *Catal. Today* **2001**, 65, 307.
- (10) Tippet, T.; Knudsen, K. G.; Cooper, B. C. *Proc. NPRA Annual Meeting 1999*, Paper AM-99-06.
- (11) Candia, R.; Clausen, B. S.; Topsøe, H. *Proc. 9<sup>th</sup> Iberoamerican Symposium on Catalysis 1984*, Lisbon, Portugal, 211.
- (12) Leliveld, R. G.; van Dillen, A. J.; Geus, J. W.; Konigsberger, D. C. *J. Catal.* **1997**, 165, 184.
- (13) Diemann, E.; Weber, Th.; Müller, A. *J. Catal.* **1994**, 148, 288.
- (14) Topsøe, H.; Candia, R.; Topsøe, N.-Y.; Clausen, B. S. *Bull. Soc. Chim. Belg.* **1984**, 93, 783.
- (15) van Veen, J. A. R.; Gerkema, E.; van der Kraan, A. M.; Knoester, A. *J. Chem. Soc. Chem. Commun.* **1987**, 22, 1684.
- (16) Vissers, J. P. R.; Scheffer, B.; de Beer, J. H. J.; Moulijn, J. A.; Prins, R. J. *Catal.* **1987**, 105, 277.
- (17) Medici, L.; Prins, R. *J. Catal.* **1996**, 163, 38.
- (18) Coulier, L.; Kishan, G.; van Veen, J. A. R.; Niemantsverdriet, J. W. *J. Phys. Chem. B* **2002**, 106, 5897.
- (19) Hinnemann, B.; Nørskov, J. K.; Topsøe, H. *submitted*.
- (20) Lauritsen, J. V.; Nyberg, M.; Nørskov, J. K.; Clausen, B. S.; Topsøe, H.; Lægsgaard, E.; Besenbacher, F. *J. Catal.* **2004**, 224, 94.

# Nature of active sites on sulfided CoMo/Al<sub>2</sub>O<sub>3</sub> and its connection with catalyst selectivity in FCC gasoline hydrodesulfurization

<sup>1</sup>Jae-Soon Choi, <sup>2</sup>Françoise Maugé, <sup>1</sup>Christophe Pichon, <sup>3</sup>Joseette Olivier-Fourcade, <sup>3</sup>Jean-Claude Jumas, <sup>1</sup>Carine Petit-Clair, and <sup>1</sup>Denis Uzio

<sup>1</sup>IFP, Solaize BP n°3, 69390 Vernaison, France

<sup>2</sup>Laboratoire Catalyse et Spectrochimie, UMR-CNRS 6506, ENSICAen, 6 Boulevard du Maréchal Juin, 14050 Caen Cedex, France

<sup>3</sup>Laboratoire des Agrégats Moléculaires et Matériaux Inorganiques, UMR-CNRS 5072, Place Eugène Bataillon, Case Courrier 015, 34095 Montpellier Cedex 5, France

## Introduction

Gasoline from Fluid Catalytic Cracking unit (FCC gasoline) has a high sulfur concentration and may contribute alone more than 90% of the sulfur contained in a total gasoline pool. Therefore, sulfur present in FCC gasoline is a key target in order to meet future sulfur specifications on gasoline. One of the viable technological options is the hydrodesulfurization (HDS) of FCC gasoline<sup>1</sup>.

Main sulfur compounds present in FCC gasoline are thiophenes and benzothiophenes, which are relatively easy to remove by conventional HDS catalysts<sup>2</sup>. However, hydrodesulfurization with conventional catalysts is accompanied by the hydrogenation (HYD) of olefins, which are also abundantly (25-50%) present in FCC gasoline. To preserve the octane number of FCC gasoline during HDS process by avoiding simultaneous olefin hydrogenation, it is necessary to improve the selectivity of the conventional catalysts (e.g., sulfided CoMo/Al<sub>2</sub>O<sub>3</sub>). One of possible ways to achieve this goal is to modify catalyst active sites distribution, if different sites are responsible for HDS and HYD, respectively. However, contradictory views still exist on the nature of active sites for HDS and HYD<sup>2-4</sup>.

The objective of the present work was to get a better insight into the relationship between different sites on sulfide and catalyst selectivity (HDS/HYD). Tin was added to sulfided CoMo/Al<sub>2</sub>O<sub>3</sub> and the resulting reactivity variations were studied. The surface organometallic chemistry (SOMC) was used for tin deposition and the local structure of Sn on sulfided CoMo/Al<sub>2</sub>O<sub>3</sub> was characterized by a multi-technique approach consisting of <sup>119</sup>Sn Mössbauer and infrared spectroscopies, as well as EXAFS.

## Experimental

**Catalyst preparation and characterization.** Tin deposition on CoMo sulfide was carried out by reacting tetraallyltin (Sn(C<sub>3</sub>H<sub>5</sub>)<sub>4</sub>, +95%, STREM CHEMICALS) with the surface of freshly sulfided CoMo/Al<sub>2</sub>O<sub>3</sub>. First, an oxide precursor (3 wt% CoO-10 wt% MoO<sub>3</sub>/Al<sub>2</sub>O<sub>3</sub>) was sulfided at 673 K in flowing 15 vol% H<sub>2</sub>S/H<sub>2</sub> under atmospheric pressure and then the sulfided sample was transferred, without air contact, to the reactor designed for the SOMC treatment. This reactor, containing the solution (complex + solvent), had been purged by Ar flow before catalyst introduction. The reaction was done at RT in flowing H<sub>2</sub> for 2 h. After reaction, the catalyst was washed with pure solvent (n-heptane) under Ar flow. To ensure complete decomposition of the anchored complexes, a post-treatment was performed by reduction under pure H<sub>2</sub> flow at 473 K.

<sup>119</sup>Sn Mössbauer spectroscopy analyses were carried out at RT using an EG & G Novelec constant acceleration spectrometer in transmission mode. A fresh Sn-containing sample was placed in the specific Pyrex cell, which was sealed under vacuum and then transferred to the spectrometer to avoid air contact. The recorded spectra were fitted with Lorentzian profiles by a least-squares

method and the isomer shifts were determined relative to the center of the BaSnO<sub>3</sub> spectrum recorded at RT.

For the infrared (IR) spectroscopy measurements, the sulfide sample previously kept under Ar was taken out in air and pressed into a self-supporting disc (10 mg, 2 cm<sup>2</sup>). It was then placed into the IR cell and re-sulfided *in situ*. First, IR spectra of fresh sulfide were obtained at RT and 100 K, then small calibrated pulses of carbon monoxide (CO) were introduced into the IR cell at 100 K up to an equilibrium pressure of 133 Pa. IR spectra were recorded after each CO introduction with a Nicolet Magna 550 FT-IR spectrometer equipped with a liquid-nitrogen-cooled MCT detector. The spectrometer operated at 4 cm<sup>-1</sup> resolution collecting 512 scans.

EXAFS experiments were performed at LURE (Laboratoire pour l'Utilisation du Rayonnement Electromagnétique, Orsay, France) using DCI, a storage ring operated with an electron energy of 1.85 GeV and a current between 260 and 360 mA. The samples were loaded under inert atmosphere and data were collected at RT for the Mo and Co K-edges.

**Catalyst performance evaluation.** Catalytic test were performed in an autoclave under constant hydrogen pressure with a model FCC gasoline feed. This feed was composed of 1000 ppm sulfur as 3-methylthiophene (> 98%, Fluka), 10 wt% olefin as 2,3-dimethyl-2-butene (> 97%, Fluka) or 1-hexene (~ 98%, Fluka), and solvent as n-heptane (> 99%, HPLC grade, Fluka). Fresh catalyst was introduced under argon (Ar) flow into the reactor containing n-heptane, which was also previously purged by Ar flow to prevent any air contact of the catalyst. The reactor was purged again by nitrogen (N<sub>2</sub>) stream, prior to the injection of reactants consisting of 3-methylthiophene and 2,3-dimethyl-2-butene or 1-hexene. Then, the temperature was increased up to the reaction temperature of 473 K under N<sub>2</sub> atmosphere. After introducing hydrogen (H<sub>2</sub>) to have a total reaction pressure of 2.5 MPa, the reaction was started by stirring the reaction mixture. The composition of the reaction mixture was monitored during the reaction, by analyzing the liquid samples using a gas chromatograph (Varian, CP-3800) equipped with a flame ionization detector and a 50-m-long and 0.2-mm-diameter (I.D.) capillary column (HP PONA, 0.5 μm film thickness).

## Results and Discussion

**Tin doping and structure changes.** Tin deposition on CoMo/Al<sub>2</sub>O<sub>3</sub> sulfide by surface organometallic chemistry of tetraallyltin seems to have taken place maintaining the initial morphology of sulfide slabs, as EXAFS spectra at the Mo and Co K-edges did not show any noticeable change with tin doping even up to 2.4%. Moreover, very high Sn dispersion seems to have been achieved, as indicated by the absence of Sn-Sn environment in <sup>119</sup>Sn Mössbauer spectra. Mössbauer spectroscopy also showed that the tin environment was rich in sulfur and oxygen. It suggests that tin-complex anchoring have proceeded through the hydrogenolysis of Sn-C bonds on SH and/or OH groups. The SH groups might be linked to Mo or Co-promoted Mo sites, H-bonded to support OH groups, or located at Al<sup>3+</sup> sites. As a result, tin doping could have led to the blocking of different sites on sulfide catalysts, according to the Sn loading. Information related to site blocking could be obtained by infrared spectroscopy analysis of CO species chemisorbed on catalyst surface at 100 K (Figure 1) or of catalyst OH groups at RT without CO chemisorption (Figure 2). The introduction of 0.5 wt% Sn decreased the numbers of support sites (OH groups, Al<sup>3+</sup> sites) and sulfide slab sulfur vacancies. Higher Sn loadings (1.6 or 2.4 wt% Sn) continued to decrease the number of sulfur vacancies but the decreasing rate was considerably lowered. On the other hand, the number of free OH groups and Al<sup>3+</sup> sites did not change any more significantly at 1.6 or 2.4 wt% Sn. On the contrary, the number of support OH groups H-bonded with sulfide slabs (which we call here

“interfacial sites”) decreased drastically at these high Sn loadings, while much less effect was observed at 0.5 wt% Sn. The site blocking by tin seems to have proceeded without significant strength change of residual sites, as no evident band shift trend was observed.

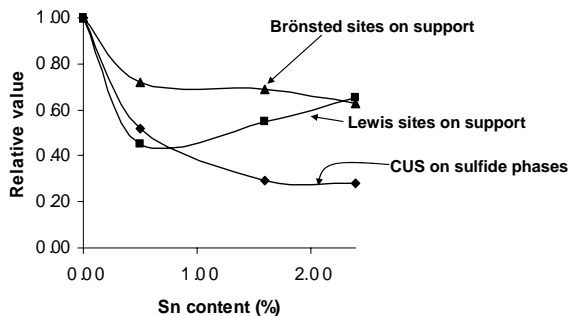


**Figure 1.** Site blocking caused by tin doping on sulfided CoMo/Al<sub>2</sub>O<sub>3</sub>. Number of sites (relative values) estimated from IR bands of different CO species adsorbed at 100 K.

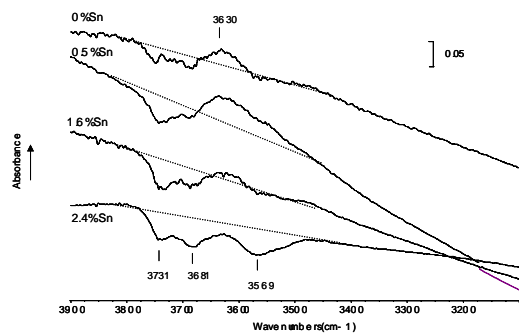


**Figure 2.** IR spectra of the OH band region of the sulfided CoMo/Al<sub>2</sub>O<sub>3</sub> with different Sn loadings, after subtraction of sulfided alumina contribution. Band at 3630 cm<sup>-1</sup> is attributed to the support OH groups H-bonded with sulfide phases<sup>5</sup>.

**Reaction networks and active sites.** The conversion of 3-methylthiophene proceeded via pre-hydrogenation of thiophenic ring and showed an apparent first-order kinetic behavior on CoMo/Al<sub>2</sub>O<sub>3</sub> sulfides with or without Sn-doping. Hydrogenation of 2,3-dimethyl-2-butene was a consecutive reaction involving intermediate isomerization to 2,3-dimethyl-1-butene. Hydrogenation of 2,3-dimethyl-1-butene started when equilibrated isomer composition was attained and had apparent zero-order kinetics. The conversion of 1-hexene involved isomerization and hydrogenation in parallel. The isomer concentration was again quickly equilibrated and hydrogenation of 1-hexene followed apparent zero-order kinetics. To assess the impact of tin doping on catalyst performance, the rates of three major reactions involved (hydrodesulfurization of 3-methylthiophene, olefin isomerization, and olefin hydrogenation) were compared in terms of tin loading (Figure 3). We could get some interesting information about active sites for the reactions involved, by analyzing the patterns of activity drop for these three reactions (see Figure 3) in connection with the site blocking patterns of different sites (see Figures 1 and 2). Tin-doping did not affect the double-bond isomerization of olefins and as it was only the number of support sites which was not decreased drastically by tin-doping, the support sites seem to play an important role in this reaction. Hydrodesulfurization and olefin hydrogenation were significantly inhibited by tin-doping. According to infrared spectroscopy, the

decreased hydrodesulfurization activity could be nicely explained by the decreased number of sulfur vacancies on sulfide phases and activity drop in hydrogenation by the disappearance of support hydroxyl groups in interaction with sulfide phases thus interfacial sites. Therefore sulfur vacancies on sulfide phases seem to play as active sites in hydrodesulfurization, having little influence on olefin hydrogenation or isomerization. The interfacial sites appear to play an important role in olefin hydrogenation reaction pathway. Further studies will however be required to examine the possible role of interfacial sites in hydrodesulfurization.

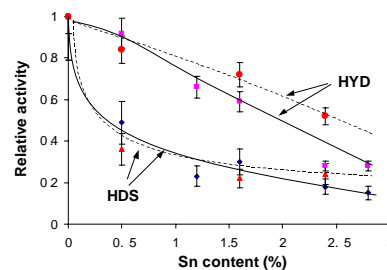


**Figure 3.** Evolution of 3-methylthiophene HDS and olefin HYD activities as a function of Sn loadings. Dashed lines correspond to the mixture of 3MT and 2,3-dimethyl-2-butene and solid lines to that of 3-methylthiophene and 1-hexene.

## Conclusions

In this work, we have investigated the nature of active sites responsible for the sulfide catalyst selectivity in FCC gasoline hydrodesulfurization process, by studying catalyst structure changes and selectivity evolution brought by tin doping via surface organometallic chemistry. Main findings can be summarized as follows:

- Tin doping of sulfided CoMo/Al<sub>2</sub>O<sub>3</sub> by surface organometallic chemistry proceeded with little change in catalyst bulk structure.
- Finely dispersed tin led to the blocking of different sites (sulfur vacancies on sulfide slabs, support sites, and interfacial sites) without significant change of site strength.
- Sulfur vacancies on sulfide slabs are essential for the conversion of 3-methylthiophene but of much less importance for olefin conversion.
- Support sites seem to play a major role in olefin isomerization with little impact on HDS or HYD.
- Interfacial sites (support hydroxyl groups H-bonded with sulfide phases) appear important in olefin hydrogenation reaction pathway. Further studies are, however, necessary to understand the exact role of interfacial sites in HDS.

## References

- (1) Baco, F.; Debuisschert, Q.; Marchal, N.; Nocca, J.L.; Picard, F.; Uzio, D., Prime G+ Process Desulfurization of FCC Gasoline with Minimized Octane Loss, AIChE Spring National Meeting, 10-14 March 2002, New Orleans.
- (2) Topsøe, H.; Clausen, B.S.; Massoth, F.E. In *Catalysis, Science and Technology*; Anderson, J.R.; Boudart, M. Ed.; Vol. 11, Springer-Verlag: Berlin, 1996.
- (3) Miller, J.T.; Reagan, W.J.; Kaduk, J.A.; Marshall, C.L.; Kropf, A.J., *J. Catal.* **2000**, *193*, 123.
- (4) Hatanaka, S.; Yamada, M.; Sadakane, O., *Ind. Eng. Chem. Res.* **1997**, *36*, 5110.
- (5) Topsøe, N.-Y.; Topsøe, H., *J. Catal.* **1993**, *139*, 641.

# DEVELOPMENT OF HYDRODEMETHALLIZATION CATALYST FOR DEEP DESULFURIZATION OF ATMOSPHERIC RESIDUE

Takehige TAKAHASHI, Hidehiro HIGASHI and Takami KAI

Department of Applied Chemistry and Chemical Engineering,  
Kagoshima University, Kagoshima 890-0065 JAPAN

## Introduction

The deep hydrodesulfurization (HDS) of an atmospheric residue (AR) has been the most important processes to produce low sulfur vacuum gas oil (VGO) for an FCC process. However, when the deep HDS (sulfur content is below 0.3 wt%) of the AR was carried out over a catalyst combination employed in commercial process, that is, demetallization catalyst (HDM), metal tolerant HDS catalyst and high active HDS catalyst, it was found that the high active HDS catalyst was easily deactivated due to the deposition of coke from an asphaltene (ASP) decomposition (1). The detailed study revealed that since the ASP and a maltene as higher reactive heavy residue than the former simultaneously decomposed on a commercial high active HDM catalyst under severe reaction conditions, a large amount of coke was deposited on the HDM surface. As the result, the pore mouth of the HDM catalyst was plugged by the coke at early operation period. In the present study, new HDM catalyst with low activity was prepared and applied to pilot plant scale (catalyst volume is 500ml) fixed bed reactor. The HDS catalyst supported on medium pore (11 nm) was supplied in the rest of the reactor. The effect of metal composition of new type HDM catalyst on catalyst deactivation has been discussed for deep HDS operation. Furthermore, the effect of reaction temperature of HDM catalyst on the catalyst life has also been discussed.

## Experimental

In the present study, two kinds of catalysts were used. CDS-R2 is the HDS catalyst ( $\text{MoO}_3=12.0\text{wt}\%$ ,  $\text{CoO}=1.0\text{wt}\%$ ,  $\text{NiO}=1.5\text{wt}\%$ ) supported on  $\gamma$ -alumina with 10.4 nm of average pore size. CDS-DM1 is new HDM catalyst ( $\text{MoO}_3=3.3\text{wt}\%$ ,  $\text{NiO}=0.7\text{wt}\%$ ,  $\text{V}_2\text{O}_5=4.0\text{wt}\%$ ) developed in the study. The sulfur and ASP contents in Khafji AR are 3.95 and 8.2 wt%, respectively. The half of sulfur in the AR is presented in the ASP. The Conradson Carbon Residue (CCR) in the AR is 13.0wt%.

The HDS reaction was carried out in a fixed bed type reactor operated at high  $\text{H}_2$  pressure. The schematic diagram of the experimental apparatus and experimental procedure were reported in a previous paper (2).

## Results and Discussion

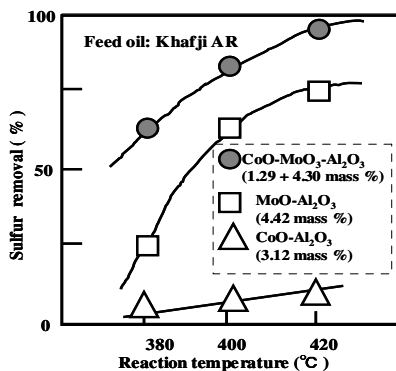


Fig.1 Effect of reaction temperature on sulfur removal over low active catalysts.

Figure 1 shows the effect of reaction temperature on sulfur removal over catalysts stipulated as an HDM catalyst for the reaction of Khafji AR. The sulfur removal activity of the Co-alumina and Mo-alumina

catalysts was very low and the activity of catalyst simultaneously modified with Mo-Co supported on alumina was high as reported in a literature (3). Furthermore, it was found that molybdenum was active metal for the HDS reaction from the figure.

Figure 2 demonstrates the effect of extent of asphaltene cracking on vanadium removal over the same catalysts as shown in Figure 1. The vanadium removal rate increases with asphaltene cracking rate. Although 50wt% of vanadium was removed at the 25wt% of asphaltene decomposition, the vanadium removal rate over 50% is proportional to the asphaltene removal rate.

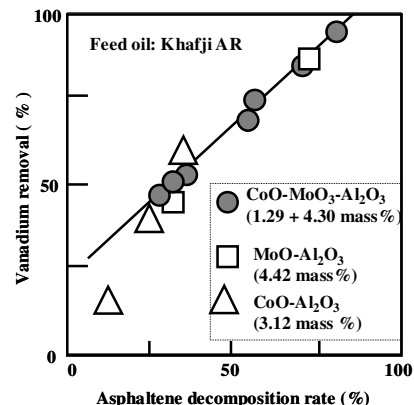


Fig.2 Effect of asphaltene decomposition rate on vanadium removal over low active catalysts.

Furthermore, the relationship between vanadium removal rate and asphaltene removal rate is laid down on the straight line as shown in Figure 1. This result indicates that vanadium removal activity over the catalysts is almost the same as each other.

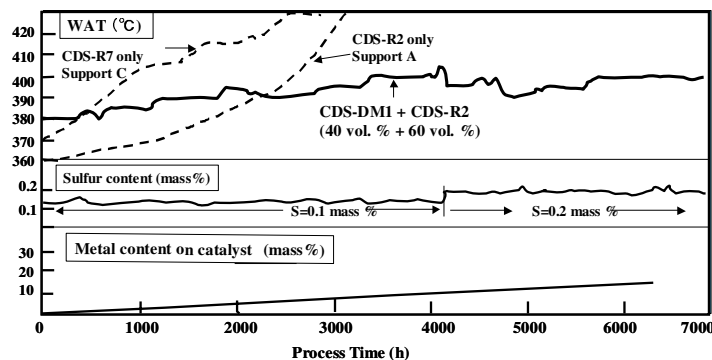


Fig.3 Relationship between WAT, sulfur content and metal on catalyst, and process time.

Figure 3 shows the relationships between reaction temperature to maintain 0.1 wt% sulfur in the product oil (Weight Average Temperature = WAT), sulfur content in the product oil, metal content on the HDM catalyst and process time (time on stream). The relationship between WAT and process time over CDS-R2 and CDS-R7 catalysts are also demonstrated in Figure 3. The WATs obtained from two HDS catalysts steeply increased with process time and reached at 683K as the temperature called as the end of reaction. On the other hand, The WAT obtained from the combination catalysts was below 673K after 4000h of process time.

The combination of low active HDM catalyst and high active HDS catalyst is effective to the deep hydrodesulfurization of atmospheric residue. The effect of reaction temperature at HDM zone on CDS-DM1 life was also discussed

## References

- Higashi, H., Takahashi, T. and Kai, T., *J. Jpn. Petro. Inst.*, in print
- Higashi, H., Takahashi, T., Kai, T., *Catalysis Survey from Japan*, 5, 111 (2002)
- Japan Petroleum Institute ed., "Petroleum Refining Process", Kodansha Scientific, pp.37-99 (1998)

## Characteristics of Maya crude hydrodemetallization and hydrodesulfurization catalysts

Mohan S. Rana\*, J. Ancheyta, S. K. Maity and P. Rayo

Instituto Mexicano del Petroleo, Eje Central Lazaro Cardenas 152, Mexico City, 07730, Mexico; \*msingh@imp.mx

### Abstract

It was found that supports prepared by ammonium carbonate and urea hydrolysis methods have improved pore size distribution (PSD) as well as pore volume. The HDM activity increases while the HDS activity decreases with increasing the average pore diameter (APD). The results of HDM and HDAs activities of catalyst protrude distinct contribution of PSD of support which has more capabilities to retain metal deposition and better diffusion of complex organo-chelating metals. It has been also proposed that deposited vanadium sulfide may act as auto-catalytic activity for HDM and HDAs.

### Introduction

The challenging task in hydrotreating of heavy oils is the hydrodemetallization (HDM) which ends up in the metal sulfide accumulation on the catalyst surface and as a result blocking of the active sites and pores [1-3]. This becomes more complicated since virtually infinite number of complex hydrocarbon like asphaltene together with the molecules containing heteroatom; mainly S, N, V and Ni etc are present in high concentration. The available information using PSD, TEM and XRD suggests that V and Ni exist as crystallite sulfides [4]. In order to draw the concept governing the effect of support preparation in HDT catalysts performance, different  $\gamma$ -Al<sub>2</sub>O<sub>3</sub> support preparation methods were employed to vary the porosity and PSD which play an important role in stability as well as in metals retention capacity on the surface of catalyst. The different characterization of the catalysts before and after reaction provides important information about the role of textural properties on metal deposition.

### Experimental

$\gamma$ -Al<sub>2</sub>O<sub>3</sub> supports were prepared by using different precipitation agents such as urea ( $\gamma$ -Al<sub>2</sub>O<sub>3</sub>-u), ammonium carbonate ( $\gamma$ -Al<sub>2</sub>O<sub>3</sub>-acs) and ammonia ( $\gamma$ -Al<sub>2</sub>O<sub>3</sub>-am). The details of the preparation of support are given elsewhere [5]. The Co-Mo promoted catalysts were prepared by the sequential incipient wetness impregnation method. The compositions and textural properties of catalysts are reported in Table 1.

The specific surface area (SSA), pore volume (PV) and PSD were carried out using N<sub>2</sub> adsorption-desorption at -196°C. X-ray power diffraction (XRD) patterns were collected on a Siemens D500 diffractometer using CuK<sub>α</sub> radiation. The TEM experiments were carried out in Jeol 100CX-II equipment.

The catalytic activities were carried out with a mixture of Maya crude and diesel 50/50 (w/w) at high pressure up-flow micro reactor [5]. The diesel was used as diluent to avoid precipitation and gum formation during the feed processing. The properties of the feed are presented in Table 2. The Metals (Ni, V), S and N were analyzed in the feed and products by flame atomic adsorption spectrometry, UV-fluorescence, chemiluminescence respectively. Asphaltene is defined as the insoluble fraction in n-C<sub>5</sub>. 10 ml of catalyst was sulfided *in-situ* with a mixture of DMDS and SRGO containing ≈2 wt. % 'S' and wet the catalyst bed at RT. The final conditions of sulfidation were 320°C, 2.8 MPa for 5h. After sulfidation, the flow was switched to the real feed and the following operating conditions were adjusted: temperature of 380°C, LHSV of 1h<sup>-1</sup>, H<sub>2</sub>/HC of 356 m<sup>3</sup>/m<sup>3</sup> and pressure of 5.4 MPa [5].

Table 1. Catalyst characterization and composition

Catalysts	Textural properties and composition					PSD % (nm)					
	SSA m <sup>2</sup> /g	PV ml/g	APD nm	Mo wt.%	Co(Ni) wt.%	5	10	20	50	100	200
CoMo/Al <sub>2</sub> O <sub>3</sub> -u	136	0.39	12.9	7.5	2.5	3.3	15	34.8	34.9	11.8	0.2
CoMo/Al <sub>2</sub> O <sub>3</sub> -acs	160	0.47	17.3	6.8	2.5	7.6	4.8	19.2	32.8	29.7	5.0
CoMo/Al <sub>2</sub> O <sub>3</sub> -am	169	0.27	6.5	7.5	2.5	32.1	59	7.0	1.0	0.0	0.0
CC	175	0.56	15.2	10.6	(2.8)	4.6	15	61.9	5.2	12.8	0.0

Table 2. Feed composition

Properties	
<i>Elemental analysis</i>	
C, wt. %	84.2
H, wt. %	8.8
N, wt. %	0.18
S, wt. %	2.21
Metal, wppm (Ni+V)	151
Asphaltene, wt. %	8.43
<i>Physical properties</i>	
Density, 20/4°C	0.88
Pour point, °C	-15
Ramscarbon, wt. %	5.45
Viscosity, g/cms, 100°c	9.45

### Results and Discussion

#### Characterization

$\gamma$ -Al<sub>2</sub>O<sub>3</sub> supports were prepared by aqueous solutions of aluminum nitrate and urea or amm. carbonate in which precipitant is obtained by *in-situ* hydrolysis. However, the different parameters such as aging time, pH, precipitating agents, concentration of solution etc. play an important role to generate the textural properties of support. A plausible explanation for high APD is that during the precipitation the CO<sub>3</sub> is trapped in a bulk between the aluminum oxyhydroxide, which escapes during the calcinations and provides larger porosity and improved PSD. The ammonia prepared alumina exhibited a *Type IV* isotherm, indicative of meso-porosity. The other two supports exhibited a *Type II* isotherm suggesting almost no micro- or meso-porosity. The CoMo/ $\gamma$ -Al<sub>2</sub>O<sub>3</sub>-acs and CoMo/ $\gamma$ -Al<sub>2</sub>O<sub>3</sub>-u supported catalysts showed greater number of pores toward macro size diameter, while CoMo/ $\gamma$ -Al<sub>2</sub>O<sub>3</sub>-am catalyst exhibits only meso-pores after active metal impregnation.

In figure 1, XRD pattern of promoted catalyst does not give any information about the active metal crystallization, which might be due to the low loading of Mo on high SSA support. Spent catalyst (after 60 h time-on stream) XRD carried out in order to see the metal deposition (Ni and V) on the outer surface of catalyst is also shown in the figure. Deposited metals exist as the sulfide compounds and are attributed to the V<sub>3</sub>S<sub>4</sub>, V<sub>2</sub>S<sub>3</sub> and Ni<sub>3</sub>S<sub>2</sub> phases [6]. These sulfided phases can be compared with the standard values (symbols in figure 1) of the Joint Committee on Powder Diffraction Standards (JCPDS).

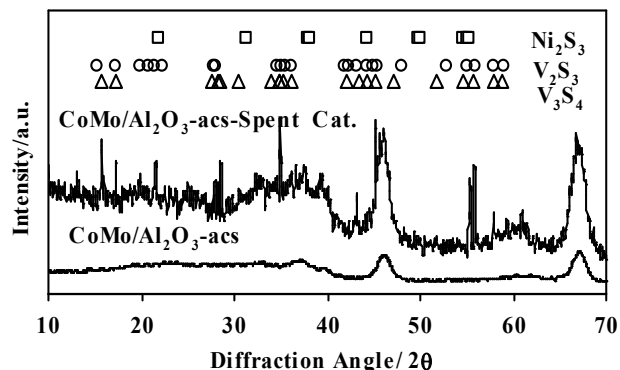


Fig. 1. XRD pattern of supported and spent catalysts

XRD results were further confirmed by spent catalysts TEM (Figure 2) which shows that V<sub>2</sub>S<sub>3</sub> phase exists in rod shaped crystallites. It is also possible that nickel may associate with vanadium [Ni(V<sub>3</sub>S<sub>4</sub>)] which grew perpendicular on the surface of support. Similar kind of TEM results were obtained by Smith and

Wei [4] for the HDM of model molecules. The MoS<sub>2</sub> slabs/stacks reduce drastically in spent catalysts due to the deposition of contaminants and crystals [3]. However, greater number of acicular or rod shaped crystallites were observed in case of CoMo/Al<sub>2</sub>O<sub>3</sub>-acs compared with commercial catalyst as shown in Figure 2. These results indicated that CoMo/Al<sub>2</sub>O<sub>3</sub>-acs is having higher capacity to retain metals (Ni, V) due to the higher amount of >50nm pores (62 %) which is less in the CC (18 %) as shown in Table 1.

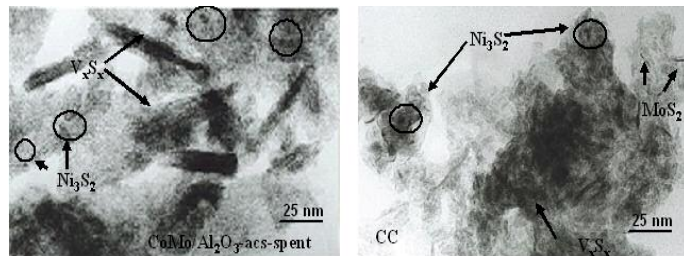


Fig.2: TEM micrographs of lab prepared and commercial catalysts

### Catalytic Activities

The catalytic activities after 60h time-on-stream (TOS) are reported in Figure 3. In general, activities decrease with time-on-stream in similar magnitude for all catalysts including commercial one. The activity decrease is due to the metal poisoning on the catalyst surface. The results of the commercial catalyst (CC) are shown in the figure, which contain higher amount of Mo as well as 3.5 wt. % of TiO<sub>2</sub>.

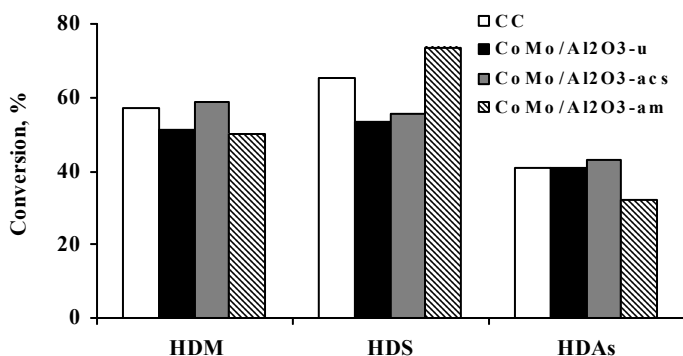


Fig. 3. Activities comparison between the catalysts after 60h TOS

The HDM activity among all lab prepared catalysts containing Co-Mo is slightly better for CoMo/γ-Al<sub>2</sub>O<sub>3</sub>-acs while smaller pore catalyst (CoMo/γ-Al<sub>2</sub>O<sub>3</sub>-am) showed lower activity for HDM. Thus, the PSD are in good agreement with HDM conversion. The low conversion in the case of CoMo/γ-Al<sub>2</sub>O<sub>3</sub>-am is due to its pore distribution in the range of 5-15 nm while the other catalysts have macro pore size profile in the range of 20-200nm.

In figure 3, the comparison between HDM and HDS showed opposite trends which revealed that HDM catalyst should be essentially macro porous in nature. Thus, HDM conversion is limited in the case of CoMo/γ-Al<sub>2</sub>O<sub>3</sub>-am due to the penetration of porphyrins or metal chelating compounds into the pores. The Maya crude contains significant amount of asphaltene, which are responsible for catalyst deactivation in hydroprocessing along with metal deposition. It is observed that the HDM as well as hydrodeasphalting (HDAs), significantly depend on the catalyst pore structure while the HDS activity showed different behavior in figure 3. This means that the HDS activity distinctively differ from the HDM and HDAs. Most probably the HDS activity appreciably depends on the surface area and the active sites. CoMo/Al<sub>2</sub>O<sub>3</sub>-am showed the lowest activity for

HDM and HDAs while maximum activity can be seen for HDS, therefore, HDM and HDAs conversions are limited due to the diffusional limitations of complex metalloid and asphaltene molecules less than 10nm pore diameter. Thus, performance of heavy oil HDT process with regard to different functionalities, such as HDM, HDS, and HDAs, is clearly linked to the porosity and nature of the heavy crude oil.

To further assess the PSD effect on different activities conversion after 60 h TOS. HDS, HDM and HDAs activities are shown in Figure 4 against average pore diameter along with metal (V+Ni) deposition on the catalyst. The HDM activity increases while the HDS activity decreases when increasing the APD. The expected reasons of decreasing HDS activity is the blocking of active sites and the deposition of carbonaceous and metallic impurities in the interstices between the catalyst particles. Different catalyst results show that the metallic deposition on the catalyst surface is more of the V metal sulfides that deposited as larger crystallite than Ni as shown by the TEM micrographs. The XRD and TEM results indicate that Ni is subtly distributed on the catalyst surface in comparison with V.

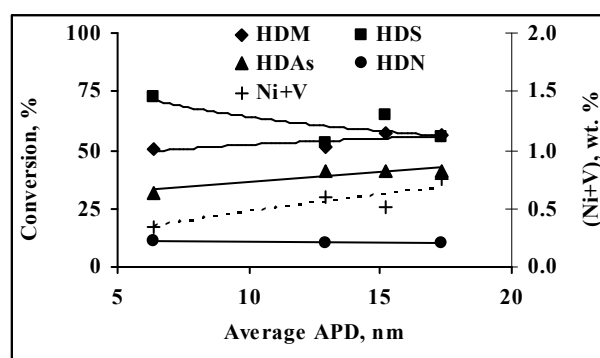


Fig. 4. Effect of average pore diameter on catalysts activity

In conclusion, the TEM and XRD results showed higher deposition of metal on bigger pores with a rod-shape crystalline phases while low porosity catalysts are randomly oriented and overlapping irregular shape of crystallites. Other characterization results of spent catalyst showed that the higher APD the greater the carbon deposition and S/Mo ratio, and hence the greater the stability or metal retention capacity of catalyst. It is also strongly expected that the deposited V<sub>x</sub>S<sub>x</sub> phases provide some auto-catalytic activity on the surface of the catalyst. Thus, HDM catalyst should be essentially macro porous in nature while HDS conversion is hardly effected by porosity.

### Conclusion

The effect of support preparation on the pore size distribution and average pore diameter apparently controls the catalytic activities of heavy crude oil. HDM and HDAs activities significantly depend on the catalyst pore size distribution while the HDS activity may depend on the metal dispersion and surface area of supported catalysts.

### References

1. E. Furimsky, F. E. Massoth, Catal. Today 52 (1999) 381.
2. E.Y. Sheu, Energy Fuels 16 (2002) 74.
3. S. Eijsbouts, Stud. Surf. Sci. Catal. 127 (1999) 21.
4. B.J. Smith, J. Wei, J. Catal. 132 (1991) 21.
5. M.S. Rana, J. Ancheyta, P. Rayo and S.K. Maity, Catal. Today, Accepted.
6. I. Kawada, M.N. Onoda, M. Ishii, M. Nakahira, J. Solid State Chem., 15 (1975) 246.

# ADSORPTIVE DESULFURIZATION OF TRANSPORTATION FUELS OVER NICKEL BASED ADSORBENTS DERIVED FROM LAYERED DOUBLE HYDROXIDES

Jennifer Clemons, Subramani Velu, Xialiang Ma and Chunshan Song\*

Clean Fuels and Catalysis Program  
The Energy Institute and  
Department of Energy and Geo-Environmental Engineering  
The Pennsylvania State University  
209 Academic Projects Building,  
University Park, PA 16802  
\* E-mail: csong@psu.edu

## Introduction

Upcoming environmental regulations are pushing towards cleaner fuels for various uses. The Environmental Protection Agency (EPA) has mandated that the sulfur content of gasoline to be below 30 ppmw by 2006, down from the current average of 300 ppmw. At the same time, the diesel fuel will be required to contain sulfur content well below 15 ppmw. Due to the current interest in fuel cells, ultra clean fuels are needed, because of the low tolerance of contaminants. The PEM fuel cell, which many consider as a good possible fuel cell for automotive applications, requires a transportation fuel with less than 1 ppmw sulfur.

Deep desulfurization has become a more difficult problem as restrictions become tighter and available crude oils contain more sulfur<sup>1</sup>. Traditionally hydrodesulfurization (HDS) has been the most common method of sulfur removal. This process is inconvenient to produce ultra-clean fuels, especially for fuel cell applications<sup>2</sup> because of the high temperature and pressure requirements<sup>1, 3</sup>, which increases the overall system cost<sup>4</sup>. To reduce the sulfur concentration of a gas oil from 500 ppmw to 10 ppmw, the hydrogen pressure in a traditional HDS is needed to be increased by 1.5 to 2 times<sup>5</sup>.

The aromatic sulfur compounds such as 4, 6-Dimethyldibenzothiophene (4,6-DMDBT) are the most difficult ones to remove by the traditional HDS systems<sup>4</sup>. Transportation fuels also contain a significant amount of aromatic compounds, so any type of sulfur removal system should selectively remove only the sulfur compounds without removing aromatics<sup>2</sup>.

Recently, our group has been working on the development of a new process termed as "Selective adsorption for removing sulfur (PSU-SARS)" to produce ultra-clean transportation fuels for fuel cell applications<sup>2, 3, 6</sup>. New adsorbents based on zeolites, supported metals, mixed oxides, metal sulfides, etc are being developed. Among them, Ni-based adsorbents perform better in removing sulfur from gasoline and jet fuels.

The object of the present study was to develop new Ni-based adsorbents derived from hydrotalcite-like layered double hydroxide (LDH) precursors. The LDH materials are represented by a general formula:  $[M(II)_{1-x}M(III)_x(OH)_2]^{x+}[(A^{n-})_{x/n}yH_2O]^{x-}$ , where M(II) = Mg, Ni, Zn, Cu, Co, Mn, etc; M(III) = Al, Fe, Cr, etc, A<sup>n-</sup> is an interlayer anion such as CO<sub>3</sub><sup>2-</sup><sup>7</sup>. These materials upon calcinations offers highly active mixed metal oxides with high metal surface area and high metal dispersion, and employed as catalysts and adsorbents in various chemical processes<sup>8</sup>. A new series of NiZnAl-mixed oxides with different Ni:Zn:Al atomic ratios were synthesized and their adsorption performance in removing organo sulfur compounds from

transportation fuels is being investigated for the first time and the preliminary results are reported here.

## Experimental

A series of NiZnAl-LDHs with different Ni:Zn:Al atomic ratios were synthesized by co-precipitation at a constant pH, around 10<sup>8</sup>. For simplicity the adsorbents are labeled as NiZnAl-A through NiZnAl-E for the Ni:Zn:Al atomic ratios 2:5:1, 3:4:1, 4:3:1, 5:2:1, and 5.5:5.5:1, respectively. A mixed aqueous solution of Ni(NO<sub>3</sub>)<sub>2</sub> \* 6H<sub>2</sub>O, Zn(NO<sub>3</sub>)<sub>2</sub>\*6H<sub>2</sub>O and Al(NO<sub>3</sub>) \* 3.9 H<sub>2</sub>O of appropriate atomic concentrations and an aqueous solution containing a mixture of KOH/K<sub>2</sub>CO<sub>3</sub> were added dropwise by maintaining a constant pH. The precipitate was aged at 65°C for 30 min, filtered, washed with distilled water, dried overnight and then calcined in air at 400°C for 6 hours. The calcined samples were reduced in H<sub>2</sub> flow in a continuous flow reactor at 500°C for 6 h, cooled down to the room temperature in H<sub>2</sub> flow and then sulfur-free n-hexane was passed through the reduced samples. The samples were then retrieved from the reactor and stored in the sulfur-free n-hexane for adsorption experiments. The reduced materials under this condition are non-pyrophoric and could be exposed to air during characterization and adsorption experiments.

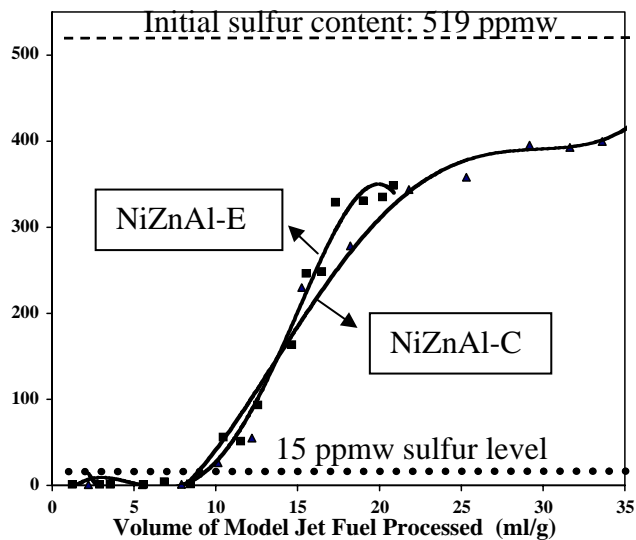
Two different model fuels, representative of diesel and jet fuel were used in the present study. The model diesel contained 100 ppmw each of benzothiophene (BT), dibenzothiophene, (DBT) 4-methylbenzothiophene (4-MDBT) and 4,6-dimethyldibenzothiophene (4, 6-DMDBT), with a total sulfur content of around 400 ppmw. On the other hand, the model jet fuel contained 130 ppmw each of benzothiophene (BT), 2-methylbenzothiophene (2MBT), 5-methylbenzothiophene (5-MBT) and dibenzothiophene (DBT) with a total sulfur content of around 520 ppmw. The model fuels also contained equimolar amounts of Naphthalene, 1-methyl naphthalene and about 10 wt % of n-butylbenzene as aromatics. The adsorbent experiments were performed 200°C using a fixed-bed flow system as described elsewhere<sup>2, 6</sup>. The reduced samples stored in n-hexane were dried in vacuum or at room temperature and then packed in a stainless-steel adsorption column as reported earlier.<sup>2, 6</sup> The materials were treated with H<sub>2</sub> gas at 200°C for 1 h, and then cooled down to the adsorption temperature (room temperature or 200°C). Model fuels with 0.2 cc/min were pumped through the adsorption bed. The treated fuels were collected periodically every 15 min and analyzed using an Antek 9000 Series Sulfur Analyzer, with a detection limit of 0.5ppmw sulfur.

## Results and Discussion

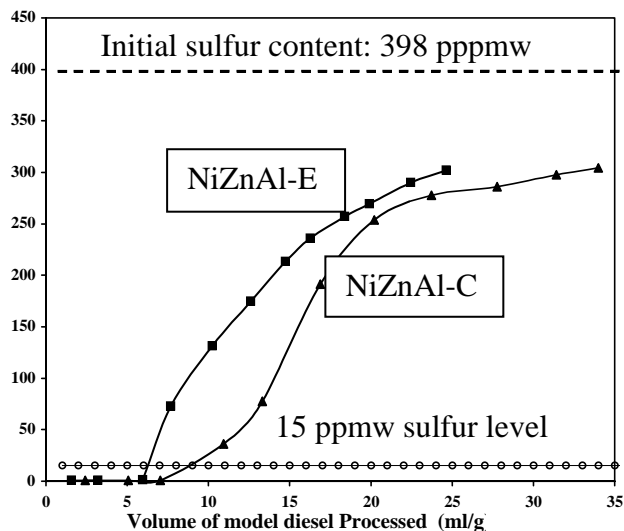
Figure 1 shows the break through curves for the adsorptive desulfurization of the model jet fuel over NiZnAl-C and NiZnAl-E adsorbents. It can be seen that under the present experimental conditions, the breakthrough capacity at 15 ppmw outlet sulfur content is about 10 ml/g of adsorbent in both cases, indicating that both adsorbents behave more or less similarly in removing sulfur compounds from the jet fuel although their chemical compositions are different. The saturation capacity was over 35 ml of the fuel/ g of the adsorbent.

Figure 2 shows the breakthrough curves for the adsorptive desulfurization of a diesel fuel over the same adsorbents tested for the model jet fuel. The breakthrough capacity at 15 ppmw outlet sulfur level over NiZnAl-C is about 8 ml/g while that over NiZnAl-E, it is 6 ml/g. These values are significantly less than that observed in the desulfurization of model jet fuel. Interestingly, the outlet sulfur content does not reach the saturation value even after 30 ml/g of the fuel treatment, which suggests that the adsorbent continue to adsorb the sulfur compounds without reaching the saturation. The early breakthrough observed in the desulfurization of model diesel fuel

compared to model jet fuel is likely due to the presence of 4, 6-DMDBT, in the former, which is more difficult to remove because of the steric hindrance exerted by the methyl groups at the 4-, and 6-positions of the Dibenzothiophene ring.



**Figure 1.** Breakthrough curves for the adsorptive desulfurization of a model jet fuel over NiZnAl-LDH based adsorbents



**Figure 2.** Breakthrough curves for the adsorptive desulfurization of a model diesel over NiZnAl-LDH based adsorbents

Further work on the optimization of chemical composition and experimental conditions in order to improve the adsorption performance is currently in progress and detailed results will be reported.

## Conclusions

New series of Ni-based materials derived from hydrotalcite-like layered double hydroxides are synthesized and their performance in the adsorptive desulfurization of model jet fuel and diesel fuel are studied using fixed-bed adsorption. Under the experimental conditions employed in the present study, these adsorbents exhibit better performance in the desulfurization of jet fuel compared to diesel fuel as the later consists of 4,6-DMDBT, which is more difficult to remove because of the steric hindrance of the methyl groups.

## Acknowledgements

The authors are grateful to the US EPA for the award of NSF/EPA STC grant.

## References

- 1 C. Song and X. L. Ma, *Applied Catalysis B-Environmental*, 2003, **41**, 207.
- 2 S. Velu, X. L. Ma, and C. S. Song, *Industrial & Engineering Chemistry Research*, 2003, **42**, 5293.
- 3 X. L. Ma, L. Sun, and C. S. Song, *Catalysis Today*, 2002, **77**, 107.
- 4 S. G. Zhang, Q. L. Zhang, and Z. C. Zhang, *Industrial & Engineering Chemistry Research*, 2004, **43**, 614.
- 5 M. Breysse, G. Djega-Mariadassou, S. Pessayre, C. Geantet, M. Vrinat, G. Perot, and M. Lemaire, *Catalysis Today*, 2003, **84**, 129.
- 6 S. Velu, X. Ma, and C. Song, *American Chemical Society, Division of Fuel Chemistry*, 2003, **48**, 693.
- 7 F. Cavani, F. Trifiro, and A. Vaccari, *Catalysis Today*, 1991, **11**, 173.
- 8 S. Velu, N. Satoh, C. S. Gopinath, and K. Suzuki, *Catalysis Letters*, 2002, **82**, 145.

# OXIDATIVE DESULFURIZATION: A NEW TECHNOLOGY FOR ULSD

Ron Gatan, Paul Barger, and Visnja Gembicki

UOP LLC  
Des Plaines, Illinois, USA

Agostino Cavanna

Eni S.p.A. Refining and Marketing Division  
Rome, Italy

Daniele Molinari

EniTecnologie S.p.A.,  
Milan, Italy

## Abstract

Oxidative desulfurization is an innovative technology that can be used to reduce the cost of producing ultra-low sulfur diesel (ULSD). The key to successful implementation of this technology in most refinery applications is effectively integrating the oxidative desulfurization unit with the existing diesel hydrotreating unit in a revamp situation.

The economics of applying oxidative desulfurization technology are dependent on the operating pressure of the existing hydrotreating capacity. A case study has been developed to illustrate how this innovative new route can be effectively utilized as an alternative to revamping existing hydrotreaters.

## Introduction

Regulations regarding the sulfur content of motor fuels continue to be enacted worldwide in response to the need for cleaner air. Today, most industrialized countries have regulations in place to reduce diesel fuel sulfur to either 15 or 10 ppm by 2009. Developing countries are progressing environmental quality improvement programs as well, with most electing to enact fuel quality regulations similar to those in place in Europe.

Refiners will meet the challenge of these new regulations at a significant cost. Technology licensors and catalyst manufacturers have continued to progress conventional hydro-desulfurization technology to reduce the capital and operating expense required. Revamping existing intermediate and lower pressure units will typically require addition of significant catalyst volume and equipment modifications to increase the hydrogen purity and circulation rate. However, there is a limit to the cost reduction that can be achieved as hydro-desulfurization (HDS) chemistry requires elevated temperature and pressure for deep desulfurization and, of course, consumes hydrogen in the process. Hydro-desulfurization also cannot readily achieve the very low sulfur levels envisaged for future "zero sulfur" fuels.

There are alternatives to using conventional hydrotreating technology for producing ULSD, including biodesulfurization, physical separation, and oxidative desulfurization. Both biodesulfurization and physical separation processes have not been shown to be economically viable on a commercial scale. Oxidative desulfurization technology, however, has progressed to the state where it is nearing commercialization. Oxidation chemistry represents an alternative route to diesel desulfurization that complements HDS chemistry. The integration of an oxidative desulfurization unit with a conventional hydrotreating unit can

improve the economics of these regulations-driven projects relative to current HDS technology.

Eni S.p.A. recognized the advantages of lower capital and operating cost that oxidative desulfurization can offer and started research efforts to develop new catalysts. UOP LLC had previously developed process technology for integrating oxidative desulfurization units with hydrotreating units that could be applied to the new catalysts.<sup>1,2</sup> In 2002, EniTecnologie S.p.A. and UOP LLC embarked on a collaborative research effort that combined each company's catalyst and process technology expertise to develop the UOP/Eni Oxidative Desulfurization Process, a new sustainable oxidative desulfurization technology that is targeted for commercialization in 2005.

The question that needs to be addressed is how best to meet future low sulfur fuel regulations such as the upcoming off-road diesel specifications in the United States and the potential for "zero sulfur" fuels at some point in the future. The preference has been to make the most with what is available, and a revamp solution is preferable to building new units. Hydrotreating is expensive, particularly for an existing low pressure unit. These units generally have been revamped to meet ULSD specifications by adding a large quantity of catalyst and reducing the available operating cycle. Hydrogen consumption is increased at the higher severity needed for ULSD, which can result in product quality give-away in some instances. The spent catalyst from these units represents a solid waste disposal issue, which combined with the additional CO<sub>2</sub> emissions associated with increased hydrogen demand, points to the need for a more sustainable technology.

A typical feedstock will contain about 30% LCO or other cracked blendstocks, with the balance being straight run diesel. Substantially higher severity is required to produce ULSD in intermediate and low pressure units. A summary of the process conditions typically required for modern HDS catalysts is shown in Table 1. Generally, a significant increase in catalyst volume is required, combined with a shorter process cycle and higher hydrogen circulation.

Table 1. Process Conditions Required for ULSD

	<i>Intermediate Pressure Original vs. New Specifications</i>		<i>Low Pressure Original vs. New Specifications</i>	
Product S, ppm	500	<10	500	<10
LHSV, 1/hr	3.0	1.0	1.5	0.5
Gas/Oil Ratio, SCFB	1500	2000	1000	1500
Cycle Length, months	36	18	24	8

Installation of a new high pressure (750<sup>+</sup> psi) hydrotreating unit is expensive, which is generally avoided unless there is no other option. Typical capital costs for a new 30,000 BPD diesel hydrotreating unit for ULSD will be \$35-\$45 MM on a US Gulf Coast (USGC), inside battery limits (ISBL) basis. High pressure units can typically be easily revamped to make ULSD by changing to a modern HDS catalyst and installation of improved reactor internals, such as UOP's Ultramix™ internals, for better flow distribution. Intermediate pressure (600 psi) units may require a significant revamp depending on the difficulty of the feedstock. A major revamp in these cases will typically include a new reactor for additional catalyst, modification or replacement of the compressors, a hydrogen purification system, and a recycle gas scrubber. This is a relatively high cost revamp, \$10-\$25 MM for a 30,000 BPD unit on the USGC, ISBL basis used by UOP. Operating cost is also higher, ranging from \$0.25/bbl to \$0.50/bbl or higher. The largest cost element is increased

hydrogen consumption in these units. The revamped unit generally operates with a shorter catalyst cycle which translates into higher catalyst cost.

Low pressure (450 psi) units will require either a major revamp or replacement with a new high pressure hydrotreating unit depending on the feedstock available. A major revamp for such a unit will include a new, much larger reactor, new recycle gas compressors, a recycle gas scrubber, and equipment to increase make-up hydrogen purity such as a Polybed™ PSA unit. These are high cost revamps, ranging from \$15-\$30 MM for a 30,000 BPD unit. Operating costs are significantly increased, ranging from \$0.50/bbl to \$0.75/bbl. As in the intermediate pressure case, the operating cycle is typically dramatically shorter in the revamped units and hydrogen consumption is increased. The difficulty of processing cracked feedstocks at low pressure also decreases the flexibility of the unit.

It is clear in this discussion that while hydrotreating is relatively expensive, a new technology has to be cost-effective to be considered as an alternative to revamping existing HDS units to meet ULSD specifications. It is easier to justify a new technology in those instances where the competitive option is a new grassroots unit, but that is only a consideration in about 25% of refineries. UOP and Eni have set development targets for the UOP/Eni Oxidative Desulfurization Process at a capital cost of \$15 MM or less for a 30,000 BPD unit and an operating cost of \$0.25/bbl or less in order to be competitive as an alternative to a major revamp of moderate to low pressure hydrotreaters. Oxidative desulfurization is not a competitive option for high pressure units where only a minor revamp or a simple catalyst replacement is required.

### Oxidative Desulfurization Technology

Oxidative desulfurization is not a new concept and has been discussed for several years in previous publications.<sup>3,4</sup> The advantage that oxidative desulfurization has over conventional HDS is that the difficult-to-desulfurize, refractory-substituted dibenzothiophenes (DBT) are easily oxidized under low temperature and pressure conditions to form the corresponding sulfones. This reaction is shown in Figure 1. The oxidant can be supplied by either hydrogen peroxide/peracid<sup>4</sup> or organic peroxide. Note that there is no hydrogen consumed in this reaction. The sulfones are highly polar compounds and are easily separated from the diesel product by either extraction or adsorption.

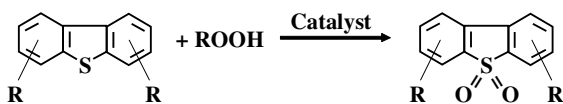


Figure 1. Dibenzothiophene Oxidation Chemistry

This oxidation chemistry is complementary to hydrotreating, as other sulfur compounds such as disulfides are easy to hydrodesulfurize, but oxidize slowly. For this reason, oxidative desulfurization is best utilized as a second stage after an existing HDS unit, taking a low sulfur diesel (~500 ppm) down to ULSD (<10 ppm) levels. In this situation, the diesel product has been depleted of difficult-to-oxidize sulfur species and has a high concentration of the more refractory DBT constituents.

The UOP/Eni Oxidative Desulfurization Process is shown schematically in Figure 2. The process consists of three process steps; an oxidant supply section, a sulfur reaction section, and finally a sulfone separation section. The UOP/Eni technology uses an organic peroxide as an oxidant. The oxidant supply section can consist either of the handling equipment associated with purchased organic peroxide such as t-butyl-hydro-peroxide, or the peroxide can be generated internally via direct oxidation of a hydrocarbon with air.

The oxidant from the oxidant supply section is first mixed with hydrotreated diesel and then sent to the sulfur reaction section. The sulfur reaction section operates at low temperature and pressure, less than 200°F and less than 100 psig. The reaction occurs in the presence of a proprietary heterogeneous catalyst in a conventional fixed bed reactor. The use of an organic peroxide as the oxidant avoids the need to recycle corrosive organic acid catalysts that are needed when hydrogen peroxide is used. Very high conversion is obtained in the sulfur reaction section, in excess of 98% conversion of organic sulfur compounds.

The final step is the sulfone separation section. The sulfones are polar molecules so they are easily separated by either extraction or adsorption. UOP and Eni have evaluated both routes, and have concluded that the adsorption route is more cost-effective. The adsorption section also serves to remove any trace by-products formed during the oxidation and reaction steps. The sulfones that are separated can either be processed in a coker or can be blended directly into the heavy fuel oil pool in some locations.

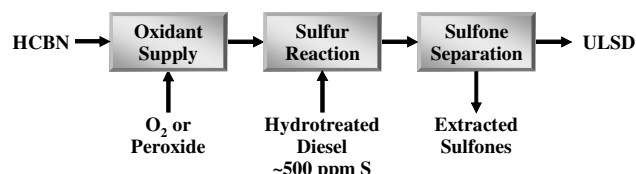


Figure 2. UOP/Eni Oxidative Desulfurization Process

During development of the process flow scheme, a number of key economic issues surfaced that are essential for the oxidative desulfurization process to compete with revamping conventional hydrotreating units for ULSD production. The major hurdles addressed were:

- Oxidant cost
- Minimize equipment
- Minimize operating costs
- Maximize ULSD yield
- Disposition of the sulfone extract

An engineering analysis of the operating and equipment costs for all sections was conducted that highlighted where innovations were needed to meet the development targets of <\$0.25/bbl operating cost and <\$15 MM capital cost. The sections that have the largest impact on cost of the unit are the oxidant supply and sulfone separation sections. This was not too surprising, as these sections have the largest number of equipment items and require product fractionation. Efforts were then focused on reducing the cost of these two sections.

There are a number of issues associated with using purchased organic peroxides in the process, the chief being the high cost and limited availability of these materials. The purchase cost adds \$0.30 to \$0.40/bbl to the operating expense, in excess of the required target operating cost. Other safety issues associated with handling and storage of organic peroxides on-site can be addressed technically but will add significant capital cost to the unit. Eni and UOP have decided that the best solution to this problem is to generate the peroxides in situ using an easily oxidizable hydrocarbon and air. We have identified catalysts that are active for the oxidation reaction and are completing the process development necessary for commercialization.

A number of different designs were evaluated for the sulfone separation section, including liquid-liquid extraction and several different adsorber configurations. Extraction is technically viable, but

has a high capital and operating cost, and can be difficult to operate. A high capacity adsorbent was identified that made the adsorption section technically feasible. UOP based the adsorber design on our commercial experience with similar separation applications in other technologies. The configuration used has a low capital cost, low diesel yield loss, and nearly complete sulfone removal from the diesel product.

### Oxidative Desulfurization Economics

UOP and Eni conduct extensive techno-economic feasibility studies as part of the development process to ensure that the technologies in development are competitive with alternatives that are available to refiners. A case study was selected to illustrate how oxidative desulfurization can be effectively applied as an alternative to revamping conventional hydro-desulfurization technology. The utility and product values used in this analysis were based on energy pricing current in 4Q03.

The value of hydrogen is critical in any comparisons of hydroprocessing technology options. In the case studies considered here, the hydrogen value used was \$2.25/MSCF. This value was calculated based on a 4Q03 Henry Hub natural gas price of \$4.50/MM BTU.<sup>5</sup> Typical hydrogen plant operating costs were used to calculate the hydrogen value used based on this assumed natural gas feedstock price.

### Case Study

The scenario assumed is an existing diesel hydrotreater, designed for processing 30 MBPD of a 70% straight run/30% LCO blend at 600 psi, producing 400 ppm low sulfur diesel. The unit design parameters are listed in Table 1 for intermediate pressure revamps. The changes required are:

- Decrease LHSV from 3 to 1 hr<sup>-1</sup>
- Reduction in process cycle from 36 to 18 months
- 33% increase in hydrogen consumption ( $\Delta$  150 SCF/bbl)
- Requires new reactor, compressors, and recycle gas scrubber

The critical performance parameters and economic values are summarized in Table 2 for both the base case operation at 400 ppm sulfur and the requirements for ULSD. A capital cost estimate for this revamp was \$18.5 MM on a USGC, ISBL basis. The operating cost increased \$0.45/bbl over the base case operation, nearly all due to the increased hydrogen consumption.

**Table 2. 600 psi Diesel Hydrotreater Revamp Case Study**

<i>Parameter</i>	<i>Base Operation</i>	<i>Conventional Revamp</i>	<i>Oxidative Desulfurization</i>
Diesel Sulfur, wt-ppm	400	<10	<10
Diesel Yield, lv-%	98.5	97.0	97.0
Capital Cost, \$MM	—	18.5	16.0
Hydrogen Cost, \$MM/yr	10.0	13.4	10.0
Utilities Cost, \$MM/yr	0.8	1.0	2.5
Catalyst Cost, \$MM/yr	0.3	1.3	1.5
Total Operating Cost, \$MM/yr	11.1	15.7	14.0
Delta Product Value, \$MM/yr	1.7	2.0	1.7
Total Operating Cost, \$bbl	0.97	1.42	1.28
ANPV, (10%, 10 yr), \$MM	—	<41>	<31>

The alternative to the conventional revamp is to install an oxidative desulfurization unit. In this case, the original HDS unit continues to produce 400 ppm sulfur product, with the oxidative desulfurization unit used to make ULSD. A capital cost of \$16 MM

was estimated for the unit, which is equivalent to \$533/bbl. The operating cost was estimated at \$0.31/bbl over the base case operation. While both values are slightly above the development target values, the economics are attractive relative to the conventional revamp. The calculated incremental net present value (10% interest rate and 10 year project life) was \$10 MM higher for the oxidative desulfurization case. This significant improvement in economics is due to eliminating the additional hydrogen consumption by installation of the oxidative desulfurization section.

### The Future of Oxidative Desulfurization

The study presented in this paper has demonstrated that oxidative desulfurization can play an important role in future technical strategies to produce ULSD. This technology can be considered to be a viable option for new ULSD projects that will be implemented in 2006 and beyond. Oxidative desulfurization technology also holds promise for both reducing operating cost and improving the sustainability for low pressure units where substantial investments have already been made. The key to success is that the oxidative desulfurization process must be cost-effective versus the HDS revamp alternatives available to refiners.

Over this coming year, UOP and Eni will continue to conduct studies in our continuous pilot plants to fully demonstrate the UOP/Eni Oxidative Desulfurization Process. The key aspects to be demonstrated include long-term catalyst stability in an integrated operation over a range of commercial feedstocks. We will continue to optimize our engineering design to improve the cost-effectiveness of the process.

Eni is considering implementation of an oxidative desulfurization unit as an alternative to revamping an existing intermediate pressure hydrotreater at an Eni refinery in Italy. The basic design of this unit is scheduled to start at the end of 2004, with construction starting in the second half of 2005. This will be a full scale commercial unit to produce ULSD meeting the 2009 regulations in Europe.

### Summary

Oxidative desulfurization technology offers a non-hydrogen consuming, lower capital cost, more sustainable alternative to conventional hydrodesulfurization technology. The technology can be applied as part of an effective strategy for both an alternative to revamping intermediate and low pressure HDS units to produce ULSD, or as a means to reduce the operating cost of low pressure units that have already been revamped. Oxidative desulfurization can also be considered as an attractive revamp opportunity for any existing unit where construction of new high-pressure HDS units is the alternative.

### References

- (1) Cabrera, C.A.; Imai, T., US Patent 6,171,478 assigned to UOP LLC.
- (2) Kocal, J.A.; Brandvold, T.A., US Patent 6,638,495 assigned to UOP LLC.
- (3) Liotta, F.J.; Yuan, Z.H., "Production of Ultra-low Sulfur Fuels by Selective Hydroperoxide Oxidation," AM-03-23, NPRA 2003 Annual Meeting.
- (4) Levy, R.E.; Pappas, A.S.; Nero, V.P.; DeCanio, S.J., "Unipure's ASR-2 Diesel Desulfurization Process: A Novel, Cost-Effective Process for Ultra-low Sulfur Diesel Fuel," AM-01-10, NPRA 2001 Annual Meeting.
- (5) *Oil and Gas Journal*, Vol. 101, Number 41, October 27, 2003, "Industry Scoreboard," pg. 4.

# REMOVAL OF HYDROGEN SULFIDE AND CARBONYL SULFIDE FOR PURIFICATION OF BIOMASS-GASIFIED SYNTHETIC GAS USING ACTIVE CARBONS

Kinya Sakanishi<sup>1)\*</sup>, Akimitsu Matsumura<sup>1)</sup>, Ikuo Saito<sup>1)</sup>, Toshiaki Hanaoka<sup>2)</sup>, and Tomoaki Minowa<sup>2)</sup>

1) Institute for Energy Utilization, National Institute of Advanced Industrial Science and Technology (AIST) Tsukuba Center West, Tsukuba, Ibaraki 305-8569, Japan

2) Biomass Technology Research Laboratory, AIST Chugoku Center, Kure, Hiroshima 737-0197, Japan

## Introduction

Removal of sulfur-containing compounds is one of the most important technologies for the utilization of gasified products derived from various feedstocks such as biomass, waste, and solid fossil fuels. Especially, gaseous sulfur compounds of H<sub>2</sub>S and COS are severe catalyst poisons against the following processes of steam reforming for hydrogen production or FT-synthesis.<sup>1,2</sup>

Various researches for H<sub>2</sub>S removal have been already reported in details for the purification of gasified products derived from various feedstocks,<sup>3-5</sup> however, removal of COS is not concerned yet as much as H<sub>2</sub>S, because COS are not the major sulfur compounds produced from the gasification of biomass and other wastes feedstocks.<sup>6,7</sup> In addition, the removal of COS is more difficult than H<sub>2</sub>S, since COS is inactive compared to H<sub>2</sub>S, probably resulting from its neutrality and similarity to CO<sub>2</sub>. What is worse, COS is sometimes produced through the reaction of H<sub>2</sub>S with CO<sub>2</sub>.

Carbon-based adsorbents such as active carbons and activated carbon fibers have been widely applied for the purification procedures of gas and water, and the selective adsorption of a specific compound from various gaseous mixtures produced from gasification and other conversion processes.<sup>8-10</sup> Although gaseous sulfur compounds such as H<sub>2</sub>S and COS contaminated in the synthetic gas products have been conventionally removed by cold and wet procedures, recently, hot gas cleaning procedures are required to be developed for the utilization of highly purified synthetic gas for F-T synthesis and hydrogen of high purity for fuel cell application. For the complete removal of H<sub>2</sub>S, higher temperatures around 500 °C are preferred because H<sub>2</sub>S is captured completely by the reaction with catalytic materials such as ZnO and Fe<sub>2</sub>O<sub>3</sub> in a absorption manner.<sup>3-5</sup>

In the present study, the adsorption behaviors of H<sub>2</sub>S and COS are investigated using active carbon adsorbents in the middle range of temperatures (300 – 400 °C), because tarry compounds produced from biomass gasification have been reported to be effectively removed in this temperature range.<sup>11,12</sup> Sulfur-containing and other contaminants such as vaporized alkali metals are expected to be captured with the tarry byproducts at the same time. Another advantage is that the following catalytic processes of F-T synthesis are operated around 300 °C, hence a directly coupled gasification process of biomass can be designed by the combination of such hot gas cleaning with catalytic F-T synthesis.

## Experimental

100 ppm of H<sub>2</sub>S and COS standard gases in N<sub>2</sub> balance was used for the adsorption treatments.

Two types of commercially available active carbons (abbreviated as AC-1 and AC-2) were used in the present study. Their surface areas and average pore diameters are 1120 m<sup>2</sup>/g, 1.7 nm and 490 m<sup>2</sup>/g, 0.97 nm, respectively.

Figure 1 illustrates the adsorption equipments applied to the present experiments.

The adsorption amounts of H<sub>2</sub>S and COS were quantified with the sampled gas out of the bottom of adsorption column by using their detector tubes which are commercially available for the detection and quantification of H<sub>2</sub>S and COS.

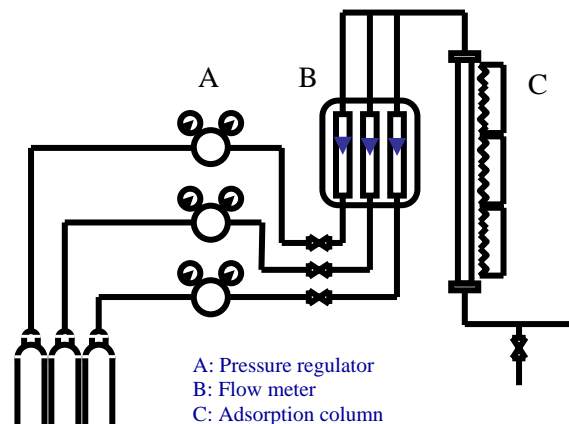


Figure 1. Adsorption apparatus for removal of H<sub>2</sub>S and COS

## Results and Discussion

**Adsorption behaviors of H<sub>2</sub>S.** Figure 2 illustrates the adsorption results of 100 ppm H<sub>2</sub>S in N<sub>2</sub> with glass beads as a blank test for H<sub>2</sub>S adsorption at variable temperatures in the temperature range from 100 to 400 °C. In the temperature range between 100 and 200 °C, about 20 % of H<sub>2</sub>S was adsorbed with glass beads, however, at the higher adsorption temperatures, about 40 % and 70 % of H<sub>2</sub>S were removed at 300 and 350 °C, respectively. It is noted that 100 ppm of H<sub>2</sub>S was completely and stationarily removed at the higher temperature of 400 °C even with glass beads. These results suggest that H<sub>2</sub>S may not only adsorb on the glass beads, but also react with each other or with some other materials at the higher temperatures in the adsorption column system.

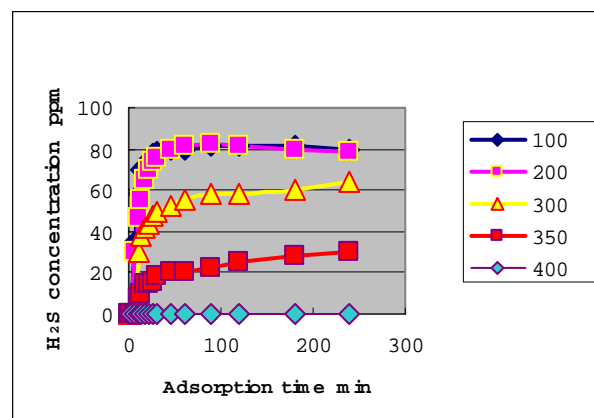
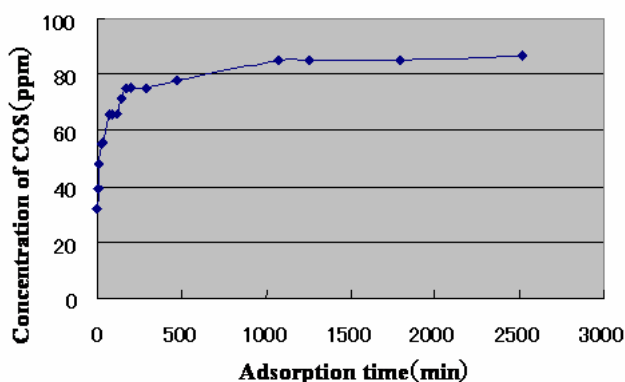


Figure 2. Blank adsorption test of 100 ppm H<sub>2</sub>S with glass beads at variable temperatures (50 ml/min H<sub>2</sub>S)

In the adsorption of H<sub>2</sub>S with active carbons of AC-1 at 300 °C, 100 ppm of H<sub>2</sub>S was completely and stationarily removed for the longer adsorption time of 80 h even with the higher flow rate of 150 ml/min of H<sub>2</sub>S.

AC-2 of the smaller surface area and pore diameter exhibited the similar adsorption behavior and capacity of H<sub>2</sub>S at 300 °C to those of AC-1, while AC-1 of the larger surface area and pore diameter showed the much higher performance in the dry removal of tarry compounds produced from biomass gasification.<sup>11,12</sup> The larger surface area and pore diameter may be essential to the efficient capture and removal of both gaseous sulfur-containing compounds and tarry by-products, although they should be carefully optimized depending upon the gasified feedstock, gas composition, and adsorption conditions.

**Adsorption behaviors of COS.** Figure 3 illustrates the adsorption breakthrough curve of COS over AC-1 at 300 °C. Unlike with the case of H<sub>2</sub>S, about 30 % of COS was eluted from the starting point, and the eluted amount of COS drastically increased in the first 500 min adsorption, being saturated to the level around 85 % from the adsorption time over 1000 min.



**Figure 3** Adsorption treatment of COS with active carbon at 300 °C (AC 2 g, H<sub>2</sub>S: 100ml/min)

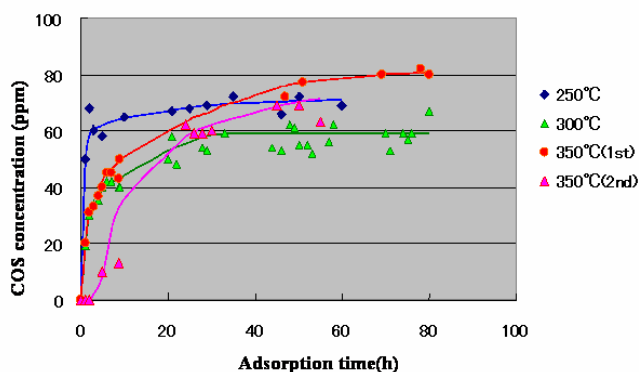


**Fig. 4** Adsorption treatment of COS with active carbon at variable temperatures

(COS initial conc.: 100 ppm, 50 ml/min, Active carbon: 5g)

Figure 4 illustrates the adsorption breakthrough curves of COS over AC-1 at variable temperatures. The breakthrough profiles were similar regardless of the adsorption temperatures, showing prompt breakthrough points within the initial 20 h, followed by gradual saturation at the longer adsorption times of 20 to 80 h. However, the

stationary adsorption levels of COS with AC-1 after the saturation were different depending upon the adsorption temperatures, showing the order of 250 °C > 350 °C > 300 °C. It is interesting to note that the adsorption capacity of COS with AC-1 is higher at 300 °C than that at 350 °C, suggesting that COS adsorption may be most favorable at around 300 °C probably because of the balanced chemical adsorption and physical desorption at 300 °C.

It is also pointed out that the repeated adsorption (2nd in Figure 4) profile of COS at 350 °C was similar to the initial breakthrough curve, although the breakthrough points looked like shifted to the longer adsorption time.

## Conclusion

The present study revealed that contrast adsorption profiles of H<sub>2</sub>S and COS over active carbon were obtained in the temperature range from 200 to 400 °C, showing the much higher adsorption capacity of H<sub>2</sub>S probably due to the stronger acidity and polarity of H<sub>2</sub>S than those of COS. The stationary adsorption capacities of H<sub>2</sub>S and COS seem to be optimized at around 400 °C and 300 °C, respectively, of which temperatures may balance the chemical adsorption and physical desorption regardless of their contrast adsorption levels. The adsorption mechanisms of H<sub>2</sub>S and COS are not clear yet, however, the possibility of chemical decomposition of H<sub>2</sub>S and COS is suggested to produce H<sub>2</sub> and CO, respectively by the direct desulfurization over the active carbon adsorbent at around 300 °C.

**Acknowledgment.** The authors are grateful to JFE Engineering Co. for their financial support and providing the active carbon samples.

## References

- Ahmed, M.A., Garcia, E., Alonso, L., Palacios, J.M., *Appl. Surf. Sci.*, **2000**, 156, 115.
- P. Hasler, P. and Nussbaumer, T., *Biomass & Bioenergy*, **1999**, 16, 385.
- Ikenaga, N., Ohgaito, Y., Matsushima, H., Suzuki, T., *Fuel*, **2004**, 83, 661.
- Slimance, R.B. and Abbasian, J., *Ind.Eng.Chem.Res.*, **2000**, 39, 1338.
- Sasaoka, E., Hatori, M., Yoshimura, H., Su, C., Uddin, M.A., *Ind.Eng.Chem.Res.*, **2001**, 40, 2512.
- Svoronos, P.D.N. and Bruno, T.J., *Ind.Eng.Chem.Res.*, **2002**, 41, 5321.
- Ferm, R.J., *Chem.Rev.*, **1957**, 57, 621.
- Cal, M.P., Strickler, BW, Lizzio, A.A., *Carbon*, **2000**, 38, 1757.
- Bandosz, T.J., *Carbon*, **1999**, 37, 486.
- Cal, M.P., Strickler, BW, Lizzio, A.A., *Carbon*, **2000**, 38, 1767.
- Hanaoka, T., Sakanishi, K., Minowa, T., *Proc. 2<sup>nd</sup> World Conf. Tech. Exhibit. Biomass for Energy, Industry and Climate Protection*, Rome, Italy, 10-14 May **2004**.
- Hanaoka, T., Sakanishi, K., Minowa, T., *J. Inst. Energy Jpn.* in submission.

# CARBON DIOXIDE REFORMING OF METHANE OVER SUPPORTED MOLYBDENUM CARBIDE CATALYSTS

D. Treacy and J.R.H. Ross

Centre for Environmental Research, University of Limerick, Ireland

## Introduction

CO<sub>2</sub> reforming of CH<sub>4</sub> is a subject of considerable interest due to the ability of the reaction to produce synthesis gas with low H<sub>2</sub>/CO ratios (~1); higher ratios can be obtained by combining the process with steam reforming or partial oxidation. Ni-based catalysts are commonly used for reforming reactions but suffer from problems due to carbon deposition. Noble metal catalysts, in particular Pt-ZrO<sub>2</sub>, have been shown to have high activities for CO<sub>2</sub> reforming while resisting significant C deposition [2,3]; however, because of their relatively high cost, their potential for use as CO<sub>2</sub> reforming catalysts is limited. The group VI transition metal carbides, WC and Mo<sub>2</sub>C, have been reported to have catalytic properties similar to those of the noble metals and York *et al.* [4,5,6] have shown that unsupported Mo<sub>2</sub>C and WC have good activities as CO<sub>2</sub> reforming catalysts. However, they found that these catalysts deactivated after short periods of use at ambient pressures. We have shown that the deactivation of the carbides is caused by the formation of the corresponding oxides [7]. In this paper, we show that when Mo<sub>2</sub>C is supported on a variety of supports, the resultant catalysts are somewhat more stable.

## Experimental

**Catalyst Preparation.** The supports used in this study, ZrO<sub>2</sub> (Norton), Al<sub>2</sub>O<sub>3</sub> (Alkan) and SiO<sub>2</sub> (Alfa), were calcined at 800°C for 15 h in a flow of 50 cm<sup>3</sup>min<sup>-1</sup> of air. The support was then impregnated with a solution of heptamolybdate (Johnson Matthey) with, when appropriate, the nitrates of the promoter species (Co, Ni or Bi) and calcined once more before carburising) in flow of 20 %v/v CH<sub>4</sub>/H<sub>2</sub> following a procedure outlined by Lee *et al.* [8], ramping the temperature to 750°C at a ramp rate of 1Kmin<sup>-1</sup>.

**Catalyst Testing.** The CO<sub>2</sub> reforming of CH<sub>4</sub> was carried out in the quartz plug flow reactor used for carburising. The reactants compositions were typically CO<sub>2</sub>/CH<sub>4</sub>/N<sub>2</sub> = 50/50/5 cm<sup>-1</sup>min<sup>-1</sup>. The N<sub>2</sub> was included as an internal standard.

**Characterisation by Raman Microprobe Spectroscopy.** The 514.5 line of an Ar<sup>+</sup> ion laser was used for excitation. Measurements were made at room temperature.

## Results and Discussion

**Catalyst Activity.** Fig. 1. shows the results of CO<sub>2</sub> reforming of CH<sub>4</sub> at 950°C and atmospheric pressure using the 5 wt% Mo<sub>2</sub>C-Al<sub>2</sub>O<sub>3</sub>, 5 wt% Mo<sub>2</sub>C-ZrO<sub>2</sub> and 5 wt% Mo<sub>2</sub>C-SiO<sub>2</sub> catalysts. The performance of a sample of unsupported Mo<sub>2</sub>C under similar reaction conditions is also shown for comparison. The Mo<sub>2</sub>C-Al<sub>2</sub>O<sub>3</sub> sample gave the highest initial activity, with a CO<sub>2</sub> conversion of 63%, while Mo<sub>2</sub>C-ZrO<sub>2</sub> also gave a relatively high CO<sub>2</sub> conversion of 48%. Mo<sub>2</sub>C-SiO<sub>2</sub> was a poor CO<sub>2</sub> reforming catalyst, giving a CO<sub>2</sub> conversion of 18%. However, the Mo<sub>2</sub>C-Al<sub>2</sub>O<sub>3</sub> deactivated almost completely after 4 h of operation whereas the ZrO<sub>2</sub>- and SiO<sub>2</sub>-supported materials remained comparatively stable over the period of the test; indeed, the Mo<sub>2</sub>C-ZrO<sub>2</sub> sample was active even after 80 h at

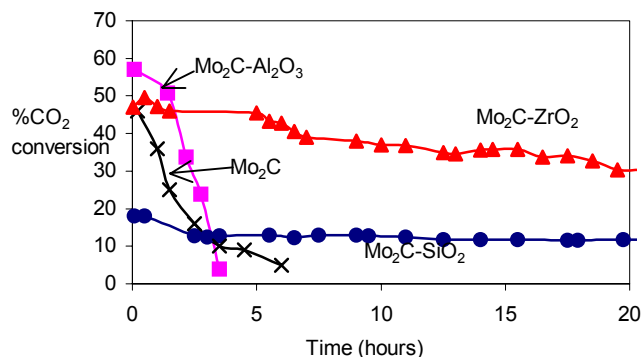


**Figure 1.** CO<sub>2</sub> reforming of CH<sub>4</sub> using (1) Mo<sub>2</sub>C, (2) 5wt% Mo<sub>2</sub>C-Al<sub>2</sub>O<sub>3</sub>, (3) 5wt% Mo<sub>2</sub>C-ZrO<sub>2</sub> and (4) 5wt% Mo<sub>2</sub>C-SiO<sub>2</sub>. [950°C, CO<sub>2</sub>/CH<sub>4</sub>/N<sub>2</sub>: 50/50/5 ml/minute, 0.33g catalyst].

950°C (not shown). The unsupported Mo<sub>2</sub>C sample deactivated after 7 h. We have previously shown [7] that the deactivation of the unsupported carbide catalyst was due to the formation of the inactive MoO<sub>2</sub> phase under conditions where re-oxidation by CO<sub>2</sub> was thermodynamically favoured. Naito *et al.* [9] have argued that the deactivation of Mo<sub>2</sub>C-supported catalysts is due not to MoO<sub>2</sub> formation but to C deposition on the catalyst surface. TG analysis showed that the level of C deposition on the Mo<sub>2</sub>C-ZrO<sub>2</sub> material during CO<sub>2</sub> reforming was relatively insignificant in comparison with that on the Mo<sub>2</sub>C-Al<sub>2</sub>O<sub>3</sub> material [10]. These results are similar to those which we have reported previously [3] for Pt supported on Al<sub>2</sub>O<sub>3</sub> and ZrO<sub>2</sub>; coke was not deposited to any significant extent on the Pt-ZrO<sub>2</sub> sample while large amounts of coke were detected during CO<sub>2</sub> reforming on the Pt-Al<sub>2</sub>O<sub>3</sub> sample. The reaction on the Pt-ZrO<sub>2</sub> appeared to take place at the interface between the Pt and the support and to involve an oxidation-reduction mechanism in which the zirconia takes part in the reaction [11]. There may be a similar explanation for the beneficial effect of the zirconia as a support for the Mo carbide phase.

**Raman Spectroscopy.** Raman spectroscopy was used to examine whether there was any difference in the surface interactions between the support and the MoO<sub>3</sub> prior to the formation of the carbide phase. Fig. 2 shows the Raman spectrum for the 5wt%MoO<sub>3</sub>-Al<sub>2</sub>O<sub>3</sub> material prior to reduction/carburisation. Although the spectrum has a poor signal to noise ratio, it is similar to that reported by Cheng and Schrader [12]. The bands at 590 and 943 cm<sup>-1</sup> are due

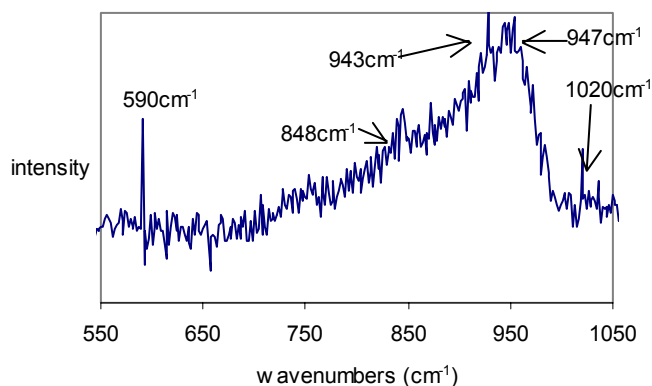


**Figure 2.** Raman spectrum of 5wt% Mo<sub>2</sub>C-Al<sub>2</sub>O<sub>3</sub>.

to the presence of the polymolybdate species,  $\text{Mo}_7\text{O}_{24}^{6-}$ , while the broad band centred at around  $970\text{cm}^{-1}$  is due to the presence of a different polymolybdate species,  $\text{Mo}_8\text{O}_{26}^{4-}$ . The weak bands at  $1020$  and  $848\text{cm}^{-1}$  also indicate the presence of crystalline  $\text{MoO}_3$  [13]; these bands are significantly smaller than that due to the  $\text{Mo}_8\text{O}_{26}^{4-}$  species. In agreement with the results of Cheng and Schrader, there was no evidence for the formation of any aluminium molybdate compounds for the sample used here (calcined at  $600^\circ\text{C}$ ). Abello *et al.* [14] also showed, using XRD, TPR and  $\text{NH}_3$ -TPD, that  $\text{Al}_2(\text{MoO}_4)_3$  formation was prevented when  $\text{MoO}_3$ - $\text{Al}_2\text{O}_3$  was calcined at  $600^\circ\text{C}$ . We therefore conclude that the predominant species on the surface of the alumina prior to carburisation are adsorbed polymolybdate species and that no amorphous  $\text{Al}_2(\text{MoO}_4)_3$  is formed.

Fig. 3 shows the equivalent Raman spectrum for the 5wt%  $\text{MoO}_3$ - $\text{ZrO}_2$  catalyst prior to carburisation. The band at  $953\text{cm}^{-1}$  indicates the presence of adsorbed polyoxomolybdate while the bands at  $749$ ,  $942$  and  $1000\text{cm}^{-1}$  can be ascribed to the presence of bulk  $\text{Zr}(\text{MoO}_4)_2$  species. There was no evidence of the presence of crystalline  $\text{MoO}_3$  species [15]. A Raman spectrum of the precarbided  $\text{MoO}_3$ - $\text{SiO}_2$  catalyst (not shown here) shows that the predominant molybdenum species on the surface of the catalyst was a silicomolybdate species [10]. Polymolybdate surface species do not interact strongly with the support and are therefore highly polarized and easily reduced [16]. The strong interactions created when Mo reacts with the support material decreases the covalency of the Mo-O bonds and therefore stabilises the Mo species; this in turn decreases the reducibility of any such compounds [17]. The presence of the

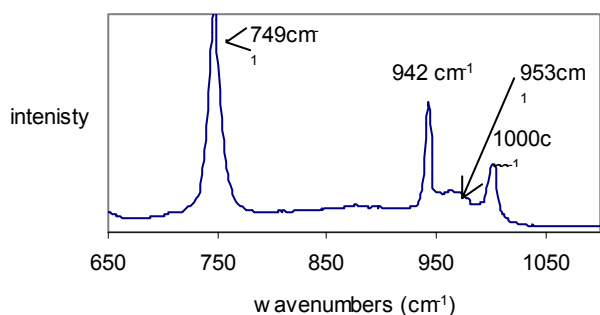


**Figure 3.** Raman spectrum of 5wt%  $\text{MoO}_3$ - $\text{ZrO}_2$ .

easily reducible polymolybdate species on  $\text{Al}_2\text{O}_3$  and, to a lesser extent, on  $\text{ZrO}_2$  enables a significant quantity of  $\text{Mo}_2\text{C}$  to be produced during the temperature programmed reduction/carburisation step of the preparation. This in turn leads to the formation of a larger number of active sites on the surface of the resultant catalyst. On the other hand, the Mo-Si material is difficult to reduce; the amount of  $\text{Mo}_2\text{C}$  produced during the temperature programmed reduction/ carburisation step for this sample (and to a lesser extent with the zirconia-supported material) is therefore probably less than that with the most active  $\text{Mo}_2\text{C}$ - $\text{Al}_2\text{O}_3$  catalyst. TPO experiments [10] support this conclusion: with the  $\text{Mo}_2\text{C}$ - $\text{Al}_2\text{O}_3$  sample, 46% of the total possible amount of carbide was formed during the TPR preparation step while, with  $\text{Mo}_2\text{C}$ - $\text{ZrO}_2$  sample, the amount of carbide formed was only 35%.

**Optimisation of the  $\text{Mo}_2\text{C}$ - $\text{ZrO}_2$  sample and the effect of promoters.** We have examined a series of  $\text{Mo}_2\text{C}$ - $\text{ZrO}_2$  catalysts doped with 1wt% metal oxide promoters (Ni, Bi, Co) to investigate their potential improvement to the activity of the catalyst. The results of this study are summarised in Table 1. The presence of Ni and Co did not significantly change the %  $\text{CO}_2$  conversion relative to that

with the unprompted  $\text{Mo}_2\text{C}$ - $\text{ZrO}_2$  catalyst. However, the 1wt%Bi-5wt% $\text{Mo}_2\text{C}$ - $\text{ZrO}_2$  catalyst gave a  $\text{CO}_2$  conversion of 74.6%, this representing an increase of 16.6% relative to the unprompted material. An explanation of this promotion is as yet unclear and further characterisation needs to be done; however, it has been suggested by Lietti *et al.* [18] that Bi changes the redox properties of the surface Mo and an effect of this sort may have a role here.

**Table 1. Results for the  $\text{CO}_2$  reforming of  $\text{CH}_4$  using different supported  $\text{Mo}_2\text{C}$  catalysts. [ $950^\circ\text{C}$ , 50/50/5 ml/minute  $\text{CO}_2/\text{CH}_4/\text{N}_2$ , 0.33g catalyst]. All the catalysts were calcined at  $400^\circ\text{C}$  prior to carburisation. Results recorded after 3 hours of testing.**

Mo phase	Promoter	Support	% $\text{CO}_2$ conversion
$\text{Mo}_2\text{C}$	-	$\text{ZrO}_2$	58
$\text{Mo}_2\text{C}$	Bi	$\text{ZrO}_2$	74.6
$\text{Mo}_2\text{C}$	Ni	$\text{ZrO}_2$	59.4
$\text{Mo}_2\text{C}$	Co	$\text{ZrO}_2$	55.6

### Conclusions

Of all the catalysts tested  $\text{Mo}_2\text{C}$ - $\text{ZrO}_2$  was the most promising due to its stability and reasonably high activity. The activity of this catalyst can be improved by increasing the reducibility of the precarbided  $\text{MoO}_3$  surface material. This could be achieved using a number of methods, including low calcination temperatures and the addition of small amounts of a Bi promoter to the catalyst.

### References

- [1] K. Seshan, H.W. ten Barge, W. Hally, A.N.J. van Keulen and J.R.H. Ross, *Stud. Surf. Sci. Catal.*, 81 (1994) 285.
- [2] A.M. O'Connor and J.R.H. Ross, *Catal. Today*, 46 (1998) 203.
- [3] J.R.H. Ross, A.N.J. van Keulen, M.E.S. Hegarty and K. Seshan, *Catal. Today*, 30 (1996) 193. 65.
- [4] A.P.E. York, J.B. Claridge, C. Marquez-Alvarez, A.J. Brungs, S.C. Tang and M.L.H. Green, *Stud. Surf. Sci. Catal.*, 110, (1997) 711.
- [5] J.B. Claridge, A.P.E. York, A.J. Brungs, C. Marquez-Alvarez, J. Sloan, S.C. Tsang and M.L.H. Green., *J. Catal.* 180 (1998) 85.
- [6] A.J. Brungs, A.P.E. York and M.L.H. Green, *Catal. Lett.*, 57 (1999).
- [7] D. Treacy, E. Xue, J.R. H. Ross, paper presented at 6<sup>th</sup> NGC Symposium, Alaska, June (2001).
- [8] J.S. Lee, S.T. Oyama, M. Boudart, *J. Catal.* 103 (1987) 125.
- [9] S. Naito, M. Tsuji, T. Miyao, *Catal. Today*, 77 (2002) 161.
- [10] D. Treacy, J.R.H. Ross, *in preparation*.
- [11] A.M. O'Connor, F.C. Meunier, J.R.H. Ross, *Stud. Surf. Sci. Catal.*, 119 (1998) 819.
- [12] C.P. Cheng, G.L. Schrader, *J. Catal.* 60 (1979) 276.
- [13] D.S. Kim, K. Segawa, I.E. Wachs, *J. Catal.* 136 (1992) 539.
- [14] M.C. Abello, M.F. Gomez, O. Ferretti, *Appl. Catal. A: Gen.*, 207 (2001) 421
- [15] B. Zhao, Z. Wang, H. Ma, Y. Tang, *J. Mol. Catal. A*, 108 (1996) 167.
- [16] M. Del Arco, S.R.G. Currazan, V. Rives, V.J. Llambias, P. Melet, *J. Catal.* 141 (1993) 48.
- [17] J.L. Brito, J. Laine, *J. Catal.* 139 (1993) 540.
- [18] L. Lietti, G. Ramis, G. Busca, F. Bregani, P. Forzatti, *Catal. Today*, 61 (2000) 187.

# A STUDY OF THE EFFECT OF DOPANTS WITH PD/CERIA IN THE WGS REACTION

Sufang Zhao and Raymond J. Gorte

Department of Chemical Engineering, University of Pennsylvania, Philadelphia, PA, 19104

## Introduction

There is a need for better water-gas shift (WGS) catalysts for the development of efficient fuel processors for fuel-cell applications [1,2]. Materials that are typically used for the WGS reaction in large-scale operations, such as Cu/ZnO, are not applicable for many fuel-cell applications due to the fact that they are sensitive to start-up/shut-down cycles and may be pyrophoric [1,2]. Ceria-supported, precious-metal catalysts are one class of materials that have been identified as exhibiting very interesting properties for the WGS reaction with fuel cells [1-5].

One of the most intriguing scientific aspects of ceria catalysis is that its properties depend strongly on pretreatment conditions and on doping with other oxides. In recent work from our laboratory [6], the effect of a large number of promoters was investigated on Pd/ceria catalysts. The majority of these "promoters" (Tb, Gd, Y, Sn, Sm, Pr, Eu, Bi, and Cr) had minimal effect on the catalytic activity. However, two kinds of "promoters" (Fe and Mo) had dramatic effect over Pd/ceria in the WGS reaction. Small amount of Fe or Mo would affect the activity by one order of magnitude.

In the present study, we set out to investigate the reason for the decrease and enhancement in the WGS activity found on Pd/ceria caused by Mo and Fe respectively. In the presentation, what we will show is that the enhanced activity associated with adding Fe<sub>2</sub>O<sub>3</sub> to Pd/ceria is due to formation of a Fe-Pd alloy. And about the Mo modified catalyst, we will show Mo ions react with surface hydroxyls on ceria and that the reducibility of the ceria surface is effectively poisoned by coverages less than 2.0 Mo/nm<sup>2</sup>.

## Experimental

**Sample preparation.** The ceria used for all of the measurements in this study was synthesized by decomposition of Ce(NO<sub>3</sub>)<sub>3</sub>·6H<sub>2</sub>O (Alfa Aesar, 99.5%) in air at 873 K. For most experiments, Fe or Mo was added to the ceria support by aqueous impregnation with Fe(NO<sub>3</sub>)<sub>3</sub>·9H<sub>2</sub>O or (NH<sub>4</sub>)<sub>2</sub>MoO<sub>4</sub> (Alfa Aesar, 99.997%). The samples were again dried at 383 K overnight and calcined in air at 873 K for 4 h. The precious metal Pd was also added to the oxide supports by wet impregnation using aqueous solutions of Pd(NH<sub>3</sub>)<sub>4</sub>(NO<sub>3</sub>)<sub>2</sub> (Aldrich, 99.99%). Following impregnation of the precious metal salts, the catalysts were dried at 383 K and calcined at 873 K.

**Catalyst Characterization.** The WGS reaction rates were measured in a 1/4-inch, Pyrex, tubular reactor using 0.10 g of catalyst. Water was introduced by saturation of a He carrier gas flowing through a bubbler with de-ionized water. While the reactor pressure was always atmospheric, the partial pressures of CO, H<sub>2</sub>O and He were controlled by adjusting the relative flow rates of each component. All of the reaction measurements in this study were collected with partial pressures for CO and H<sub>2</sub>O of 25 torr. All the reaction rates were measured under differential conditions, with the conversions of CO and H<sub>2</sub>O kept below 10%. To avoid potential transients associated with catalyst oxidation and reduction, we always allowed the reaction to run for at least 30 min before analyzing the products. To ensure that the results were reproducible, the rates at each point were measured at least three times. The concentration of the effluent from the reactor was determined using an on-line gas chromatograph, SRI8610C, equipped with a Haysep Q column and a TCD detector.

The transient-pulse experiments were performed on a system that has been described previously. Computer-controlled switching valves allowed the composition of reactants admitted to a tubular reactor to undergo step changes. The product gases leaving the reactor could be analyzed by an on-line quadruple mass spectrometer. Integration of the partial pressures as a function of time allowed accurate determination of the amounts of oxygen that could be added or removed at different temperatures. The carrier gas was pure He, with relatively dilute amounts of CO (5% in He), O<sub>2</sub> (7% in He), and H<sub>2</sub>O (2% in He) added in the pulses. The amount of catalyst used in the pulse studies was 1.0 g.

Phase identification in the samples was performed via x-ray diffraction with a Rigaku X-ray diffractometer, using Ni-filtered, Cu K $\alpha$  radiation ( $\lambda = 1.54184 \text{ \AA}$ ). The diffraction measurements were performed in the range of  $2\theta = 30^\circ - 50^\circ$  with a scanning speed of  $2^\circ/20\text{min}$ .

## Results and Discussion

The first evidence that the addition of Fe to the ceria support must do more than simply modify the properties of the ceria support came from WGS rate measurements with various Fe:Pd ratios, with representative data for the Fe-impregnated ceria catalysts reported in **Fig. 1**. Fig.1 summarizes the activity measurements at 453 K for the catalysts with different Fe loading. The activities of the Pd catalysts prepared with Fe-doped ceria were higher than that with undoped ceria; and there is an optimal Fe content for maximizing the rates. The catalyst shows the highest activity with Fe:Pd molar ratio 3:1. It indicates the possibility of the alloy formation between Fe and Pd.

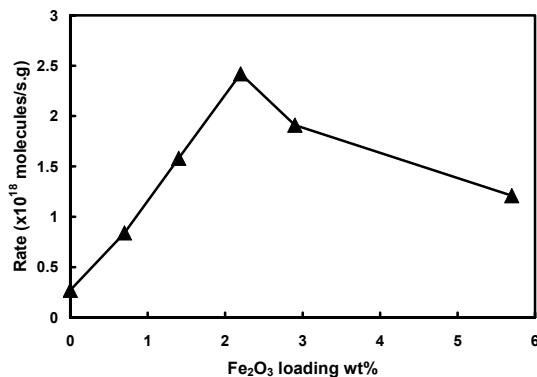


**Figure 1.** The activity rate measurements for Fe-modified Pd/ceria in WGS reaction at 453K.

To identify the phases responsible for the high activity in the Pd-Fe/ceria catalyst, we prepared the following catalysts: 6 wt% Pd on ceria; 13 wt% Fe<sub>2</sub>O<sub>3</sub> on ceria; and 6 wt% Pd, 13 wt% Fe<sub>2</sub>O<sub>3</sub> on ceria. Each sample was then exposed to the same WGS reaction conditions at 473 K for 2 h, then cooled in He to room temperature. Because initial experiments showed that the samples were re-oxidized when exposed to air at room temperature, we first passed 1-butene over the catalysts for 30 min at room temperature, before taking the samples out of the reactor, since the carbon-covered catalysts are not as susceptible to re-oxidation. **Figure 2** shows a comparison of XRD patterns on the three catalysts in the range of 30 to 50 degrees  $2\theta$ . The metallic Pd peak at 40.12 degrees  $2\theta$  was clearly observed for 6 wt% Pd/ceria. On the Fe<sub>2</sub>O<sub>3</sub>/ceria sample, the peak at 36.85 degrees  $2\theta$  shows that Fe remains in an oxidized form, but as Fe<sub>3</sub>O<sub>4</sub>. The 6 wt% Pd, 13 wt% Fe<sub>2</sub>O<sub>3</sub> sample still shows the peak that we associate with Fe<sub>3</sub>O<sub>4</sub>, but now the peak associated with Pd has shifted upward to near 41.22 degrees  $2\theta$ , which would be associated with the (111) plane of the alloy, FePd.

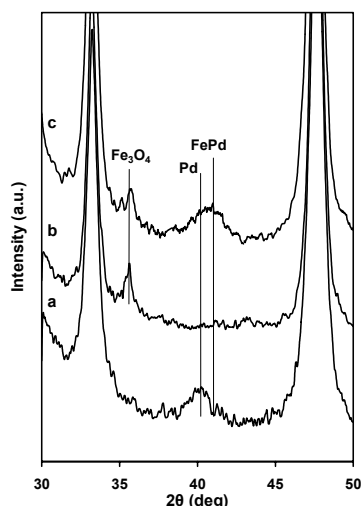


**Figure 2.** XRD data for (a) 6%Pd/ceria, (b) Fe/ceria (13wt%  $\text{Fe}_2\text{O}_3$ ) and (c) 6%Pd/Fe-ceria (13wt% $\text{Fe}_2\text{O}_3$ )

The effect of added Mo on the water-gas-shift rates is shown in **Figure 3**. Clearly, the Pd/ceria catalyst without added Mo showed the highest rates, with Mo-containing samples exhibiting rates that decreased with increasing Mo content. It is also interesting to consider that the addition of 1.25 wt% Mo decreased the WGS rate by almost a factor of 10. This coverage of Mo corresponds to  $1.8 \times 10^{18}$  Mo/m<sup>2</sup>, a specific coverage that is less than one would normally associate with a monolayer capable of blocking the surface of ceria.

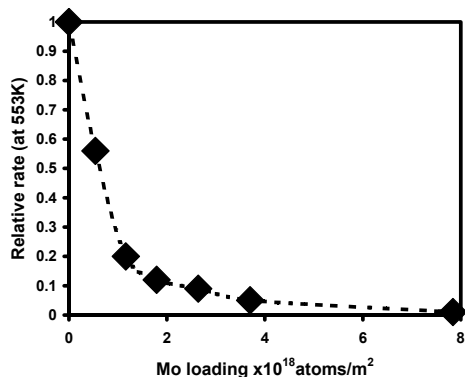


**Figure 3.** Relative activity rate for the Mo-modified Pd/ceria at 553 K in the WGS reaction.

To understand how Mo modifies the properties of ceria, CO-O<sub>2</sub> pulse studies were performed on catalysts with 1 wt% Pd on the ceria and 1-wt% Mo-ceria samples. Typical data for these two catalysts are shown in **Figure 4** for measurements at 473 K. For Pd/ceria, Fig. 4a), the initial CO pulse (m/e=28) partially reduces the catalyst, forming 135  $\mu\text{mol/g}$  CO<sub>2</sub> (m/e=44,28). A subsequent pulse of CO on this reduced catalyst forms only negligible amounts of additional CO<sub>2</sub>. More CO<sub>2</sub> is formed (115  $\mu\text{mol/g}$ ) in a sharp peak when the reduced sample is exposed to O<sub>2</sub> (m/e=32). In the previous study, it was shown that the CO<sub>2</sub> formed during the O<sub>2</sub> pulse is due to decomposition of a surface carbonate that is stable only with Ce<sup>3+</sup>, an assignment that was confirmed by FTIR measurements. The data for Pd on 1-wt% Mo-ceria, shown in Fig. 4b), have a similar appearance to that for Pd/ceria, with the exception that much less CO<sub>2</sub> (38

$\mu\text{mol/g}$ ) is formed during the O<sub>2</sub> pulse. According to the FTIR results, the surface carbonate is not formed on the Mo-containing sample and most of this CO<sub>2</sub> is likely formed by reaction of O<sub>2</sub> with CO adsorbed on Pd. The total oxygen transfer in the redox process can be quantified by summing CO<sub>2</sub> formed in the CO and O<sub>2</sub> pulses. We interpret the CO-O<sub>2</sub> pulse results as showing that Mo prevents oxidation and reduction of the ceria surface.

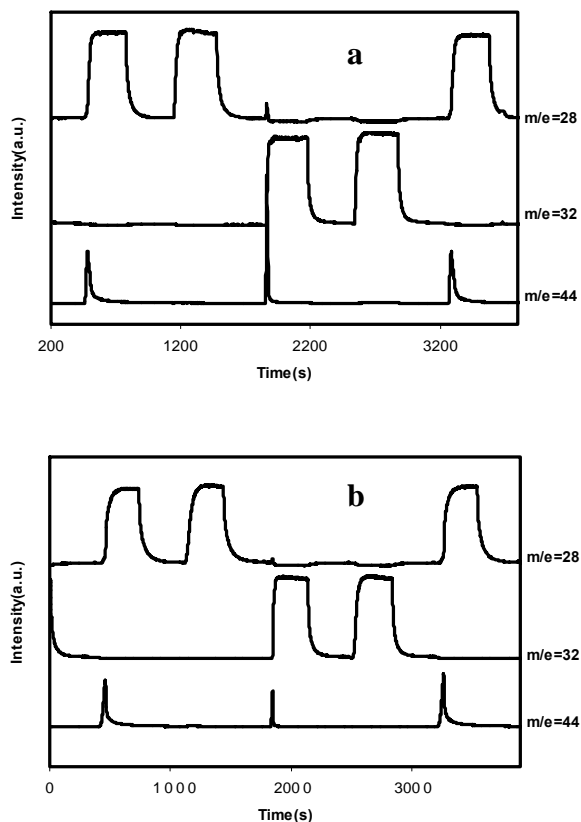


**Figure 4.** Pulse measurements on (a) 1%Pd/ceria and (b) 1%Pd/1wt%Mo-ceria at 473 K.

### Conclusions

We have demonstrated that the enhanced WGS activity observed upon the addition of Fe to Pd/ceria catalysts is probably due to the formation of a Fe-Pd alloy. Our study shows that Mo affects the activity by blocking the surface redox ability of ceria.

**Acknowledgement.** This work was supported by the DOE, Basic Energy Sciences, Grant #DE-FG03-85-13350.

### References

- (1) Ghenciu, A.F. *Current Opinion in Solid State and Materials Science*, **2002**, 6, 389.
- (2) Ladebeck, J.R.; and Wagner, J.P. In *Handbook of Fuel Cell Technology-Fundamentals, Technology, and Applications*; Vielstich, W., Ed.; Wiley, 2003, chapter 17.
- (3) Fu, Q.; Saltsburg, H.; and Flytzani-Stephanopoulos, M. *Science*, **2003**, 301, 935.
- (4) Swartz, S.L.; Seabaugh, M.M.; Holt, C.T.; and Dawson, W.J. *Fuel Cell Bull.* **2001**, 4, 7.
- (5) Hilaire, S.; Wang, X.; Luo, T.; Gorte, R.J.; and Wagner, J. *Appl. Catal. A* **2001**, 215, 271.
- (6) Wang, X.; and Gorte, R.J. *Appl. Catal. A* **2003**, 247, 157.

# DEVELOPMENT OF BIMODAL COBALT CATALYSTS FOR FISCHER-TROPSCH SYNTHESIS

Yi Zhang, Yoshiharu Yoneyama, Noritatsu Tsubaki

Department of Applied Chemistry, School of Engineering,  
Toyama University, Toyama 930-8555, Japan

## Introduction

Metallic cobalt is an excellent catalyst for CO hydrogenation, yielding higher hydrocarbons in F-T synthesis. The activity of supported cobalt catalyst in the F-T synthesis should be proportional to the area of the exposed metallic cobalt atoms. For F-T synthesis, the reaction performance of the supported metal catalysts was controlled by a number of factors, such as support property, metal precursor identity and calcination temperature. Among these factors, support pore size has great effect on the mass transfer of reactants and products. The bimodal catalyst where both large pore and small pore coexist can guarantee high diffusion efficiency and large supported metal area meantime, as theoretically proved by Levenspiel.<sup>1</sup>

Until now, several preparation methods were reported to form bimodal catalyst support. But these methods used very corrosive reagents such as aqua regia, and the size of large pore of the obtained bimodal structure was as high as several hundred nanometer that the effect of bimodal structure was not obvious. Furthermore, all the reported methods are only effective for one specific oxide support, such as Al<sub>2</sub>O<sub>3</sub> or SiO<sub>2</sub>. A general method to prepare bimodal structure, especially containing hetero-atom structure, is expected.

To find a simple, clean, and general preparation method to form tailor-made bimodal structure, it is proposed here a new method to introduce silica or zirconia sols into large-pore silica gel directly, to realize high catalytic activity through higher diffusion efficiency in large pore and higher metal dispersion via the increased surface area. As an application of this kind of bimodal support, it was used for liquid-phase FTS reactions where cobalt was supported. Meanwhile, as a promoter of Co/SiO<sub>2</sub> FTS catalyst, zirconia should promote the catalytic activity as well.

## Experimental

The bimodal support was prepared by incipient-wetness impregnation of a commercially available silica gel (Cariact Q-50, Fuji Silysia Chemical Ltd., specific surface area: 70 m<sup>2</sup> g<sup>-1</sup>, pore volume: 1.2 ml g<sup>-1</sup>, pellet size: 74-590 μm and mean pore diameter: 50 nm), with zirconia sol (Seramic G 401, Nibban Institute Co., particle size: 1.7-2.4nm, content: 21wt%, alcohol solution) or silica sol (Snowtex XS, Nissan Chemicals Industry Ltd., particle size: 5nm, content 20wt%, aqueous solution), where the volume of zirconia or silica sol was the same with the silica gel support pore volume. After the impregnation, the support was calcined in air at 673 K or 873 K for 2 h directly without drying, for zirconia or silica bimodal, respectively.

Cobalt-supported catalyst with 10wt% metal loading was prepared by incipient-wetness impregnation of different supports, including the bimodal support, with cobalt nitrate aqueous solution. The catalyst precursors were dried in air at 393 K for 12 h, and then were calcined in air from room temperature to 673 K with a ramping rate of 2 K min<sup>-1</sup> and kept at 673K for 2 h. After calcination, the catalysts were activated in flowing hydrogen at 673 K for 10 h and at last, passivated by 1 % oxygen in nitrogen.

FTS reaction was carried out in a semi-batch autoclave, slurry-phase reactor with the inner volume of 80 ml. The passivated catalyst (1.0 g, under 149 μm) and 20 ml liquid medium (n-

hexadecane) were loaded in the reactor. During the reaction, effluent gas released from the reactor was analyzed by on-line gas chromatography. CO and CO<sub>2</sub> were analyzed by using an active charcoal column equipped with a thermal conductivity detector (TCD). The hydrocarbons were also analyzed on-line using FID for C<sub>1</sub>-C<sub>5</sub> (Porapak Q) and for C<sub>6</sub>-C<sub>20</sub> (SE-30, uniport), respectively. Argon was employed as an internal standard with concentration of 3 % in the feed gas. The reaction conditions were P (total) = 1.0 MPa, CO/H<sub>2</sub> = 1/2, W/F (CO + H<sub>2</sub> + Ar) = 10 g-cat. h mol<sup>-1</sup>, T = 513 K.

Pore size distribution, BET surface area and pore volume were determined by using Shimadzu ASAP 2000, where nitrogen was used as absorbent. Supported cobalt crystalline size of the passivated catalysts was detected by TEM (TOPCON EM-002B, acc.volt: 200kV, Point resolution: 0.18nm, line resolution: 0.14nm) and XRD (Rigaku, RINT2000).

In-situ DRIFT spectra were collected on a Nexus 470 FT-IR spectrometer supplied with a diffuse reflectance attachment and with a MCT detector. In-situ absorbance spectra were collected with collecting 32 scans at 2 cm<sup>-1</sup> resolution.

Temperature-programmed reduction (TPR) experiments were carried out in a quartz-made microreactor using 0.2g calcined catalysts. The gas stream, 5 % H<sub>2</sub> diluted by nitrogen as reducing gas, was fed via a mass flow controller. After the reactor, the effluent gas was led via a 3 Å molecular sieve trap to remove the produced water.

## Results and Discussion

The characteristics of obtained bimodal supports and silica gel Q-50 were shown in **Table 1**. It is clearly proved that the obtained bimodal support contains distinctly-distributed two kinds of pores, according to the bimodal structure. The increased BET surface area and the decreased pore volume indicated that the particles from sols entered the large pores of Q-50, and deposited on the inner wall of Q-50 to form the small pores. If the sol particles deposited the entrance of large pores of Q-50, the large pores of bimodal support would be blocked, and the BET surface area of the bimodal support would decrease significantly. These data provided evidences that particles from the sols indeed entered the large pores of Q-50 gel and the bimodal support was formed. Based on these findings, it is able to conclude that the obtained bimodal support formed according to the designed route, as introducing the sols into the large pores of silica gel directly.

**Table 1. Characteristics of various supports**

Support	SiO <sub>2</sub> or ZrO <sub>2</sub> loading [wt%]	BET [m <sup>2</sup> /g]	Pore diameter [nm]	Pore volume [ml/g]
Q-50	0.0	70	50.0	1.20
Q-3	0.0	546	3.0	0.30
Silica bimodal	11.2	106	6.0-45	0.46
Zirconia bimodal	16.8	201	3.2-45	0.41

Meanwhile, a lot of oxides, such as zirconia or alumina, were used as promoter to synthesize highly active silica-base catalyst.<sup>2,3</sup> By introducing different sol other than SiO<sub>2</sub> sol into silica pellet, it is considered that the multi-function bimodal support can be formed, where besides spatial effect of bimodal structure, new chemical phenomenon or effect might appear with the hetero-atom formation between different oxides. In this study, the zirconia-silica bimodal was formed by using zirconia sol and silica pellet to obtain the multi-function bimodal support.

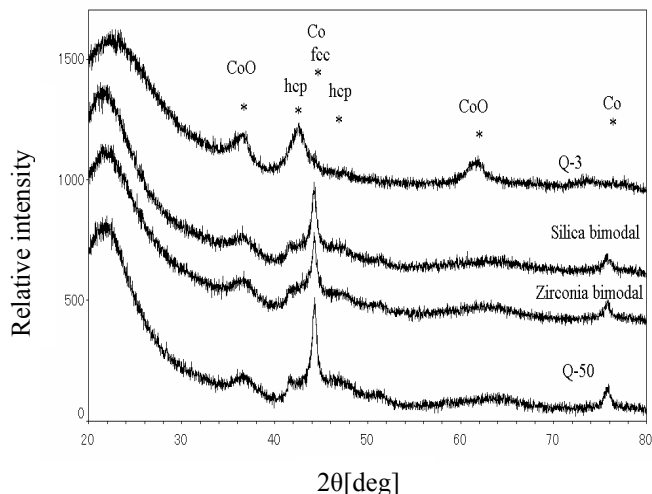
**Table 2. Characteristics and reaction performance of various catalysts**

Catal.	CO Conv [%]	Sel. [%]		Co Crystal size [nm]		Red. Deg. <sup>a</sup> [%]	TOF <sup>b</sup> [s <sup>-1</sup> ]	$\alpha$
		CH <sub>4</sub>	CO <sub>2</sub>	XRD	TEM			
Q-50	17	7.1	3.2	35.0	37.0	98.6	0.035	0.86
Silica bimodal	33	10.1	2.7	20.2	22.6	86.2	0.044	0.86
Zirconia bimodal	86	11.0	3.2	23.6	21.6	88.1	0.134	0.87
Q-3	26	22.0	20.5	4.5	1.4	62.3	0.009	0.84

Reaction conditions: 513 K, 1.0MPa, W/F = 10 g-cat.h/mol, H<sub>2</sub>/CO = 2, cobalt loading: 10wt%

a: reduction degree was calculated by TPR from 373 K to 1073 K.  
b: used the reduction degree from TPR.

In this study, both the bimodal catalysts, which derived from silica or zirconia sol, showed the best properties such as higher activity and lower methane selectivity, as compared in **Table 2**. For the catalyst prepared from silica bimodal support, the CO conversion was higher than that of catalyst derived from Q-50 and Q-3, and meanwhile selectivities of CH<sub>4</sub> and CO<sub>2</sub> were as low as to those of the catalyst prepared from Q-50. For the zirconia bimodal catalyst, the CO conversion was significantly increased from that of silica bimodal catalyst as the highest in this study, and the selectivities of

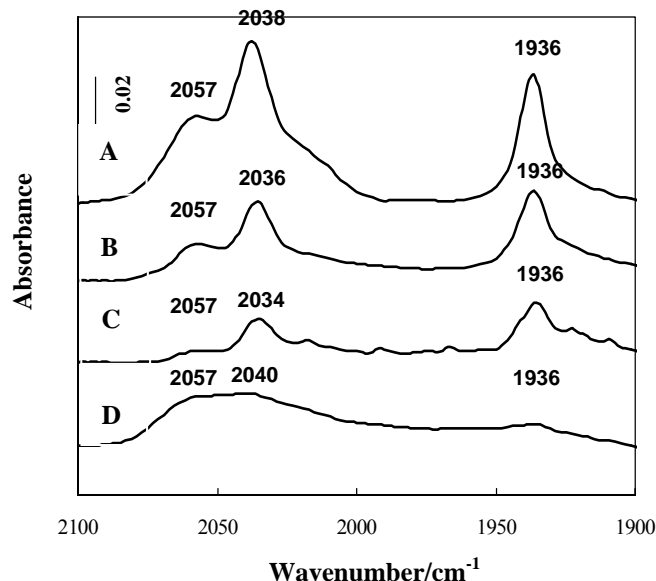


CH<sub>4</sub> and CO<sub>2</sub> were almost the same as that of silica bimodal catalyst.  
**Figure 1.** The XRD patterns of various reduced catalysts

The supported cobalt crystalline size was detected by TEM and XRD. In **Table 2**, the metal particle size calculated by XRD data is generally in accordance with that from TEM. The XRD spectra of various catalysts were shown in **Fig 1**. This clearly displays that the catalysts prepared from bimodal supports had smaller particle sizes than that of the catalyst prepared from silica gel Q-50. Based on these findings, it was proved that the dispersion of the supported cobalt was improved by the bimodal structure of bimodal supports.<sup>4</sup> The TOF of different catalysts was calculated. As shown in **Table 2**,

the TOF of zirconia bimodal catalyst was significantly higher than that of silica bimodal catalyst, even though their reduction degree and crystalline size of supported cobalt were almost the same. Hence, the results suggest that the activity of Co sites might be increased due to the presence of ZrO<sub>2</sub> in zirconia bimodal catalyst. ZrO<sub>2</sub> might form an active interface with Co, which was responsible to some extent for the enhancement in Co activity.<sup>5</sup>

**Figure 2.** In-situ DRIFT spectra of various catalysts.



A: Zirconia bimodal pore catalyst; B: Silica bimodal pore catalyst; C: Q-50 catalyst; D: Q-3 catalyst.

As in-situ DRIFT spectra illustrated in **Fig 2**, for both of silica and zirconia bimodal pore catalysts, the peaks of bridged adsorbed CO, which was easily dissociated, were stronger than that of Q-50. The high activity of bimodal catalysts could be attributed to the increase in bridge-type adsorbed CO, which was easily dissociated to carbon and oxygen, contributing to higher reaction rate of FTS.

## Conclusions

From described above, it is clear that building up micropores using zirconia particles inside silica large pores realized two functionality, chemical promotion and spatial promotion, at the same time to enhance the activity for liquid phase FTS reaction. These results indicate that a new, simple and general method for preparing bimodal support is developed by manipulation of zirconia nanoparticles from its sol inside the pores of silica gel. By this method, the multi-functional bimodal support with both large pore of the desired size and micropore can be easily prepared and the large pore size of the bimodal structure is successfully controlled.

## References

- (1) Levenspiel, O. *Chemical Reaction Engineering*, 2<sup>nd</sup> ed., Wiley, New York, 1972; pp. 496.
- (2) Withers, H. P.; Eliezer, Jr., K. F.; and Mitchell, J. W. *Ind. Eng. Chem. Res.* **1990**, 29, 1807.
- (3) Takahashi, R.; Sato, S.; Sodesawa, T.; Yabu, M. *J. Catal.* **2001**, 200, 197.
- (4) Tsubaki, N.; Zhang, Y.; Sun, S.; Mori, H.; Yoneyama, Y.; Li, X.; Fujimoto, K. *Catal. Comm.* **2001**, 2, 311.
- (5) Zhang, Y.; Yoneyama, Y.; Tsubaki, N. *Chem. Comm.* **2002**, 1216.

# Leaching Studies of a Highly Active Cu-Pd Bimetallic Catalyst Supported on Nanostructured CeO<sub>2</sub> for Oxygen-Assisted Water-Gas-Shift Reaction

Elise S. Bickford\*<sup>+</sup>, Subramani Velu and Chunshan Song

Clean Fuels and Catalysis Program, The Energy Institute

\*Intercollege Graduate Program in Materials

Department of Energy and Geo-Environmental Engineering

Pennsylvania State University

209 Academic Projects Building

University Park, PA 16802, USA

<sup>+</sup>Presenting Author

## Introduction

Fuel Cell technology is rapidly on the rise. With an increased demand for fuel and energy efficiency over the modern combustion engine, fuel cells are a viable alternative.<sup>1</sup> There is also an added benefit of being more environmentally friendly by reducing exhaust emissions. With the introduction of proton exchange membrane fuel cells (PEMFCs) for the use in automotive technology, it has become increasingly important to decrease the CO concentration of the feed gas to less than 10 ppm. In an early study by Sekizawa et al.<sup>2</sup> on the catalytic activity of Cu on alumina-mixed oxides supports, it was found that Cu(30)/Al<sub>2</sub>O<sub>3</sub>-ZnO had the highest activity for the water-gas-shift reaction. They also found that if half the stoichiometric amount of oxygen/carbon monoxide was added to the gas feed, the CO removal in the system was greatly enhanced.

However, CuZn-based catalysts are highly pyrophoric and less stable during on stream operation. Thus, new catalysts that are non-pyrophoric, more active, selective for the conversion of CO in the H<sub>2</sub>-rich atmosphere and less expensive are required for the down-stream CO clean-up of the reformed gas for fuel cell applications.<sup>3</sup> Since CeO<sub>2</sub> has oxygen storage and release properties, it is anticipated that base metals such as Cu supported on CeO<sub>2</sub> would be less pyrophoric than the CuZn-based catalysts. The pyrophoricity of the Cu/CeO<sub>2</sub> catalyst may be further improved by the addition of a small amount of noble metal due to the synergistic interaction between them. Thus, a new series of Cu-Pd bimetallic catalysts containing various amounts of Cu and Pd supported on a high surface area CeO<sub>2</sub> obtained by urea gelation method have been developed recently in our laboratory for the oxygen-assisted water-gas shift reaction.<sup>4, 5</sup> Among the catalysts tested, the one containing 30 wt % Cu and 1 wt % Pd (Cu(30)Pd(1)/CeO<sub>2</sub>) exhibited the best performance with a CO conversion exceeding 99 % under H<sub>2</sub>-rich conditions around 210°C. Scanning electron microscopic studies of the catalyst showed the existence of separate Cu-rich and CeO<sub>2</sub>-rich regions. This raised a question if the bulk CuO or small CuO clusters dispersed on CeO<sub>2</sub> are active in the OWGS reaction.

In the present study, leaching of CuO by HNO<sub>3</sub> and NH<sub>4</sub>OH has been undertaken in order to investigate the nature of active species involved in the OWGS reaction over a highly active CuPd/CeO<sub>2</sub> catalyst identified in our laboratory. The unleached as well as leached catalysts are characterized by

XRD, TPR, XPS and SEM techniques. This study is also expected to help developing a new, highly active and more stable catalyst containing less Cu metal supported on CeO<sub>2</sub> for the deep removal of CO from the reformed gas for fuel cell applications.

## Experimental

### Catalyst Preparation and characterization:

The support CeO<sub>2</sub> was prepared by urea gelation method as described elsewhere and had a BET surface area of about 215 m<sup>2</sup>/g.<sup>5</sup> Cu and Pd metals were deposited on the support surface using an incipient wetness impregnation (IWI) method, dried at 120°C overnight and calcined at 400°C for about 4 h using a heating rate of 2°C/min. TPR data were acquired on a Micromeritics AutoChem 2910 instrument. About 0.1 g of the catalyst was loaded in the reactor and heated in 5% H<sub>2</sub>/Ar gas (25 cc/min) between room temperature and 500°C at a heating rate of 5°C/min. The H<sub>2</sub> consumption due to the reduction of constituent metal ions is monitored by a TCD detector equipped in the instrument.

### Catalytic Studies:

Oxygen-assisted water-gas shift reaction was performed at 240°C in a fixed-bed down-flow reactor. A gas mixture containing 4% CO, 10% CO<sub>2</sub>, 2% O<sub>2</sub> and balance (about 84%) H<sub>2</sub> was used as reactants. The CO/H<sub>2</sub>O molar ratio was kept at 1/10. The effluent of the reactor was analyzed on-line using an Agilent 3000 A Micro GC equipped with thermal conductivity detectors with a CO detection limit of below 10 ppm. Prior to the reaction, the catalyst was reduced *in situ* at 225°C for 1h in H<sub>2</sub> flow.

## Results and Discussion

Our recent study on the OWGS reaction over Cu-Pd/CeO<sub>2</sub> catalyst containing 30 wt % Cu and 1 wt % Pd indicated that Cu forms bulk-like CuO particles.<sup>5</sup> The bulk CuO can be easily dissolved in nitric acid.<sup>6</sup> Thus, the catalyst, Cu(30)-Pd(1)/CeO<sub>2</sub> was immersed in equivalent amounts of H<sub>2</sub>O and HNO<sub>3</sub> for 5, 10 and 15 h. For comparison, the same catalyst was also immersed in aqueous 30% free NH<sub>3</sub> solution (NH<sub>4</sub>OH) for 15 h as Cu can also be leached by using NH<sub>4</sub>OH.<sup>7</sup> The leached catalysts were filtered, washed with de-ionized water and dried around 400°C for 3-4 h. The catalytic performance of leached catalysts in the OWGS reaction under H<sub>2</sub>-rich conditions is compared with that of the unleached catalyst. As can be seen from Fig. 1, under the present experimental conditions, the unleached catalyst exhibited a CO conversion over 99 %. Interestingly, the catalyst leached in HNO<sub>3</sub> for 15 h shows a CO conversion even slightly higher than that of the unleached catalyst although there is a small drop in conversion for catalysts treated for 5 and 10 h. The inlet CO content of about 4 % has been reduced to below 40 ppm in a single step under the H<sub>2</sub>-rich condition over the catalyst leached in HNO<sub>3</sub> for 15 h. On the other hand, the CO conversion drops to below 60% over the catalyst treated with NH<sub>4</sub>OH.

TPR experiments are performed over the leached catalysts in order to understand the effect of HNO<sub>3</sub> and

NH<sub>4</sub>OH treatments on the redox properties, and the results are shown in Fig. 2. For comparison, the profiles of Cu(30)Pd(0)/CeO<sub>2</sub> catalyst without Pd and that of Cu(0)Pd(1)/CeO<sub>2</sub> catalyst without Cu are also presented. The catalyst Cu(0)Pd(1)/CeO<sub>2</sub> without Cu shows a single reduction peak centering at 153°C, which can be attributed to the reduction of PdO interacting with the CeO<sub>2</sub> support. On the other hand, the 30% Cu/CeO<sub>2</sub> catalyst exhibits reduction peaks at two different temperature regions, one below 200°C, with a doublet centering at 159 and 179°C, and the other above 200°C. The peak below 175°C has been generally assigned to the reduction of dispersed CuO clusters while the peak above 200°C has been attributed to the reduction of CuO particles, similar to that of bulk CuO. Interestingly, the catalyst, Cu(30)Pd(1)/CeO<sub>2</sub> possesses an intense peak centering around 160°C together with a broad envelop up to 310°C, indicating the formation of at least two different CuO clusters dispersed on the CeO<sub>2</sub> support together with some bulk-like CuO particles. No separate peak for the reduction of PdO could be seen, suggesting that the presence of Pd along with Cu makes the CuO and PdO reduction as a single broad peak. This reveals that in addition to the Pd-Ce and Cu-Ce interactions, a Cu-Pd interaction also exists in the catalyst. The synergistic interaction between Cu and Pd further improves the reducibility of Cu and Pd species. In fact, a recent *in situ* XANES (X-ray absorption near edge structure) study on the similar Cu-Pd/CeO<sub>2</sub>-ZrO<sub>2</sub>-Al<sub>2</sub>O<sub>3</sub> catalyst confirmed the formation of Cu-Pd alloy and this significantly improved the catalytic performance of CO-O<sub>2</sub>-NO reaction.<sup>9</sup>

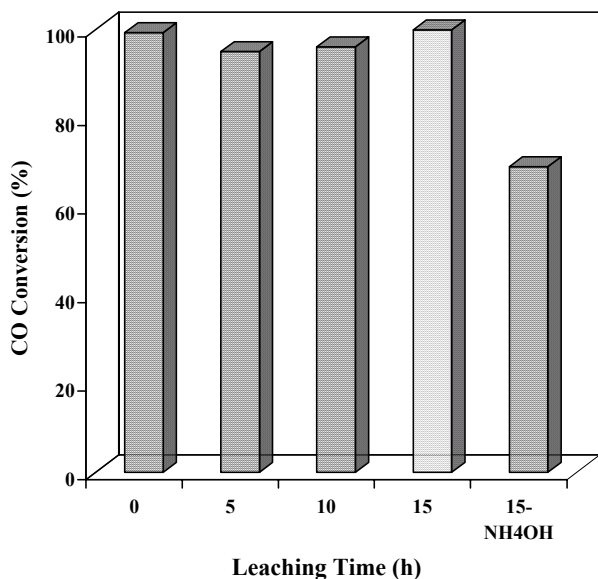


**Figure 1.** Conversion of 4% CO under H<sub>2</sub>-rich conditions over leached and unleached Cu(30)Pd(1)/CeO<sub>2</sub> catalysts in the oxygen-assisted water-gas shift reaction.

A comparison of the TPR profiles of unleached and leached samples offers several interesting results. The peak positions are shifted towards lower temperature in the leached

samples, suggesting that the metal ions become easily reducible after leaching treatments. In addition, the peak width is narrowed down and the area under the curve decreased dramatically indicating that there is a significant loss in the quantity of reducible cations. This also reveals that the nature of reducible species are identical, particularly in the catalyst leached by HNO<sub>3</sub> as only a sharp reduction peak centering around 130°C is noticed in contrast to a broad H<sub>2</sub> consumption peak around 190°C together with a sharp peak centering at 140°C are observed in the NH<sub>4</sub>OH treated sample.

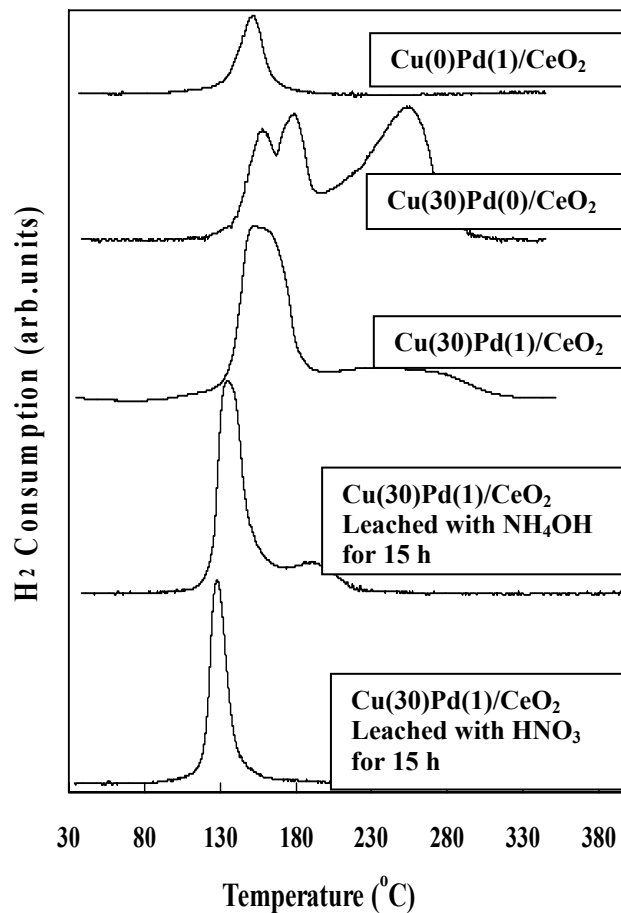


**Figure 2.** TPR profiles of leached and unleached CuPd/CeO<sub>2</sub> catalysts.

The sharp peak centering at 130°C in the HNO<sub>3</sub> treated sample can be attributed to the reduction of CuO clusters, highly dispersed on the CeO<sub>2</sub> and interacting closely with PdO. The sharpening of the peak and the absence of the high temperature shoulder clearly indicates that significant amounts of bulk-like CuO species are removed by the HNO<sub>3</sub> treatment. Since the CO conversion remains above 99% even after removing significant amount of bulk-like CuO (see Fig. 1), it is tentatively concluded that small CuO clusters dispersed on CeO<sub>2</sub> surface and interacting closely with PdO

species contribute significantly to the conversion of CO in the OWGS reactions. The existence of a broad shoulder around 200°C in the NH<sub>4</sub>OH treated sample suggests that NH<sub>4</sub>OH treatment retains some amount of bulk-like CuO. In addition, a dramatic decrease in the CO conversion over this sample (see Fig. 1) reveals that there is a significant loss in the active species upon NH<sub>4</sub>OH treatment. It is likely that the NH<sub>4</sub>OH treatment removes in addition to the bulk-like CuO, significant amount of highly dispersed CuO that are responsible for the catalytic activity.

Further characterization of the leached samples by using XRD, XPS and SEM to understand the changes in the structural features, surface chemical compositions and morphology upon leaching treatments are currently in progress and the detailed results will be reported.

### Conclusion

Leaching experiments on a highly active Cu(30)Pd(1)/CeO<sub>2</sub> catalyst under H<sub>2</sub>-rich conditions indicated that the catalyst retains the CO conversion well above 99 % CO even after leaching with HNO<sub>3</sub> for 15 h in the oxygen-assisted water-gas shift reaction. On the other hand, the catalyst leached with NH<sub>4</sub>OH loses about 40 % of the catalytic activity. It is tentatively concluded that in the Cu(30)Pd(1)/CeO<sub>2</sub> catalyst, CuO clusters dispersed on CeO<sub>2</sub> and interacting closely with PdO contribute significantly to the catalytic activity.

### References

- (1) Song, C. *Catalysis Today* **2002**, 77, 17.
- (2) Sekizawa, K.; Yano, S.-i.; Eguchi, K.; Arai, H. *Appl. Catal. A-Gen.* **1998**, 169, 291.
- (3) Fu, Q.; Saltsburg, H.; Flytzani-Stephanopoulos, M. *Science* **2003**, 301, 935.
- (4) Bickford, E.S.; Velu, S.; Song, C. *Prepr. Pap.-Am.Chem.Soc., Div. Pet. Chem.* **2003**, 48, 810.
- (5) Bickford, E.S.; Velu, S.; Song, C. *Catal.Today* **2004** (Submitted).
- (6) Liu, W.; Flytzani-Stephanopoulos, M. *J.Catal.* **1995**, 153, 304.
- (7) Burkin, A. R. *The Chemistry of Hydrometallurgical Processes*; D. Van Nostrand Inc.: Princeton, NJ, 1966.
- (8) Li, K.; Fu, Q.; Flytzani-Slephanopoulos, M. *Appl. Catal. B-Environ.* **2000**, 27, 179-191.
- (9) Hungria, A. B.; Iglesias-Juez, A.; Martinez-Arias, A.; Fernandez-Garcia, M.; Anderson, J. A.; Conesca, J. C.; Soria, J. J. *Catalysis* **2002**, 206, 281-294.

..

## DEVELOPMENT OF SYNTHESIS GAS PRODUCTION CATALYST AND PROCESS

Fuyuki Yagi<sup>\*1</sup>, Shuhei Wakamatsu<sup>1</sup>, Ryuichi Kanai<sup>1</sup>,  
Ryuichirou Kajiyama<sup>1</sup>, Yoshifumi Suehiro<sup>2</sup>, Mitsunori Shimura<sup>1</sup>

<sup>1</sup> R&D Center,  
Chiyoda Corporation,  
Kawasaki, Kanagawa, 210-0855, Japan

<sup>2</sup> Oil&Gas Technology Research & Development,  
Japan Oil, Gas and Metals National Corporation,  
Mihama, Chiba, 261-0025, Japan

### Introduction

Gas To Liquid(GTL) processes have recently been praised as effective technologies for the utilization of natural gas fields on medium or small scales which are not available for LNG. The capital cost of synthesis gas production section in GTL processes has been accounted for around 60% of the total capital cost<sup>(1),2)</sup>. Therefore the development of more compact synthesis gas production processes with high energy efficiency is desired.

We have been developing new CO<sub>2</sub>/H<sub>2</sub>O reforming catalyst and process through Japan Oil, Gas and Metals National Corporation (JOGMEC) GTL National project since 1999. The new process by using a tubular reformer which does not need an expensive oxygen plant can directly generate the stoichiometrically balanced synthesis gases which have no excess of H<sub>2</sub> and CO as suitable feed gases for Fisher-Tropsch(FT) synthesis, methanol and dimethyl ether and so forth. This proprietary catalyst with a high resistance to carbon deposition can produce synthesis gases by lower CO<sub>2</sub>/Carbon and H<sub>2</sub>O/Carbon molar ratio in the feed gas composition with low energy consumption. For elucidation and bluish up of catalyst performance, several characterizations (for example: XPS, TPD, TPR and TEM etc.) have been carried out.

The simulator to predict the temperature profile and gas compositions in the catalyst bed has also been developed for the design of the tubular reformer.

The pilot plant tests of this process were successfully carried out at Yufutsu gas field in Japan, and high economics were shown on the feasibility study.

### Experimental

**Catalyst.** The commercial size ring catalysts of 16mm outer diameter, 8mm inner diameter and 16mm length were prepared by loading of novel metals (Rh, Ru and Pt etc.) on basic metal oxide supports. An average side crushing strength of the catalysts was 500N/piece. Catalyst surface property, Lewis acidity and basicity, was designed precisely to exhibit high activity and decoking nature.

**Pilot test.** For the pilot plant operations, about 120L of commercial size catalysts were charged in mono-tube reformer which has 12.0m length and 11.0cm inner diameter, and were reduced at around 800□ under atmospheric pressure before starting the reaction tests. Synthesis gas with H<sub>2</sub>/CO=2 was generated directly by CO<sub>2</sub> and H<sub>2</sub>O reforming of natural gas. Feed H<sub>2</sub>O/CO<sub>2</sub>/Carbon ratio was 1.15-1.64/0.40-0.60/1, and reaction conditions were at 865-890, 1.5-1.9MPaG and GHSV=3000 1/HR. The total content of higher hydrocarbons in natural gas, for example ethane and propane, was around 13% and total sulfur content was around 1ppm.

**Characterization.** The XP spectra were measured with a apparatus use a JEOL JPS-9010MC spectrometer equipped with a single-channel detector, employing Al K $\alpha$  radiation (1486.6eV, anode operated at 10kV x 30mA). O(1s) spectra were recorded with the

analyzer in constant pass-energy mode (pass energy at 50eV). Measurement samples were calcined with pure O<sub>2</sub> at 400□ followed by reduction with 1% H<sub>2</sub>/He gas at 300, 500 and 900□, respectively.

**Simulator.** The concept of the simulator is shown in Fig. 1.

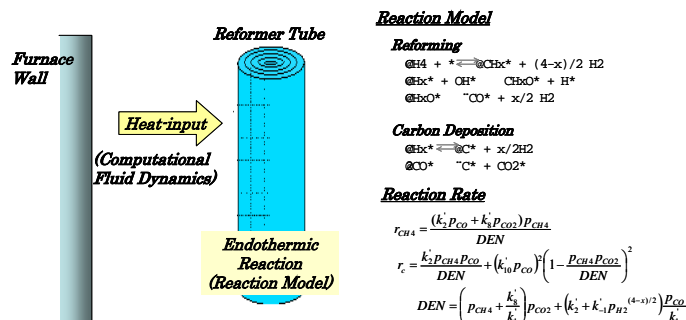


Figure 1. Concept of CO<sub>2</sub> reforming Simulator

The heat-input of the reformer tube from the burners is calculated by computational fluid dynamics, and the endothermic heat-flux is calculated by the simulator. The modeling of reactions for reforming and carbon formation on the catalyst surface is conducted with consideration from the laboratory experimental results and information on literatures<sup>3)</sup>. Catalysts life under optional operation conditions can be estimated because the carbon formation rate is taken into the consideration. Representative elementary reactions are shown. The reaction rate of CH<sub>4</sub> and the carbon formation reaction rate are expressed by the rate constant on elementary reactions and the partial gas pressures.

### Results and Discussion

Fig.2 shows the relation between volume of feed gases and compositions of those to obtain constant amount of synthesis gases with H<sub>2</sub>/CO molar ratio of 2.0.

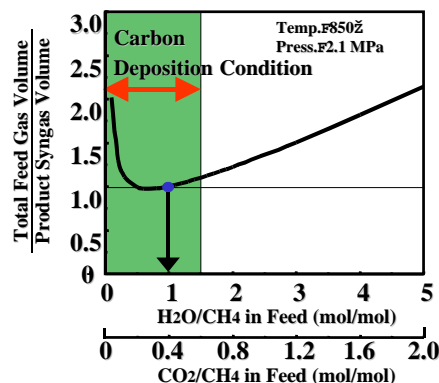
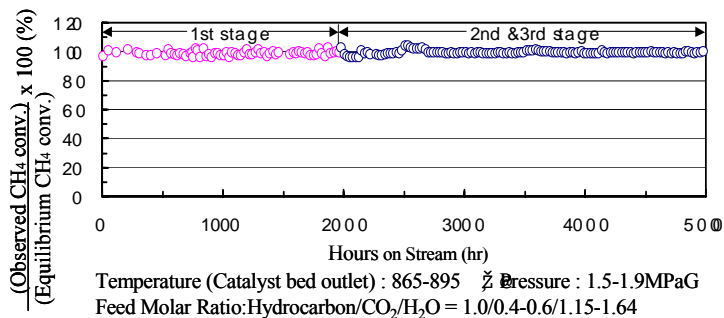


Figure 2. Optimal CO<sub>2</sub>/CH<sub>4</sub> and H<sub>2</sub>O/CH<sub>4</sub> Molar Ratio in Feed Gas to Produce Syngas (H<sub>2</sub>/CO=2.0) for FT Synthesis

The volume of synthesis gases was estimated by the equilibrium calculation of steam reforming and water-gas shift reactions at 850°C and 2.1MPa. At the point of nearby feed molar ratio of CH<sub>4</sub>:CO<sub>2</sub>:H<sub>2</sub>O=1.0:0.4:1.0, volume of feed gas is minimized and it is predicted that preferable operations with lower energy consumption can be accomplished. But on CO<sub>2</sub>/H<sub>2</sub>O reforming with ordinary reforming catalysts, the selection of these operating conditions is prohibited by higher potential for carbon formation, and particular technologies for decoking will be required<sup>4),5)</sup>.

The results of the pilot plant operation are shown in Fig. 3. In this figure, the conversions of natural gas are presented by comparison with the percentage of the equilibrium values at the same reaction conditions.



**Figure 3.** Results of Pilot Plant Tests for CO<sub>2</sub> Reforming

Although catalyst reloading was done after 1<sup>st</sup> stage operation, some parts of discharged catalysts were recharged at the same position which had been loaded before. So we could investigate total experience of the catalysts. As shown in Fig. 3, the stable operation for more than 5,000 hours has been attained under the target reaction condition. During the operation, little change of the temperature and pressure drop of the catalyst bed was observed. After the total tests, the catalyst was discharged from the reformer and the carbon content of the catalysts was analyzed. The amounts of the carbon deposition on the catalysts which have been loaded during the total test were less than 0.1wt%. From the results, the carbon-free operation has been demonstrated.

The result of the characterization (XPS(O1s)) is shown in Fig. 4.

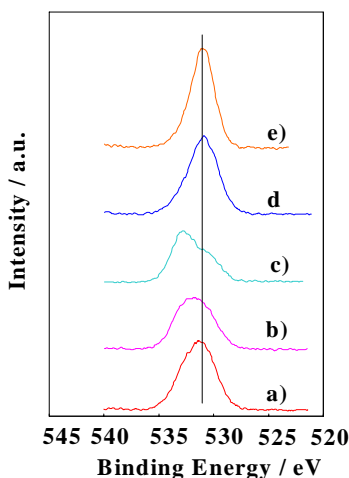


**Figure 4.** Results of X-ray photoelectron spectroscopy(O1s); a)Before reduction, b), c), d)300, 500, 900 °C reduction, e)Support

This catalyst was the same as the one that had been installed in pilot test, and it had exhibited high decoking property. The shapes of O (1s) spectra were changed by H<sub>2</sub> reduction at various temperatures. Especially, O (1s) spectrum on the one reduced at 500 °C showed two major peaks. The peak observed at higher binding energy of 532.9eV is originated from the oxygen with lower electron density. Katzer et al. assigned these two peaks to the oxygen of the support (531.9eV) and hydroxyl group terminating the support (532.9eV)<sup>6)</sup>. Hydroxyl

group could be generated with hydration of support because H<sub>2</sub>O would be originated by the reduction of loaded metal oxide. These results suggest that the interaction between loading metal and support is strong and/or the metal-support interfaces are active for hydration. Such properties are considered to be some of the reasons on the decoking nature of the reforming catalysts<sup>4),5)</sup>. By using other characterization methods (TPD, TPR and TEM etc.), we confirmed that it was effective method to control the acidity and basicity of the support for the suppression of carbon deposition.

Typical fitting results to determine kinetics parameters are shown in Fig. 5. This figure stands each gas compositions with the reaction times. The plots represent the observed value, and corresponding curves present the calculation results. As shown in this figure, calculation results fitted with observed value well, and kinetics parameters in reaction model could be obtained.

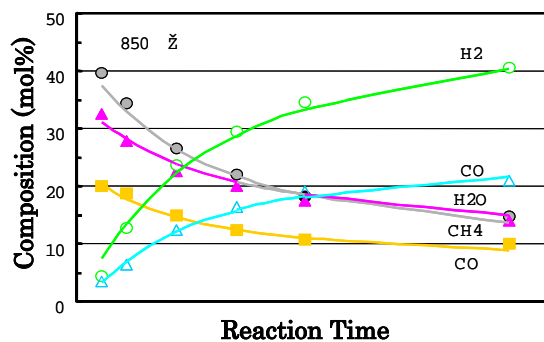


**Figure 5.** Results of parameter fitting

Through the analysis of the pilot plant test results by the simulator incorporated that reaction model, it was confirmed that it could be effectively used for the CO<sub>2</sub> reformer design.

The feasibility studies of the new GTL process for the utilization of those gas fields have been done. In the Southeast Asia, a lot of gas fields of those sizes containing a certain amount of CO<sub>2</sub> are found. In those natural gas fields, the CO<sub>2</sub> reforming process will be successfully applied to the synthesis gas production as feed for FT synthesis. The basic assumptions of the feasibility studies are as follows, Gas Field Size ; 1.75TCF, Plant Capacity; 15000BPSD (Stand Alone/Grass Roots), Natural Gas Composition; CH<sub>4</sub>/C<sub>2</sub>H<sub>6</sub>/C<sub>3</sub>H<sub>8</sub>/C<sub>4</sub><sup>+</sup>/N<sub>2</sub>/CO<sub>2</sub> = 77.5/1.0/0.3/0.3/0.8/20.1 (vol%). It is estimated that the plant cost is 560 million US\$, and the product oil price COE (Crude Oil Equivalent price) is around 18 US\$/bbl.

#### Acknowledgements

Grateful acknowledgements for the financial support is made to Japan Oil, Gas and Metals National Corporation.

#### References

1. P. J. Lakhapate, V. K. Prabhu, *Chemical Engineering World*, **2000**, 35, 77.
2. *Oil & Gas Journal*. June 15 (1998) 34.
3. M. C. J. Bradford and M. A. Vannice, *Appl. Catal.*, **1996**, 142, 97.
4. I. Alstrup, B.S. Clausen, C. Olsen, R. H. H. Smith and J. R. Rostrup Nielsen, *Studies in Surface Science and Catalysis(Natural Gas Conversion V)*, **1992**, 119, 5
5. Y-G. Chen, K. Tomishige, K. Yokoyama, K. Fujimoto, *Appl. Catal. A*, **1997**, 165, 335.
6. M. A. Baltanas, J. H. Onuferko, S. T. Mcmillan and J. R. Katzer, *J. Phys. Chem.*, **1987**, 3772, 91.

# OXYGENATE SYNTHESIS VIA HYDROFORMYLATION ON SOLID CATALYSTS

Yi Zhang, Youhei Shiki, Yoshiharu Yoneyama,, Noritatsu Tsubaki

Department of Applied Chemistry, School of Engineering, Toyama University, Gofuku 3190, Toyama 930-8555, Japan

## Introduction

Hydroformylation, the addition of synthesis gas (CO and H<sub>2</sub>) to alkenes, is one of the most important syngas-related reactions. The hydroformylation reaction was first discovered on a heterogeneous Fischer-Tropsch (F-T) catalyst.<sup>1</sup> It recognized that cobalt carbonyls generated from the heterogeneous cobalt metal during the reaction were responsible for the catalysis. All current commercial processes are based on homogeneous catalysts, mostly using rhodium. The successful development of a heterogeneous catalyst for hydroformylation would avoid the drawbacks of homogeneous catalysis, such as, very high pressure, the catalyst separation and recovery steps. A great number of papers and patents concerning olefin hydroformylation catalyzed by rhodium complexes or other noble metals supported on inorganic carriers have been published.<sup>2</sup> Whereas rhodium is the most active hydroformylation catalytic component; efforts have been made to study and exploit cheaper metals, thus replacing rhodium in catalysis for economic reasons.

Cobalt is extensively applied in homogeneous process of this reaction due to its high activity and low cost. Supported cobalt catalysts were known to be highly active for Fischer-Tropsch synthesis (FTS). Nevertheless, supported cobalt catalysts usually show low catalytic activity and selectivity for olefin hydroformylation because of high catalytic activity for olefin hydrogenation proceeding at same time.<sup>3</sup> Thus far, only a limited number of papers relating to supported cobalt catalyzed hydroformylation have appeared. However, it was reported that the activity and selectivity of supported cobalt catalysts for hydroformylation could be promoted by various promoters. Qiu et al.<sup>4</sup> reported that the Pd promoted Co/SiO<sub>2</sub> catalyst was very active and selective for the hydroformylation of 1-hexene. The promoting effect of iridium was also founded for the gas-phase hydroformylation of ethane over Co/SiO<sub>2</sub> catalyst.<sup>5</sup> In the present work, the promotional effect of noble metals, such as Pt, Pd and Ru, was studied for active carbon-supported cobalt catalyzed hydroformylation of 1-hexene.

## Experimental

**Catalyst Preparation.** The active carbon-supported cobalt catalyst was prepared by impregnation of cobalt nitrate aqueous solution onto active carbon (Kanto Chemical Co., specific surface: 1071.7 m<sup>2</sup>/g, pore volume: 0.43m<sup>3</sup>/g, pellet size: 20-40 mesh). The noble metals promoted Co/A.C. catalysts were prepared by co-impregnation of cobalt nitrate and noble metal salts aqueous solution with different noble metal loading. The cobalt loading of all of catalysts was 10wt%. After impregnation, the catalyst precursors were dried at 393 K for 12 h, and then calcined at 673 K for 6 h under the nitrogen flow. At last, the catalysts were reduced by hydrogen at 673 K for 6 h and passivated by 1% oxygen.

**Hydroformylation Reaction.** Hydroformylation reaction was carried out at in a magnetically-stirred autoclave with inner volume of 85 ml. The catalyst of 20-40 mesh and 1-hexene were loaded into the reactor with a stirrer. The reaction conditions were 403K, 5.0MPa, CO/H<sub>2</sub>=1. The weight of catalyst was 1.0g, and that of 1-Hexene was 40mmol. The reaction time was 2h. After the reaction, the reactor was cooled to 273K and depressurized. After filtration to remove the solid catalyst, the liquid products were analyzed quantitatively by gas

chromatograph (Shimadzu GC 14A) with a capillary column and a flame ionization detector (FID).

## Results and discussion

The main products of 1-hexene hydroformylation were normal and iso-heptanal with Co/A.C. catalysts. Meanwhile, small amounts of heptanol and condensation products (C<sub>13</sub>+C<sub>14</sub>) were also produced.

### 3-1) The effects of noble metals addition to Co/A.C. catalyst

For silica-based catalyst, it was reported that the noble metals, such as Pt, Ru and Pd, were not active for hydroformylation. However, the hydroformylation activity would be increased by addition of small amount of noble metals to cobalt silica catalysts.<sup>4</sup> Based on this, the promotional effect of addition of various metals to cobalt active-carbon catalysts was studied. **Table 1** showed the reaction performance of cobalt active carbon catalysts promoted by various metals. For the supported cobalt catalyst, conversion of 1-hexene gave 37.8%, and oxygenates, including aldehydes (C<sub>7</sub>-al) and alcohols (C<sub>7</sub>-ol), predominated the product, as 60.8% nal and nol selectivity. The additions of only 1wt% of Pt, Pd and Ru promoters improved the catalyst performance significantly, as increasing the conversion of 1-hexene and selectivity of oxygenate, while ruthenium exhibited the best promoting effect. 97.04% 1-hexene conversion and 79.13% selectivity of oxygenate products were obtained on Co/A.C. catalyst promoted by 1wt% Ru. The 1wt% Pt promoted Co/A.C. catalyst also presented higher activity for hydroformylation of 1-hexene as 96.35% 1-hexene conversion and 66.68% oxygenate selectivity. For the Co/A.C. catalyst promoted by Pd, the activity and selectivity were lower than those of Co/A.C. catalysts promoted by Pt or Ru in this study, even though, Pd showed significantly promotional effect than Pt and Ru for Co/SiO<sub>2</sub> catalyst in hydroformylation of 1-hexene.<sup>4</sup> The additions of alkaline earth oxide, such as Mg, Sr and Ca, did not present promotional effect for hydroformylation of 1-hexene in this study. For Mg promoted Co/A.C.catalyst, the conversion slightly increased than Co/A.C. catalyst, but isomerization and hydrogenation of 1-hexene were significantly promoted by Mg, leading to the decreased selectivity of oxygenate. The catalysts added by Sr or Ca showed lower activity and selectivity than cobalt active carbon catalyst.

### 3-2) The contribution of Ru loading for cobalt active carbon catalyst.

Although supported ruthenium and supported cobalt were much less active than supported rhodium in olefin hydroformylation, the combination of these two metals has been demonstrated to exert a striking influence on the rate enhancement of oxygenate formation in F-T synthesis and olefin hydroformylation. In this study, the promotional effect of Ru for hydroformylation of 1-hexene was carried out with different Ru loading. Different amounts of Ru, such as 0.05wt%, 0.10wt%, 0.5wt% and 1.00wt%, were added to 10wt% Co/A.C. catalyst, respectively. Hydroformylation reaction was carried out at 403K for 2h. The reaction performance of various Ru-promoted Co/A.C. catalysts was shown in **Table 2**. The conversion of 1-hexene increased with increased Ru loading. The conversion of 0.5wt% Ru promoted Co/A.C. catalyst was almost 100%. As blank test, the Ru/A.C. catalysts was prepared and tested in hydroformylation of 1-hexene. This kind of catalyst showed a negligible activity for 1-hexene hydroformylation, as no oxygenate was produced and 1-hexene was only converted to hydrogenation and isomersization products. It was proved that Ru supported active carbon catalyst had no catalytic activity of 1-hexene hydroformylation to form oxygenates.

The observed rate enhancement of 1-hexene hydroformylation with Ru promoted Co/A.C. catalyst accounted for a synergy of ruthenium and cobalt, which might be explained

in terms of catalysis by bimetallic particles or by ruthenium and cobalt monometallic particles in intimate contact. On the other hand, it was considered that the increased noble metal loading would increase the active site number on the surface of catalysts, contributing to the improved reaction rate. It was reported that the addition of ruthenium to cobalt base catalyst could significantly improve the reduction degree.<sup>6</sup> The higher reduction degree of catalyst can provide more cobalt metal centers for the reaction and lead to higher catalytic activity. Based on this, it was considered that the active cobalt site remarkably increased due to the addition of ruthenium.

On the other hand, the atoms at the corners and edges of metal particles are thought to be advantageous for hydroformylation reaction.<sup>5</sup> Therefore, the high dispersion or small particle size of metal on the catalyst, where the number of atoms at the corners and edges of metal particles is more, is also important for the improvement of catalytic performance. It is considered for Ru promoted Co/A.C. catalyst, the reduction degree was significantly improved, while the dispersion of supported cobalt was also very well. The small particle size of supported cobalt was advantageous for CO insert reaction, contributing to form the oxygenate products.

The hydrogenation and isomerization of 1-hexene decreased with the increased ruthenium loading. It is considered that with the increased active site number on the surface of catalyst, the CO

adsorption was improved, contributing to CO insert reaction and inhibiting the isomerization of 1-hexene. The formation of oxygenate was advantageous with increasing Ru loading.

### Conclusion

The addition of small amount of Pt, Pd and Ru exhibited significant effect on the Co/A.C. catalyst. The Ru promoted Co/A.C. catalyst was very active and selective for the hydroformylation of 1-hexene.

### References

1. Cornils, B., in: Falbe, J. (Ed.), *New Synthesis with Carbon Monoxide*, Springer, New York, 1980.
2. Lenarda, M.; Storaro, L.; Ganzerla, R., *J. Mol. Catal. A* **1996**, 111, 203-211.
3. Arakawa, H.; Takahashi, N.; Hnaoka, T.; Takeuchi, K.; Matsuzaki, T.; Sugi, Y., *Chem. Lett.* **1988**, 1917-1918.
4. Qiu, X.; Tsubaki, N.; Fujimoto, K., *Catal. Comm.* **2001**, 2, 75-80.
5. Takahashi, N.; Tobise, T.; Mogi, I.; Sasaki, M.; Mijin, A.; Fujimoto, T.; Ichikawa, M., *Bull. Chem. Soc. Jpn.* **1992**, 65 2565-2572.
6. Tsubaki, N.; Sun, S.; Fujimoto, K., *J. Catal.*, **2001**, 199, 236-246.

**Table.1 The effect of noble metals on Hydroformylation of 1-Hexene over 10 wt% Co/A.C.**

Catalyst	Conv.(%) 1-Hexene	Sel. (%)						Yield (%)	
		Hexane	Isomer	iso-Heptanal	1-Heptanal	C7-nol	nal and nol	Oxygenate	n/iso
10wt%Co	37.80	9.38	18.82	33.37	26.84	0.60	60.80	25.13	0.80
+ 1 wt%Ru	97.04	5.57	10.06	42.11	32.64	4.38	79.13	81.58	0.78
+ 1 wt%Pt	96.35	20.74	6.50	36.40	28.37	1.90	66.68	68.88	0.78
+ 1 wt%Pd	84.01	19.51	6.08	36.08	33.78	1.26	71.12	60.84	0.94
+ 1 wt%Mg	56.78	31.02	13.66	26.71	17.52	0.65	44.88	29.79	0.66
+ 1 wt%Sr	38.23	9.53	22.07	31.62	28.14	0.58	60.34	24.22	0.89
+ 1 wt%Ca	28.45	11.46	22.52	31.91	26.74	0.40	59.05	17.73	0.84

Reaction conditions: catalyst: 20-40 mesh, 0.10 g; 1-Hexene: 40.0 mmol; reaction temperature: 403K; reaction time: 2h

**Table.2 The effect of content on Hydroformylation of 1-Hexene over 10 wt% Co/A.C.**

Catalyst	Conv.(%) 1-Hexene	Sel. (%)						Yield (%)		n/iso
		Hexane	Isomer	iso-Heptanal	1-Heptanal	C7-nol	nal and nol	Oxygenate		
10wt%Co	37.80	9.38	18.82	33.37	26.84	0.60	60.80	25.13	0.80	
+0.05wt%Ru	26.25	14.17	28.45	29.22	19.57	0.42	49.21	14.49	0.67	
+0.10wt%Ru	44.20	0.00	37.40	30.13	20.56	0.59	51.29	26.29	0.68	
+0.50wt%Ru	97.81	0.00	24.56	36.26	30.67	2.69	69.61	72.26	0.85	
+1.00wt%Ru	97.04	5.57	10.06	42.11	32.64	4.38	79.13	81.58	0.78	

Reaction conditions: catalyst: 20-40 mesh, 0.10 g; 1-Hexene: 40.0 mmol; reaction temperature: 403K; reaction time: 2h

# THERMOGRAPHICAL STUDIES ON NOBLE METAL CATALYSTS DURING REFORMING AND COMBUSTION OF METHANE

Baitao Li, Kenji Maruyama, Mohammad Nurunnabi,  
Kimio Kunimori, and Keiichi Tomishige

Institute of Materials Science  
University of Tsukuba  
1-1-1, Tennodai, Tsukuba  
Ibaraki 305-8573  
Japan

## Introduction

In the presence of oxygen, the hot spot is always a serious problem concerning to the autothermal reaction and/or partial oxidation, because the combustion reaction is much faster than the reforming reaction, it usually proceeds on the catalyst near the bed inlet, while the reforming reaction takes place over the catalyst bed after oxygen is consumed [1, 2]. Generally, the combustion zone does not overlap the reforming zone. Therefore, the temperature of the catalyst in combustion zone is expected to be very high. As a result, a large temperature gradient will appear in the catalyst bed during the catalytic partial oxidation of methane [3-5]. In addition, the hot spot, in which the temperature expectedly becomes much higher than other places in the reactor, is one of the main difficulties in operating the partial oxidation [6-8].

The purpose of this study is to evaluate the possibility of hot spot formation over granule  $\text{Al}_2\text{O}_3$  supported Rh, Pt and Pd catalysts in autothermal reforming of methane by means of IR thermographical observation. From the fundamental viewpoint, the investigation on the temperature profiles in autothermal reforming of methane is quite attractive to develop a catalytic process in which the exothermic combustion and endothermic reforming zones can overlap so as to exert a heat transfer with high efficiency.

## Experimental

**Catalyst preparation.** Preparation of alumina supported noble metal (Rh, Pt, Pd) catalysts were performed by an impregnation method. Alumina was prepared by the calcination of JRC-ALO-1 in air at 1473 K for 3 h. The JRC-ALO-1 support material has a spherical shape (diameter of 2-3 mm and surface area of 143  $\text{m}^2/\text{g}$ ). However, after the calcination at 1473 K, the micro structure of JRC-ALO-1 was changed to  $\alpha\text{-Al}_2\text{O}_3$  from  $\gamma\text{-Al}_2\text{O}_3$ , although the spherical shape was maintained. BET analysis showed that the surface area of the calcined alumina was 6  $\text{m}^2/\text{g}$ . Loading of Rh, Pt and Pd on this alumina was carried out by impregnating the support material with aqueous solution containing precursor salts. The precursor of Rh, Pt and Pd was  $\text{RhCl}_3 \cdot 3\text{H}_2\text{O}$ ,  $\text{H}_2\text{PtCl}_6 \cdot 6\text{H}_2\text{O}$  and  $\text{PdCl}_2$ , respectively. After evaporation and dry, the catalyst was calcined in air at 773 K. The loading amount of the noble metal was  $3.0 \times 10^{-5}$  mol/g-catalyst.

**Performance testing.** Activity test of methane reforming was carried out in a fixed bed flow reactor under atmospheric pressure. Schematic diagram of the fixed bed reactor is illustrated in Figure 1. A quartz tube of 1.5 mm i.d used as a thermowell was inserted from the bottom of the reactor and the tip was located near the outlet of the catalyst bed. Reaction temperature was controlled by a thermo-controller with this thermocouple for monitoring. An electronic furnace was connected with the thermo-controller, and it had a window (15 mm x 15 mm) for the observation of the temperature profile of catalyst granules. The temperature profile was measured with IR thermography equipment (TH31 from NEC San-ei Instruments Ltd.). The concentration of  $\text{CO}$ ,  $\text{CO}_2$  and  $\text{CH}_4$  in the

effluent gas was determined by FID-GC equipped with a methanator using a stainless steel column packed with Porapak N. The concentration of  $\text{H}_2$  was determined by TCD-GC using a stainless steel column packed with a molecular sieve 13 X.

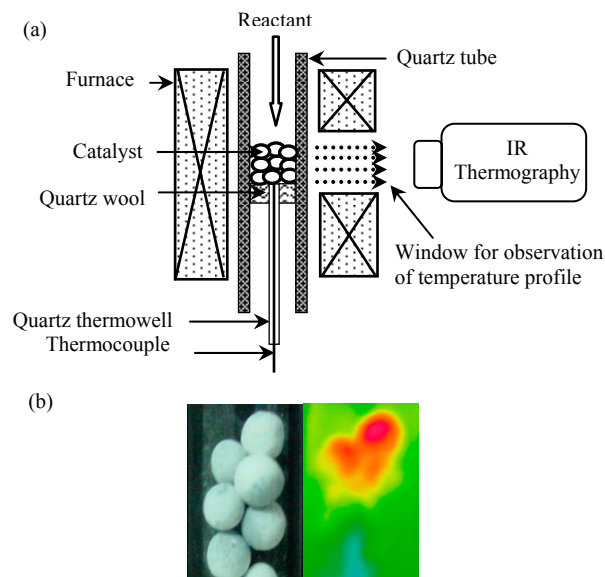


**Figure 1.** (a) Schematic diagram of the reactor unit in the reforming of methane, (b) Temperature profile observation before reaction (left) and during reaction (right).

## Results and Discussion

The combustion activity was measured under the partial pressure of  $\text{CH}_4/\text{H}_2\text{O}/\text{O}_2/\text{Ar}=10/0/20/70$ , which corresponded to the complete combustion of methane. The temperature profiles in the combustion reaction over  $\text{Rh}/\text{Al}_2\text{O}_3$ ,  $\text{Pt}/\text{Al}_2\text{O}_3$  and  $\text{Pd}/\text{Al}_2\text{O}_3$  catalysts are shown in Figure 2(a). Under this condition, only the methane combustion occurred, and the formation of  $\text{CO}$  and  $\text{H}_2$  were not observed. In this case, the methane conversion over three catalysts was almost 100%. In the temperature profiles of the catalyst bed, high temperature section was observed clearly over all three catalysts. In addition, a high temperature region at a rather small size was detected near the catalyst bed inlet. These indicate that the combustion reaction proceeded in the small region and this was related to high reaction rate of combustion. The highest temperature in this methane combustion was 1256 K, 1322 K and 1323 K over  $\text{Rh}/\text{Al}_2\text{O}_3$ ,  $\text{Pt}/\text{Al}_2\text{O}_3$  and  $\text{Pd}/\text{Al}_2\text{O}_3$ , respectively. Since it is thought that high temperature could be caused by high combustion activity, the order of combustion activity is as follows:  $\text{Pt} \sim \text{Pd} > \text{Rh}$ .

Figure 2(b) depicts the results of temperature profiles in the methane reforming with steam and  $\text{CO}_2$  over  $\text{Rh}/\text{Al}_2\text{O}_3$ ,  $\text{Pt}/\text{Al}_2\text{O}_3$  and  $\text{Pd}/\text{Al}_2\text{O}_3$  catalysts. The reaction was performed under  $\text{CH}_4/\text{CO}_2/\text{H}_2\text{O}/\text{Ar}=30/10/50/10$ , which corresponds to the gas composition when methane combustion only proceeded under  $\text{CH}_4/\text{H}_2\text{O}/\text{O}_2/\text{Ar}=40/30/20/10$ . In this case, only endothermic reaction (steam and  $\text{CO}_2$  reforming of methane) proceeded, and the endothermic profiles were observed by IR thermography. At  $W/F=0.4$   $\text{gh mol}^{-1}$ , the lowest temperature in the catalyst bed over  $\text{Rh}/\text{Al}_2\text{O}_3$  was detected as 1023 K; however, it was 1073 K over  $\text{Pt}/\text{Al}_2\text{O}_3$  and increased to 1085 K over  $\text{Pd}/\text{Al}_2\text{O}_3$ . It can be concluded that  $\text{Rh}/\text{Al}_2\text{O}_3$  exhibited higher reforming activity than  $\text{Pt}/\text{Al}_2\text{O}_3$ , and  $\text{Pd}/\text{Al}_2\text{O}_3$  exhibited much lower activity than  $\text{Rh}/\text{Al}_2\text{O}_3$  and  $\text{Pt}/\text{Al}_2\text{O}_3$ .

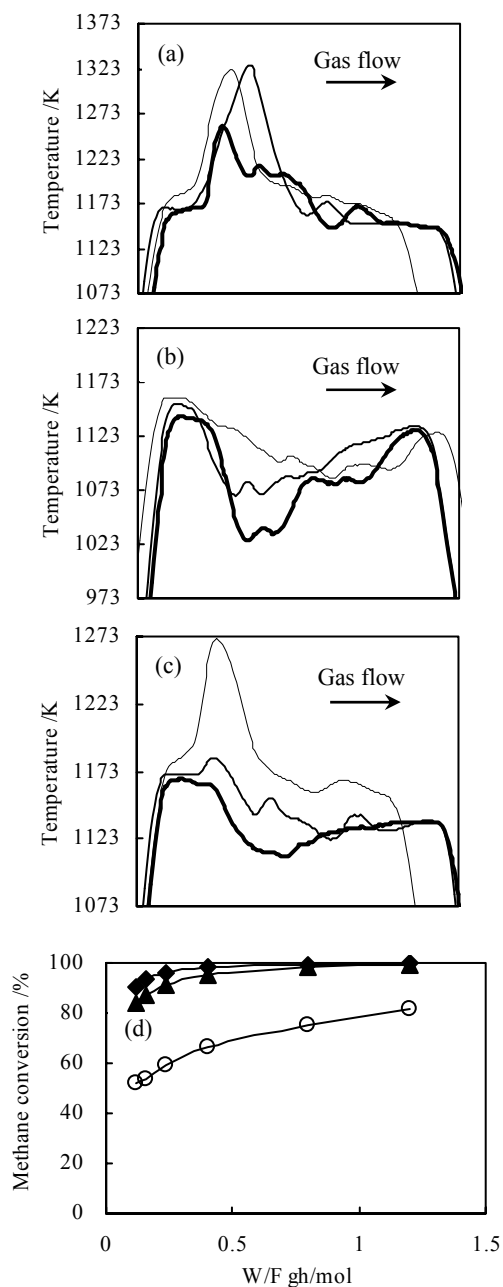


**Figure 2.** Temperature profiles under different partial pressure of CH<sub>4</sub>/CO<sub>2</sub>/H<sub>2</sub>O/O<sub>2</sub>/Ar (a)-(c). {(a) 10/0/0/20/70 (combustion reaction), (b) 30/10/50/0/10 (reforming with H<sub>2</sub>O and CO<sub>2</sub>), (c) 40/0/30/20/10 (autothermal reforming). Rh/Al<sub>2</sub>O<sub>3</sub> (bold solid line), Pt/Al<sub>2</sub>O<sub>3</sub> (solid line), Pd/Al<sub>2</sub>O<sub>3</sub> (thin solid line).} and methane conversion in the autothermal reforming of methane (d). {Rh/Al<sub>2</sub>O<sub>3</sub> (◆), Pt/Al<sub>2</sub>O<sub>3</sub> (▲), Pd/Al<sub>2</sub>O<sub>3</sub> (○).} Reaction conditions: temperature 1123 K, W/F=0.4 gh/mol (except in (d)), total pressure 0.1 MPa, catalyst weight 0.14 g, H<sub>2</sub> pretreatment 1123 K 0.5 h.

Figure 2 (c) displays the feeding gas at the partial pressure of CH<sub>4</sub>/H<sub>2</sub>O/O<sub>2</sub>/Ar=40/30/20/10 containing the combustion gas (CH<sub>4</sub>/O<sub>2</sub>=10/20) and the steam reforming gas (CH<sub>4</sub>/H<sub>2</sub>O=30/30), and

whose composition was close to the autothermal condition. At the reaction temperature of 1123 K, the inlet temperature was 1173 K and 1183 K over Rh/Al<sub>2</sub>O<sub>3</sub> and Pt/Al<sub>2</sub>O<sub>3</sub>, respectively, where the exothermic profiles were not observed. However, the bed temperature jumped to 1273 K over Pd/Al<sub>2</sub>O<sub>3</sub>, so that a large exothermic peak was clearly detected at the catalyst inlet. The reason for this high temperature is due to the very small overlap of combustion zone with reforming zone, and combustion activity of Pd/Al<sub>2</sub>O<sub>3</sub> was as high as that of Pt/Al<sub>2</sub>O<sub>3</sub>, as shown from the temperature profiles of combustion (Figure 2(a)). In addition, the effect of W/F on catalytic properties was also performed, the results is presented in Figure 2 (d). Methane conversion over Rh/Al<sub>2</sub>O<sub>3</sub> and Pt/Al<sub>2</sub>O<sub>3</sub> catalysts was dramatically lower than that over Pd/Al<sub>2</sub>O<sub>3</sub>. The results strongly reveal that Rh catalyst exhibited high methane conversion and low inlet temperature in the autothermal reforming of methane. Based on the findings, it is suggested that this behavior can contribute to the effective inhibition of the hot spot formation.

### Conclusions

From the temperature profiles in the combustion reaction, the order of the combustion activity was as follows: Pd≈Pt>Rh. In the activity test of methane reforming with H<sub>2</sub>O and CO<sub>2</sub>, the order of the reforming activity was as follows: Rh>Pt>Pd. It was found that Rh is the most effective catalyst for autothermal reforming in terms of high reforming activity, low combustion activity, and the overlap between two reaction zones.

**Acknowledgement.** A part of research was supported by Chiyoda Corporation and Japan Oil, Gas and Metals National Corporation.

### References

- (1) Mallens, E. P. J.; Hoebink, J. H. B. J.; and Marin, G. B. *Catal. Lett.* **1995**, 33, 291.
- (2) Dissanayaki, D.; Rosynek, M. P.; and Lunsford, J. H. *J. Phys. Chem.* **1993**, 97, 3644.
- (3) Heitnes, K.; Lingberg, S.; Rokstad, O. A.; and Holmen, A. *Catal. Today* **1995**, 24, 211.
- (4) De Groot, A. M.; and Froment, G. F. *Appl. Catal. A* **1996**, 138, 245.
- (5) Basile, F.; Fornasari, G.; Trifiro, F.; and Vaccari, A. *Catal. Today* **2001**, 64, 21.
- (6) Tomishige, K.; Kanazawa, S.; Sato, M.; Ikushima, K.; and Kunimori, K. *Catal. Lett.* **2002**, 84, 69.
- (7) Tomishige, K.; Kanazawa, S.; Suzuki, K.; Asadullah, M.; Sato, M.; Ikushima, K.; and Kunimori, K. *Appl. Catal. A* **2002**, 233, 35.
- (8) Tomishige, K.; Kanazawa, S.; Ito, S.; and Kunimori, K. *Appl. Catal. A* **2003**, 244, 71.

# ENHANCED FORMATION OF MIDDLE ISOPARAFFINS THROUGH TWO-STAGE FISHER-TROPSCH REACTION

Tian-Sheng Zhao, Yoshiharu Yoneyama and Noritatsu Tsubaki\*

Department of Material System and Life Science,  
School of Engineering, Toyama University,  
Gofuku 3190, Toyama 930-8555, Japan

Tel/Fax : (81)-76-445-6846 Email: tsubaki@eng.toyama-u.ac.jp

## Introduction

Fischer-Tropsch synthesis (FTS) has found increasing applications as the world economical development. Selectivity control of the products is of significant for this purpose. FTS using supported metal catalysts yields a wide range of hydrocarbons, which are mainly normal paraffins. Both catalysts renovate as well as reactor design have been conducted for desired product distribution. For instance, zeolite supported various metals were employed as catalysts for syngas conversion to limit product chain growth.<sup>1, 2</sup> Improved product distribution can also be realized using the hybrid of FT catalysts with zeolites.<sup>3-6</sup>

In this work, enhanced synthesis of middle isoparaffins from syngas was reported through two-stage Fischer-Tropsch reaction. Isoparaffins can be used as gasoline component with high-octane number.

In the first stage reactor, a hybrid catalyst by Co/SiO<sub>2</sub> FTS catalyst and H-ZSM-5 zeolite was used for limiting the formation of long chain hydrocarbons by the cracking of primary FTS products. Meanwhile the activity and lifetime of Co/SiO<sub>2</sub> was sustained due to the removal of wax accumulation. In the second stage reactor, H-zeolites alone or their hybrid with Pd/SiO<sub>2</sub> catalysts were employed to enhance the formation of C<sub>4</sub>-C<sub>6</sub> isoparaffins by further cracking and isomerizing the first stage reaction products in the presence of hydrogen, with the lowest amount of olefinic hydrocarbons. Pd/SiO<sub>2</sub> addition was expected to extend the lifetime of the H-zeolites by means of hydrogen spillover.

In addition, having Fischer-Tropsch reaction conducted in two-stage reactor was based on the consideration of reaction temperatures. The desired temperatures for FTS catalyst and zeolite in the present work were 513-523K and 553-593K, respectively.

## Experimental

**Catalyst preparation.** Co/SiO<sub>2</sub> (20 wt%) as the FTS catalyst was prepared by the incipient wetness impregnation method with commercially available silica gel (Fuji Silysia Chem, ID, BET surface area: 120 m<sup>2</sup>/g, pore volume: 1.2 ml/g) and an aqueous solution of Co(NO<sub>3</sub>)<sub>2</sub>. Pd/SiO<sub>2</sub> (2.5 wt%) catalyst was prepared by the similar method to that of Co/SiO<sub>2</sub> with the precursor of Pd(NH<sub>3</sub>)<sub>2</sub>(NO<sub>3</sub>)<sub>2</sub> acidic solution (Tanaka Co.). H-ZSM-5(23), H-Beta(27), H-USY(6.3) and H-Mordenite (19) were commercially available zeolite powder (Tosoh, data in parenthesis stand for the SiO<sub>2</sub>/Al<sub>2</sub>O<sub>3</sub>). The desired H-zeolites were physically mixed well with the above two catalysts in certain weight ratio without binder, respectively. All the catalysts including the mixed ones were pressed to 20-40 mesh pellets at 60.0 MPa. The first stage catalyst was reduced in flowing hydrogen at 673 K for 10 h. The second stage catalyst was activated in hydrogen gas flow at 673 K for 1 h under atmospheric pressure.

**Reaction procedure.** Both the first reactor and the second reactor were the flow-type fixed-bed pressurized ones with the dimension of 8 mm i.d.× 300mm. Reaction conditions were as follows unless

otherwise noted: first stage reaction: Co/SiO<sub>2</sub> + H-ZSM-5, 1:1(wt.), total weight, 1.0 g; H<sub>2</sub>/CO=2, contact time W(Co/SiO<sub>2</sub>)/F, 5.0 g h/mol; temperature, 513-523K; pressure, 1.0 MPa; second stage reaction: Pd/SiO<sub>2</sub> + H-Zeolite, 1:4(wt.), total weight, 1.25 g (Pd/SiO<sub>2</sub> 0.25g + H-Zeolite 1.0g), in the case of no Pd/SiO<sub>2</sub> addition, H-Zeolite weight, 1.0g; H<sub>2</sub>/CO=3; contact time W(H-zeolite)/F, 7.5 g h/mol; temperature, 553-593K; pressure, 1.0 MPa. H<sub>2</sub> flow rate in the inlet of the second stage reactor was additionally adjusted to H<sub>2</sub>/CO=3, assuming that H<sub>2</sub>/CO=2 syngas in the first stage reactor has no reaction. The effluent hydrocarbon products were analyzed on-line by FID gas chromatograph (GL Science GC390B), with a capillary column (Neutrabond-1) coupled with V Station software. CO, CH<sub>4</sub> and CO<sub>2</sub> were analyzed by TCD gas chromatograph, with an activated carbon column. All the products were assigned on a GC-MS (Shimadzu GCMS 5050A) with the same column and temperature program.

## Results and Discussion

In order to understand the hydrocracking and isomerization of hydrocarbons on acidic catalysts, four kinds of H-zeolites were used in the second stage reactor. The reaction conditions and the hydrocarbon distributions are showed in Figure 1. In this case, the CO conversions were between 74% and 75.3%, which is attributable to the same first stage reaction at 513K. The CO<sub>2</sub> selectivity was below 3.2%. The selectivity of C<sub>4</sub>-C<sub>6</sub> isoparaffins changed from 26.5% to 58.4%. C<sub>7</sub><sup>+</sup> hydrocarbons were not produced when using H-Beta and H-USY as the second stage catalysts, while the selectivity of C<sub>7</sub><sup>+</sup> hydrocarbons was 9.4% and 15.8% in the cases of H-ZSM-5 and H-Mordenite, respectively. Furthermore, no C<sub>4</sub>-C<sub>6</sub> olefins were found except for using H-Mordenite. The activity in terms of C<sub>4</sub>-C<sub>6</sub> isoparaffin selectivity increased in the order: Co/SiO<sub>2</sub> + H-ZSM-5 || H-Mordenite < Co/SiO<sub>2</sub> + H-ZSM-5 || H-ZSM-5 < Co/SiO<sub>2</sub> + H-ZSM-5 | H-Beta < Co/SiO<sub>2</sub> + H-ZSM-5 | | H-USY.

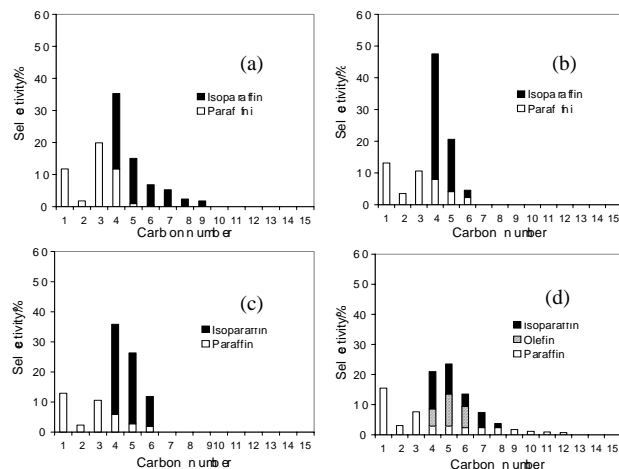


**Figure 1.** Hydrocarbon distributions for two-stage FTS reaction 1st stage temp., 513K, 2nd stage temp., 573K. 2nd stage cat.: (a) H-ZSM-5; (b) H-Beta; (c) H-USY; (d) H-Mordenite.

These results indicate that the products from the first stage reaction were further converted to isoparaffins as the main product components. The distinct changes in hydrocarbon distributions can be explained in terms of the secondary reactions following conventional FTS reaction, such as hydrocarbon cracking, skeletal isomerization and hydrogen transfer, as the longer chain hydrocarbons were easily hydrocracked. The products from the first

stage catalysts diffused to the surfaces of the second stage catalysts and were further hydrocracked or isomerized to the lighter isoparaffins and the  $C_7^+$  hydrocarbons were therefore eliminated. In addition, the activity sequence can be attributable to the disparity in the instinct acidity and microporous structure of the H-zeolites. The second stage reactions were simultaneously effected by the acidity and microporous structure of the H-zeolites.

The results and the product distributions for using the hybrid of H-zeolites with Pd/SiO<sub>2</sub> as the second stage catalysts are shown in Figure 2. The CO conversions remained unchanged compared with the above results and the CO<sub>2</sub> selectivity and methane selectivity were below 3.2 % and 12.9 %, respectively. The  $C_7^+$  fraction in the products did not appear and the carbon number of the products terminated at 6, while the selectivity of C<sub>2</sub>-C<sub>6</sub> normal paraffins changed to a certain extent. The selectivity of C<sub>4</sub>-C<sub>6</sub> isoparaffins increased slightly, compared to that without Pd/SiO<sub>2</sub> addition. H-Beta + Pd/SiO<sub>2</sub> in the second stage exhibited as high C<sub>4</sub>-C<sub>6</sub> isoparaffins selectivity as 64.4%. Similarly, it is clear that the olefin formation was completely suppressed. The olefins from FTS reaction were mainly 1-olefins and 1-olefins were effectively hydrogenated on the added Pd/SiO<sub>2</sub>. The hydrocracking of n-octane used as a model compound of FTS reaction over hybrid catalyst composed of Pd/SiO<sub>2</sub> + H-ZSM-5 has shown high activity, giving more isoparaffin-rich hydrocarbons than on those without Pd/SiO<sub>2</sub> catalyst.<sup>6</sup> The activity in terms of C<sub>4</sub>-C<sub>6</sub> isoparaffins increased in the order: Co/SiO<sub>2</sub> + H-ZSM-5 | H-ZSM-5 + Pd/SiO<sub>2</sub> < Co/SiO<sub>2</sub> + H-ZSM-5 | | H-Beta + Pd/SiO<sub>2</sub>.

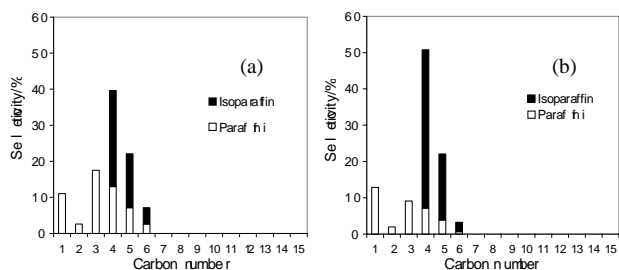


**Figure 2.** Hydrocarbon distributions for two-stage FTS reaction 1st stage temp., 513K, 2nd stage temp., 573K. 2nd stage cat.: (a) H-ZSM-5 + Pd/SiO<sub>2</sub>; (b) H-Beta + Pd/SiO<sub>2</sub>.

The time-on-stream change in CO conversion and hydrocarbon selectivity of the two-stage reaction is shown in Figure 3. It can be seen that within 30 h, the CO conversion was stabilized at 83%. The selectivity of C<sub>4</sub>-C<sub>6</sub> isoparaffins was around 50%, while there were no olefins to be found. These results showed that the catalysts for the present two-stage reaction were very stable. H-ZSM-5 zeolite in the first stage catalysts cracked timely the formed waxy components; the disappearance of wax layer on the FTS catalyst could accelerate diffusion of syngas and produce hydrocarbons. The coexisting of Pd in the second stage catalysts activated hydrogen from gaseous H<sub>2</sub> to stabilize or strengthen the acidic sites of zeolite via spillover effect.<sup>7</sup> Because the H-zeolite coexistence in the first stage catalyst released the reaction from diffusion-controlled regime and the hydrogen spillover effect of Pd/SiO<sub>2</sub> on H-zeolite in the second stage catalysts, the lifetime of hybrid catalyst was therefore extended remarkably.

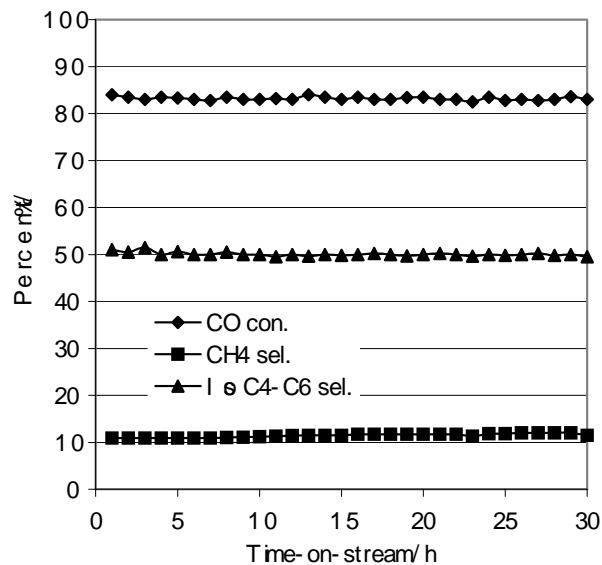


**Figure 3.** CO conversion and product distributions as time-on-stream for two-stage FTS reaction. 1st stage cat.: Co/SiO<sub>2</sub> + H-ZSM-5; T: 523K; 2nd stage catalyst: H-Beta + Pd/SiO<sub>2</sub>; T: 553K.

By this modified two-stage FTS, high selectivity of C<sub>4</sub>-C<sub>6</sub> branched hydrocarbons was achieved directly from syngas using hybrid catalysts with different functions. High selectivity of C<sub>4</sub>-C<sub>6</sub> isoparaffins resulted from the secondary cracking of heavy hydrocarbons in the first stage reaction to some extent, and mainly from further hydrocracking, isomerization of the first stage reaction products to more desired products in the second stage reaction. Furthermore, conducting the FTS in this reactor can avoid the mismatch of most suitable temperature for Co/SiO<sub>2</sub> and H-zeolites. In the case of using Co/SiO<sub>2</sub> + H-ZSM-5 for the first stage catalyst and H-Beta + Pd/SiO<sub>2</sub> for the second stage catalyst, the highest selectivity for C<sub>4</sub>-C<sub>6</sub> isoparaffins was obtained and the products terminated in C<sub>6</sub> hydrocarbon with the CO conversion of 74.8%. With H-ZSM-5 hybrid in the first stage catalyst, wax deposition was restrained and with Pd/SiO<sub>2</sub> hybrid in the second stage catalyst the acid sites of H-zeolites could be maintained by hydrogen spillover effect. The catalytic performance of the total hybrid catalysts was therefore remarkably improved.

**Acknowledgement.** The grant from NEDO, Japan is greatly appreciated.

## References

- Nijs, H. H., Jacobs, P. A., Uytterhoeven, J. B., *J. Chem. Soc. Chem. Commun.*, **1979**, 180.
- Tatsumi, T., Shul, Y. G., Sugiura T., Tominaga, H., *Applied Catalysis.*, **1986**, 21, 119.
- Udaya, V., Rao, S., Gormley, R. J., *Catalysis Today*, **1990**, 6, 207.
- Fujimoto, K., Adachi, M., Tominaga, H., *Chem. Lett.*, **1985**, 783.
- Tsubaki, N., Yoneyama, Y., Michiki, K., Fujimoto, K., *Catalysis Communications.*, **2003**, 4, 108.
- Li, X., Asami, K., Luo, M., Michiki K., Tsubaki, N., Fujimoto, K., *Catalysis Today*, **2003**, 84, 59.
- Zhang, A., Nakamura, I., Aimoto, K. and Fujimoto, K., *Ind. Eng. Chem. Res.*, **1995**, 34, 1074.

# IMPACT OF PROMOTERS ON THE PERFORMANCE OF THE SKELETON IRON CATALYST IN THE APPLICATION TO FISCHER-TROPSCH SYNTHESIS PROCESS

Yijun Lu, Peizheng Zhou

R & D Center  
Hydrocarbon Technologies, Inc.  
1501 New York Ave.  
Lawrenceville, NJ 08648

## Introduction

As all we realized, this painful gasoline price fly will occur inevitably and frequently in the coming future. Natural gas and remote coal resources have been consistently considered as the alternative fuel by most of the big energy consuming countries. However, Gas-To-Liquid conversion processes was traditionally defined being competitive only when the crude oil price is over US\$ 35/bbl, although it yields ultra-clean hydrocarbon based fuels. As one key part of the increased worldwide interest of GTL technology, HTI has developed a series of proprietary Raney Fe catalyst and the related Integrated Hydrocarbon/Ammonia Production process. As detailed in other places, Raney Fe catalyst, patented as ZIP catalyst, possesses most advantages that the current used precipitated and supported iron catalysts do not have<sup>1,2,3</sup>. Along with the scaling-up of Raney Fe catalyst application, it brought up many interesting points for both research and commercialization purpose. This presentation is to discuss the effect of principle FTS iron catalyst promoters on this novel iron catalyst and its performance of said reaction. The major promoters (elements) addressed here are K, Cu and Mn.

## Experimental

**Catalyst Samples.** The Raney Fe catalysts used in this study are the basis HTI patent ZIP catalyst, and the modified one. All samples are prepared form an amorphous alloy precursor by a way of caustic solution leaching and impregnation process.

The preparation procedure has been provided in the related US patents and other literatures. The distinct skills for controlling the alloy and catalyst chemical formula and physics properties include screening proper additive substance, operating optimum melting procedure, immediate organic-inorganic exchange and discreet transfer under vacuum condition. All catalyst samples before test were stored in ethanol alcohol or slurry phase medium, Durasyn 164.

**Characterization & Analysis.** The typical measurement data in terms of catalyst chemical, morphological properties have been published in other documents. The techniques contain BET surface area, N<sub>2</sub>-adsorption for pore size distribution, X-ray diffraction for chemical phase and crystallization extent, scanning electron microscope and surface element probe analysis.

**Catalyst Evaluation.** Fischer-Tropsch synthesis was conducted in a 1 liter CSTR and operated under commercial conditions (270°C, 2.5MPa, 2.0NI/gcat/h, 15wt% catalyst loading). Most of the test lasted over 300 hours. All promoters in this study were primarily added in the parent precursor of Raney Fe catalyst, except that K was impregnated onto the skeleton bulk iron particle.

## Results and Discussion

Before any test data investigation, it is necessary to clarify one experimental observation that the Raney Fe catalyst does not need any activation or induction period. **Figure 1** indicates the reaction conversion of CO with TOS from zero and there is insignificant

induction stage after dramatic temperature increasing to 270°C. The no activation can be simply attributed to the metallic phase (XRD) of Raney Fe catalyst, nevertheless the no induction phenomenon is strongly against the popular point that active Fe catalyst requires to be carbonized to some extent but not reduced to  $\alpha$ -Fe phase.

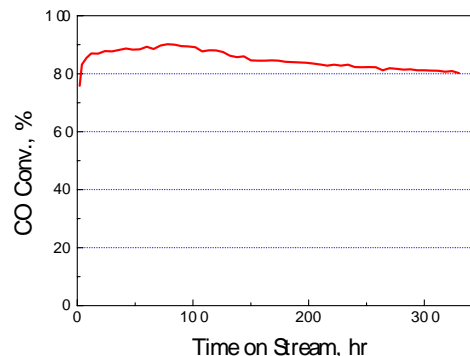


**Figure 1.** The CO hydrogenation reaction activity as a function of time.

Based on the characterization (XRD & Mossbauer spectra) of Raney Fe catalyst samples after reaction, and the experiment data that FTS product selectivity and activity slightly changed after 1000hours evaluation, Raney Fe catalyst can be concluded as one physical/chemical stable iron cell. The magnetite phase Fe<sub>3</sub>O<sub>4</sub> was discovered as the dominant component mixed with trace FeC<sub>x</sub> and  $\alpha$ -Fe. A recent study reported that using nano-iron unsupported catalyst to undergo CO activation (reduction) and 120hours Fischer-Tropsch synthesis test, the catalyst sample was not converted to most carbide (12wt%) yet. While the micro size iron catalyst showed higher percentage of FeC<sub>x</sub> (40wt%). The conclusion was that nano-iron ( $\alpha$ -Fe<sub>2</sub>O<sub>3</sub>) is subject to be stable in Fe<sub>3</sub>O<sub>4</sub> phase, i.e., with the iron particle size increasing, the tendency to be carbonized is enhanced. However, for the novel Raney Fe case, amorphous physics property helped greatly to harness the carbonization of Fe. One fact we have to realize that, the composition relationship with catalytic properties of Fe-based FTS catalysts during reaction and identity of active phase still remain controversial.

**Potassium Promotion.** K as the most important alkali promoter, has been extensively utilized in fused, supported, precipitated FTS iron catalyst<sup>4,5,6,7</sup>. Different authors gradually come to the same conclusion about the K role (or experiment observation) in these different iron catalysts. It was believed that there is an optimum of K/Fe ratio, and among this range the yield of CH<sub>4</sub> and higher paraffins decreased and olefins increased as K amount increased. Besides, the ratio CO<sub>2</sub>/H<sub>2</sub>O in products increased with increasing K/Fe, and the carburization of Fe in synthesis gas proceeded more rapidly on K promoted catalysts.

For the well-known precipitated-Fe catalyst preparation, originally, potassium was added by mixing an aqueous solution of ferric nitrate, potassium nitrate/carbonate and with other nitrate compound if necessary (like copper nitrate). After high temperature calcinations and complete reduction, the K promoter was thought rich on the surface of catalyst and interacting with Fe atoms strongly. Since the recent application of precipitated Fe catalyst has involved in the spray-dried step (which is purposing on the K<sub>2</sub>O and SiO<sub>2</sub> promoters addition) in the preparation process, K promoter was assumed to mostly bind with SiO<sub>2</sub> rather than Fe atoms. This poor K-Fe interaction obviously led people to increase K concentration in the catalyst (1~4% comparing with the optimum range 0~0.4 conclude from the co-precipitated Fe catalysts)<sup>6,7,8</sup>.

Before starting the K promoter impregnation onto Raney Fe particles, the difficulty that metallic Fe catalyst is air sensitive and water sensitive when the temperature is over room temperature had to be resolved. The methanolic solution of potassium and vacuum rotate evaporator were chosen to accomplish the loading object. Impregnating temperature was controlled below 70°C and after 3 hours loading/drying the inert paraffins was introduced to protect active catalyst exposing to air. Catalyst was subsequently transferred into the CSTR and heat treated at 300°C and 0.7 MPa under N<sub>2</sub> or H<sub>2</sub> for 20 hours in order to purge and vaporize out all possible oxidant substance that may contacting with the active catalyst particles. The reactant gas was fed in a ratio of H<sub>2</sub>/CO=1, and the Fischer-Tropsch synthesis occurred instantly as confirmed from the first 1 hour vent gas analysis.

**Table 1. Comparison of the FTS performance on Raney Fe catalyst containing different K loading**

Run No.	224-77	224-88	224-101	224-89
Raney Catalyst	Fe/Al/Mn Base			
K/Fe, wt%	0	0.3	0.6	1.1
Conv., mol%				
CO	84.4	89.3	85.1	89.7
H <sub>2</sub>	44.0	64.1	54.3	71.0
CH <sub>4</sub> sel., %	12.0	10.1	8.3	7.1
Deactivation rate, %/d	1.45	0.88	0.83	0.30

(CH<sub>4</sub> selectivity here is represented as the percentage to whole HC product).

**Table 1** demonstrated that K promoter played an incredible role in the Raney Fe catalyst. It was apparent that methane selectivity was decreased and deactivation rate was minimized as well as the hydrogenation activity enhanced by increasing the K/Fe ratio. However the impregnated K amount was relatively lower comparing with those over precipitated Fe catalysts which have obtained much nearly catalytic performance.

**Copper Promotion.** Copper is another extensively researched promoter to Fe-based FTS catalysts. Especially for the precipitated iron catalyst, copper (CuO) was proved by sufficient studies to play great role in reducing the iron oxide reduction temperature, and believed contributive to the initial carburization, extent of carburization and the stability of higher FTS rate. It was clearly recommended by many authors to use copper and potassium both at the same time, so as to possibly increase the activation sites and subsequently form multiple and smaller carbide crystallites<sup>9</sup>. Nevertheless, the Raney Fe catalyst in this presentation showed very slight requirement of copper as structural promoter. After a series FTS tests over different copper promoter percent and different copper chemical phase (Cu and CuO), it was found the copper in Raney Fe catalyst system had little effect on the activity or stability, except led slight increase in oxygenates yield.

**Manganese Promotion.** In fact the manganese was traditionally defined as active element for the FTS reaction, and some literatures have used manganese content over 40wt% iron catalyst. The mostly agreed effect of manganese on the iron based catalyst was the enhancement of olefin selectivity especially the low molecular olefins. The catalyzing/promoting mechanism was thought to form bi-metallic catalyst surface sites, so as to reduce hydrogenation probability and increase thermal stability as well as the carburization inhabitation or carbide deposition. X. Li et al have suggested to adjust the manganese amount during the co-precipitation process

could obtain unique Fe/Mn oxides in the form of spinel compound (MnFe<sub>2</sub>O<sub>4</sub>) after relative high temperature calcinations (1100°C)<sup>10</sup>.

Three different manganese type catalysts were studied in this work, MnCO<sub>3</sub>, Mn<sub>2</sub>O<sub>3</sub>, Mn were all separately added to the parent alloy of Raney Fe catalyst, the ratio to Fe was controlled as < 5wt%. The steady state test data demonstrated that manganese addition to the Raney Fe catalyst greatly enhanced the activity and stability comparing with the one has no manganese promoter. But the proper reaction temperature to reach satisfying performance was found increased by 10-30°C. One possible explanation about this temperature difference was that the reduction tendency of iron surface oxide species was inhibited when manganese added, the characterization results of the proof of spinel compound somewhat supported the observation. Once FeMnO<sub>x</sub> crystallite is formed, surface active sites were smaller than the iron clusters. **Table 2** lists the manganese promoted Raney Fe catalyst and their FTS catalytic properties.

**Table 2. Comparison of FTS performance over Raney catalyst with manganese promoters**

Run No.	224-68	224-83	224-104	224-89
Raney Catalyst	Fe/Al Base			
Manganese, wt%		*Mn <sub>2</sub> O <sub>3</sub>	*Mn	MnCO <sub>3</sub>
Potassium, wt%	0	4	2	5
Conv., mol%	0	0	0	1.1
CO	67.7	69.3	86.2	89.7
H <sub>2</sub>	30.0	45.7	53.1	71.0
CH <sub>4</sub> sel., %	8.56	6.8	7.3	7.1
Deactivation rate, %/d	3.60	4.01	0.75	0.30

- Reaction temperatures were 290°C.

## Conclusions

From the above discussion, it can simply be concluded that Cu had little influence on the CO hydrogenation activity comparing with the significant K contribution. Mn promoter was proved playing positive role in the CO hydrogenation and olefin selectivity but turned out negative effect on the reaction stability when both Mn and K were present in the Raney Fe catalyst. The reason was thought to be the high selectivity in wax that inevitably enhanced the viscosity and primary product transfer resistance, particularly the oxidizing by-products. Further characterization by morphological, species analysis and H<sub>2</sub>/CO adsorption in-situ could provide better explanation of these observations.

**Acknowledgment.** Catalyst characterization was provided by the Material Science & Engineering Center of New Jersey, Institute of Technology.

## References

1. Lu, Y.J., et al., ACS Preprints, Fuel Chemistry Division, 2001, 46(2), 500
2. Zhou, J.L., et al., US Pat. No. 6265451
3. Zhou, P. Z., et al., US Pat. No. 6277895
4. Davis, B.H., Catalysis Today 84(2003)83-98
5. Bukur, D.B., et al., Ind. Eng. Chem. Res., 1990,29,1588-1599
6. Bukur, D.B., et al., Applied Catalysis A; General 186(1999)255-275
7. Mahajan, D., et al., Catalysis Communications 4(2003) 101-107
8. Anderson, R.B., The Fischer-Tropsch Synthesis, Academic Press, Inc. 1984
9. Li, Senzi, et al., J. Phys. Chem. B 2001,105,5743-5750
10. Li. X. G., et al., Hyperfine Interactions, 1991,69(1-4), 867

## Synthetic Fuels from Synthesis Gas Activities in Japan

Kaoru FUJIMOTO

Faculty of Environmental Engineering  
The University of Kitakyushu  
Hibikino 1-1, Wakamatsu-ku, Kitakyushu,  
Fukuoka 808-0135, Japan

### Introduction

Production of liquid fuels from raw materials other than petroleum is exclusively important for Japan, which consumes huge amount of petroleum, coal, and natural gas, while their domestic production is negligibly small. The production of sulfur free liquid fuel from natural gas or coal from outside of Japan and its transportation to Japan is one of effective method of importing petroleum substitute and clean fuels.

Synthetic fuel is not limited to liquid hydrocarbons. Dimethyl ether (DME), fuel methanol, and liquid petroleum gas (LPG) are also promising synthetic fuels in Japan. Among many methods of synthetic fuel production (Fig. 1), the route which passes through synthesis gas is most promising and well studied.

Japan has long history for developing sciences and technologies of synthetic fuel production and some of them are now on the way of commercialization.

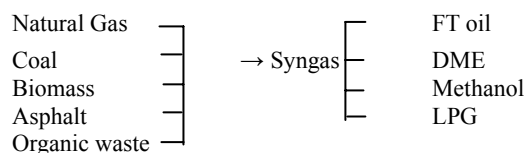
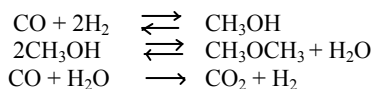


Figure 1. Synthetic Fuel Production Scheme

### Dimethyl Ether (DME)

The direct synthesis of DME from synthesis gas has been published by the present authors in 1982, where the catalyst was composed of the methanol synthesis catalyst and methanol dehydration catalyst<sup>1,2</sup>. The essential of this study is that the quick conversion of methanol, whose unfavorable synthesis equilibrium from synthesis gas can be overcome, giving a much higher one-pass yield than that of methanol synthesis. This technique can be applied



to the effective syngas to gasoline (STG) process. The DME synthesis technology was converted to the liquid slurry process which utilizes the modified catalyst. The slurry process has run on the path for commercialization which pass through small bench plant (50 kg/d), pilot plant (5t/d), and demonstration plant (100 t/d, running since 2003) promoted by JFE group<sup>3</sup>.

Indirect process, which passes through the methanol synthesis, has been also developed by Mitsubishi Gas Chemical and Tokyo Engineering.

DME utilization is now on the road in many directions.

### Fischer-Tropsch Synthesis (FTS)

The basic research of FTS after so-called "oil crisis" has started in 1975, which clarified the behaviors of adsorbed CO on various supported noble metals by TPR and IR method, concluding that the active species for CO hydrogenation is formed by the dissociation of carbon-oxygen bonding on the metal surface<sup>4</sup>.

Since then numerous studies have been made by many groups mainly on cobalt and ruthenium catalysts from the stand point of developing catalyst with higher activity and a higher carbon chain growth. The present authors have developed the FTS process under super-critical (SC) conditions, which make it possible to extract heavy hydrocarbons from the catalyst surface and quick transfer of the product<sup>5</sup>. The FTS in the SC phase results in the extraordinary high concentration of olefins in the product and high yield of wax<sup>6,7</sup>.

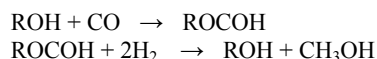
The kinetic and catalytic analysis of slurry phase FTS with supported cobalt catalyst clarified the effect of pore structure and additives on the rate and the product selectivity<sup>8</sup>. Also, it was proved that the small amount of added noble metal promoted the degree of cobalt under reaction conditions to promote the catalytic reaction<sup>9</sup>. This analysis made it possible the development of high performance of cobalt catalyst (1 kg-oil/kg-cat h and  $\alpha = 0.9$ ) proven in the pilot plant operation.

### Iso-paraffin Synthesis

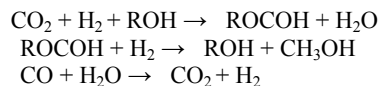
Conventional FTS gives straight chain aliphatic hydrocarbons as the main product. Linear olefins can be utilized as chemicals while linear paraffins with suitable boiling range is excellent diesel fuel. However, the straight chain hydrocarbons are unsuitable for Otto-cycle engine because of their low octane number. The present authors has been developing reaction systems which makes iso-paraffin rich hydrocarbons whose catalyst is composed of cobalt-base FTS catalyst and modified zeolite in either one stage or two stages the products are mostly distributed over C<sub>3</sub>-C<sub>6</sub> hydrocarbons which are rich in iso-paraffins<sup>10</sup>.

### Methanol Synthesis

Methanol synthesis with Cu-Zn catalyst is the well established process and is thought to have little room to be developed. It has been tried to develop technologies by utilizing the liquid phase carbonylation of alcohol with methoxide catalysts to formic acid ester, and its hydrocracking to methanol and alcohol. However,



This process (especially the carbonylation step) is strongly poisoned by either water or CO<sub>2</sub>, which make it difficult to commercialize. The present authors have developed two types of low temperature liquid phase methanol synthesis. One is the utilization of carbonates or formates of alkali for the carbonylation step and the utilization of special hydrogenation catalyst<sup>11</sup>. Another system is the utilization of new concept of methanol formation<sup>12,13</sup>.



Both systems are operated at around 150-160 °C under pressurized conditions, giving 60-70% one-pass yield of methanol from synthesis gas even in the presence of H<sub>2</sub>O or CO<sub>2</sub>.

### Liquid Petroleum Gas (LPG)

LPG is one of the most important home fuel and transportation fuel in Asian countries. LPG is the by product of crude oil production or natural gas production and the mixture of C<sub>3</sub> and C<sub>4</sub> paraffins. Selective production of LPG from synthesis gas by FTS catalyst is difficult because of the limitation of ASF distribution and the formation of large amount of CH<sub>4</sub>. The present authors have shown that the synthesis gas conversion on the hybrid catalyst composed of methanol synthesis catalyst and zeolite gives the mixture of hydrocarbon composed of C<sub>2</sub> - C<sub>5</sub> paraffins with high selectivity and with very low CH<sub>4</sub> selectivity<sup>14,15</sup>. The high

LPG selectivity is attributed to the quick carbon-carbon bond formation from methanol (or DME) on zeolite to olefins and their quick hydrogenation to paraffins.

The combination of the heat tolerant methanol synthesis catalyst and suitable zeolite shows excellent catalyst stability and product selectivity. This technology is going to start its industrial application.

### Conclusion

Synthetic fuel production technologies including FTS reaction, which can produce sulfur-free fuel, are now becoming the stage of industrial development depending on the local conditions and technology level.

### References

1. K. Fujimoto, K. Asamai, T. Shikada, H. Tominaga, Chem. Lett., **1984**, P2051
2. Fujimoto, K., Asamai, K., Saima, H., Shikada, T., and Tominaka, H., Ind & Eng. Chem., Prod. Res. Dev. **1986**, **25**, P262.
3. Y. Adachi, M. Komoto, I. Wantabe, Y. Ohno, K. Fujimoto, Fuel **2000** **79**, (4), P229-234.
4. Fujimoto, K., Kameyama, I. Abe, T. Kunugi, J. Japan Petrol. Inst., **1981**, **24**, P233.
5. Yokota, K., and Fujimoto, K., Fuel, **1989**, **68**, P225.
6. K. Yokota and K. Fujimoto, Ind and Eng. Chem. Res., **1991**, **45**, P95.
7. K. Fujimoto, L. Fan and K. yoshii, Topics in Catalysis, **1995**, **2**, P259-266.
8. L. Fan, K. Yokota, and K. Fujimoto Topics in Catalysis, **1995**, **2**, P267-283.
9. S. Sun, K. Fujimoto, Y. Yoneyama, N. Tsubaki, Fuel, **2002**, **81**, P1583-1591.
10. Xiaohong Li, Kenji Asami, Mengfei Luo, Keisuke Michiki, Noritatsu Tsubaki, and Kaoru Fujimoto, Catalysis Today, **2003**, **84**, P59-65.
11. Yoshitada S., Fan, Li., Kaoru F., Sekiyu Gakkaishi **1998**, **41**, (5), P354-375 Jianqing Zeng, Kaoru Fujimoto, and Noritatsu Tsubaki, Energy & Fuels, **2002**, **16**, P83-86.
12. Jian-Qing Zeng, Noritatsu Tsubaki, Kaoru Fujimoto, Fuel, **2002**, **81**, P125-127
14. Saima, H., Fujimoto, K., and Tominaga, H., J. Catalysis, **1985**, **94**, P16.
15. Fujimoto, K., Saima, H., and Tominaga, H., I & EC Research, **1998**, **27**, P920.

# CATALYSTS FOR HYDROGEN PRODUCTION FROM METHANE

Huifang Shao, Edwin L. Kugler and Dady B. Dadyburjor

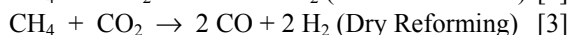
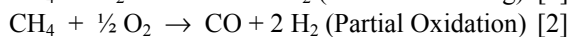
Department of Chemical Engineering  
West Virginia University, Morgantown WV 26506-6102

## Abstract

Bimetallic carbides such as  $\text{Co}_6\text{W}_6\text{C}$  have been synthesized and used for the reforming of methane to synthesis gas. These catalysts are active, selective and stable when they have been pretreated above  $750^\circ\text{C}$ . Reactivity experiments, coupled with characterization by XRD, show the effect of preparation procedure.

## Introduction

Three processes exist for the production of hydrogen from methane: steam reforming, partial oxidation and dry reforming. The three main reactions are indicated below.



Side reactions of importance include:



Dry reforming produces a product (synthesis gas, or syngas) of a lower  $\text{H}_2/\text{CO}$  ratio than the other two processes. However, there are advantages to this process, including the use of the greenhouse gas  $\text{CO}_2$  as a reactant.

Traditionally, a supported nickel catalyst has been used for dry reforming (1). However, this material deactivates rapidly, due to coke formation. Addition of alkali or alkaline-earth metals or passivation of the catalyst with, e.g., sulfur has been shown (2,3) to be effective. Noble-metal catalysts, e.g., Pt, have also been used. They are active and stable, but may be prohibitively expensive. Metal carbides are reasonably active and reasonably priced. (4).

Our work has concentrated on the use of bimetallic carbides as a way to modify the behavior of the carbides. Early work (5,6) used commercial material from Nanodyne. We have now started preparing the material in-house. In the current work, we report on a series of preparation and pretreatment techniques and show how they influence the reactivity behavior of these materials as well as their bulk characteristics.

## Experimental

**Catalyst Preparation.** The procedure is similar to that of Polizzoti *et al.* (7,8) In brief, precursor solutions of ammonium triethylenediamine tungstate and cobalt chloride are mixed at room temperature. The tungstate solution is prepared by dissolving 14.5 g tungstic acid in 400 ml of a 1:1 aqueous ammonium chloride solution and 300ml of ethylenediamine, followed by heating and stirring until the solution is clear. The cobalt solution is prepared by dissolving 13.8 g of the hexahydrate in 50 ml of distilled water. After mixing the two precursor solutions, the volume is reduced by 50% by evaporation. Pure cobalt triethylenediamine tungstate

( $\text{Co(en)}_3\text{WO}_4$ ) is obtained by filtering, washing with acetone, and drying the filter cake in the hood for 24 h.

The bimetallic carbide is obtained by a temperature-programmed reaction (TPRx) of this material, using a mixture of CO and  $\text{CO}_2$  of specified ratio. The process is carried out at 1 atm in a fixed-bed reactor. In the TPRx procedure, the temperature is first ramped up to  $650^\circ\text{C}$  during the flow of 130 sccm of an equimolar mixture of Ar and  $\text{H}_2$ , and the temperature held for 3 h. Then the mixture is flushed with Ar at 190 sccm for 0.5 h while the temperature is increased to  $850^\circ\text{C}$ . Last, the  $\text{CO}_2$ -CO mixture flows through for 24 h with a total flow rate of  $60(1+x)$  sccm, where x is the ratio  $\text{CO}_2 / \text{CO}$ . The reactor is then purged by flowing Ar at 190 sccm, and cooled down to room temperature.

**Catalyst Characterization.** The material was characterized by  $\text{N}_2$  BET and by x-ray diffraction. XRD measurements were carried out both before and after reaction.

**Reactor Setup.** Reactions were performed in a stainless-steel reactor (SS 304L) with an outer diameter of 0.5 in and a length of 25 in, which was placed in an 18-in single zone furnace from Applied Test Systems. A stainless-steel sheathed thermocouple was inserted into the center of the catalyst bed to monitor and control the reaction range. The products were sampled immediately downstream at preset intervals using a Valco six-port gas-sampling valve. To prevent the outlet from heating up the valve beyond its operating range, a cooling system was added between the reactor outlet and the sampling valve, using circulating silicone oil at  $90^\circ\text{C}$ . The composition of the outlet gas was analyzed using an on-line Hewlett-Packard 5890 gas chromatograph (GC) equipped with a thermal-conductivity detector (TCD), which provided quantitative analysis for  $\text{H}_2$ , CO,  $\text{CH}_4$ ,  $\text{CO}_2$ , and  $\text{H}_2\text{O}$ .

Typically 0.3 g of the catalyst sample was used for each test. The catalyst was pretreated by reducing with flowing hydrogen at 60 sccm for 1 h, followed by another hour of flushing with argon at  $400^\circ\text{C}$ . The reaction started once the pretreatment finished. The reactor was operated at 3.4 atm and  $850^\circ\text{C}$  with equal amounts of methane and carbon dioxide in the feed stream. The gas-hourly space velocity was kept constant at 9000 scc/hr/g cat. The conversions of the feed gases, the yields of the products, and the carbon balance, given by

Carbon Balance = (carbon out – carbon in) / (carbon in) [5]  
could then be calculated.

## Results and Discussion

Characterization and reactivity data are discussed below for values of x equal to 0.1, 0.2, 0.5 and 0.75.

**Catalyst Characterization.** BET results indicate that the surface area of the fresh catalyst does not depend on the value of x. Typical surface area values were found to be 2-3  $\text{m}^2/\text{g}$ . This is approximately equal to the values for the Nanodyne materials, approximately 5  $\text{m}^2/\text{g}$ .

XRD patterns are shown in Figures 1-4 for the different catalyst materials. The major components present in the bulk are summarized in Table 1. Here  $\text{Co}_3\text{W}_3\text{C}$  represents an interstitial carbide with twice the amount of C present than in the bimetallic carbide  $\text{Co}_6\text{W}_6\text{C}$ .

**Table 1. Bulk Components of Catalyst Materials as a Function of Pretreatment Conditions**

$x = \text{CO}_2 / \text{CO}$	Bulk Components
0.1	$\text{Co}_3\text{W}_3\text{C}$ , Co, WC
0.2	$\text{Co}_3\text{W}_3\text{C}$
0.5	$\text{Co}_6\text{W}_6\text{C}$
0.75	$\text{Co}_6\text{W}_6\text{C}$

Clearly the bulk components are dependent upon the ratio  $x (= \text{CO}_2 / \text{CO})$ , at least for values less than or equal to 0.5. Table 1 indicates that the relative amount of carbon present in the bulk compounds decreases, in general, as  $x$  increases, at least up to  $x = 0.5$ . This is consistent with the decreasing chemical activity of carbon,  $a_C$ , as the  $\text{CO}_2/\text{CO}$  ratio decreases.

More importantly, Table 1 indicates that the bulk compounds present for the material made with  $x = 0.1$  are those found in the Nanodyne catalyst after it reached its steady-state catalytic performance (6). This would seem to imply that the catalytically active material could be made directly by using in-house techniques.

**Catalyst Reactivity and Stability.** The catalytic performance of the bimetallic carbides prepared and characterized as described above is shown in Figures 5-7. While the individual behaviors are different, note that all three catalysts are characterized by an unsteady-state period of approximately 20 h, after which the catalyst is stable for at least the next 80 h. Clearly, the catalyst is still undergoing a solid-state reaction to

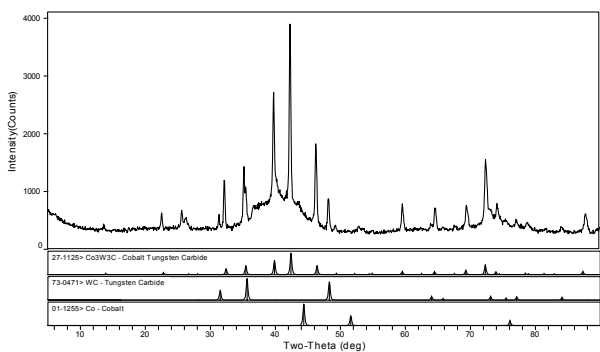


**Figure 1.** XRD spectrum from material made with  $x (= \text{CO}_2 / \text{CO}) = 0.1$

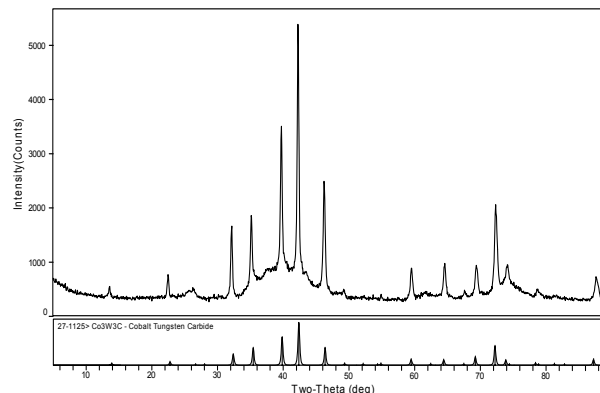


**Figure 2.** XRD spectrum from material made with  $x (= \text{CO}_2 / \text{CO}) = 0.2$

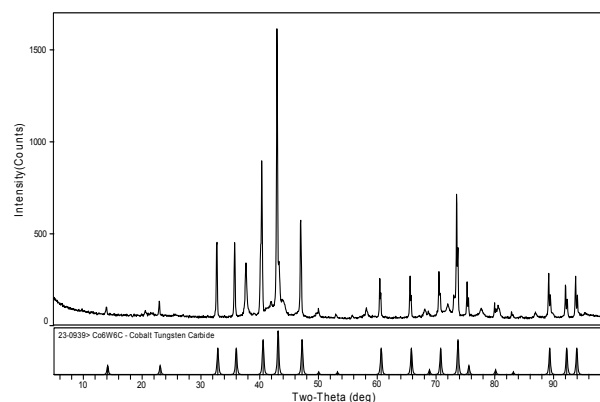


**Figure 3.** XRD spectrum from material made with  $x (= \text{CO}_2 / \text{CO}) = 0.5$ .

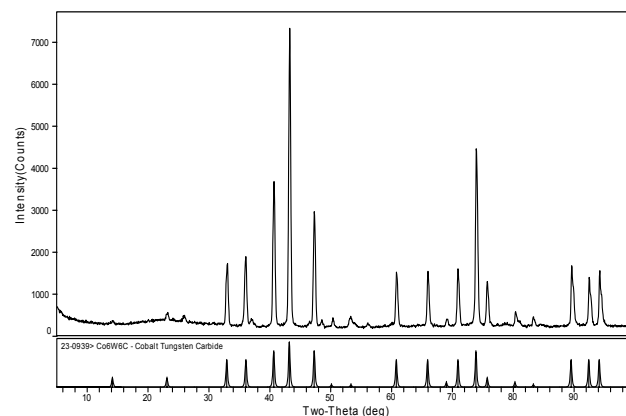


**Figure 4.** XRD spectrum from material made with  $x (= \text{CO}_2 / \text{CO}) = 0.75$ .

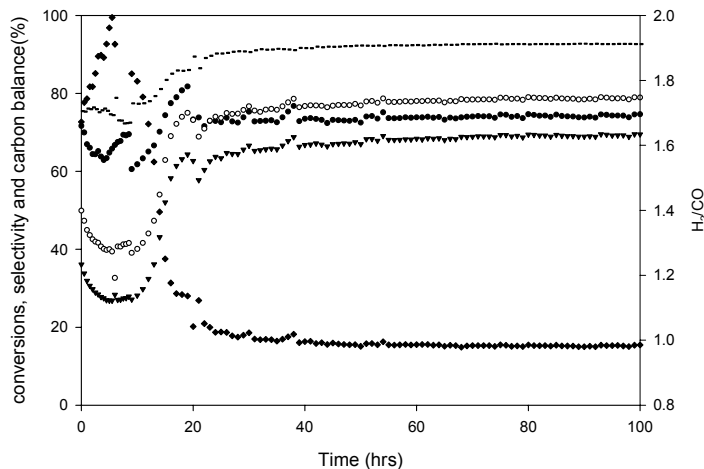


**Figure 5.** Catalytic performance of material made with  $x (= CO_2 / CO) = 0.1$ . Closed circles =  $CH_4$  conversion, open circles =  $CO_2$  conversion, triangles = CO yield, diamonds =  $H_2/CO$ , dashed lines = carbon balance.

a more-stable phase, which is also the more catalytically active phase. The unsteady-state period is characterized by  $H_2/CO$  ratios much higher than the expected (stoichiometric) value of 1 and a relatively low carbon balance of 70-80%. These observations are consistent with a laydown of carbon on the catalyst surface. Hence, in all cases, it would appear that carbon deposition leads to a more-stable, more-active phase on the catalyst surface.

From Table 1, the material prepared using  $x = 0.75$  has the same bulk structure as the Nanodyne material. Hence it is worthwhile comparing the catalytic performance of these two materials. The Nanodyne material reaches its steady-state

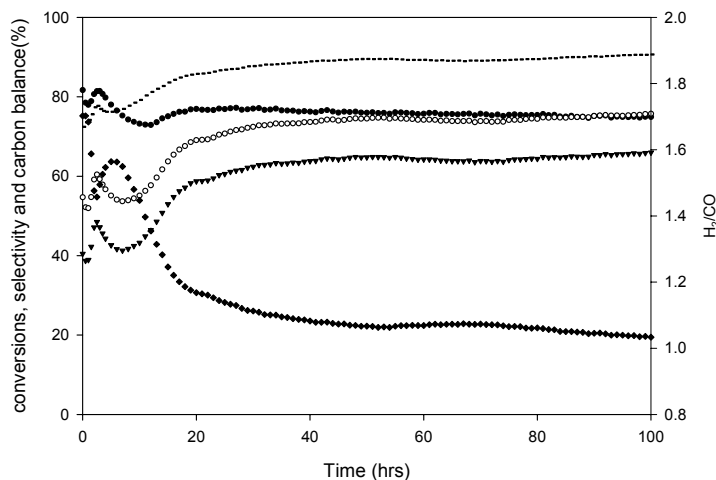


**Figure 6.** Catalytic performance of material made with  $x (= CO_2 / CO) = 0.2$ . Symbols have the same meaning as in Fig. 5.

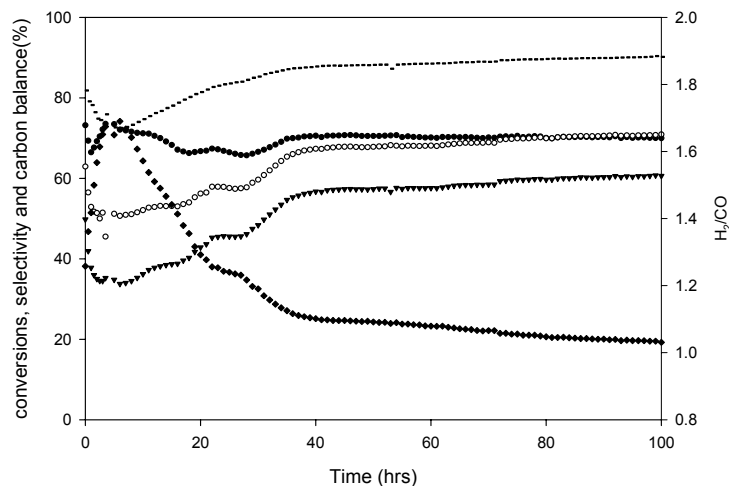


**Figure 7.** Catalytic performance of material made with  $x (= CO_2 / CO) = 0.75$ . Symbols have the same meaning as in Fig 5.

value in well under 20h (6), whereas the in-house material takes longer to approach steady state. The  $CH_4$  conversion is greater than the  $CO_2$  conversion in Figure 7, at least initially, whereas the reverse is observed (6) for the Nanodyne material, and at all times on stream. The ratio of  $H_2/CO$  is significantly greater than the stoichiometric value (1.0) for the in-house material, especially during the unsteady-state period. All these observations imply that the in-house material results in greater carbon deposition and more water-gas shift products. The in-house material is also further from its final, catalytically active state than is the Nanodyne material.

As mentioned earlier, Table 1 indicates that the material prepared using  $x = 0.1$  has the same bulk constituents found in the Nanodyne material (or the material prepared with  $x = 0.75$ ) after it had reached its final, active state. Hence, one would expect the catalytic performance of the former material to require little or no time on stream to reach steady-state behavior, and for this behavior to be comparable to the steady-state behavior of the  $x = 0.75$  (or Nanodyne) material. However, Figure 5 shows that steady-state behavior still requires 20 h on stream to be achieved, even though this amount is less than the comparable period for Figure 7. Clearly, even the catalyst that contains WC and Co in the bulk phase at the start needs pretreatment. Further, the  $H_2/CO$  at unsteady state is much higher than the corresponding value in Figure 7. The  $CO_2$  conversion at steady state is somewhat greater than the  $CH_4$  conversion, implying less water-gas shift than for the  $x = 0.75$  (or Nanodyne) material.

Finally, we consider the catalytic performance of the  $x = 0.2$  material (Figure 6). The time to reach steady state in Figure 6 lies in between those in Figures 5 and 7. The catalytic performance in Figure 6 is more closely related to that in Figure 7 than that in Figure 5. This would appear to be counter-intuitive, given the values of  $x$  used in these three procedures and the bulk materials obtained from XRD. Again,

the nature of the catalytically active surface needs to be determined.

Figures 8 and 9 represent XRD patterns for materials after the reactions. For the  $x = 0.75$  material (Figure 8), the bulk species after reaction are those obtained with the Nanodyne material, *viz.*, WC, Co and C. For the  $x = 0.1$  material (Figure 9), the bulk materials observed after reaction, in addition to C, are similar to those observed before, *viz.*,  $\text{Co}_3\text{W}_3\text{C}$ , WC and Co, but in different relative amounts than before.

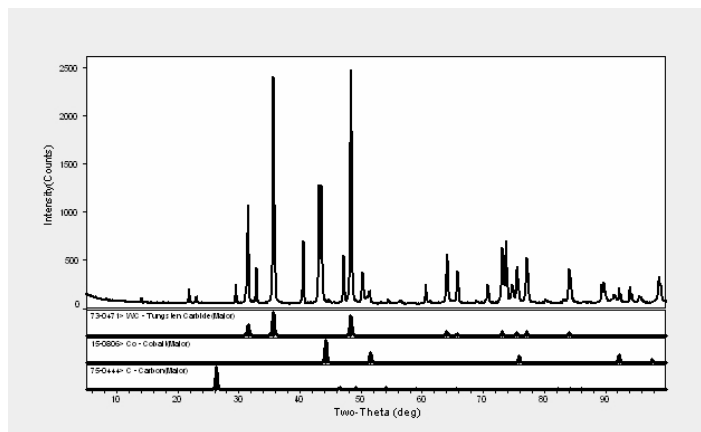


**Figure 8.** XRD after reaction for material prepared with  $x = 0.75$ .

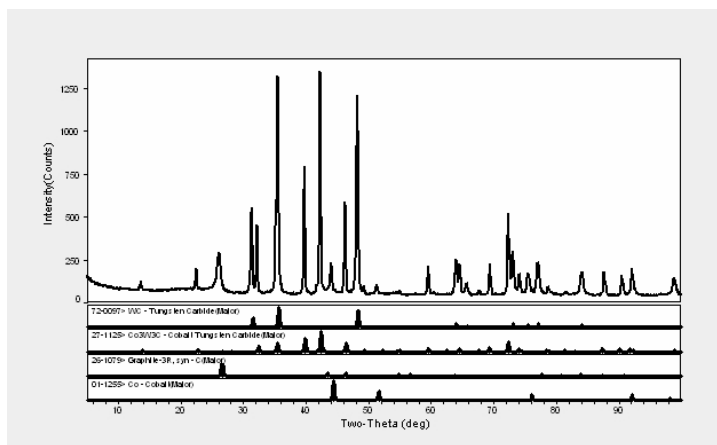


**Figure 9.** XRD after reaction for material prepared with  $x = 0.1$

## Conclusions

Bimetallic carbides such as  $\text{Co}_6\text{W}_6\text{C}$  have been synthesized and used for the reforming of methane to synthesis gas. These catalysts are active, selective and stable when they have been pretreated at  $850^\circ\text{C}$ . Reactivity experiments, coupled with characterization by XRD, relate the activity data to the formation of various chemical species in bulk. In all cases, there is an initial unsteady-state period characterized by carbon deposition and solid-state

transformation of the material to a more catalytically active phase. However, it would appear that the connection between bulk structure and reactivity is ambiguous. Clearly, the surface nature of the catalyst needs to be obtained.

**Acknowledgement.** Financial support from the U.S. Department of Energy under Cooperative Agreement DE-AC22-99FT40540 with the Consortium for Fossil Fuel Science is gratefully acknowledged. The assistance of Professor M.S. Sehra, Department of Physics, in obtaining the XRD patterns is appreciated.

## References

- (1) Bradford, M. C. J.; Vannice, M. A. *Applied Catalysis A: General* **1996**, *142*, 73-96.
- (2) Osaki, T.; Mori, T. *J. Catal.* **2001**, *20*, 89-97.
- (3) Rostrup-Nielsen, J. R. *J. Catal.* **1984**, *85*, 31-43.
- (4) Babilius, A. *Materials Science* **2003**, *7*, 183-186.
- (5) Iyer, M.V.; Norcio, L.P.; Kugler, E.L.; Dadyburjor, D.B. *Ind. Eng. Chem. Res* **2003**, *442(12)*, 2712-2721.
- (6) Iyer M.V.; Norcio, L.P.; Punnoose, A.; Kugler, E.L.; Sehra, M.S.; Dadyburjor, D.B. *Topics in Catalysis*, in press.
- (7) Kugler, E.L.; McCandlish, L.E.; Jacobson, A.J.; Chianelli, R.R. *U.S. Patent 5,138,111*; **August 11, 1992**.
- (8) Polizzoti, R.S.; McCandlish, L.E.; Kugler, E.L. *U.S. Patent 5,338,330*; **August 16 1994**.

# HYBRID CATALYSTS WITH MICROCRYSTALLINE ZEOLITE AND SILICA-ALUMINA FOR WAX HYDROCRACKING

Nobuo Aoki, Hiroyuki Seki, Masahiro Higashi,  
Toshio Waku, and Masakazu Ikeda

Central Technical Research Laboratory  
Nippon Oil Corporation  
8 Chidori-cho, Naka-ku,  
Yokohama, 231-0815 JAPAN

## Introduction

The demand for heavy residues such as asphalt is decreasing while that for clean fuels is increasing in order to reduce particulate matter and others in automobile exhaust. One possible solution to this situation is the development of asphalt-to-liquid (ATL) process. ATL process consists of three steps: gasification of asphalt, wax production by F-T synthesis, and production of clean fuels by wax hydrocracking. This paper focuses on the development of catalyst for wax hydrocracking.

There are two major requirements for wax hydrocracking catalysts, high activity and high selectivity of middle distillates (MD). As is well known, it is quite challenging to meet the both requirements. For instance, silica-alumina shows high MD selectivity,<sup>1</sup> but its activity is insufficient. On the contrary zeolites show high activity, but their MD selectivity is generally lower than silica-alumina since their high activity causes overcracking of MD.

We have clarified in our last report, however, that both requirements are satisfied at a fairly high level with the catalysts which contain microcrystalline USY zeolite (MC-USY).<sup>2</sup> The higher MD selectivity of MC-USY based catalysts is assumed to be achieved by shorter pore lengths of MC-USY which has a particle size of less than 0.5  $\mu\text{m}$ , with less overcracking of

In order to enhance the performance of MC-USY based catalysts further we are trying to hybridize this key material with various amorphous solid acids. This paper reports the performance of the hybrid catalyst with MC-USY and silica-alumina. The mechanism of collaboration of the two components is also discussed.

## Experimental

**Catalysts.** MC-USY was prepared by crystallizing smaller seeds than usual, followed by steaming and acid treatment. Its  $\text{SiO}_2/\text{Al}_2\text{O}_3$  ratio was adjusted to 30, according to the method in our previous report.<sup>2</sup> Commercially available amorphous silica-alumina (alumina 14 mass %) powders were used in combination with MC-USY. Extrudates with a composition of 3 mass% MC-USY, 57 mass% silica-alumina and the rest alumina binder were prepared using a usual method. On these extrudates a given amount of platinum was loaded with an aqueous solution of nitric acid (1N) containing hexachloroplatinum acid by the incipient wetness method. The Pt-loaded extrudates were calcined at 500 °C for 1 h.

Catalysts containing single acid component, MC-USY or silica-alumina, were also prepared.

**Performance Tests.** Tests were carried out with a flow reactor. The catalysts (100 ml) were first reduced at 340 °C for 1 h before the reaction started. Feed wax was treated under the condition below:

pressure: 3 MPa,  $\text{H}_2/\text{oil}$ : 3500 scf/b, LHSV: 2  $\text{h}^{-1}$ .

The product oil was fractionated into naphtha (<145 °C), kerosene (145-260 °C), gas oil (260-360 °C), and wax (>360 °C). The term of middle distillates (MD) means the total of kerosene and gas oil.

## Results and Discussion

The performance of the hybrid catalyst loaded with 0.8 mass % Pt is shown in **Figure 1** and **Figure 2** with those of catalysts containing single acid component

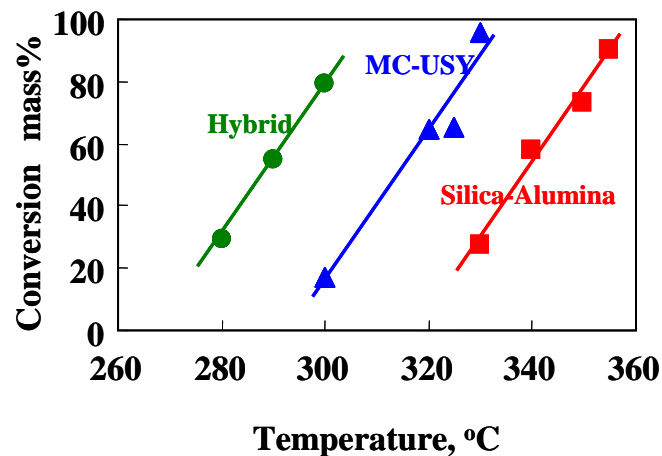


**Figure 1.** Cracking activity of tested catalysts. Pt: 0.8 mass %

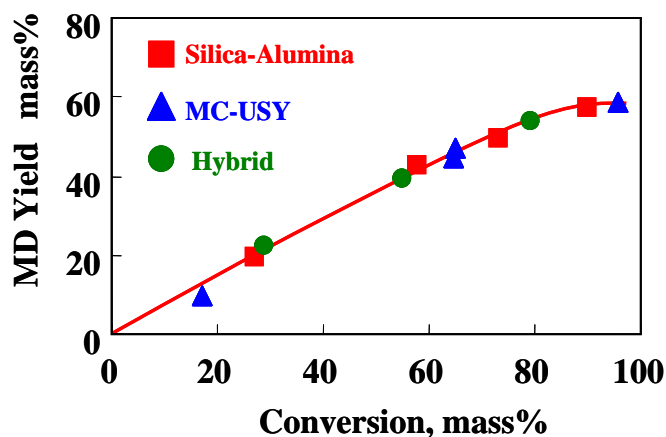


**Figure 2.** Middle distillates (MD) selectivity of tested catalysts. Pt: 0.8 mass %

**Figure 1** shows that cracking activity increases in the order of silica-alumina, MC-USY, and Hybrid. This indicates the hybrid catalyst can hydrocrack wax at lower temperature range where the catalysts containing single acid component cannot.

It is clear from **Figure 2** that despite the high activity of the hybrid catalyst it maintains the same level of high MD selectivity as the catalyst containing only silica-alumina as acid component.

There has already been a widely accepted reaction mechanism for wax hydrocracking by USY zeolite based catalysts with Pt, as is shown in **Figure 3**. This mechanism consists of four steps below.

- (1) olefin formation by dehydrogenation of wax on Pt
- (2) isomerization on acid sites of USY zeolite
- (3) cracking of the isomers on acid sites of USY zeolite
- (4) stabilization of cracked products through hydrogenation on Pt

In this mechanism, step (2) is considered to be rate determining.<sup>3</sup> Silica-alumina in the hybrid catalyst is assumed to accelerate step (2) and consequently enhance the overall reaction rate.

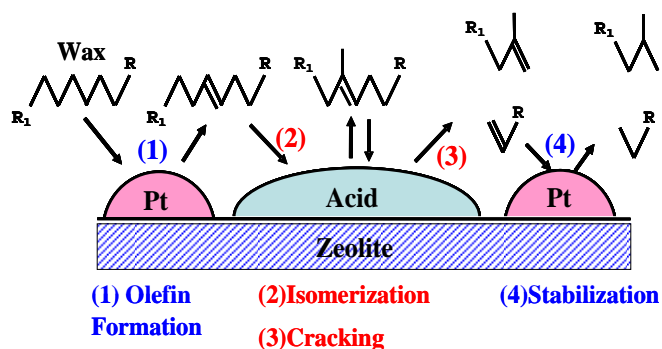


**Figure 3.** Reaction mechanism for wax hydrocracking by USY zeolite based catalysts with Pt.

The type of silica-alumina affects the performance of the hybrid catalyst. For instance, the high MD selectivity of the hybrid catalyst is not obtained when another silica-alumina is used which contains 5 mass % of alumina and has higher acid strength than silica-alumina of this report.

The ratio of silica-alumina to MC-USY can also affect the performance and we have started to optimize the ratio. The result will be reported in near future.

Because Pt plays an important role in wax hydrocracking, the effect of the amount of Pt on the catalytic performance was studied. The results are presented in **Figure 4** and **Figure 5**.

**Figure 4** shows that the hybrid catalyst exhibits constant cracking activity even with Pt less than 0.8 mass %. This indicates that the rate determining step of this hybrid catalyst is still step (3) in **Figure 3**. However it can be seen from **Figure 5** that MD selectivity of the hybrid catalyst decreases gradually, depending on the amount of Pt, in the range less than 0.8 mass %. This tendency is not observed in the case of the catalysts containing single acid component except for the range less 0.2 mass %. This means that the stabilization ability in step (4) in **Figure 3** is insufficient in the hybrid catalyst with Pt less than mass 0.8 % and that the hybrid catalyst requires more Pt than the catalyst containing single acid component to gain the same level of MD selectivity.

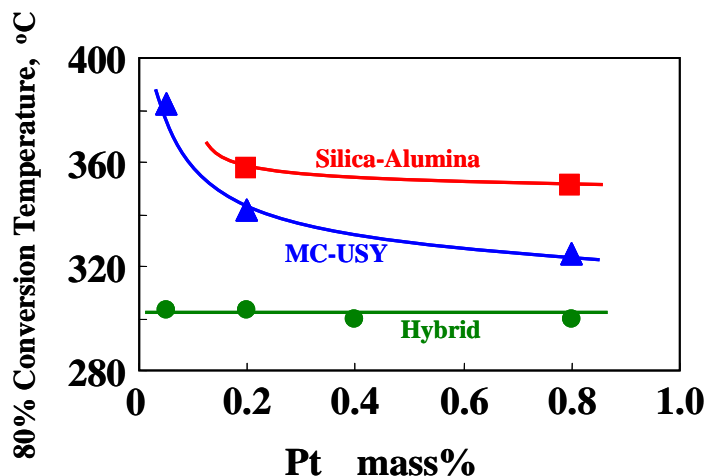


**Figure 4.** Effect of the amount of Pt on cracking activity. Vertical axis shows the temperature at which 80% of conversion is gained and relates to cracking activity.

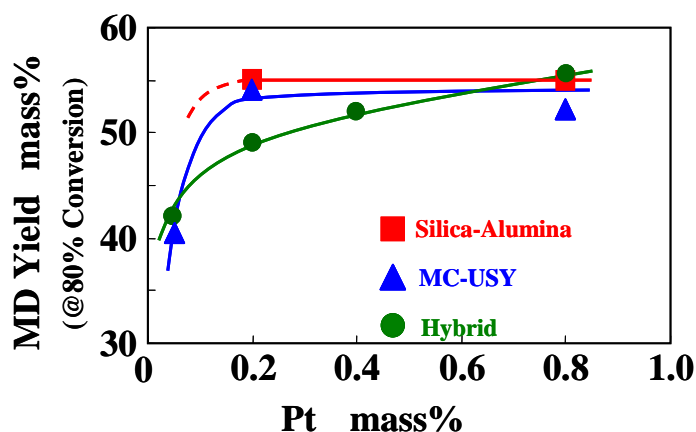


**Figure 5.** Effect of the amount of Pt on MD selectivity.

**Table 1** presents the properties of the gas oil obtained with the hybrid catalyst (Pt 0.8 mass %) along with that of the catalyst containing only MC-USY. By hybridization more preferable gas oil with lower pour point is obtained.

**Table 1. Properties of Gas Oil**

	Density, @ 15° C	Cetane Index	Pour point °C
MC-USY	0.7876	94	-17.5
Hybrid	0.7876	94	-22.5

## Conclusions

- The hybrid catalyst with both MC-USY and silica-alumina exhibits higher activity than that containing only MC-USY and has the same level of high selectivity as that containing only silica-alumina.
- Silica-alumina in the hybrid catalyst is assumed to accelerate the isomerization step that is considered to be rate determining in an accepted reaction mechanism.
- While cracking activity of the hybrid catalyst is independent of the amount of Pt, MD selectivity is sensitive to it

**Acknowledgement.** This work was done as a part of the Asphalt-to-Liquid (ATL) research project of the New Energy and Industrial Technology Development Organization (NEDO) of Japan with a subsidy from the Ministry of Economy, Trade and Industry

## References

- Calemma, V.; Peratello, S.; Pavoni, S.; Clerici, G.; and Perego, C., *Stud. Sur. Sci. Catal.*, **2001**, 136, 307.
- Seki, H.; Aoki, N.; and Ikeda, M., Prepr. Pap. -*Am.Chem.Soc., Div. Pet. Chem.*, **2003**, 48 (3), 139.
- Weitkamp, J. and Ernst, S., *Catalysis. Today*, **1994**, 19, 107.

# A NEW LOW-TEMPERATURE METHANOL SYNTHESIS FROM LOW-GRADE SYNGAS

Prasert Reubroycharoen<sup>a</sup>, Yamagami Tetsuji<sup>a</sup>, Yoshiharu Yoneyama<sup>a</sup>, Tharapong Vitidsant<sup>b</sup>, Noritatsu Tsubaki<sup>a\*</sup>

<sup>a</sup>Dept. of Material System & Life Science, School of Engineering, Toyama University, Gofuku, Toyama, 930-8555, Japan

<sup>b</sup>Dept. of Chemical Technology, Faculty of Science, Chulalongkorn University, Bangkok, 10330, Thailand

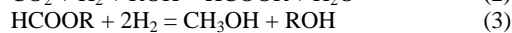
\* Tel/Fax: (81)-76-445-6846; E-mail: tsubaki@eng.toyama-u.ac.jp

## Introduction

Methanol, which is an alternative fuel, is being produced by 30-40 million ton per year around the world from CO/CO<sub>2</sub>/H<sub>2</sub>. It is now commercially produced by ICI process under high temperature and high pressure (523-573 K, 50-100 bar), using Cu/ZnO catalyst developed by ICI Co.. However, the efficiency of methanol synthesis is severely limited by thermodynamics,<sup>1,2</sup> theoretic CO conversion is around 20% at 573 K and 50 bar.<sup>3</sup> Therefore, developing a low-temperature process for methanol synthesis will greatly reduce the production cost by utilizing the intrinsic thermodynamic advantage at low temperature.<sup>4</sup>

Brookhaven National Laboratory of USA (BNL) realized this synthesis at 373-403 K and 10-50 bar, using very strong base catalyst (mixture of NaH, alcohol and acetate) and pure syngas (CO + H<sub>2</sub>). However, a remarkable drawback of this process is that trace amount of carbon dioxide and water in the feed gas (CO + H<sub>2</sub>) or reaction system will deactivate the strongly basic catalyst soon,<sup>5,6</sup> which implies high cost from the complete purification of the syngas from the methane reformer or the gasification plant, as well as the re-activation process of the deactivated catalyst.

The present authors proposed a new method of low-temperature synthesis of methanol from CO/H<sub>2</sub> containing CO<sub>2</sub>.<sup>7,8</sup> It consists of the following fundamental steps:



In this study, the influence of chemical composition of Cu/ZnO catalyst was studied in a batch reactor. The effects of reaction condition on the synthesis of methanol from CO/CO<sub>2</sub>/H<sub>2</sub> on Cu/ZnO catalyst were investigated. A flow-type semi-batch reactor was employed, where catalyst lifetime change could be observed.

## Experimental

**Catalyst Preparation.** The catalyst was prepared by the conventional co-precipitation method of an aqueous solution containing copper, zinc nitrates and an aqueous solution of sodium carbonate at 338 K and pH of 8.3-8.5. The molar ratio of Cu/Zn was varied.

**Low-temperature Methanol Synthesis.** The reaction apparatus was a flow-type semi-batch autoclave reactor with an inner volume of 85 ml. The configuration of the reactor is shown in Figure 1. 3.0 g (Cu:Zn = 1:1 and 100-200 mesh) of passivated catalyst and 20 ml of alcohol (purity > 99.5 %) were used. The temperature of reactor exit and cold trap was controlled. After purging the system with feed gas at room temperature, increasing the pressure of reactor to 50 bar, the temperature was enhanced to 443 K in 20 min. The

composition of feed gas was CO/CO<sub>2</sub>/H<sub>2</sub>/Ar = 32.6/5.2/59.2/3.0, in which argon was employed as an internal standard. The effluent gas was introduced to TCD. The liquid products in the cold trap and those remaining in the reactor were collected together and then analyzed by FID with methanator after the reaction. All liquid products were confirmed on GC-MS (Shimadzu GCMS 1600).

The reaction of activity test of home-made Cu/ZnO catalyst with different Cu/Zn ratio was conducted in a closed batch reactor with the inner volume of 85ml.

Total carbon conv. = CO conv. × a/(a+b) + CO<sub>2</sub> conv. × b/(a+b)  
(a, b were the contents of CO, CO<sub>2</sub> in the feed gas)

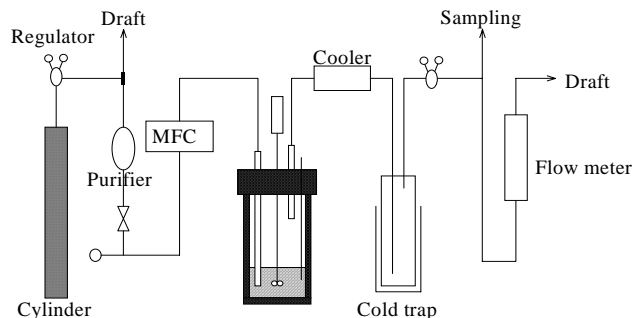


**Figure 1.** The semi-batch continuous apparatus for methanol synthesis reaction.

## Results and Discussion

In Figure 2, the reaction activity and its relationship with the chemical composition of Cu/ZnO in a closed reactor were displayed. It is clear that too much Cu or Zn percentage was not favorable to the catalyst activity. Cu/ZnO with the molar ratio of 1 exhibited the best reaction activity. More interestingly, while the total conversion was lower, the selectivity of ethyl formate was high. With the enhanced conversion, the selectivity of methanol increased, indicating that methanol was the final product and formate was intermediate in this consecutive reaction series.

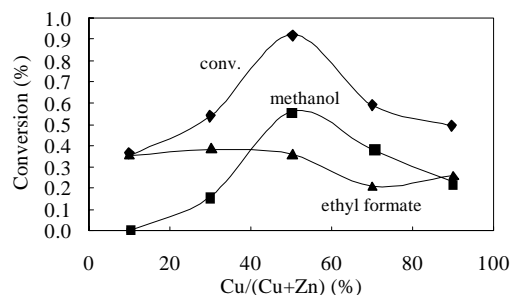


**Figure 2.** The reaction performances of Cu/ZnO catalysts with different Cu/(Cu + Zn) molar ratio in a batch reactor. Temperature = 443 K; initial pressure = 30 bar; reaction time = 2 h; Cu/ZnO = 0.20 g; ethanol 10 ml; stirring speed = 1260 rpm.

In Figure 3, the conversion and yield of methanol increased with increasing in time of reaction. Methanol yield gradually increased with the decreased ethyl formate yield, while the latter correspondingly decreased and became equilibrium at about 2 h, indicating that ethyl formate was an intermediate of methanol synthesis.

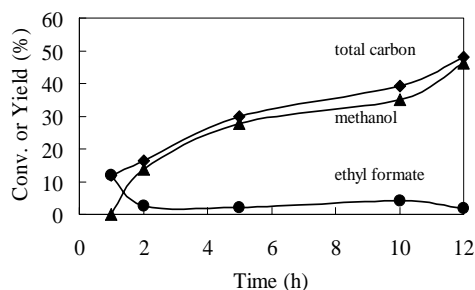


**Figure 3.** The effect of reaction time in batch reactor. Temperature = 443 K; initial pressure = 30 bar; Cu/ZnO = 1.00 g; ethanol = 20 ml; stirring speed = 1260 rpm.

In Figure 4, it is shown the time-on-stream and conversion on Cu/ZnO during 20 h. The conversions were very low at initial stage due to the dead volume of the reactor and trap filled by the feed gas. The total carbon conversion was about 47%. Furthermore, at the initial 10 h, the CO<sub>2</sub> conversion dropped to minimum -42% and then increased again to about 3%.

According to the time-on-stream of the conversions above, that CO was converted to CO<sub>2</sub>, and then CO<sub>2</sub> converted to methanol through the designed routes, step (1) - (3). It should be noted that if no alcohol was used as solvent, for example, in the case where hexane was used instead as an inert solvent, no activity was observed.

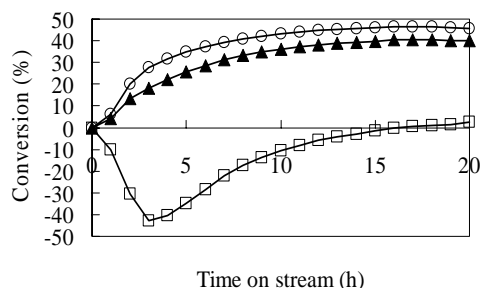


**Figure 4.** Variations of conversions with time on stream for the methanol synthesis from CO/CO<sub>2</sub>/H<sub>2</sub>. Temperature = 443 K; pressure = 50 bar; Cu/ZnO = 3.00 g; 2-butanol 20 ml; stirring speed = 1260 rpm; 20 ml/min; (○) CO%; (□) CO<sub>2</sub>%; (□) total carbon%.

In Figure 5, the relationship between conversion and reaction pressure is shown. It was found that the total carbon conversion increased gradually with increasing reaction pressure.

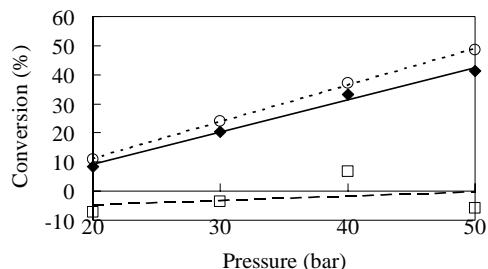


**Figure 5.** Variations of conversions with for the methanol synthesis from CO/CO<sub>2</sub>/H<sub>2</sub>. Temperature = 443 K; Cu/ZnO = 3.00 g; 2-butanol 20 ml; stirring speed = 2000 rpm; 20 ml/min; (○) CO%; (□) CO<sub>2</sub>%; (□) total carbon%.

In Figure 6, it is shown the conversion and reaction temperature. It is interesting that the conversion continuously increased with increasing in temperature of reaction without changing in the methanol selectivity (>98%). In contrary with high temperature methanol synthesis, high reaction temperature lowers the methanol selectivity.

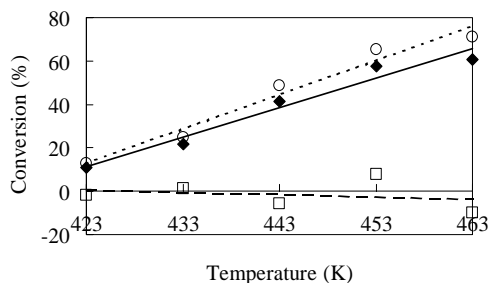


**Figure 6.** Variations of conversions with temperature for the methanol synthesis from CO/CO<sub>2</sub>/H<sub>2</sub>. Pressure = 50 bar; Cu/ZnO = 3.00 g; 2-butanol 20 ml; stirring speed = 2000 rpm; 20 ml/min; (○) CO%; (□) CO<sub>2</sub>%; (□) total carbon%.

In Table 1, the results on catalyst weight showed the conversion can be improved by increasing the catalyst weight, in contrary to high-temperature gas phase reaction, the increased catalyst weight indeed improved the conversion due to relief of thermodynamic limitation.

**Table 1** Methanol synthesis with various weight of catalyst

Cat. (g)	Conversion (%)			CH <sub>3</sub> OH selectivity (%)
	CO	CO <sub>2</sub>	Total C	
3.0	48.5	-5.8	41.4	98.5
6.0	63.8	-11.5	53.9	99.2

Temperature = 443K Pressure = 50 bar; 2-butanol 20 ml; stirring speed = 2000 rpm; 20 ml/min.

## Conclusions

The low-temperature methanol synthesis from CO/CO<sub>2</sub>/H<sub>2</sub> using 2-butanol as solvent has exhibited very high activity and selectivity for methanol formation at temperature as low as 443 K and 50 bar. Since the reaction employed conventional solid catalyst, very mild reaction conditions and syngas containing CO<sub>2</sub> and H<sub>2</sub>O, it might be a promising practical method for methanol synthesis at low temperature. The total carbon conversion increased with the increasing of reaction temperature, pressure, and catalyst weight. The high conversion of methanol synthesis at low-temperature was produced from CO and H<sub>2</sub> containing small amount of CO<sub>2</sub>.

## References

- (1) Herman, R. G.; Simmons, G. W.; Klier, K. *Studies in Surf. Sci. Catal.* **1981**, *7*, 475.
- (2) Graaf, G. H.; Sijtsema, P.; Stamhuis, E. J.; Oosten, G. *Chem. Eng. Sci.* **1986**, *41*, 2883.
- (3) Marchionna, M.; Lami, M.; Galletti, A. *CHEMTECH*, 1997, April, 27.
- (4) Zheng, J.; Tsubaki, N.; Fujimoto, K. *Fuel* **2002**, *81*, 125.
- (5) Haggin, J. *Chem. & Eng. News* **1986**, Aug. 4, 21.
- (6) Brookhaven National Laboratory, U.S. Patent, 4,614,749, 4,619,946, 4,623,634, 4,613,623 (1986), 4,935,395 (1990).
- (7) Tsubaki, N.; Sakaiya, Y.; Fujimoto, K. *Appl. Catal.* **1999**, *180*, L11.
- (8) Tsubaki, N.; Ito, M.; Fujimoto, K. *J. Catal.* **2001**, *197*, 224.

## Development of high-performance F-T synthesis catalyst and demonstrative operation of a pilot plant with the catalyst by JOGMEC-GTL project in Japan

Ken-ichiro Fujimoto<sup>1</sup>, Kimihito Suzuki<sup>1</sup>, Masato Kageyama<sup>1</sup>,  
Yasuhiro Ohnishi<sup>2</sup>, Noriyuki Yamane<sup>1</sup>, Ikuo Jitsuvara<sup>1</sup>,  
Yoshifumi Suehiro<sup>3</sup>

<sup>1</sup> Technical Development Bureau

Nippon Steel Corporation  
20-1 Shintomi, Futtsu-city, Chiba 293-8511, Japan

<sup>2</sup> Energy Facilities, Civil Engineering & Marine Construction Div.

Nippon Steel Corporation  
5-9-1 Nishihashimoto, Sagami-hara-city, Kanagawa 229-1131, Japan

<sup>3</sup> Oil & Gas Technology Research & Development

Japan Oil, Gas and Metals National Corporation  
1-2-2 Hamada, Mihama-ku, Chiba-city, Chiba 261-0025, Japan

### Introduction

Natural gas is now reconsidered as a promising energy source, because of its environmental friendliness and abundances in reserves. While its demand will be thought to increase, there are many stranded gas fields untapped in South East Asia and Oceania regions that were found in marginal location. These have been left uncommercialized by the conventional means of LNG form or through pipeline as their reserves are not large enough to invest in such infrastructures. GTL technology seems to be one of the attractive ways to develop these gas fields. By GTL technology, natural gas can be transformed to liquid hydrocarbon that is easy to be handled and transported.

Japan Oil, Gas and Metals National Corporation (JOGMEC) and five private companies (Japan Petroleum Exploration Co., Ltd., Chiyoda Corporation, Cosmo Oil Co., Ltd., Nippon Steel Corporation, and INPEX Corporation) have been making collaboration in the development of new GTL technology as JOGMEC-GTL project. Authors joined to this project and have been developing non-precious metal based F-T synthesis catalysts, and doing some research of simulation for F-T synthesis process. And we made a demonstrative operation of pilot plant last year with using our developed catalyst at Yufutsu in Hokkaido, Japan.

In this paper, we would like to report the obtained results introduced above.

### Development of catalysts for F-T synthesis in laboratory scale

Nippon Steel Corporation joined to this project in 2001, and has been developing cobalt-based catalysts using modified silica support. In this project, some target values for the catalyst performance shown in **Table 1** are set, and the catalyst also should have very high attrition resistance since the slurry phase reactor (slurry bubble column reactor: SBCR) is employed as a F-T reactor, and it is operated at very high superficial gas velocity (0.16m/s).

**Experimental.** Autoclaves (capacity: 100ml, 300ml) were used for F-T synthesis, and desired amount of catalyst and n-hexadecane as a solvent were put in the autoclave. After the autoclave was purged with nitrogen, syngas ( $H_2/CO=2.0$ ) containing Ar as an internal standard was introduced to the autoclave and pressurized to desired pressure. Then temperature was raised to desired temperature stirring the slurry at 800 rpm, and F-T synthesis reaction was started in this CSTR system. The effluent gas that contained unreacted syngas and light hydrocarbons was introduced to gas chromatography (TCD, FID) after getting through the trap that was kept at 273 K, and CO conversion,  $CH_4$  selectivity, and  $CO_2$

selectivity were calculated. Standard reaction conditions were as follows;

Temperature: 503 K

Pressure: 2.2 MPaG

W/F( $H_2+CO$ ): 5 g.h/mol

**Results and discussion.** Optimizing the properties of silica-based support and the preparation method of catalyst, the catalyst that shows splendid properties has been developed. This catalyst cleared all the target values shown in **Table 1** and was tested in 800-hour long run of F-T synthesis. The result is shown in **Figure 1**. Induction period is observed for the first 100 hours. It seems that this phenomenon is due to solvent replacement from n-hexadecane to heavy hydrocarbons produced by F-T synthesis. After this period, the catalyst activity is fairly stable. Re-designing the silica-based support, we could increase the physical strength and the attrition resistance of the catalyst. The particle size distribution of the catalyst was measured not only before and after 500-hour long run of F-T synthesis but also before and after ultrasonic attrition test<sup>(1)</sup>. By this series of tests, destruction and pulverization of the catalyst particle was not observed, and high attrition resistance of the catalyst was confirmed, so that applicable catalyst to SBCR was obtained. We also analyzed the by-product water. Although it showed weak acidity (pH=3.3 @ 298 K) as organic acids were formed a little, concentrations of other oxygenated organic compounds were low as expected, so it could not be problems for the operation of F-T synthesis reaction.

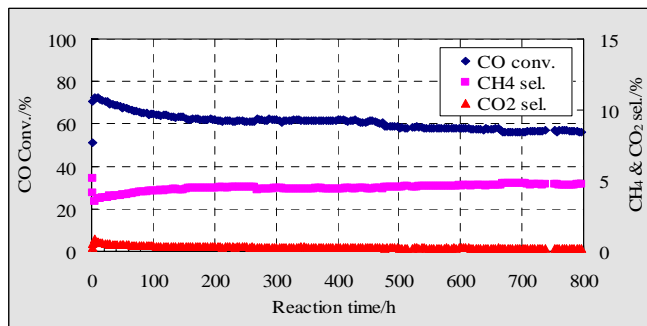


**Figure 1.** The result of long term F-T synthesis test. 503 K, 2.2MPaG,  $H_2/CO=2.0$ , W/F=1.5 g.h/mol



**Figure 2.** GTL pilot plant at Yufutsu in Hokkaido, Japan.

**Table 1. Catalyst Performance Demonstrated at Yufutsu Pilot Plant.**

	Temperature K	W/F g.h/mol	CO conv. %	C <sub>5</sub> <sup>+</sup> sel. %	$\alpha$ –	C <sub>5</sub> <sup>+</sup> Productivity g/kg-cat.h	Production bbl/d
Target	–	–	> 60	> 85	> 0.9	–	–
	513	1.8	62.3	85.2	0.91	1325	5.0
	503	4.5	75.3	88.7	0.91	689	2.6

2.2MPaG, H<sub>2</sub>/CO=2.0

### Demonstrative operation of pilot plant with developed catalyst

As shown above, the high-performance catalyst that is applicable for the pilot plant has been developed. So, the demonstrative operation was carried out last year at Yufutsu pilot plant (Figure 2). The results are shown in Table 1. All target values were cleared by this series of operation, and full load operation was attained at 7.3 bbl/d, which was beyond designed capacity of 7 bbl/d. And remarkably, very high C<sub>5</sub><sup>+</sup> productivity of over 1300 g/kg-cat.h was also recorded.

### Development of scale-up technology for F-T synthesis reactor

As scale-up technology for a slurry phase reactor, techniques based on mathematical models like a axial dispersion model and tank-in-series model are mainly adopted (2). But, these techniques need experimental parameters that describe the hydrodynamics in a gas-liquid system, and these parameters are usually obtained in a

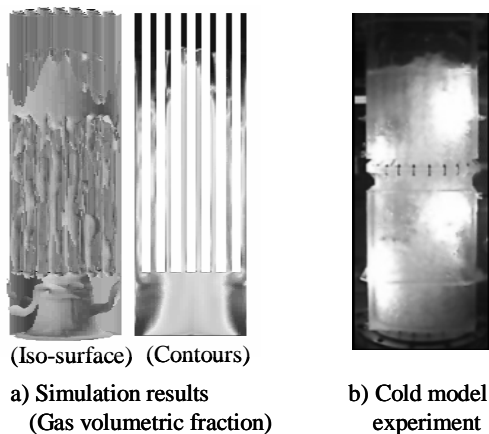


Figure 3. Visualization of the hydrodynamics.

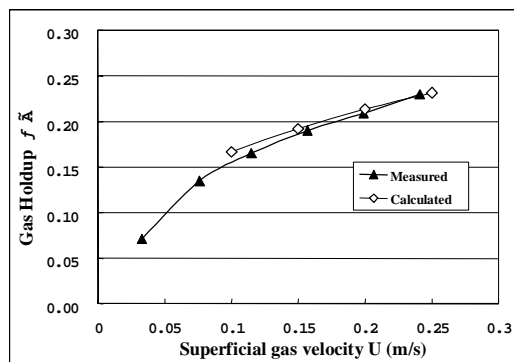


Figure 4. Comparison of calculated and measured gas holdup.

completely different system in dimension and physical properties from those of real plant like water-air system with using small-scale apparatus. Therefore, when these parameters are used for designing the real plant, an inaccuracy due to extrapolation should be taken into account. Then, in this research, we decided to

develop the simulation technology of gas-liquid fluid aided with CFD (Computational Fluid Dynamics) technique that has made remarkable progress in the area of scale-up technology.

**CFD technique for gas-liquid fluid.** Though there are some methods for a gas-liquid fluid simulation technique by CFD like averaging method, bubble-tracking method, and VOF method (3), averaging method was employed as designing method in this research, because of the realistic calculation load for simulation industrially.

**Cold model experiment.** For the accuracy verification of this simulation method, cold model experiment was conducted with using water and air in our laboratory. In this research, fairly large apparatus (ID: 0.58 m, L: 3 m) made of acrylic resin that was easy to be observed inside was used. 34 tubes were set inside the apparatus as mock cooling tubes, and then air was introduced from its bottom (0.04-0.32 m/s).

**Calculation results.** The simulated results that visualize gas volumetric fraction is shown in a) of Figure 3. Iso-surface of gas volumetric fraction is shown in left side, and gas volumetric fraction contours in vertical centerline plane of the column is shown in right side. White linear parts in figures indicate cooling tubes. A photo of cold model experiment is shown in b) of Figure 3 for a reference. Calculation results are depicting the waves of top surface and the hydrodynamics very well.

Calculated relation between gas holdup and superficial gas velocity is shown in Figure 4 with experimental data obtained from cold model experiment. Calculated results are in accordance with the results obtained by experiment.

Considering the results mentioned above, this simulation method is well describing the hydrodynamics in the reactor with accuracy. Authors will make fluid analysis of the commercial size reactor with this method, and design the commercial scale plant.

### Summary

With the high-performance F-T synthesis catalyst developed in this project, the first stable operation of GTL pilot plant in Japan at full load ended in success, and the outstanding properties of the catalyst could be demonstrated at the plant. Authors will continue the pilot plant operation and establish the scale-up technology with applying the simulation.

**Acknowledgment.** Authors acknowledge collaborators of this project (JAPEx, Chiyoda Corp, Cosmo Oil, and INPEX), and thank Yufutsu GTL for dedicated operation of the pilot plant and ChAS for computer calculations and Professor Akio Tomiyama for helpful discussions and suggestions.

### References

- (1) Zhao, R.; Goodwin Jr., J. G.; Oukaci, R. *Appl. Catal. A.* **1999**, *189*, 99.
- (2) Deckwer, W.-D., *Bubble Column Reactors*, John Wiley & Sons, **1992**.
- (3) Tomiyama, A., "The state of the art and perspective of computational bubble dynamics.", *Trans. JSME, B.* **2000**, *66*, 1618.

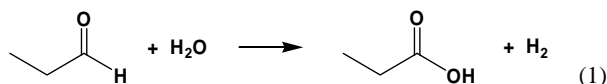
## Aldehyde-Water Shift Catalysis: H<sub>2</sub> Production from Water and Aldehydes via a Homogenous Dirhodium Tetraphosphine Catalyst

George G. Stanley,\* David A. Aubry, Novella Bridges, Bobby Barker and Brandy Courtney

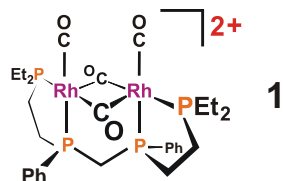
Department of Chemistry, Louisiana State University, Baton Rouge, LA 70803-1804, USA

### Introduction

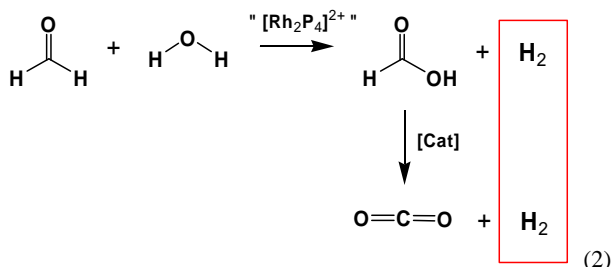
A new catalytic reaction to produce H<sub>2</sub> from aldehydes and water has been discovered (eq. 1).



This is called aldehyde-water shift catalysis in analogy with the water-gas shift reaction:  $\text{CO} + \text{H}_2\text{O} \rightleftharpoons \text{CO}_2 + \text{H}_2$ . The aldehyde-water shift reaction is thermodynamically downhill with  $\Delta G^\circ(363\text{K}) = -28.4 \text{ kJ/mol}$ ,  $\Delta H^\circ = -9.6 \text{ kJ/mol}$ , and  $\Delta S^\circ = 51.9 \text{ J/molK}$ . The proposed catalyst for this reaction is  $[\text{rac-Rh}_2(\mu\text{-CO})_2(\text{CO})_2(\text{et,ph-P4})](\text{BF}_4)_2$ , **1**, shown below.



The potential of this catalysis for fuel cell applications comes from the possibility of using formaldehyde to make formic acid and H<sub>2</sub>, followed by decomposition of the formic acid to make another H<sub>2</sub> and CO<sub>2</sub> (eq. 2):



A formaldehyde-water mixture has one of the highest H<sub>2</sub> energy storage capacities on a per weight basis for fuel cell applications.

### Experimental

The catalyst precursor used was  $[\text{rac-Rh}_2(\text{nbnd})_2(\text{et,ph-P4})](\text{BF}_4)_2$  (nbnd = norbornadiene) prepared according to literature methods,<sup>1</sup> or  $[\text{rac-Rh}_2(\text{CO})_4(\text{et,ph-P4})](\text{BF}_4)_2$  prepared and isolated from the carbonylation of the norbornadiene complex (details available from the principle author). 1-hexene, heptaldehyde, acetaldehyde, and acetone were all obtained from Aldrich and degassed with N<sub>2</sub> prior to use. 1-hexene was further purified by passing it through a short alumina column under N<sub>2</sub> prior to use. This removes any peroxide impurities that can deactivate the dirhodium catalyst. Water was normal distilled water from our in-house system and also degassed with N<sub>2</sub> prior to use.

Catalytic reactions were performed in 150 mL Parr 4560 mini-reactors equipped with standard thermocouples, pressure transducers and Parr packless magnetic stirrers. Data was collected and partially

analyzed on Parr 4850 or 4870 process controllers. The autoclave is configured to run under constant pressure with gas being supplied from a 1 L high pressure reservoir equipped with a pressure transducer and dual stage regulator. The autoclave set-up is shown in Figure 1. Products were analyzed on HP 5890 GC using a DB-1 30m capillary column or on a HP GC-MS system.

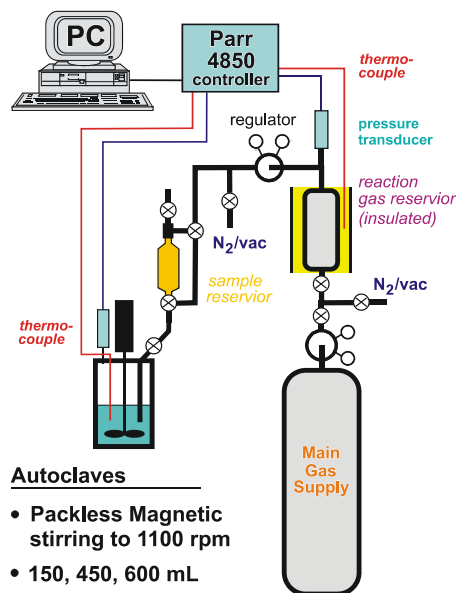


Figure 1. Schematic of autoclave setup.

### Tandem Hydroformylation and Aldehyde-Water Shift Catalysis.

With our current batch autoclave setup the most consistent results are obtained by first starting the catalysis under hydroformylation conditions using 1-hexene as the starting substrate and a 1:1 mixture of H<sub>2</sub>/CO gas. The autoclave was loaded under an inert atmosphere with 1.0 mM  $[\text{rac-Rh}_2(\text{nbnd})_2(\text{et,ph-P4})](\text{BF}_4)_2$  and 80 mL of 30% water (by volume) in acetone. The autoclave was then purged three times with H<sub>2</sub>/CO, and the catalyst solution stirred at 1000 rpm stirring for 15-20 min under 45 psig 1:1 H<sub>2</sub>/CO as the temperature was increased to 90°C. After the temperature has stabilized at 90°C the pressure of the reaction vessel was decreased to ~45 psig and 1000 equivalents of 1-hexene (99+% and passed through a neutral alumina column under inert atmosphere immediately prior to use,  $8.9 \times 10^{-2} \text{ mol}$ , 11 mL) was pushed into the autoclave with 90 psig of H<sub>2</sub>/CO. The progress of the reaction was monitored by gas uptake from a higher pressure gas storage reservoir connected to a two-stage regulator delivering synthesis gas at a constant pressure of 90 psig to the reaction vessel.

After 10 min of hydroformylation (representing approximately 80% conversion of the 1-hexene to heptaldehyde) the gas supply to the autoclave is turned off and the H<sub>2</sub>/CO gas in the high pressure reservoir is replaced with pure CO. This takes about 5 mins. The autoclave is then opened to the pure CO reservoir. Aldehyde-water shift catalysis occurs during this period converting the heptaldehyde to heptanoic acid and H<sub>2</sub>. The rapid build-up of H<sub>2</sub> in the autoclave typically stops the aldehyde-water shift catalysis at about 75-80% conversion of the aldehyde to carboxylic acid.

**Simple Flow-Reactor Studies.** Aldehyde can be directly reacted with water to make carboxylic acid and H<sub>2</sub> using a simple flow setup in our autoclaves. After the initial catalyst precursor ( $[\text{rac-Rh}_2(\text{nbnd})_2(\text{et,ph-P4})](\text{BF}_4)_2$ ) soaks under 1:1 H<sub>2</sub>/CO at 90 °C to generate the active catalyst, the feed gas is switched to 90 psig of pure CO and a needle valve is employed to constantly purge the

reaction vessel. 1000 equivalents of heptaldehyde are pressure added to the catalyst solution and a CO purge rate of 4-5 psig/min (based on the pressure drop in the high pressure reservoir cylinder) provided good conditions for aldehyde-water shift catalysis. A maximum of about 75% conversion to carboxylic acid was achieved, with an approximate turnover frequency of 1000 TO/hr (from GC analysis) and with undetectable side products. The aldehyde-water shift catalysis is quite sensitive to reaction conditions and both timing and proper purge rates are critical to achieve good conversion. These are still being optimized.

## Results and Discussion

The most consistent results for the aldehyde-water shift catalysis have been obtained by first performing hydroformylation catalysis on 1000 equivalents (1M concentration) of 1-hexene (smaller 1-alkenes are expected to work fine for this as well) under our standard reaction conditions: 90°C, 90 psig 1:1 H<sub>2</sub>/CO, and 30% water (by volume) and acetone as the solvent.<sup>2</sup> Water-acetone solvent dramatically stabilizes our highly active and selective dirhodium catalyst system by inhibiting fragmentation to unreactive species.<sup>2</sup> After 10 mins of rapid hydroformylation, approximately 80% of the 1-hexene has been converted to heptaldehyde. At this point the H<sub>2</sub>/CO gas feed to the autoclave is turned off and then switched over to pure CO. The continuing hydroformylation rapidly generates H<sub>2</sub>-deficient conditions in the autoclave that shifts the dirhodium catalyst equilibrium away from the hydroformylation dihydride catalyst,<sup>1b</sup> [rac-Rh<sub>2</sub>H<sub>2</sub>(μ-CO)<sub>2</sub>(et,ph-P4)]<sup>2+</sup>, to simple dirhodium carbonyl complexes that we believe are important for the aldehyde-water shift catalysis.

It is at this point under hydrogen depleted conditions that the aldehyde-water shift catalysis initiates. Average turnover frequencies (based on GC analysis) range from 1700 hr<sup>-1</sup> up to 2100 hr<sup>-1</sup>. A representative reactant-product consumption-production plot is shown in Figure 2. We have not directly measured the H<sub>2</sub> being produced, but the stoichiometry of the reaction, number of turnovers, and high selectivity of the reaction leaves little doubt that H<sub>2</sub> is one of the products.

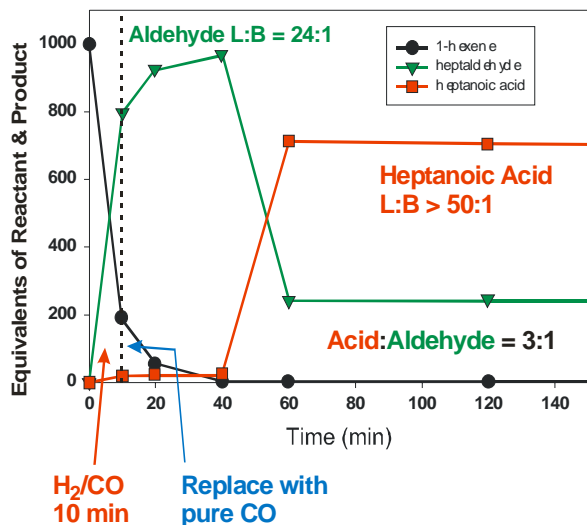


**Figure 2.** GC analysis of a tandem hydroformylation and aldehyde-water shift catalysis experiment.

The rapid production of H<sub>2</sub> leads to rapid inhibition of the aldehyde-water shift catalysis as seen after the 60 min mark in Figure 2. We typically get conversions of about 75% (750 turnovers), although we have seen one of our early runs with over 90%

conversion that had a relatively rapid accidental leak that purged hydrogen gas out of the autoclave.

We propose that the active catalyst species for the aldehyde-water shift catalysis is the dirhodium complex [rac-Rh<sub>2</sub>(μ-CO)<sub>2</sub>(CO)<sub>2</sub>(et,ph-P4)](BF<sub>4</sub>)<sub>2</sub>, **1** (see introduction for structural drawing). Under normal hydroformylation conditions with a 1:1 ratio of H<sub>2</sub>/CO no aldehyde-water shift catalysis is observed. We have established that the aldehyde-water shift catalysis is inhibited by the presence of too much H<sub>2</sub>, although we have not established the precise amount. Interestingly, some hydrogen is necessary to form the CO-bridged species, **1**. We believe that hydrogen addition to the “open-mode” (non-CO bridged) isomer [rac-Rh<sub>2</sub>(CO)<sub>4</sub>(et,ph-P4)]<sup>2+</sup> makes a Rh dihydride complex that can far more readily close up to make the bridged CO hydroformylation catalyst complex [rac-Rh<sub>2</sub>H<sub>2</sub>(μ-CO)<sub>2</sub>(et,ph-P4)]<sup>2+</sup>. Reductive elimination of H<sub>2</sub> from this species produces the bridged CO complex **1** critical for the aldehyde-water shift catalysis. **1** only exists in very low concentrations during hydroformylation catalysis when there is considerable H<sub>2</sub> present.

DFT quantum calculations on **1** indicate that the bridging CO ligands link and stabilize the lowest unoccupied molecular orbital (LUMO) making it a far better acceptor for activating the aldehyde for nucleophilic attack by water. The π\* systems of both the terminal and bridging CO ligands form bonding interactions with the Rh p<sub>z</sub> orbitals. This lowers the energy of the LUMO of **1** by 0.8 eV relative to the open-mode, non-CO bridged isomer of **1**.

The direct conversion of aldehyde and water is more difficult because our autoclave systems are not designed as flow reactors. Nevertheless, we have successfully performed aldehyde-water shift catalysis by activating the catalyst precursor under H<sub>2</sub>/CO, then using a constant purge of pure CO to react heptaldehyde and water (using 30% water in acetone as the solvent) to make heptanoic acid and H<sub>2</sub>. The generality of the reaction was partially demonstrated by converting acetaldehyde and water to acetic acid and H<sub>2</sub>. The volatility of the acetaldehyde, however, made this a considerably more difficult experiment and a slower purge rate had to be used to reduce the loss of acetaldehyde. Due to these experimental difficulties only 100 equivalents of acetaldehyde were converted. The ability to convert both heptaldehyde and acetaldehyde indicates that this reaction may work for aldehydes in general.

We are currently upgrading one of our autoclaves with a mass flow controller, condenser, and automated back-pressure regulator to setup a more sophisticated flow reactor system to study more volatile reactants such as acetaldehyde and especially formaldehyde.

## Conclusions

Aldehyde-water shift catalysis is a new reaction for producing H<sub>2</sub> from water and aldehyde. The use of water both as an oxidizing agent and a source of the H<sub>2</sub> being produced is remarkable. We believe that bimetallic cooperativity in the proposed dirhodium catalyst [rac-Rh<sub>2</sub>(μ-CO)<sub>2</sub>(CO)<sub>2</sub>(et,ph-P4)](BF<sub>4</sub>)<sub>2</sub>, **1**, is playing an important role in helping to activate the aldehyde and to provide a low energy route for hydrogen production.

**Acknowledgement.** We thank the NSF for funding (CHE-0111117).

## References

- (1) Broussard, M. E.; Juma, B.; Train, S. G.; Peng, W. J.; Laneman, S. A.; Stanley, G. G. *Science* **1993**, *260*, 1784. (b) Matthews, R. C.; Howell, D. K.; Peng, W.-J.; Train, S. G.; Treleaven, W. D.; Stanley, G. G. *Angew. Chem., Int. Ed. Engl.* **1996**, *35*, 2253.
- (2) Aubry, D. A.; Bridges, N. N.; Ezell, K.; Stanley, G. G. *J. Am. Chem. Soc.*, **2003**, *125*, 11180.

# COMBUSTION CHARACTERIZATION OF GTL DIESEL FUEL

*André L. Boehman, James P. Szybist, Juhun Song,  
Vince Zello and Mahabubul Alam*

The Energy Institute  
The Pennsylvania State University  
405 Academic Activities Building  
University Park, PA 16802

*Kirk Miller*

ConocoPhillips  
600 N. Dairy Ashford  
Houston, TX 77252

## Introduction

Synthetic diesel fuel production from natural gas offers the potential of both monetizing stranded natural gas resources and providing a supply of ultra clean transportation fuels. Gas-to-liquids (GTL) diesel fuels produced by the Fischer-Tropsch process typically have very high cetane number and zero sulfur content and can provide reductions in particulate and NO<sub>x</sub> emissions [1]. ConocoPhillips is developing a demonstration scale plant in Ponca City, OK to produce GTL diesel. The present study is part of an Ultra Clean Fuels project entitled "Ultra Clean Fuels from Natural Gas," sponsored by U.S. Department of Energy under Cooperative Agreement No. DE-FC26-01NT41098.

In this paper, we present results from in-cylinder imaging in a Cummins 5.9L, turbocharged, six-cylinder, 4-stroke direct injection (DI) diesel engine using an engine videoscope system. The imaging studies provide a comparison of the fuel injection timing, ignition timing, spray formation and flame luminosity between different fuels. Results are presented for an ultra low sulfur diesel fuel with 15 ppm sulfur content ("BP15") and for a GTL diesel fuel produced by ConocoPhillips. Also, we present experimental results on combustion and emissions with this ConocoPhillips Fischer-Tropsch diesel fuel (COP F-T diesel), in comparison with an ultra low sulfur diesel fuel. Together, these results show the potential impact of GTL diesel fuel on injection, combustion, and emissions formation in diesel engines.

## Experimental

Two different experimental systems were used in the work described here: a highly instrumented 6-cylinder DI turbodiesel engine equipped with an in-cylinder visualization capability and a highly instrumented, single-cylinder DI diesel engine equipped with in-cylinder and fuel injector sensors.

**In-Cylinder Imaging.** Tests were performed with a Cummins ISB 5.9L turbodiesel engine (MY2000, 235 HP max output) connected to a 250 HP capacity, eddy current absorbing dynamometer. The engine has been heavily instrumented, with a 0.1 crank angle resolution crank shaft encoder, a cylinder pressure sensor, a needle lift sensor and in-cylinder visualization using an AVL 513D Engine Videoscope. The engine and dynamometer are operated through an automated control system. Results are presented at an engine setting of 1800 rpm and 10% load.

**Injection Timing and Heat Release Analysis.** The single-cylinder engine tests were performed in a Yanmar L70 EE air-cooled, 4-stroke, single cylinder, DI diesel engine with a maximum power output of 7 hp was operated at 25% and 75% load and 3600 RPM (two operating modes from the G2 test from the ISO 8178-4.2 [2]). Cylinder pressure and fuel-line pressures were measured using

Kistler piezoelectric pressure transducer models 6052B1 and 601B1, respectively. A Hall-effect proximity sensor, installed by Wolff Controls Corporation, was used to measure needle-lift in the injector. An AVL 364 shaft encoder installed on the engine crankshaft, along with a Keithley DAS 1800 data acquisition board enabled 0.1 CA degree resolutions of these signals. NO<sub>x</sub> emissions were measured using an Eco-Physics NO<sub>x</sub> analyzer integral in an AVL GEM 110 emissions bench.

## Results and Discussion

**In-Cylinder Imaging.** Results from the in-cylinder imaging are shown in Figures 1 and 2. The figures compare the structure of the spray and flame for the BP15 and COP F-T diesel fuels at the same point in time after the start of injection (SOI), shown in terms of crank angle degrees after SOI. In the Cummins ISB engine it was observed that the BP15 fuel was injected at 0.2 crank angle degrees earlier than the COP F-T diesel, so comparisons are made relative to SOI. Also, each figure shows two views of each spray or flame. The viewing angle and orientation of the videoscope camera probe can provide different perspectives on the injection and combustion processes. In both Figures 1 and 2, a close-up view of the spray provides a clear view of the spreading angle and both the start and end of injection, while a view from a greater distance can provide an image of the entire length of the spray showing differences in penetration into the combustion chamber. Figure 1 shows images at 4 crank angle degrees after SOI (ASOI). Figure 2 shows images at 10 crank angle degrees ASOI. In both sets of images, Figure 1 showing the spray prior to ignition and Figure 2 showing flame structure well after ignition, there are no significant differences in the general structure of the spray or flame that are visible in this qualitative comparison, despite the significant differences in fuel properties.

**Injection Timing and Heat Release Analysis.** With the engine set at 25% load, Figures 3 and 4 compare injection timing and heat release results at two injection timing settings, set using shims between the fuel injection pump and the cylinder block. For the ultra low sulfur diesel fuel, BP15, combustion is delayed as injection is delayed leading to degraded combustion, which is particularly evident at the retarded injection timing. The higher cetane number of the COP F-T diesel causes the F-T diesel blend to perform well despite retarded injection timing, as seen for the late injection timing in Figure 4. As Figure 5 shows for the "late" static fuel injection timing, the differences in the heat release rate are not as significant at higher load where the ultra low sulfur fuel does not display degraded combustion as it does at the light load. Nonetheless substantial differences in emissions and fuel consumption are observed between the test fuels as injection timing and load are varied. Figure 6 presents brake specific fuel consumption, NO<sub>x</sub> emissions and CO emissions at 25% load for the "early" and "late" fuel injection timings. At the late injection timing, CO emissions increase and fuel consumption increases for the ultra low sulfur diesel fuel relative to the COP F-T diesel. NO<sub>x</sub> emissions are observed to have a more complex trend with fuel type. NO<sub>x</sub> decreases with retardation of injection timing, as expected. But, at light load NO<sub>x</sub> emissions are slightly lower for the ultra low sulfur diesel fuel than for the F-T diesel. However, the lower NO<sub>x</sub> with the ultra low sulfur diesel fuel at light load and retarded injection timing is at the substantial expense of CO and fuel consumption. At the higher load setting, NO<sub>x</sub>, CO and fuel consumption are always lower for the COP F-T diesel fuel.

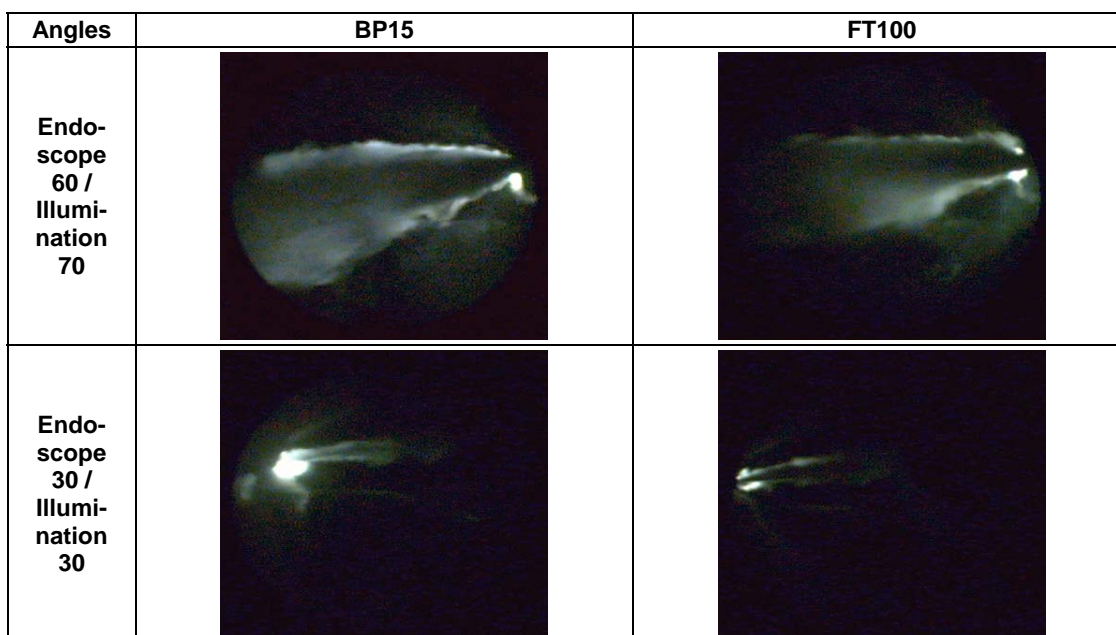


**Figure 1.** Videoscope images of injection of BP15 and COP F-T diesel within Cummins ISB 5.9L turbodiesel engine at 4 degrees ASOI.

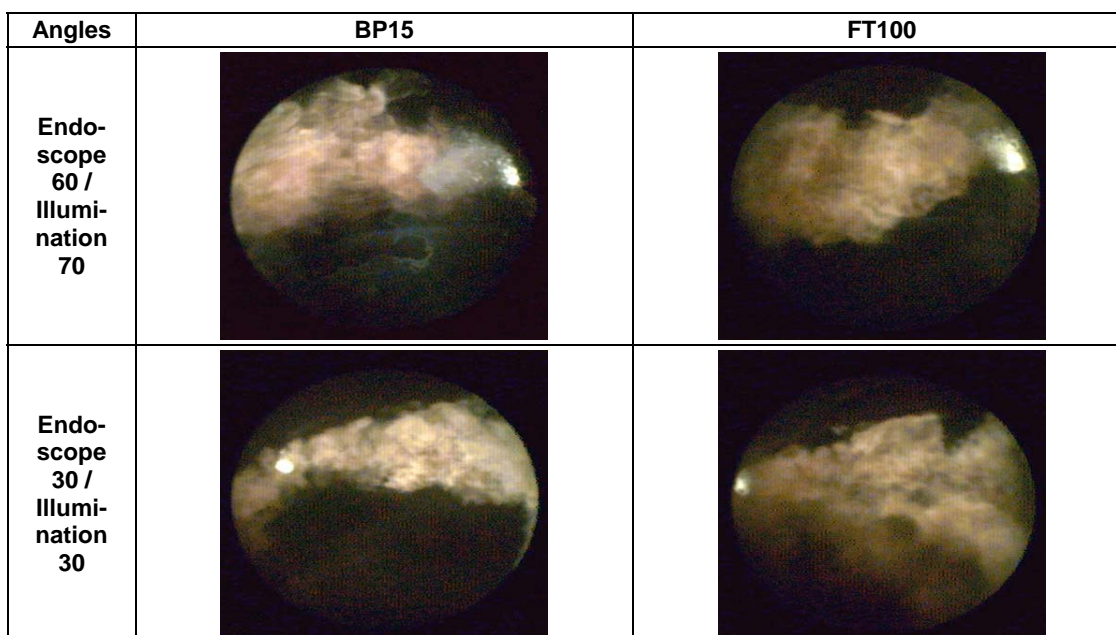


**Figure 2.** Videoscope images of injection of BP15 and COP F-T diesel within Cummins ISB 5.9L turbodiesel engine at 10 degrees ASOI.

### Conclusions

While in-cylinder imaging comparisons of ultra low sulfur diesel fuel and synthetic diesel fuel show no significant differences in spray or flame structure, injection timing and heat release analysis show that the high cetane number and low bulk modulus of compressibility of the F-T diesel fuel lead to significant differences in heat release and pollutant formation.

**Acknowledgement.** The authors wish to thank ConocoPhillips, Cummins Engine Company, the U.S. Department of Energy and the Pennsylvania Department of Environmental Protection for their support of this work. The authors especially wish to thank Etop

Esen, Doug Smith, Keith Lawson, Ed Casey, Raphael Espinoza and Jim Rockwell of ConocoPhillips, and John Wright and Edward Lyford-Pike of Cummins Engine Company for their support of this work.

This paper was written with support of the U.S. Department of Energy under Cooperative Agreement No. DE-FC26-01NT41098. The Government reserves for itself and others acting on its behalf a royalty-free, nonexclusive, irrevocable, worldwide license for Governmental purposes to publish, distribute, translate, duplicate, exhibit, and perform this copyrighted paper.

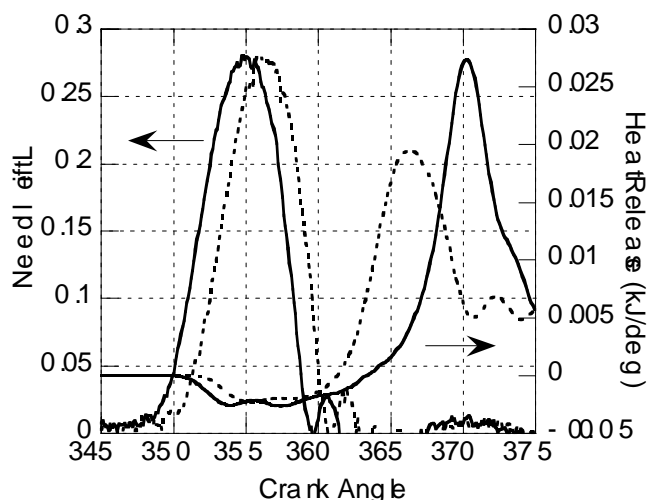


**Figure 3.** Needle lift and heat release versus crank angle for the “early” static injection timing at 25% load and 3600 rpm, in a Yanmar L70 DI diesel engine. (—) BP15 ultra low sulfur diesel fuel and (---) COP Fischer-Tropsch diesel fuel.

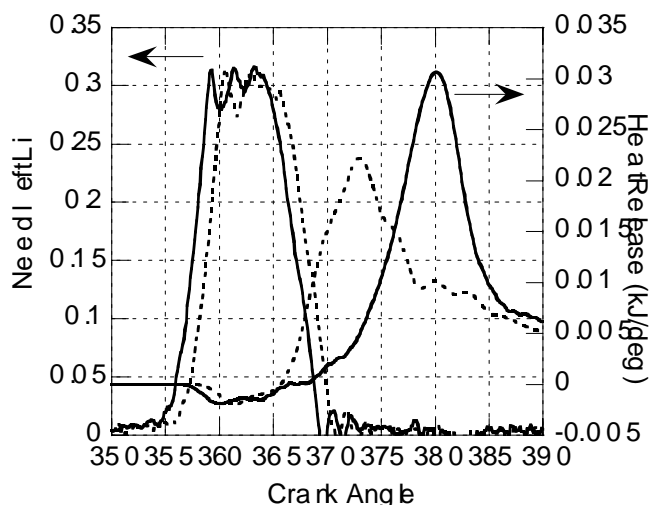


**Figure 5.** Needle lift and heat release versus crank angle for the “late” static injection timing at 75% load and 3600 rpm, in a Yanmar L70 DI diesel engine. (—) BP15 ultra low sulfur diesel fuel and (---) COP Fischer-Tropsch diesel fuel.

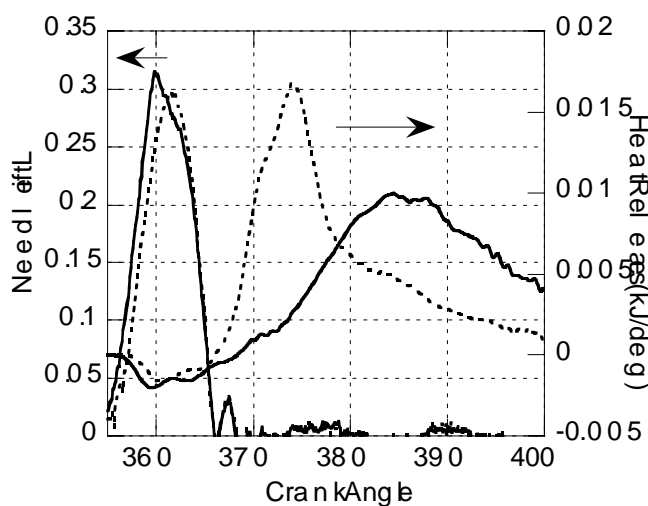


**Figure 4.** Needle lift and heat release versus crank angle for the “late” static injection timing at 25% load and 3600 rpm, in a Yanmar L70 DI diesel engine. (—) BP15 ultra low sulfur diesel fuel and (---) COP Fischer-Tropsch diesel fuel.

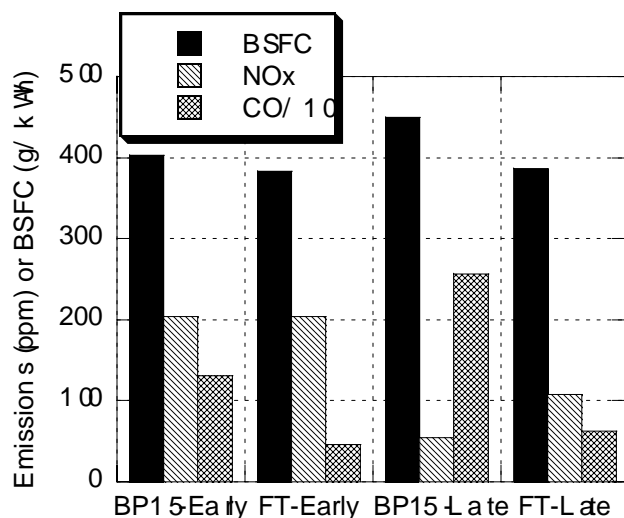


**Figure 6.** Brake specific fuel consumption, NOx emissions and CO emissions for BP-15 and COP F-T diesel fuels at 25% load and 3600 rpm, at the “early” and “late” injection timing settings.

This material was prepared with the support of the Pennsylvania Department of Environmental Protection. Any opinions, findings, conclusions, or recommendations expressed herein are those of the author(s) and do not necessarily reflect the views of the DEP.

## References

- (1) Lloyd, A.C. and Cackette, T.A., *J. Air & Waste Manage. Assoc.*, **2001**, 51, 809-847.
- (2) International Organization for Standardization, ISO 8178: Reciprocating internal combustion engines - Exhaust emissions measurement - Part 4. Test Cycles for different engine applications. 1995.

# SELECTIVE PRODUCTION OF GASOLINE-RANGED ISOPARAFFINS OVER Co/SiO<sub>2</sub> AND METAL/ $\beta$ CATALYSTS FROM SYNGAS

Zhong-Wen Liu<sup>†, ††</sup>, Xiaohong Li<sup>\*†</sup>, Kenji Asami<sup>†</sup>, Kaoru Fujimoto<sup>†</sup>

<sup>†</sup>Department of Chemical Processes and Environments, Faculty of Environmental Engineering, The University of Kitakyushu, Kitakyushu, Fukuoka 808-0135, Japan

<sup>††</sup>College of Chemistry and Chemical Engineering, Nanjing University of Technology, Nanjing 210009, P. R. China

## Introduction

The Fischer-Tropsch (FT) synthesis is an effective route to convert coal or natural gas derived synthesis gas (syngas, CO + H<sub>2</sub>) to liquid fuels and high-value added fine chemicals.<sup>1</sup> However, the FT products which are composed mainly of mixture of normal paraffins are nonselective and the product distribution is controlled by the so-called Anderson-Schulz-Flory (ASF) polymerization kinetics.<sup>1</sup> To selectively synthesize desired products such as diesel or high-octane gasoline, it is essential to circumvent the ASF distribution. Several groups have tried to selectively produce isoparaaffins by utilizing FT active components supported on acidic zeolites.<sup>2,3</sup> However, acidic zeolites are not a stable support under FT reaction conditions, and typical results show low activity and high methane selectivity. In our previous investigations,<sup>4,5</sup> a fundamental concept on direct production of isoparaaffins over physical mixture of a FT catalyst to synthesize long-chain hydrocarbons and a Pd-supported zeolite catalyst to hydroconvert the FT products was proposed and preliminary experiments were carried out both in one reactor and a consecutive dual reactor system. Results showed that high selectivity to isoparaaffins of C<sub>4</sub> ~ C<sub>8</sub> can be more efficiently and easily achieved in a dual reactor system by loading Pd/ $\beta$  catalyst in the downstream reactor.<sup>5</sup> In this investigation, Pt- and Pd-supported zeolite  $\beta$  catalysts were comparatively studied at different time on stream (TOS) for selective production of isoparaaffin from syngas in a consecutive dual reactor system, i.e., Fischer-Tropsch (FT) synthesis over Co/SiO<sub>2</sub> catalyst in the up-stream reactor and hydrocracking & hydroisomerization of FT hydrocarbons over the metal-supported zeolite  $\beta$  catalyst in the down-stream reactor.

## Experimental

The Co/SiO<sub>2</sub> catalyst (20 wt% Co) was prepared by the incipient wetness impregnation of aqueous solution of cobalt nitrate on the silica gel (Fujisilicia Q-15). The zeolite  $\beta$  (Sud Chemie, SiO<sub>2</sub>/Al<sub>2</sub>O<sub>3</sub>=25) was ion-exchanged at 353 K for 6 h in the solution of Pt(NH<sub>3</sub>)<sub>4</sub>Cl<sub>2</sub> and Pd(NH<sub>3</sub>)<sub>4</sub>(NO<sub>3</sub>)<sub>2</sub>, respectively, for the preparation of Pd/ $\beta$  and Pt/ $\beta$  catalysts (0.5 wt% loading). The final catalysts were dried overnight at 393 K and then calcined at 723 K for 2 h.

The reaction was carried out in consecutive dual fixed-bed reactors (SUS tube, 8mm I.D.), in which 0.4 g Co/SiO<sub>2</sub> mixed with 0.1 g  $\beta$  and diluted with 0.5 g quartz sands was loaded in the upper reactor and 0.5 g metal/ $\beta$  catalyst diluted with the same amount of quartz sands was in the lower reactor. Before reaction, the catalysts were pretreated at 673 K for 3 h in a flow of hydrogen. The operating conditions were P (system)=1.0MPa, H<sub>2</sub>/CO=2.0, W/F(syngas)=4.97 g·h·mol<sup>-1</sup>. The effluent hydrocarbons, which were cooled at 453 K, were analyzed by an on-line GC equipped with a NB-1 capillary column and a FI detector. The CO, CH<sub>4</sub>, and CO<sub>2</sub> in the effluent after cooling in an ice-water trap were on-line analyzed by a GC with a packed active carbon column and TC detector. The selectivity of hydrocarbons in this study was calculated on the basis of carbon number.

## Results and Discussion

To comparatively study the effect of catalyst loaded in the lower reactor on the isoparaaffin selectivity, the catalyst in the upper reactor and its operating conditions were kept the same for all the experiments. For simple expression, only the metal/ $\beta$  catalyst loaded in lower reactor will be mentioned. The product distribution over Pd/ $\beta$  catalyst in the dual reactor system was given in Figure 1. It is clear that the ASF distribution of the FT products was significantly changed, i.e., long-chain hydrocarbons produced in FT synthesis was dominantly hydrocracked and high selectivities toward C<sub>4</sub> to C<sub>7</sub> hydrocarbons were observed. It is a common fact that very less isoparaaffins was produced from FT synthesis over Co/SiO<sub>2</sub> catalyst. However, in the present case, very high selectivities of isoparaaffins with carbon numbers from 4 to 7 were observed as shown in Figure 1. At the present operating conditions, CO conversion was about 55%, indicating that an appreciable amount of unreacted hydrogen from the upper reactor was available in the lower reactor. Therefore, it is reasonable to propose that the main reactions occurred over Pd/ $\beta$  catalyst were hydrocracking and hydroisomerization. Comparing the carbon number distribution at different TOS, a slight decrease of the isoparaaffin selectivity was observed. This can be reflected clearly from the molar ratio of total isoparaaffins to C<sub>4</sub>+ hydrocarbons (I/C<sub>4</sub>+). The I/C<sub>4</sub>+ decreased from 62.1 at TOS of 2.5 h to 58.5 at TOS of 7 h.

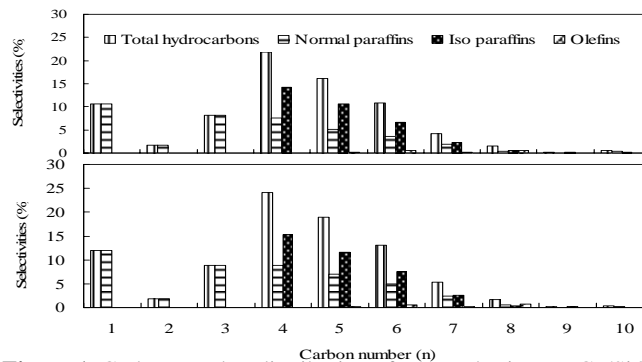


**Figure 1.** Carbon number distribution of FT synthesis over Co/SiO<sub>2</sub> and Pd/ $\beta$  catalysts in a dual reactor system (T=508 K (upper reactor), T=573 K (lower reactor)) at time on stream of 2.5 h (upper) and 7 h (lower).

From Figure 2, which was the carbon number distribution over Pt/ $\beta$  catalyst, it was clear that the ASF distribution of FT products was also significantly altered. But, in comparison with the results over Pd/ $\beta$ , an appreciable amount of hydrocarbons with carbon number larger than 11 was still observed, suggesting that heavy hydrocarbons produced on Co/SiO<sub>2</sub> was less hydrocracked over Pt/ $\beta$  than that over Pd/ $\beta$ . Furthermore, obvious higher olefin selectivities were found over Pt/ $\beta$  catalyst than that over Pd/ $\beta$  catalyst, especially at the later stage of the reaction. These results suggest that hydrocracking of FT products over Pt/ $\beta$  catalyst is less efficient than that over Pd/ $\beta$  catalyst. It should be pointed out that a significant decrease of isoparaaffin selectivity occurred by comparing the carbon number distribution at TOS of 2 h and 10 h. This was more clearly reflected from the sharp decrease of calculated I/C<sub>4</sub>+ ratios, i.e., from 67.3 at TOS of 2 h to 36.7 at TOS of 10 h. It is worthy to note that the sharp decrease of isoparaaffins with TOS was accompanied with significant increase of olefin selectivity as shown in Figure 2.

To compare the selectivities of individual isoparaaffin with the corresponding normal paraffin at different TOS, C<sub>4</sub>, C<sub>5</sub> and C<sub>6</sub> were chosen and calculated respectively, and the results were given in

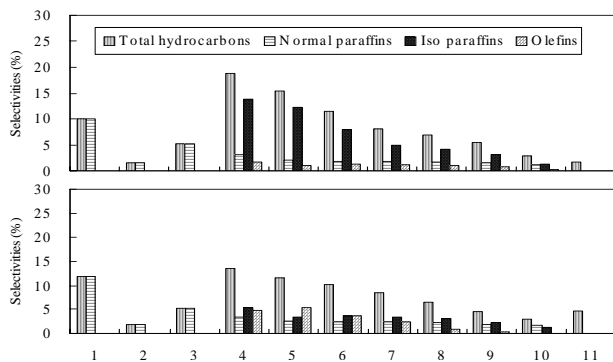


**Figure 2.** Carbon number distribution of FT synthesis over Co/SiO<sub>2</sub> and Pt/ $\beta$  catalysts in a dual reactor system (T=505 K (upper reactor), T=573 K (lower reactor)) at time on stream of 2 h (upper) and 10 h (lower).

Figures 3 and 4. Over Pd/ $\beta$  catalyst, the ratio of isobutane to n-butane was low even at TOS of 2.5 h (1.9) and decreased slightly to 1.7 at TOS of 7 h. When pentane and hexane were considered, almost same values and changing trends with TOS were observed. In the case of Pt/ $\beta$  catalyst, a quite different pattern appeared. A very high molar ratio of isoparaffin to the corresponding normal paraffin was produced at TOS of 2 h, and then decreased sharply with TOS and reached 1.66, 1.65, and 1.55 for butane, pentane and hexane, respectively.

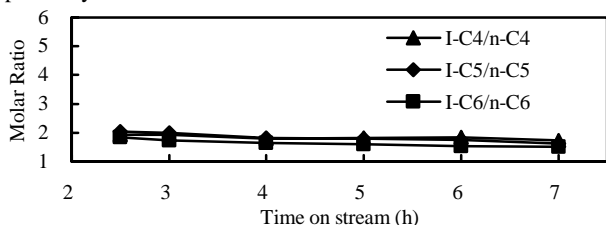


**Figure 3.** TOS I/C4+ molar ratios of FT synthesis over Co/SiO<sub>2</sub> and Pd/ $\beta$  catalysts in a dual reactor system (T=508 K (upper reactor), T=573 K (lower reactor)).

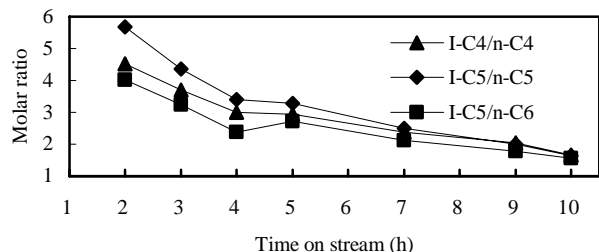


**Figure 4.** TOS I/C4+ molar ratios of FT synthesis over Co/SiO<sub>2</sub> and Pt/ $\beta$  catalysts in a dual reactor system (T=505 K (upper reactor), T=573 K (lower reactor)).

Blank tests showed that CO conversion was less than 2% at the present operating conditions when only either Pt/ $\beta$  or Pd/ $\beta$  was loaded. As mentioned above, the catalyst and operating conditions in the upper reactor were kept the same for each experiment, almost the same CO conversion and CH<sub>4</sub> selectivity were obtained irrespective of the catalyst used in the lower reactor. Therefore, the above phenomena must only be related to the hydroconversion function of the metal/ $\beta$  catalysts loaded in the lower reactor.

For the hydroconversion of normal paraffins over metal/solid acid catalysts, it is generally accepted that acid sites are responsible

for the cracking or isomerization reactions although the action mechanism of metal is still controversial.<sup>6</sup> However, zeolite  $\beta$  used in this study is the same for both Pd/ $\beta$  and Pt/ $\beta$  catalysts. Thus, the possible explanation on the different performance of Pd/ $\beta$  and Pt/ $\beta$  in the titled reaction may be from the interaction of metal and  $\beta$  zeolite. It is believed that Pt has high activity for hydrogenation/dehydrogenation of hydrocarbons and Pd doesn't have while both metals show high activity for the dissociation of hydrogen. Therefore, it is reasonable to propose that hydroconversion reactions of the FT hydrocarbons may be preceded in different mechanisms over the two catalysts.

Because water was produced in FT synthesis and the activity of water-gas shift reaction over Co was low, steam was always present in the lower reactor. Furthermore, it is a common fact that steam has a negative effect on solid acids. Therefore, the slight decrease isoparaffin selectivity over Pd/ $\beta$  catalyst may be caused by the deteriorative effect of steam on the acid sites over zeolite  $\beta$ . Another reason may be from the accumulation of coke on the catalyst as coke formation always accompanied with the hydroconversion of hydrocarbons over solid acid. Presently, anyone of the above reasons cannot be ruled out.

It is surprising that the Pt/ $\beta$  catalyst deactivated sharply for the titled reaction, additional reasons must be there. To the best of our knowledge, there is no report on the application of Pt/ $\beta$  catalyst for hydroconversion reactions in the FT conditions although Pt-supported solid acid catalysts were intensively investigated for hydroconversion of pure normal alkanes. In the present conditions, besides paraffins with a wide range of carbon number, olefins, steam and unreacted CO were also fed to the lower reactor. The fast deactivation of Pt/ $\beta$  catalyst may be arisen from these factors. Deteriorative effect of CO on the hydroconversion of n-butane over Pt/sulfated ZrO<sub>2</sub> was observed.<sup>7</sup> Moreover, the hydrocracking ability of Pt supported sulfated zirconia was severely reduced when n-C16 was co-fed with a C16 olefin.<sup>8</sup> In another work for the hydroconversion of n-C24 in a batch reactor<sup>9</sup>, the same authors found that Pt supported on WO<sub>3</sub>/ZrO<sub>2</sub> showed much lower hydrocracking ability. These findings support our present explanation. However, to clearly answer why Pt/ $\beta$  catalyst showed a fast deactivation in comparison with Pd/ $\beta$  catalyst, purposefully designed experiments and characterization works are in progress.

**Acknowledgment.** The authors acknowledge the financial support by Japan Oil, Gas and Metals National Corporation (JOGMEC).

## References

- (1) Vannice, M. E. *Cat. Rev. Sci. Eng.* **1976**, *14* (2), 153–191.
- (2) Jothimurugesan, K.; Gangwal, S. K. *Ind. Eng. Chem. Res.*, **1998**, *37*, 1181.
- (3) Koh, D.J.; Chung, J.S.; Kim, Y.G. *Ind. Eng. Chem. Res.*, **1995**, *34*, 1969.
- (4) Li, X.; Luo, M.; Asami, K. *Catal. Today*, 2004, in press.
- (5) Li, X.; Asami, K.; Luo, M.; Michiki, K.; Tsubaki, N.; Fujimoto, K. *Catal. Today*, **2003**, *84*, 59.
- (6) Fujimoto, K. In *Hydrotreatment and Hydrocracking of Oil Fractions*; B. Delmon, B.; Froment, G.F.; Grange, P.; Ed.; Elsevier Science B. V.: Amsterdam, 1999, Vol.127, p37.
- (7) Song, X.; Sayari, A. *Energy Fuels*, **1996**, *10*, 561.
- (8) Venkatesh, K.R.; Hu, J.; Wang, W.; Holder, G.D.; Tierney, J.W.; Wender I. *Energy Fuels*, **1996**, *10*, 1163.
- (9) Zhou, Z.; Zhang, Y.; Tierney, J.W.; Wender I. *Fuel Proc. Tech.*, **2003**, *83*, 67.